

DEVELOPMENT OF AN APPARATUS TO INVESTIGATE THE THERMAL
CHARACTERISTICS OF REGENERATIVE HEAT EXCHANGERS

Submitted in fulfilment of the requirements for the degree
of Doctor of Philosophy

at

The University of Leeds

by

S.J. HOLLINS, B.Sc.

Under the direction of

P.J. HEGGS, B.Sc., Ph.D., C.Eng., M.I.Chem.E.

Department of Chemical Engineering,
Houldsworth School of Applied Science,
The University of Leeds,
Leeds, LS2.9JT.

Summary

Cyclic thermal regenerators have an important industrial application, however most of the design techniques are old and use many simplifying assumptions. With the advent of digital computers many of these simplifying assumptions can be examined, however there is very little scope for practical verification. An apparatus has been designed, built and fully commissioned to investigate thermal regenerator characteristics. The analog operation of the apparatus is enhanced by four computer aspects. Commissioning of the regenerator highlighted how the response of apparatus can be influenced by the peripheral pipework around the test section, radiation effects from the heaters and jetting of air into the regenerator packed bed section.

A series of experiments, comprising runs (a maximum of ten period changes) within a set-up (a known air flowrate and packed bed length) were formulated to examine the regenerator response, using three types of spherical packing, steel lead glass and alumina. A method of obtaining convective heat transfer coefficients was produced and represented in two forms. One in a graphical form which can be used for cyclic regenerator designs without the prior knowledge of a heat transfer coefficient, whilst the other form is data stored on a computer disc which produces convective heat transfer coefficients for regenerator raw data. Analysis of the practical data clearly shows the importance of the number of cycles required to reach equilibrium, test bed heat leak and packing intraconduction.

Finally, prior to each cyclic set-up a single shot run was performed and the convective heat transfer coefficient obtained using Darabi's(1981) graphical technique. This offered a unique opportunity to compare cyclic and single shot characteristics for the same physical system.

ACKNOWLEDGEMENTS

Many thanks to Dr. P.J. Heggs for his constant advice and helpful discussion throughout this research and the compiling of this thesis. Thanks to Professor McGreavy for allowing me the use of the Departmental facilities and to the many members of the Department, friends and colleagues who have given assistance. In particular thanks are given to Mr. L. Bailey for his help with the computation and also to the Departmental technicians for their help during the design and construction of the apparatus. Financial support given by the S.R.C. is also gratefully acknowledged.

Additional thanks go to L. Flutter and A. Ralph for typing this text and to Air Products Ltd. for their help.

Finally this work owes a great deal to the patience and constant encouragement given by my beloved wife Julie.

<u>CONTENTS</u>	<u>PAGE NUMBER</u>
Summary	i
Acknowledgements	iii
Contents	iv
List of Tables	ix
List of Figures	x
Chapter 1 Introduction	1
Chapter 2 Previous Regenerator Theory, Design and Practical Investigations	10
2.1 Introduction	10
2.2 Theoretical Advancements	10
2.3 Previous Cyclic Regenerator Experimental Work	13
2.3.1 Experimental Work Above Ambient Temperature	15
2.3.2 Experimental Cryogenic Work	16
2.4 Cyclic Regenerator Design Methods	17
2.5 Approximate Solutions	22
2.6 Single Blow Techniques	23
2.7 Pilot Plant Applications	28
Chapter 3 Design of a Regenerative Apparatus	29
3.1 Introduction	29
3.2 Conceptual Regenerator Design	29
3.2.1 Apparatus to Operate at Ambient Temperature	29
3.2.2 Mode of Operation	30
3.2.3 Single Horizontal Fixed Bed	30
3.2.4 Process Fluid	31
3.2.5 Initial Regenerator Conception	31
3.3 Cyclic Regenerator Design	32
3.3.1 Regenerator Matrix Housing	32

CONTENTS Contd.

PAGE NUMBERS

3.3.2	Regenerator Bed Design	32
3.3.3	Regenerator Test Bed Characteristics	36
3.3.4	Imbalanced Systems	37
3.3.5	Regenerator Switching	38
3.3.6	Heater Design	38
3.3.7	Temperature Indication	41
3.3.8	Design for Plug Flow	45
3.4	Proposed Regenerator Operation	45
3.4.1	Front End Section	45
3.4.2	Main Regenerator Section	46
3.4.3	Chimney Section	47
3.5	Chapter Conclusion	48
Chapter 4	Mechanical Construction and Analog Instrumentation Installation	49
4.1	Introduction	49
4.2	Front End Section	49
4.3	Main Regenerator Section	59
4.4	Chimney Section	69
4.5	Chapter Conclusions	70
Chapter 5	Computer Control and Data Logging Facilities	71
5.1	Introduction	71
5.2	Computer Interfacing	74
5.3	Description of Digital Computers	75
5.4	Period Switching	77
5.4.1	Timing Hardware	77
5.4.2	Overall Operational Procedure Software Programme	80

CONTENTS Contd.PAGE NUMBERS

5.4.3	Overall Timing Procedure	80
5.5	Flowrate Logging	81
5.5.1	Flowrate Logging Hardware	81
5.5.2	Overall Flowrate Computer Logging	85
5.6	Computer Data Logging	89
5.6.1	Temperature Logging Hardware	90
5.6.2	Computer Temperature Logging Procedure	93
5.7	Front End Computer Control	93
5.7.1	Control Hardware	96
5.8	Conclusion	96
Chapter 6	Apparatus Commissioning	97
6.1	Introduction	97
6.2	Radiation Effects on the Resistance Thermometers	97
6.3	Control of the Inlet Temperature to the Test Bed Section	104
6.3.1	Computer Control	104
6.3.2	Analog Control	106
6.4	Thermal Inertia	109
6.5	Further Rig Commissioning	118
6.5.1	Analog Commissioning	118
6.5.2	Mechanical Commissioning	118
6.5.3	Computer Commissioning	120
6.6	Chapter Conclusions	123
Chapter 7	Experimental Programme	124
7.1	Introduction	124
7.2	Choice of Packing	128
7.3	Apparatus Simulation	130

<u>CONTENTS Contd.</u>		<u>PAGE NUMBERS</u>
7.3.1	Model Solution	131
7.4	Test Bed Simulation	140
7.5	MISP Simulation for Operational Procedure	145
7.6	Convective Heat Transfer Coefficient Prediction	148
7.6.1	Suitable Method	148
7.6.2	Convective Heat Transfer Coefficient Determination	149
7.7	Experimental Start Up and Shut Down	156
7.8	Data Collection	156
7.8.1	Set-Up Data Collection	157
7.8.2	Run Data for a Set-Up	158
7.9	Chapter Conclusions	160
Chapter 8	Analysis of Results	161
8.1	Introduction	161
8.2	Single Shot Analysis	161
8.3	Cyclic Analysis	170
8.4	Effect of the Number of Cycles to Reach Equilibrium	178
8.5	Discrepancy Between the Hot and Cold Efficiencies	182
8.6	Dimensionless Length Prediction	187
8.7	Intraconduction Analysis of the Cyclic Set-Ups	197
8.8	Comparison of Cyclic and Single Shot Heat Transfer Coefficients	213
8.9	Chapter Conclusions	214
Chapter 9	Summary of Conclusions and Proposals for Future Work	215
9.1	Conclusions	216
9.2	Future Work	220

CONTENTSPAGE NUMBER

Appendices:

A	Instrument Characteristics	222
B	Manual and Computer Interface Switching Actions	225
C	Computer Interfacing Equipment	230
D	S/7 and Eclipse Software Facilities	233
E	Flow Diagrams Showing the ON and OFF Line Programmes Required for Computer Operation of the Apparatus	237
F	Front End Steady State Radiation Calculations	247
G	Prediction of the Temperature Response Within the Front End Section for a Known Step Heat Input	251
H	Published Paper by P.G. Heggs and S.J. Hollins	258
I	Logic Diagram for Computer Programme SJHEFF2	262
J	Apparatus Start Up and Shut Down	263
K	Set-Up Data	278
L	Run Data for Each Set-Up	279
	Nomenclature	285
	References	289

<u>LIST OF TABLES</u>	<u>PAGE NUMBER</u>
3.1 Higgs (1967) Packed Bed Correlations	33
6.1 Wheatstone Bridge Resistance Values	101
6.2 Data Required for a MISP program Run to Examine a 4 inch (101.6 mm) Packed Bed Section with Internal Insulation and a Flowrate of 0.001 and 0.0463 M ³ /s	108
6.3 MISP output for the Seven Regenerator Sections	111
6.4 Regenerator Section Time Constants	114
6.5 MISP Output for just a 4 inch (101.6 mm) Packed Bed	116
7.1 Efficiency Values at $\Lambda = 15$ and 20 for $\Pi/\Lambda \leq 2.0$ obtained using the Schumann model programme SJHEFFI	139
7.2 MISP Simulation Results for Steel and Lead Glass at $\Lambda = 25, 10, 15$ and 10	141
7.3 MISP and Schumann Model responses for Steel at $\Lambda = 20$	146
8.1 Single Shot Set-Up Data	166
8.2 Values of Efficiency from the Cyclic Matrix Method Using Single Shot Values of Lambda	179
8.3 Heat Leak Calculation Data	184
8.4 Λ Results from Set-Ups A to F	193
8.5 Data Used in Intraconduction Analysis	201
8.6 Λ Comparison for the Cyclic and Single Shot Set-Ups.	212

<u>LIST OF FIGURES</u>	<u>PAGE NUMBER</u>
1.1 Fixed Matrix Regenerators	2
1.2 Rotary Regenerator	2
2.1 Closed Basket Weave Setting	14
2.2 Hausen's Effectiveness Chart	18
2.3 Peiser and Lehner's Design Chart for Symmetric Regenerators	19
3.1 Graph of Superficial Gas Mass Velocity (G) Versus Lambda (Λ) for Various Packed Bed Lengths (L) of 6.35 mm Diameter Spheres	34
3.2 Various Test Bed Lengths for a Packed Bed Section up to 355.6 mm	35
3.3 Tufnol Housing for Heater and Resistance Thermometer Elements	39
3.4 Detail of Heater Wire Positioning	40
3.5 Detail of Resistance Wire Positioning	42
3.6 Regenerator Diffuser Containing a Temperature Dampening Section	43
3.7 Schematic Diagram of the Regenerator	44
4.1 Mains Contact Breaker	50
4.2 Front End Step Temperature Unit	50
4.3 Indicator Controller Wiring	53
4.4 C.S.R. Thyristor Regulator Wiring	53
4.5 Front End Analog and Computer Control Set-Up	54
4.6 Pressure Indication Layout	58
4.7 Two P.O.42 LGM electronic Timers Wired for Dissimilar Timing actions	60
4.8 Manual and Computer Timing Interfacing with Test Bed Heater Set-up	61
4.9 Heenan 180/6 (Test Bed Heater Unit) Wiring	63

<u>LIST OF FIGURES Contd.</u>	<u>PAGE NUMBER</u>
4.10 Temperature Indication Procedure	63
4.11 Wheatstone Bridge Set-Up	64
4.12 308 Amplifier in the Non Inverting State	64
4.13 Resistance Thermometer Representation on the Multi Point Kent Mk 3 Recorder	66
4.14 Orifice Unit	67
4.15 Orifice Calibrations	68
5.1 Hierarchical Computer System for the Thermal Regenerator Showing the Front End Control Loop	72
5.2 Computer Reed Relay Timing Circuit	78
5.3 Block Diagram of the Computer Timing	78
5.4 Differential Pressure to Analog Voltage Circuit	82
5.5 Block Diagram of the Computer Flowrate Logging	82
5.6 Flowrate Versus Time for one Cycle at Low Flowrate	83
5.7 Flowrate Versus One Cycle at High Flowrate	84
5.8 Regenerator Response for Five Thirty Minute Cycles	86
5.9 Two Consecutive Thirty Minute Cycles	87
5.10 Cycle Efficiency Versus Total Number of Thirty Minute Cycles	88
5.11 Thumbwheel Switch Circuit	91
5.12 0.27 Inch Logic Hexidecimal L.E.D. Circuit	91
5.13 Block Diagram of the Computer Temperature Logging Procedure	92
5.14 Digital to Analog Converter	94
5.15 Block Diagram of the Front End Computer Control Loop	95

<u>LIST OF FIGURES Contd.</u>	<u>PAGE NUMBER</u>
6.1 Radiation Shield and Tufnol Housing	99
6.2 Graph of Temperature Versus Resistance for all Seven Resistance Thermometers	100
6.3 Radiation Shield Test Runs	102
6.4 Control Block Diagram Representing the Front End	105
6.5 Test Bed Sections Used in the MISP program	107
6.6 Graph of MISP Output, Regenerator Bed Temperature Versus Distance	110
6.7 Graph of Water Manometer Height Versus Voltage for Calibration of the D/P-Emitter Follower Circuit	121
6.8 Graph of BITS Versus Voltage Output for the D/A Converter	121
7.1 Heggs et al Intraconduction Design Chart for Spherical Packings	125
7.2 Peiser and Lehner's Design Chart for Symmetric Regenerators	127
7.3 Hausen's Effectiveness Chart	129
7.4 Numerical Scheme for the Schumann Model	134
7.5 Number of Cycles Required to Obtain Equilibrium Versus $\frac{\pi}{\Lambda}$ for Lambda 25(5)5. $\frac{\pi}{\Lambda}$ Decreasing	137
7.6 Number of Cycles Required to Obtain Equilibrium Versus $\frac{\pi}{\Lambda}$ for Lambda 25(5)5. $\frac{\pi}{\Lambda}$ Increasing	138
7.7 Representation of Array A	150
7.8 Matrix Method Linear Design graph. Efficiency Versus $\frac{\pi}{\Lambda}$ for Lambda	151
7.9 Matrix Method Semi Log Design Chart. Log Inefficiency versus $\frac{\pi}{\Lambda}$ for Lambda	152
7.10 Representation of Array A	150
7.11 Representation of Array B.	150

<u>LIST OF FIGURES Contd.</u>	<u>PAGE NUMBER</u>
8.1 Temperature Response for a Single Shot Run	162
8.2 Darabi's Graph of $\overline{\Pi} / \Lambda_{SS}$ Versus Λ_{SS}	163
8.3 Bi Versus $\overline{\Pi}_{SS}$ for the Six Single Shot Runs Made Prior to Each Set Up	165
8.4 An Example of the Difference Between Schumann and Plain Wall Effectiveness	169
8.5 η Versus $\overline{\Pi} / \Lambda$ for Steel Set-Up 'A'	171
8.6 η Versus $\overline{\Pi} / \Lambda$ for Steel Set-Up 'B'	172
8.7 η Versus $\overline{\Pi} / \Lambda$ for Lead Glass Set-Up 'C'	173
8.8 η Versus $\overline{\Pi} / \Lambda$ for Lead Glass Set-Up 'D'	174
8.9 η Versus $\overline{\Pi} / \Lambda$ for Alumina Set-up 'E'	175
8.10 η Versus $\overline{\Pi} / \Lambda$ for Alumina Set-Up 'F'	176
8.11 Section through the Regenerator Bed	183
8.12 Brethertons Set-Up at $\Lambda = 178$ for 0.08 inch (2.03 mm) Lead Shot	188
8.13 Brethertons Set-Up at $\Lambda = 250$ for 0.08 inch (2.03 mm) Lead Shot	189
8.14 Λ_{av} Versus $\overline{\Pi} / \Lambda$ for Steel Set-Ups 'A' and 'B'.	190
8.15 Λ_{av} Versus $\overline{\Pi} / \Lambda$ for Lead Glass Set-Ups 'C' and 'D'	191
8.16 Λ_{av} Versus $\overline{\Pi} / \Lambda$ for Alumina Set-Ups 'E' and 'F'	192
8.17 Schumann-Sphere Comparison $\Lambda = 2.5$	198
8.18 Schumann-Sphere Comparison $\Lambda = 5$	199
8.19 Schumann-Sphere Comparison $\Lambda = 10$	200
8.20 Bi Versus $\overline{\Pi}$ for Steel Set-Ups 'A' and 'B'	208
8.21 Bi Versus $\overline{\Pi}$ for Lead Glass Set-Ups 'C' and 'D'	209
8.22 Bi Versus $\overline{\Pi}$ for Alumina Set Ups 'E' and 'F'	210

LIST OF FIGURES Contd.PAGE NUMBERS

F.1	Diagram of the Front End Experimental Run	350
F.2	Diagram of the Front End Simulation	250
G.1	Diagram of the Control Set-Up	256
G.2	Simulated Temperature Response According to Fig. G.1.	257

LIST OF PLATES

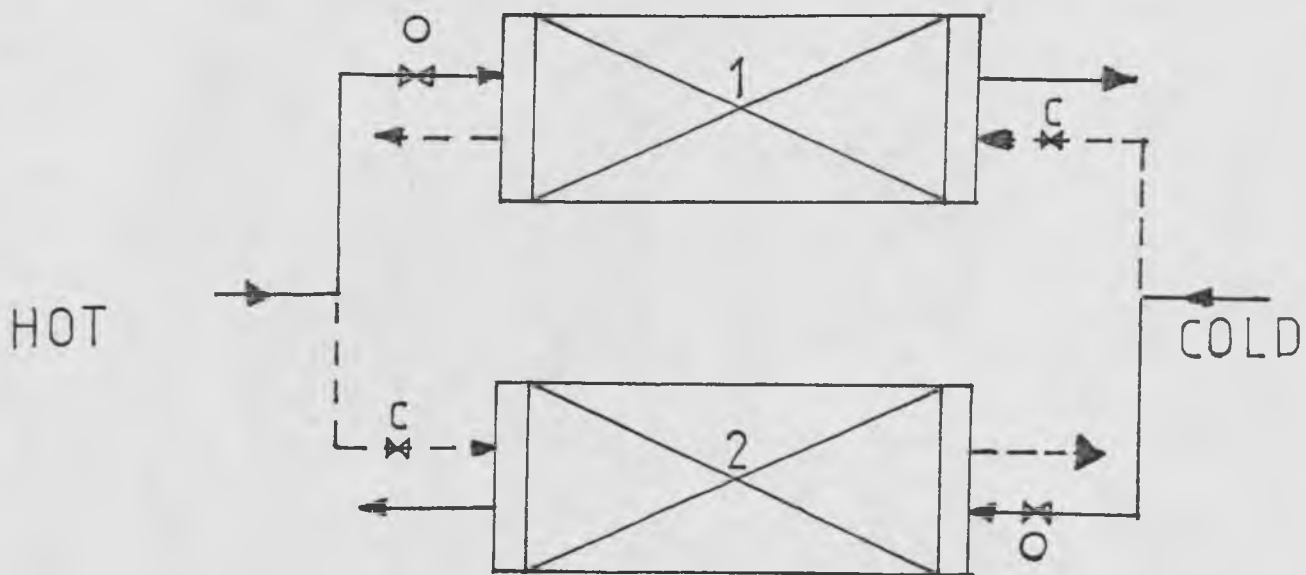
4.1	Control Panel	51
4.2	Regenerator Test Bed	57

Chapter 1

Introduction

In a thermal regenerator heat is transferred between two fluid streams. The hotter fluid gives up its heat to a packing and subsequently this heat is released to a colder fluid. This heat transfer is a combination of several competing mechanisms, namely: convection, conduction and, at high temperatures, radiation. Regenerator design should allow for all heat transfer contributions. Before the advent of digital computers regenerators were mainly designed by analogy with recuperators. Heat capacity, cycle times and conduction effects were incorporated in a modified overall heat transfer coefficient. Computational advances now allow a more thorough analysis and design of such systems, but practical validation for these techniques has not been substantiated.

Regenerators have been used for many years in the process industries and fall into two main categories; fixed bed and rotary matrix type. For the fixed bed system two regenerators are required for continuous operation. More commonly, three and four bed arrangements are used in the iron and steel industry for pre-heat of blast furnace air. Fig. 1.1 shows the operation of a two-bed countercurrent regenerator system. Bed 1 is being heated whilst bed 2 is being cooled. At the end of a fixed timing period the fluid flows are switched over, which reverses the procedure.



o OPEN c CLOSED

FIGURE 1-1

FIXED MATRIX REGENERATORS

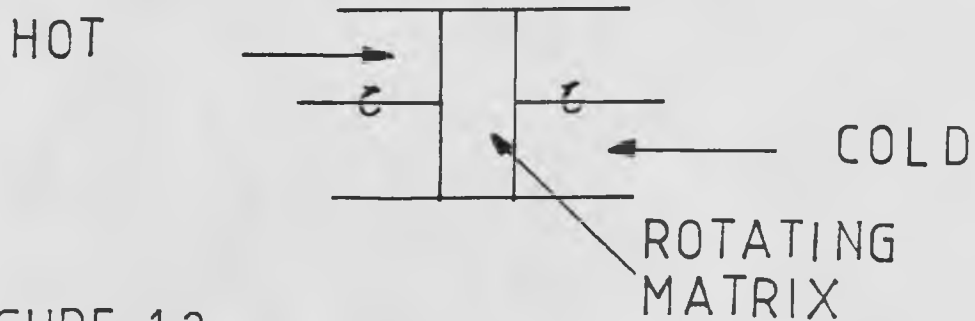


FIGURE 1-2

ROTARY REGENERATOR

Rotary regenerators do not employ reversing fluid streams. Periodic operation, as shown by Fig. 1.2, is achieved by rotating the solid matrix about a central axis, so that the matrix alternately passes through each flowing fluid stream. The time taken for the solid matrix to pass through one fluid stream is equivalent to a fixed regenerator bed period.

Many *INDUSTRIES* employ regenerators ranging from cryogenics to high temperature processes. Typical types of high temperature applications are Cowper stoves in the steel industry Petit (1964), preheat regenerators in the glass industry Ruheman (1940) gas turbine plants as discussed by Hrynszak (1958), power plants Poletavkin and Malygin (1972) and waste heat recovery systems, particularly for stack gases, Orr (1976). At the other end of the temperature scale thermal regenerators are used to retain coldness within processes. Such as the Linde-Frankl process for air separation and the Gifford McMahon (1965) cycle, which is used in refrigeration.

Regeneration models normally consider only interphase convective heat transfer, although other mechanisms may be accounted for by lumped parameters. The assumptions inherent in this model are as follows:-

1. The thermal conductivity of the solid may be regarded as being infinite in the direction normal to the surface.
2. The thermal conductivity of the matrix parallel to the gas flow may be assumed to be zero.

3. The fluid does not disperse heat within itself.
4. There is constant fluid mass flow which is dispersed equally across the flow area.
5. There are constant solid properties throughout the regenerator.
6. The fluid properties and heat transfer coefficients are constant throughout each period.
7. The flow changeover is instantaneous.

It may be reasonably assumed that the thermal conductivity of the solid normal to the surface may be regarded as infinite for regenerator packings comprising Frankl packings, very small metal shot, thin metal plates and gauzes of metal wires. However, this assumption may well be questioned when packings of quartz pebbles, glass ceramic screens, quartz wire gauzes and refractory chequers are used.

The assumption of zero conductivity parallel to the gas flow is valid in particulate regenerator packings, such as spheres, rods and gauzes, because there is only point contact between the packing elements. However in non-particulate packings, such as Frankl packings and those constituting Lungstrum rotary regenerators, axial conduction combinations may be significant.

The assumption of negligible fluid maldistribution and no dispersion of heat within the fluid phase are justified in non-cryogenic processes where there are large fluid flowrates, large amounts of heat transferred and the matrix size is large compared to the void dimensions. In cryogenic regenerators however, the fluid flowrates and amount of heat transferred is small. The possible significance of these mechanisms must therefore be borne in mind when considering such regenerator systems.

Many regenerators operate with a constant fluid mass flow. However, there are situations where the flow varies throughout the period of operation in order to provide a fixed process outlet temperature. These are primarily used in the steel industry and the systems employ a by-pass for a portion of the mass flow. In most industrial regenerators the temperature range is considerable and the assumption of constant solid and fluid properties is most questionable. In addition, any variations in these properties will subsequently affect the heat transfer coefficient.

An additional assumption is made that there is no heat loss or pick up from the surroundings. This is valid for just above and below ambient temperature, but the regenerator must be adequately insulated at both ends of the temperature scale to concur with theory.

Furthermore, it is assumed that the regenerator wall heat capacity is negligible. This is true for large

regenerators, such as Cowper stoves, where the wall heat capacity is negligible compared to the large heat capacity of the checkerwork constituting the packing. However, in cryogenic refrigeration units the regenerator wall has a considerable heat capacity in comparison to the packing material. In such cases, therefore, the wall heat capacity is significant and should be allowed for within the design calculations, as discussed by Granville et al (1966).

Operational and constructional considerations must also be accounted for in design calculations. Theory assumes that the inlet fluid temperatures do not vary with time. However in practice this is not always the case. The peripheral pipework has a finite heat capacity and this causes the inlet temperature to vary with time.

A feature common to all types of regenerator systems is cyclic equilibrium operation. This occurs when the efficiencies of the hot (η_H) and cold (η_C) strokes are equal, where:

$$\eta_H = \frac{(G C_g P)_H (T_{HI} - T_{HOM})}{(G C_g P)_{Min} (T_{HI} - T_{CI})} \quad (1.1)$$

$$\eta_C = \frac{(G C_g P)_C (T_{COM} - T_{CI})}{(G C_g P)_{Min} (T_{HI} - T_{CI})} \quad (1.2)$$

G = Superficial gas mass velocity (kg/s m^2)

C_g = Fluid specific heat (J/kg K)

P = Time of a period (S)

T_{HI} = Hot inlet temperature (K)

THOM = Mean hot outlet temperature (K)

TCI = Cold inlet temperature (K)

TCOM = Mean cold outlet temperature (K)

Subscript H = Hot stroke

Subscript C = Cold stroke

MIN = Smaller of the hot and cold values

MAX = Larger of the hot and cold values

Another parameter used in regenerator design is the dimensionless fluid outlet temperature swing, defined as follows:

$$\sigma_{TC} = \frac{(TCO_{MAX} - TCO_{MIN})}{(THI - TCI)} \quad (1.4)$$

$$\sigma_{TH} = \frac{(THO_{MAX} - THO_{MIN})}{(THI - TCI)} \quad (1.5)$$

Cyclic equilibrium exists when the temperature time history of one complete cycle is identical to that of the previous and subsequent cycles. For a fixed bed regenerative system, this assumes that the hot and cold periods follow each other exactly. However, in large flowrate applications such as Cowper stoves the switch-over valves are pneumatic and can take up to 2 minutes to open or close, so affecting the outlet temperature.

At the other extreme, in cryogenic refrigeration cycles, such as the Gifford McMahon cycle (1965) there is rapid switching between the fluid streams. The single stage cryogenic gas balancing refrigeration is an application of

the Gifford McMahon cycle and typically operates at one to three cycles per second. The very rapid switching *BETWEEN* flows means that the fluid residence time in the packing voids may become the same as or even *MORE* than the very short period. However, conventional regenerator design techniques assume negligible fluid residence time, which is clearly untrue in this situation and can lead to inaccurate design as shown by Heggs and Carpenter (1976).

It is evident that the theoretical assumptions used in design need practical verifications for the different types of regenerator usage.

This research project is therefore undertaken to design, build and operate a small scale fixed bed thermal regenerator, operating just above ambient temperature and incorporating the majority of the above assumptions. The operational procedure provides computer temperature and flowrate data logging, computer control of the inlet fluid temperature and flow stream reversals. The computer aspects allow a much wider range of operating parameters as well as a far greater accuracy. In addition the computer is used 'off-line' to process the experimental data and to provide direct evaluation of thermal efficiency and outlet temperature swings.

After consulting the literature it was evident that a more accurate and concise method of obtaining cyclic regenerator packing heat transfer coefficients had to be

found. A unique method is proposed and used to obtain overall heat transfer coefficients for balanced regenerator systems.

Chapter 2

Previous Regenerator Theory, Design and Practical Investigations

2.1 Introduction

Recent theoretical advances in thermal regenerator technology, as discussed by Carpenter (1976), have shown how regenerator design can be markedly improved. However practical investigations have not kept pace with theory.

2.2 Theoretical Advancements

Industrial design applications have remained unaltered for many years. This is typified by Petit (1964), who quoted Cowper stoves as the 'good children of the steel industry' because they fully met their design criteria over 100 years ago but were subsequently ignored as operating conditions gradually changed, particularly as higher output temperatures were required.

Initially overall heat transfer coefficients were only required for regenerator design. However, recent mathematical modelling techniques in conjunction with digital computers allow previous design assumptions to be investigated.

The first computer technique representing a cyclic fixed bed regenerator was developed by Willmott (1964) using the

Schumann (1929) assumptions for heat transfer between the gases and the solid matrix. Willmott (1969), later compared his intraconduction model to a Schumann type system in which he used a lumped heat transfer coefficient h_0 to relate fluid and mean solid temperatures. He obtained this lumped coefficient from the zero order eigen function of Hausen's (1942) solution, in which Hausen gives h_0 as:

$$\frac{1}{h_0} = \frac{1}{h_c} + \frac{\phi w}{3K} \quad (2.1)$$

where ϕ is given by :

$$\phi = 1 - \frac{1}{15} \left(\frac{1}{F_{oH}} + \frac{1}{F_{oC}} \right) \quad \text{when } \frac{1}{F_{oH}} + \frac{1}{F_{oC}} \leq 5 \quad (2.2)$$

$$\phi = \frac{2.142}{0.3 + 2 \left(\frac{1}{F_{oH}} + \frac{1}{F_{oC}} \right)} \quad \text{when } \frac{1}{F_{oH}} + \frac{1}{F_{oC}} \geq 5 \quad (2.3)$$

where F_o = Fourier number

Despite this theoretical work, Carpenter (1976) concluded that the ranges of applicability of the Schumann (1929) system and the intraconduction model have never been clearly defined. He solved the intraconduction model using finite difference techniques and found it essential to employ the simple model whenever possible, hence a dividing line between the simple and combined mechanism models was produced based upon 1% and 5% maximum error in any heated fluid outlet temperature. This allows a prior estimation of the error associated with using the simple convection model and neglecting intraconduction effects. This technique was used to examine spheres, rods and planar packings. Heggs and Carpenter (1979) also developed an

intraconduction factor which enables the simple interphase convection model with modified parameters to reproduce the rigorous intraconduction model results, giving considerable savings in computer time. The factor they proposed is time dependent and accurately reproduces the true time variation of the fluid temperatures in the intraconduction system.

Willmott (2, 1968) mathematically investigated the requirement of a regenerative system to produce a constant outlet temperature for the preheated gas by means of a by-pass main system. The method developed accommodated the **TIME** dependence of the heat transfer coefficient and the gas and solid specific heats. Just prior to this however, Willmott (1, 1968) used this technique to investigate Cowper stove improvements. Willmott and Burns (1977) later examined the effect of transient response of a thermal regenerator in step changes in either inlet gas temperature or gas rate. They extended (1978) this work examining balanced and unbalanced systems, and then (1980) heat transfer coefficient correlations for thermal regenerators. Razelos and Benjamin (1978) have more recently solved the differential equations which govern the non-linear heat transfer process within regenerators to give a smooth outlet air temperature using a by-pass mechanism, with temperature dependent properties; fluid, solid and heat transfer coefficient.

Using computational studies for both convection and intraconduction effects, Heggs and Carpenter (1978)

examined the effect of packing material (fireclay, alumina and silicon carbide), size (a range of brick sizes) and arrangement on temperature swing. The theoretical treatment of the effects of fluid residence time in the packing voids for rapid switching regenerators, which conventional design does not allow for, was first developed by Thomas (1972). This work was later extended by Willmott and Hinchcliffe (1976) then Heggs and Carpenter (1976).

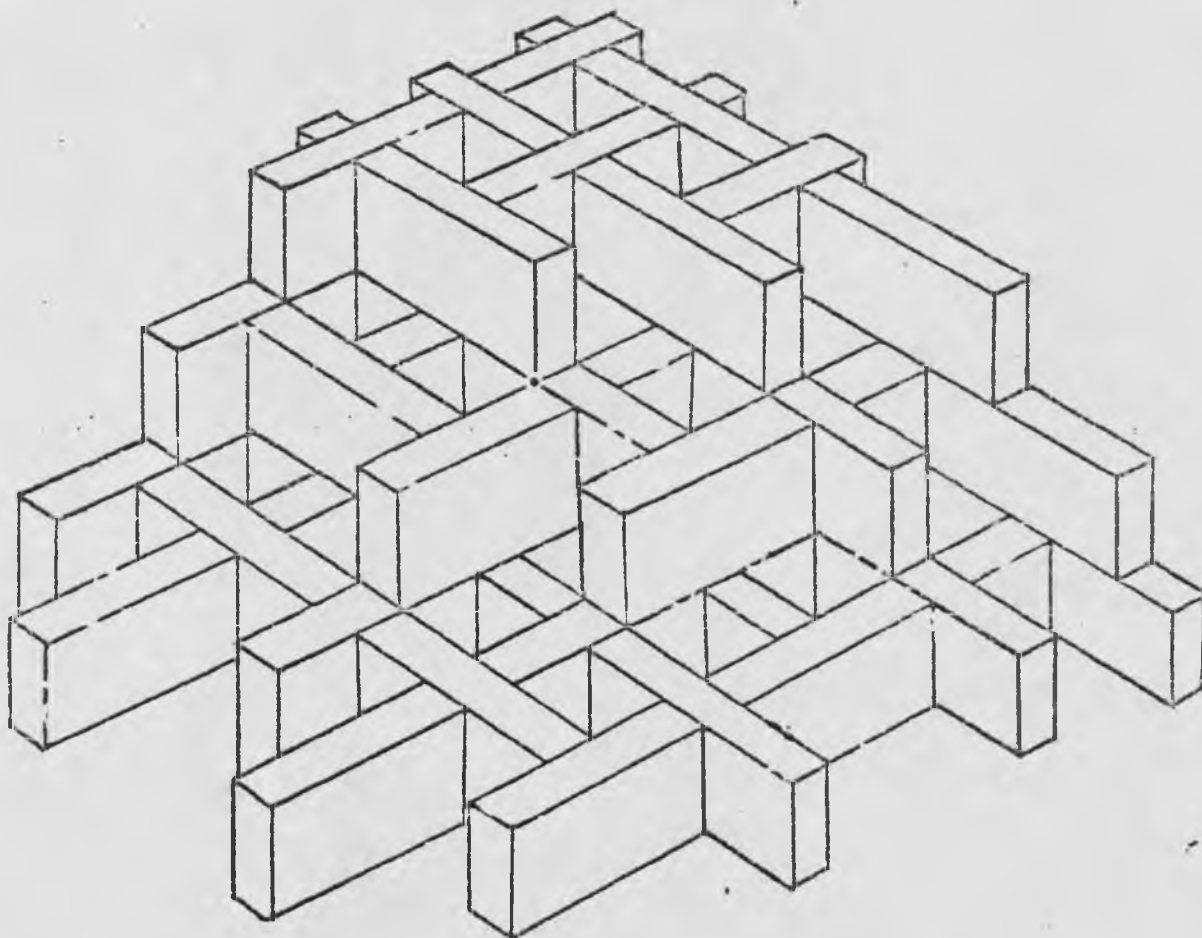
These theoretical representations offer great advantages in the understanding of regenerator design. However, the results of these theories need to be validated on a pilot plant scale of operation prior to industrial application.

2.3 Previous Cyclic Regenerator Experimental Work

Experimental cyclic regenerator investigations have been in two distinct fields, high and low temperature. Most of this work has been concerned with the production of overall heat transfer coefficients. However excessive temperature differences cause large changes in the fluid and solid specific heats as well as the fluid viscosity. Rio and Smith (1967) give an account of the problem of very large variations in the specific heat of metal packings at low temperatures.

The heat transfer correlations that have been produced are only specific to the particular packings or regenerator

FIG 2.1 CLOSED BASKET WEAVE SETTING



characteristics which were examined. Very little attempt has been made to produce a comprehensive method of obtaining heat transfer coefficients for various systems, either for experimental treatment or design purposes.

2.3.1 Experimental Work Above Ambient Temperature

Kistner (1929/30) was one of the first to have studied heat transfer coefficients in regenerator basket weave checker flues. The data was obtained from a pilot plant regenerator. A diagram of a closed basket weave set up is shown in Fig. 2.1. However, he encountered great difficulties in measuring both flowrates and temperatures, whilst Böhm (1932/33) did not, because he used a single horizontal brick lined square flue. Böhm produced a laminar and turbulent heat transfer coefficient for various degrees of roughness and widths of packing.

Elukhin and Storavijskii (1964) obtained the following equation using twin bed regenerators :

$$Nu = 0.3 Re^{0.8} P_v^{0.75} \quad (2.4)$$

for various types of packing such as Lump basalt (3.5, 6.5 and 10.5 mm diameter), aluminium spiral rings (6.1 x 6.6 x 1.5 mm diameter), shavings of carbon and stainless steel, copper raschig rings (10. x 10 x 0.5 mm) and steel balls (8.7 mm diameter). Ridgion and Kerrison (1964), using two pilot plant Cowper stoves obtained heat transfer coefficient data for Freyn checkers. The runs were under full automatic control until equilibrium was reached. The convective heat transfer coefficient was then obtained using

a form of the Tipler (1947) equation, derived by Willmott (1963).

$$\lambda \text{ reduced length} = \frac{\log \left(\frac{1+x'}{1-x'} \right)}{v - \frac{1}{2} \log \left(\frac{1+x'}{1-x'} \right)} \quad (2.5)$$

$$\text{where : } \lambda = \text{reduced length} = \frac{h.A}{W.C_s}$$

$$v = \text{utilisation factor} = \frac{W.C_g.P}{M.C_s}$$

$$x' = v.\eta$$

However this solution contains Tipler's inbuilt assumption of linear solid temperature profiles. The form of the results was a linear plot of log surface heat transfer coefficient versus log air flowrate. Stacey (1970) recently built a novel cylindrical regenerator, and obtained heat transfer coefficients from an overall heat balance. The temperature rise was 1000°C across the regenerator and the superficial gas mass velocity varied due to radial flow.

2.3.2 Experimental Cryogenic Work

The study of cryogenic regenerators has led to extensive experimental work, such as Bretherton's (1970) proposal of lumped heat transfer coefficients calculated by a modified Tipler (1947) equation which correlates any deviations from Schumann's (1929) simplifying assumptions. However there was considerable scattering of results.

Granville et al (1966) have shown for small regenerators how the reduced length may be modified to account for the effects of heat storage in the regenerator walls. Gifford et al (1968) and Ackerman and Gifford (1969) have also shown the differences in performance of small regenerators with stainless steel and phenolic walls.

Lund and Dodge (1948) obtained overall heat transfer coefficients and friction factors for air flowing through Frankl regenerator packings using a pilot plant scale apparatus, at temperatures and pressures encountered in actual air separation plants. The effects of variables such as reversal time, inlet temperature, inlet humidity, flowrate, packing geometry and the ratio of length to diameter on the heat transfer coefficient were studied.

However the design of regenerators has been successfully undertaken without the necessary practical verification of the theory and the inadequacy of the heat transfer coefficient data.

2.4 Cyclic Regenerator Design Methods

The earliest solutions to models of cyclic regenerator operation are those of Nusselt (1928) and Hausen (1929), being well reported by Jakob (1957). Hausen (1929) essentially adopted the same approach and assumptions as Schumann (1929), though independently. He showed that under these assumptions the performance of a regenerator is a function of two

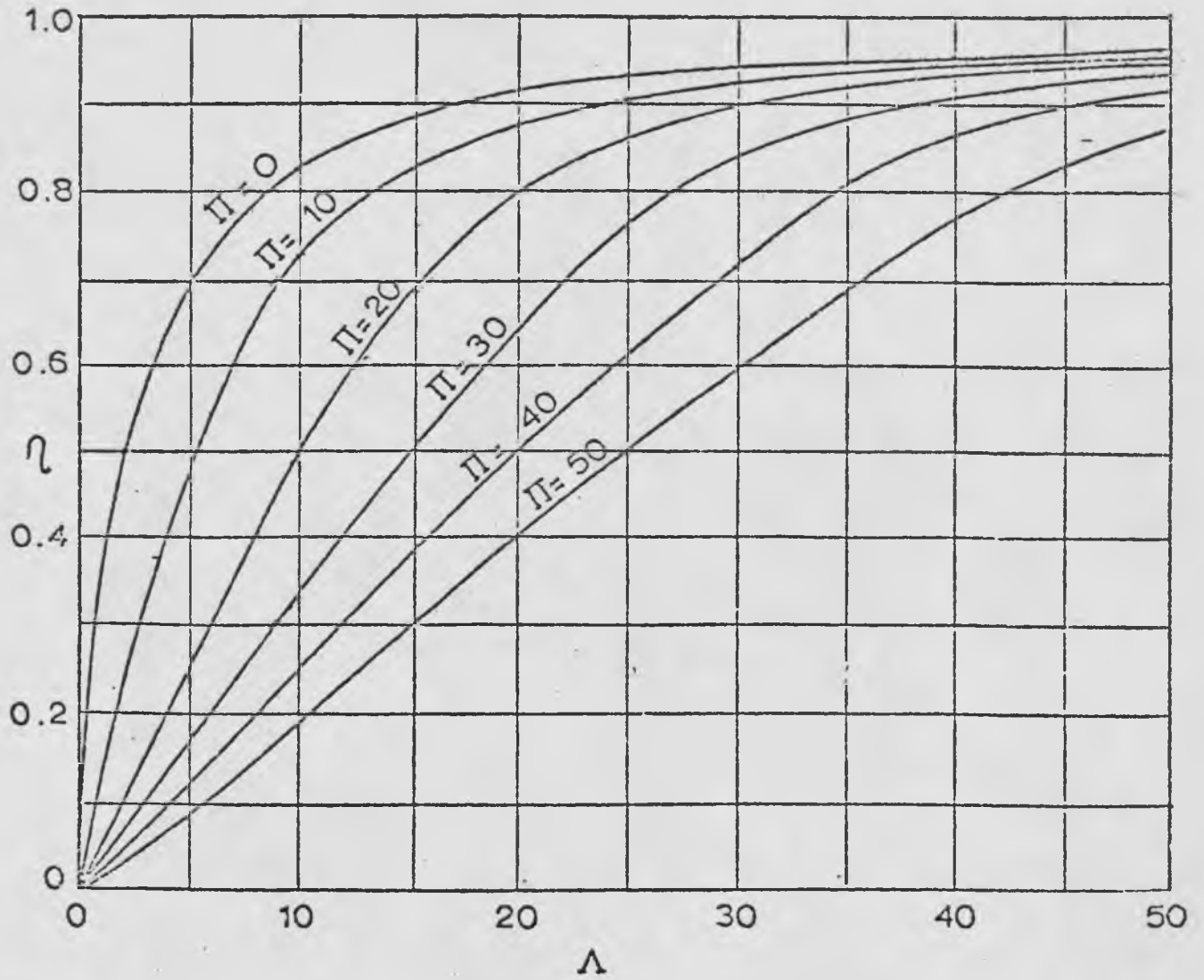
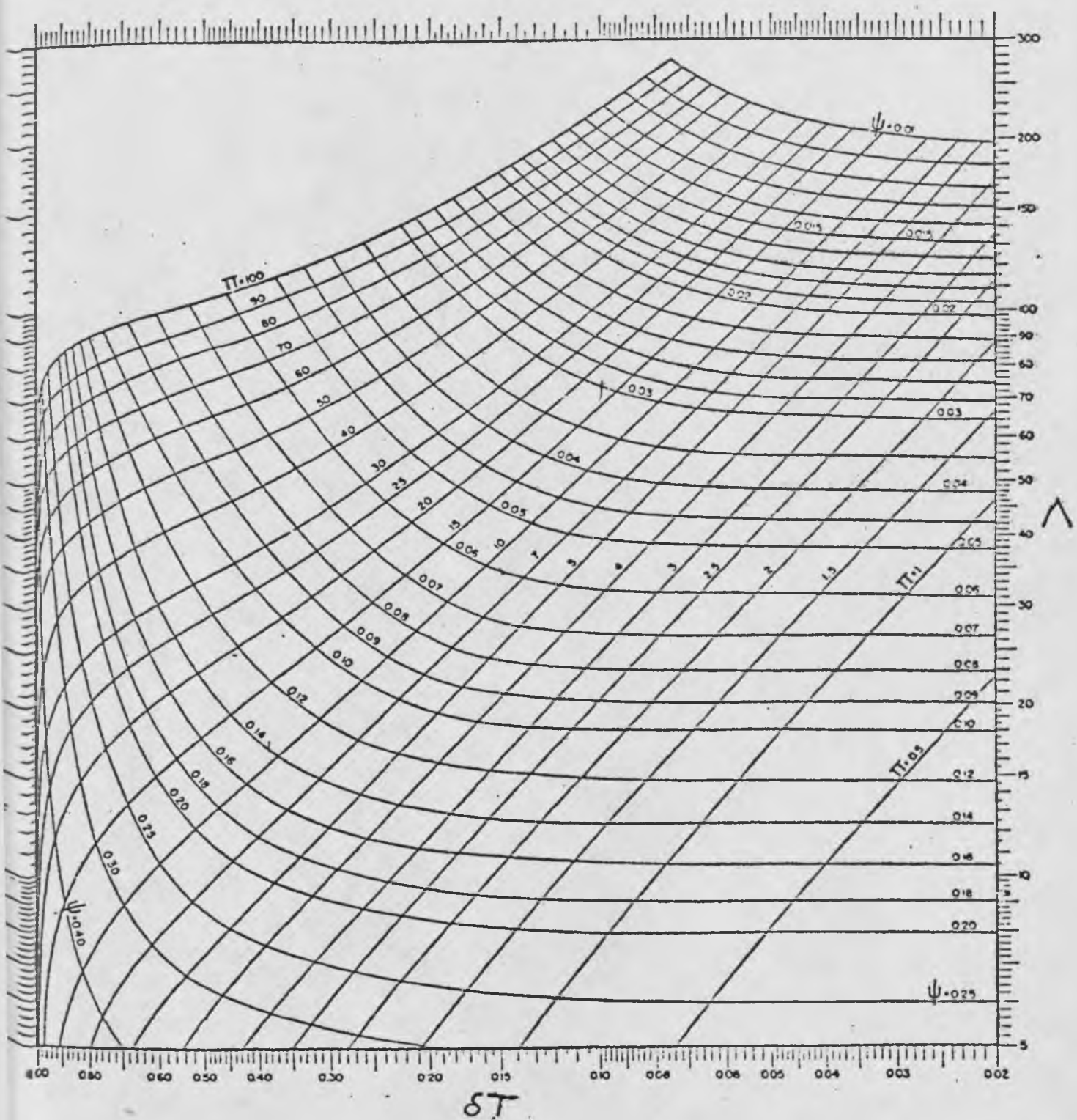
FIG 2-2 HAUSEN'S EFFECTIVENESS CHART

FIG 2-3 PEISER AND LEHNER'S DESIGN CHART FOR SYMMETRIC REGENERATORS



δT
DIMENSIONLESS EXIT TEMPERATURE SWING

$\psi = 1 - \eta = \text{INNEFFICIENCY}$

parameters. These are dimensionless length Λ and the dimensionless period Π , which are defined as follows :

$$\Lambda = \frac{h.A.L}{G.Cg} \quad (2.6)$$

$$\Pi = \frac{h.A.P}{\rho_s C_s} \quad (2.7)$$

Figure 2.2 shows Hausen's (1929) design chart which gives the effectiveness (η) in terms of these parameters. His charts cover a limited range and are restricted to balanced regenerators, although for unbalanced cases he recommends the use of 'harmonic mean' parameters, for example

$$\frac{1}{\Lambda} = \frac{1}{2} \left(\frac{1}{\Lambda_H} + \frac{1}{\Lambda_C} \right) \quad (2.8)$$

and
$$\frac{1}{\Pi} = \frac{1}{2} \left(\frac{1}{\Pi_H} + \frac{1}{\Pi_C} \right) \quad (2.9)$$

Later, Hausen (1931) developed a more approximate method called the 'Heat pole method', as reported by Jakob (1957).

Peiser and Lehner (1953) seemingly unaware of Hausen's work produced a design chart using Schumann type assumptions, Fig. 2.3, which as well as including dimensionless time and length (of much larger range than Hausen's), and efficiency, also included dimensionless temperature swing for 'symmetric' regenerative systems.

Recently Heggs et al (1980) have theoretically examined symmetrical regenerators for spherical, cylindrical and planar packings. Intraconduction effects have been considered and design charts have been obtained of log inefficiency ($1 - \eta$) against log dimensionless temperature

swing for Λ and Π , and various values of Biot number. Kay's and London (1964) produced cyclic and fixed bed regenerator design charts with effectiveness a function of the number of transfer units, heat capacity of the bed and the matrix capacity rate when considering cyclic regenerators. The information required was provided by Lambertson (1958) and Bahnke and Howard (1964) who used computer techniques to solve the complex mathematical equations.

Hlinka et al (1961) produced a Manual for thermal design of open hearth regenerators. Paschkis and Razelos (1966) extended Hlinka's work to establish a similar procedure for the design of blast furnace stoves. Larsen (1967) obtained by a single hand calculation method fluid and solid temperatures at any time and location in a regenerative heat exchanger. Schofield et al (1961) gave a good report of applying Hausens (1939) procedure to Cowper stove design and Butterfield et al (1963) have refined this approach to include non uniformities in thermal constants and fluid flowrates. Holmes et al (1964) briefly compared these methods. They suggest the original approach as adequate for normal Cowper stove design purposes, whilst the refined analysis may be used when extrapolations are to be made in unusual areas of operation.

Even the earliest simple regenerator solutions were very complex and only provided an estimate of the

effectiveness. This situation led to the development of less rigorous, but less accurate solutions to regenerator problems. Indeed in many cases the birth of the approximate technique advanced the practical investigation of regenerators, because of the simplicity of data treatment, in particular the production of overall convective heat transfer coefficients.

2.5 Approximate Solutions

The initial work in this field is that of Lubbock and Bowen (1946) which was refined by Tipler (1947). He found that provided $\Pi \ll 10$, the maximum error in effectiveness is of the order of 4%. This being mainly due to his assumption of linear solid temperature profiles. His equation for the effectiveness of a balanced countercurrent regenerator is :

$$\eta = \frac{\Lambda}{\Pi} \tanh \left(\frac{\Pi}{2 + \Lambda} \right) \quad (2.10)$$

A feature common to all approximate solutions is that as $\Pi \rightarrow 0$, with equal Λ per period the effectiveness is given by :

$$\eta = \frac{\Lambda}{\Lambda + 2} \quad (2.11)$$

which is equivalent to the expression for countercurrent recuperator effectiveness, as given by Kays and London (1964). This relationship between regenerator and recuperator analogy is the basis for many design methods and is well reported by Carpenter (1976).

In all these methods it is necessary to have heat transfer coefficient data. Much of the data has been obtained, not from cyclic regenerator experiments, but from single blow regenerator investigations.

2.6 Single Blow Techniques

The investigations in this area have been reviewed by Barker (1965), Price (1964), Heggs (1967) and Main (1978). The spread of results illustrated by these reviews is considerable despite similar experimental techniques. These discrepancies are due mainly to the different experimental methods employed and the various mathematical models used to interpret the experimental data.

Main (1978) categories single shot experimental investigations into 3 parts: transient response, steady state and heat and mass transfer analogy. The easiest, and hence most used technique is that of transient response. A change is introduced into the inlet fluid temperature to the packed bed, and the variation of outlet fluid temperature is measured and used by various analyses to evaluate the fluid to particle heat transfer coefficient within the bed. However, the ultimate accuracy of this parameter depends on the closeness of the assumptions incorporated in the analysis and those pertaining to the experimental conditions.

The dynamics of heat transfer in fluid flow through a packed bed indicate a linear behaviour. Therefore the type of change in the inlet fluid temperature is arbitrary as long as it is accurate and well defined. Experimental investigations have used a number of forms: step, Price (1964) and Heggs (1967), exponential, Coombs (1970), ramp, Bradshaw et al (1970), sinusoidal, Gunn and De Souza (1974) and square wave, Absjornsen and Wang (1971). The easiest and quickest method experimentally is the step technique, which is the only method found for experimental determination of cyclic regenerator heat transfer coefficients.

Schumann (1929) as described earlier, derived with various simplifying assumptions an analytical solution for the outlet fluid temperature in response to a step change in inlet fluid temperature. Following this solution many experimental investigations were carried out to obtain heat transfer coefficient data for packings of varying materials shapes and sizes, as reviewed by Barker (1965). Early techniques utilised curve matching of the theoretical and experimental breakthrough curves to determine the heat transfer coefficients. Price (1964) developed a numerical solution to Schumann's (1929) model and incorporated it into an iterative computer to calculate heat transfer coefficients. Heggs (1967) and Main (1978) used and extended this solution in their investigations.

However, many single shot investigations have been concerned in the area where particles are non isothermal

and intraparticle conduction is important. This is not accounted for in Schumann's (1929) solution. Heggs (1967) from his theoretical studies and experimental results on lead, phosphor bronze and steel spheres, lead and soda glass ballotini proposed the criterion, $\Lambda_{Bi} < 60$ for the importance of intraconduction. Heggs, also studied Hasche tile configurations (1970) and parallel plate systems (1969) for which he deduces the criteria $\Lambda/Bi < 60$ and $\Lambda/Bi < 80$, respectively. Coombs (1970) concluded from a parametric investigation of cross-inclined tube bundles that $\Lambda^2/Bi < 100$.

In particulate packings, axial conduction is negligible except at very low Reynolds numbers, Main (1976) quotes < 2 . However when the bed consists of plates set parallel to the fluid flow then these effects become important. Heggs (1967) from experiments with aluminium plates, proposed that longitudinal conduction should be accounted for when $\Lambda K_1 < 0.1$ and $\Lambda > 4$.

Recent attention into heat transfer measurements in packed beds has involved investigation of axial fluid dispersion. This subject has been comprehensively reviewed by Main (1978).

Main proposes from his experimental and theoretical work that Pe_L (Peclet number) is the optimum parameter in the difference between the single Schumann model and the more complex axial dispersion model. If $Pe_L > 400$ the simple model can be used with only small error, but if $Pe_L < 400$

axial dispersion should be taken into account. Main defines Pe_L as $L/w * Ped$ and for $Re \gg 10$, $Ped = 2$, then for $Re \gg 10$ L/w must be above 200 in order that axial dispersion may be ignored. Main also describes that in his practical investigations L/w does not exceed 70 and therefore axial dispersion is important and does affect all heat transfer coefficients obtained.

The effect of the wall heat capacity of a packed bed and the amount of radial heat loss from the bed have not been dealt with by many workers, even at temperatures markedly different from ambient. Many experimental investigators have simply used low thermal conductivity test sections or internal insulation with varying amounts of external insulation. Saunders and Ford (1940) measured the temperature of the test section wall and applied natural convection correlations to measure heat loss. This method was used by Coombs (1970) in his experimental investigations to measure the heat transfer characteristics of cross-inclined tube bundles. Main (1978) concluded from his theoretical and experimental investigations that wall heat capacity effects may be assumed negligible for the following ranges :

$$Aw \leq 0.001 \text{ for } Az \geq 0.001 \quad (2.12)$$

$$Aw = 0.001 \text{ for } Az \geq 0.1 \quad (2.13)$$

$$Aw = 0.01 \text{ for } Az \geq 10.0 \quad (2.14)$$

where Aw = ratio of the heat transfer resistance to the packing and the wall.

A_z = ratio of packing heat capacity to that of the wall times A_w .

Single shot methods of representing heat transfer coefficients for packed beds are usually of the form

$$J_h = f_n(Re) \quad (2.15)$$

No account is taken of bed voidage or particle shape.

However Gupta and Thodos (1963) proposed

$$J_h \cdot P_v = f_n(Re) \quad (2.16)$$

to correlate fluid to particle heat transfer. Price (1964) adapted this expression plotting $J_h \cdot Re \cdot P_v$ versus Re in a linear manner and was later used by Main (1978), highlighting surface roughness effects. Heggs (1967) was concerned with comparing regenerator packings, and found that the most suitable means of comparison was of the form $(J_h \cdot P_v / f_v)$ plotted against $(Re \cdot m)$ where f_v is a friction factor and m the hydraulic mean radius.

Where cyclic regenerator heat transfer coefficient data is not available for design single shot correlations are used, as in this work. However the single shot data does not take into account the periods of switching and subsequent finite times of heat soakage and disruption experienced by the packing, due to the cyclic nature of the regenerator. Carpenter (1976) has also shown that intraconduction effects vary according to (τ) , due to the available time for heat

soakage, whereas single shot correlators assume constant intraconduction properties with time.

Advancement in the single shot area has become widespread because this mode of operation is easier to model theoretically and the experimental apparatus is easier to design, construct and operate, over a cyclic system.

2.7 Pilot Plant Applications

It is clear that more experimental work has been undertaken in the single shot field than the cyclic field. From the above therefore, there is a great need to examine practically the theoretical cyclic advancements and also compare this with the single shot theoretical and experimental work, which has accelerated much faster. This situation could be due to the complexity of the boundary conditions imposed by the nature of the cyclic arrangement which could not be investigated until the advent of digital computers using numerical techniques to solve the mathematics.

A pilot plant apparatus using normal analog methods, but enhanced greatly by computer control and temperature and flowrate logging techniques is now available to experimentally examine more thoroughly the cyclic theoretical models.

Chapter 3

Design of a Regenerative Apparatus

3.1 Introduction

Regenerators have existed in various forms for many years and were initially designed using many simplifying assumptions, as discussed earlier in Chapter 1.

However more recently, as shown by Carpenter (1976), with the advent of digital computers a thorough theoretical analysis of regenerator designs and operation is possible. He examined in detail such effects as surface heat transfer data, intraconduction and axial conduction in the packing material, axial dispersion in the fluid phase and zones of different packing shape size and material. For these various design criteria to be valid on an industrial scale they must primarily be examined using a pilot plant apparatus embracing as many of the theoretical assumptions as possible. These theoretical advances once proven on a pilot plant apparatus can then be used with confidence in the design of industrial regenerators.

3.2 Conceptual Regenerator Design

3.2.1 Apparatus to Operate at Ambient Temperature

As discussed earlier in chapter 2, previous cyclic regenerator experimentation was carried out over large

temperature ranges from ambient, either down to cryogenic or up to high temperatures. These excessive temperature differences have a significant effect upon the solid and fluid specific heats, as well as the fluid viscosity. However, these properties are assumed constant in many design methods as well as in most computer simulations. The apparatus will therefore operate at ambient conditions with at most a 10°C temperature difference between hot and cold fluids to avoid physical property variation.

3.2.2 Mode of Operation

Again as discussed in chapter 1, two types of industrial regenerator exist, fixed bed and rotary. A fixed bed arrangement was chosen in preference to a rotary type, because of ease of changing the regenerator geometry and with a rotary system fluid carry over is possible.

3.2.3 Single Horizontal Fixed Bed

Industrial fixed bed systems comprise two or more matrices, such as in the Linde Frankl production of oxygen as reported by Ruheman (1940), where two regenerators are used, and in the production of hot air for blast furnaces by a combination of usually three Cowper stoves as reported by Petit (1964). A two bed four valve switching arrangement is shown in Fig. 1.1. In order to obtain a completely balanced system, ie. where $\Lambda_H = \Lambda_C$ and $\Pi_H = \Pi_C$, as is assumed in

many theoretical modelling investigations, only one test bed is used. For the same fluid flow rate and for identical hot and cold strokes this arrangement inherently provides a balanced system. The regenerator test bed will be horizontal for ease of access with the capability of housing various packing lengths.

3.2.4 Process Fluid

The process fluid used is air, supplied by a Broom and Wade compressor capable of delivering up to $6.29 \times 10^{-2} \text{ m}^3/\text{s}$. The air properties may be assumed constant with very little water vapour and carbon dioxide present. However Price (1964) previously discovered that the air temperature leaving the compressor drifts markedly, which is inadequate when considering constant temperature inputs used in theoretical design criteria. The air flowrate through the apparatus is obtained by measuring the pressure drop across a sharp edged orifice plate with one inch taps, as proposed by Spink (1961).

3.2.5 Initial Regenerator Conception

An experimental apparatus which fulfills the requirements mentioned earlier must include a single fixed bed regenerative system operating at around ambient temperature, a switching arrangement to direct a single flow of air in either direction through the regenerator, a front end section to produce a smooth air inlet temperature into the apparatus, a means of

increasing the air temperature at one entrance to the regenerator and a method by which the air flowrate through the apparatus can be measured accurately.

3.3 Cyclic Regenerator Design

3.3.1 Regenerator Matrix Housing

With the pilot plant scale operation it became necessary to design a metallic test section which can accommodate packings similar to those used in industrial applications. Heggs (1967) investigated spheres, cylinders, Raschig rings, Lessing rings and various orientations of plate packings using a 76.2mm inside diameter cylindrical copper test section. The 76.2mm inside diameter copper test section used in this work is adequate for the 6.35mm ($\frac{1}{4}$ inch) particulate packings investigated.

3.3.2 Regenerator Bed Design

Mathematical treatment of fixed bed cyclic regenerators using Schumann (1929) assumptions predicts that effectiveness (η) is a function of (Π_H , Π_C , Λ_H and Λ_C). Carpenter (1976) concluded that most industrial regenerators have dimensionless lengths in the range $1 \leq \Lambda \leq 20$. The most comprehensive set of overall heat transfer coefficient data for various packing geometries was obtained from Heggs (1967) work, who used a single blow technique to obtain the following correlations, shown in table 3.1.

Table 3.1Heggs (1967) Packed Bed Correlations

1.	Steel spheres Re 100 → 4,500	$Jh * Re * Pv = 0.255 Re^{0.665}$
2.	Lead spheres 9mm Re 100 → 4,500	$Jh * Pv = 0.255 Rem^{-0.332}$
3.	Bronze 0.375" spheres Re 100 → 4,500	$Jh * Pv = 0.255 Rem^{-0.332}$
4.	Stainless Steel Cylinders D = 0.25" $\frac{1}{4}$ " x $\frac{1}{4}$ " Re = 100 → 2,000	$Jh * Pv = 0.129 Rem^{-0.271}$
5.	Porcelain Rings D = 0.09" $\frac{1}{4}$ " x $\frac{1}{4}$ " Re = 100 → 2000	$Jh * Pv = 0.291 Rem^{-0.348}$
6.	Aluminium Plates D = 0.37" Ax = 0.104 ft ² Re = 1000 → 4,000	$Jh * Pv = 0.448 Rem^{-0.357}$
7.	Aluminium Plates D = 0.35" Ax = 0.234 ft ² Re = 1000 → 4,000	$Jh * Pv = 0.317 Rem^{-0.347}$
8.	Aluminium Plates D = 0.4" Ax = 0.052 ft ² Re = 1000 → 4,000	$JhPv = 0.532 Rem^{-0.372}$

Where:- $Jh = StPr^{2/3}$

$$St = \frac{h}{G C_g} \quad Pr = \frac{\mu C_g}{K} \quad Rem = \frac{4.G.m}{Pv}$$

$$m = \frac{PvD}{6(1-Pv)}$$

FIG 3-1

GRAPH OF SUPERFICIAL GAS MASS
VELOCITY (G) VS LAMBDA (Λ) FOR
VARIOUS PACKED BED LENGTHS (L)
OF 635mm DIAMETER SPHERES

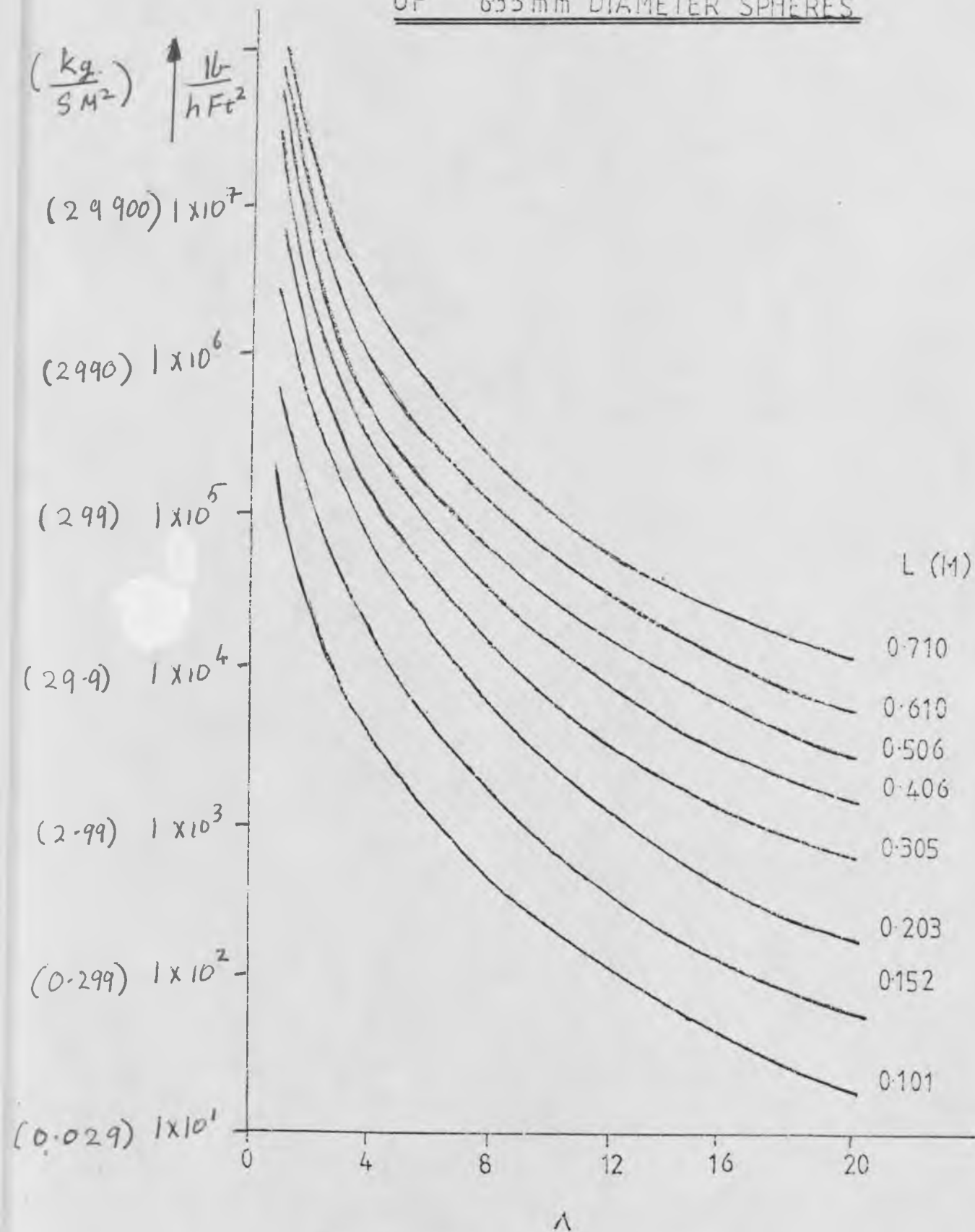
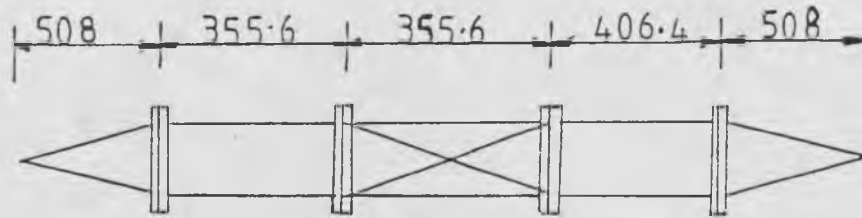


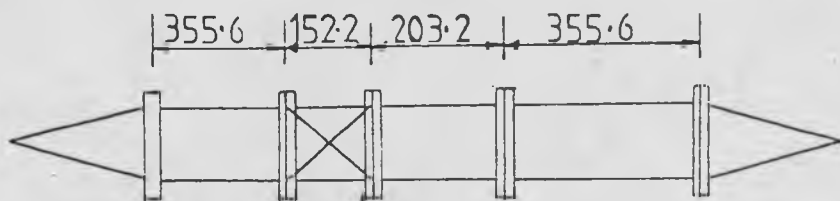
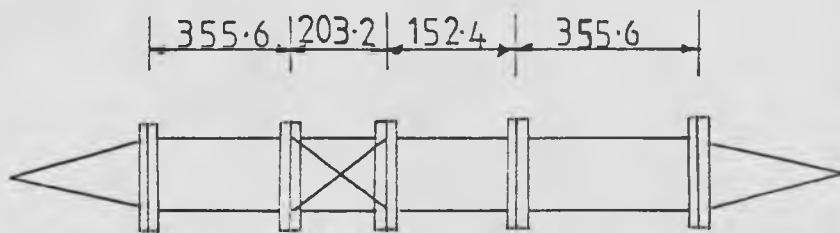
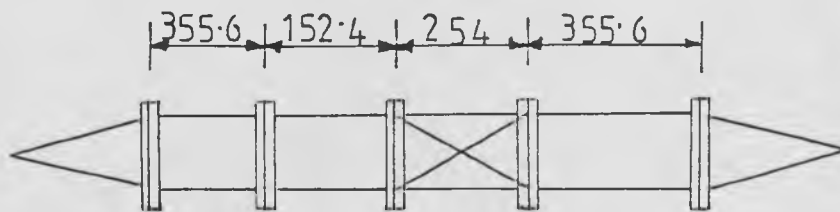
FIG 3-2

VARIOUS TEST BED LENGTHS FOR
A PACKED BED SECTION UP TO 355.6mm



ALL DIMENSIONS: mm

NO TO SCALE



TOTAL LENGTH WITHOUT
 TUFNOL HOUSING = 1117.6

In order to produce a thorough regenerator test bed length design, numerous graphs of superficial gas mass velocity (G) versus dimensionless length (Λ) for various bed lengths (L), were analysed for the correlations shown in table 3.1. All the correlations give a nest of curves similar to those for spheres, shown in Fig. 3.1. Analysis of the 0.4 inch (10.16mm) alumina plates produced a maximum bed length of 3 feet (914.4mm), however as shown in Fig. 3.1, for a dimensionless length (Λ) range of 0-20 for spheres the bed length required is less than 3 feet (914.4mm), so the bed matrix is designed to comprise varying length sections down to 76.2mm (3 inch). The arrangement of the test bed to obtain matrix lengths from 355.6 to 152.2mm is shown in Fig. 3.2.

Carpenter (1976) suggests that the range of dimensionless period should be $1 \leq \Pi \leq 10$. This range has been adequately catered for by analysing the particulate packings to be considered and producing real time periods in the range 1 (1) 99 minutes for manual timing and 1 (1) ∞ seconds using computer timing.

3.3.3 Regenerator Test Bed Characteristics

Wall heat capacity effects for single blow and cyclic operation have been studied by Main (1978) and Granville (1966) respectively, showing how this can affect the overall heat transfer coefficient of the system. Due to design

restriction many previous experimental workers have had to suffer a considerable wall heat capacity effect, which theoretical design does not allow for, by using large wall sections of mild or stainless steel. Internal insulation using 1mm Triton Kaowool is used to reduce this effect, produced not only by the $\frac{1}{16}$ " (4.233mm) copper tube section, but by the $2\frac{1}{2}$ " (63.5mm) mild steel table 'E' flanges used for test section coupling.

The internal insulation also reduces the excess voidage produced at the tube wall by the $\frac{1}{4}$ inch (6.35mm) and $\frac{1}{2}$ inch (12.7mm) particulate packings. In addition, heat loss from the apparatus is also reduced by external $\frac{3}{4}$ inch (19.05mm) polyurathane insulation and working just above ambient temperature.

3.3.4 Imbalanced Systems

Many existing industrial applications are imbalanced, mainly due to different fluid flows in each stroke and the unequal switching times when more than two fixed beds are employed in a regenerator system. To this end the apparatus has been designed to produce dissimilar dimensionless periods by making $P_H \neq P_C$ and dissimilar dimensionless lengths by reducing the flowrate through the apparatus at a given stroke, so $\Lambda_H \neq \Lambda_C$.

3.3.5 Regenerator Switching

Mathematical representation of regenerative systems assume instantaneous stream switching. This feature can never be totally achieved. However, using Dewrance Asco 24 V.D.C. solenoid valves with a maximum opening time of 24 milli-seconds coupled with electronic or computer timing and 'continental series' relay interfacing, rapid switching is possible.

Exploiting the speed with which these valves actuate and the capability of the computer timing to produce one second periods, fluid hold up may be examined as reported by Carpenter (1976). However this type of system would require an almost instantaneous heat source and temperature measurement capability.

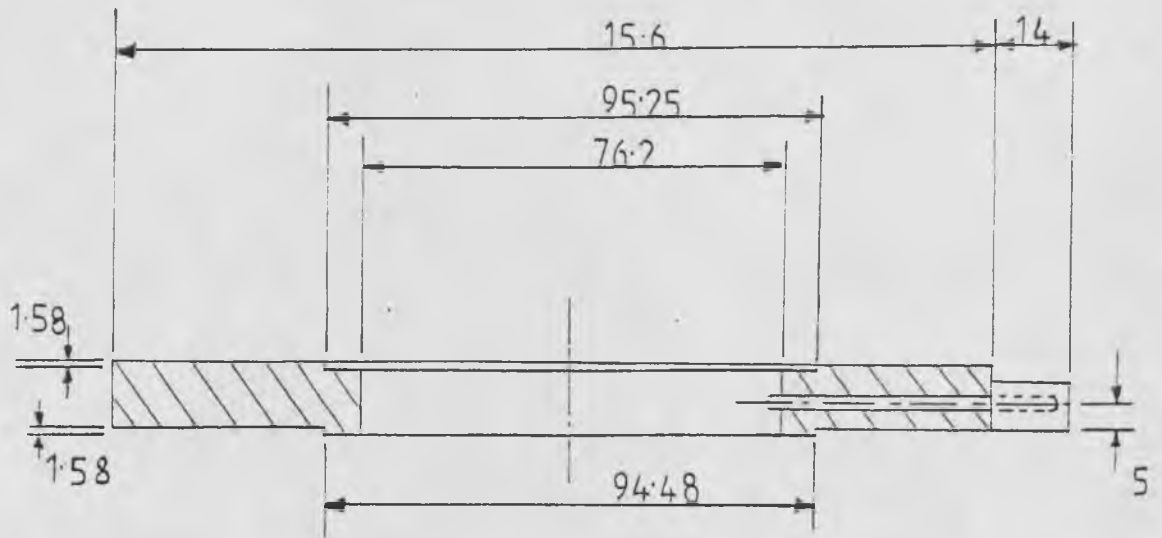
3.3.6 Heater Design

For rapid heat input two distinct design problems are encountered. The production of power to provide a step temperature input and the correct type of heater appliance unit.

The power is supplied by a 'crane motor' control unit (Heenen 180/6) capable of delivering 1080 watts of stabilized voltage and capable of actuation by a relay. The heater element is constructed of $\frac{1}{2}$ inch (12.7mm) Tufnol Carp sheet and incorporates a male female rebate. This assists location

FIG 3-3

TUFNOL HOUSING FOR HEATER AND
RESISTANCE THERMOMETER ELEMENTS



SECTION AA

TUFNOL HOUSING

ALL DIMENSIONS: mm
 SCALE: FULL SIZE

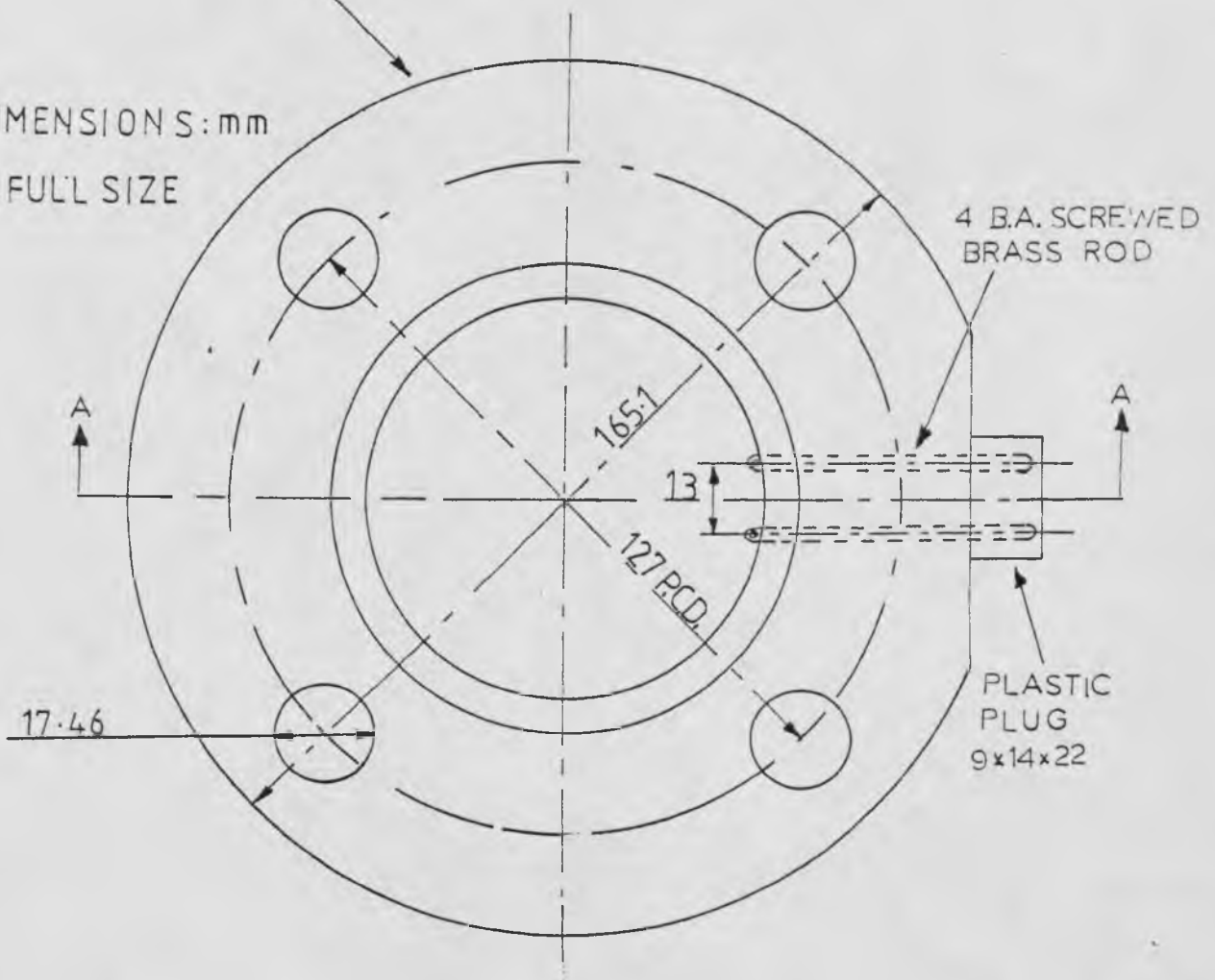
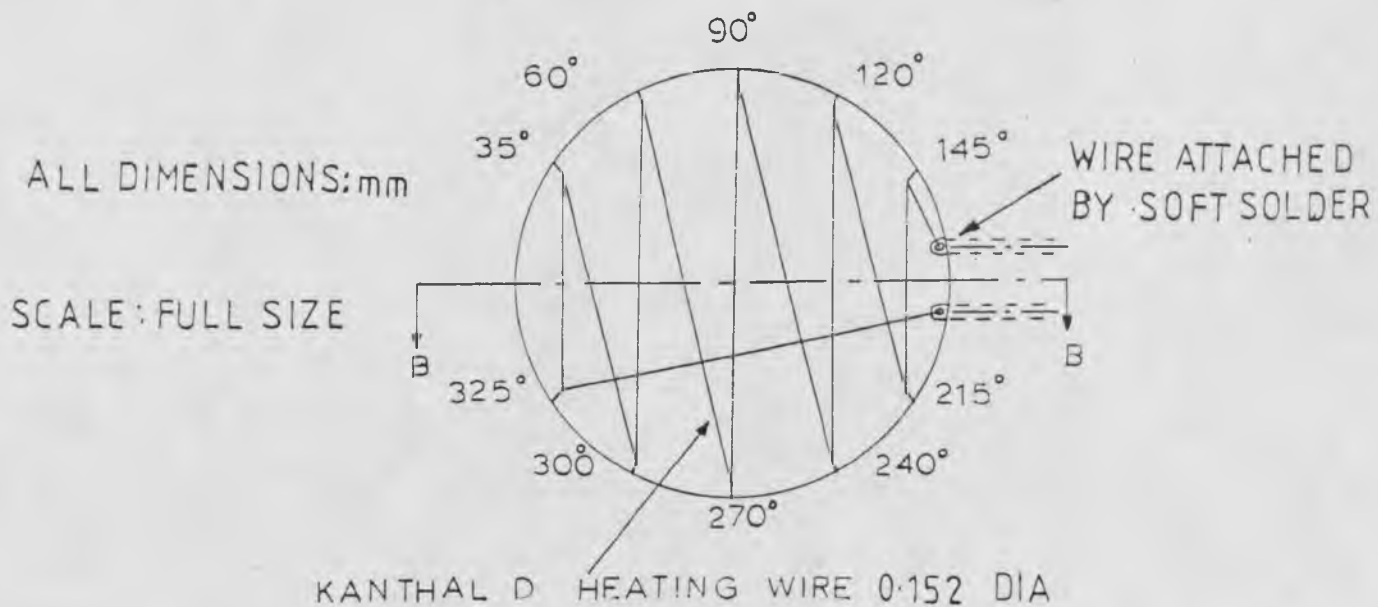
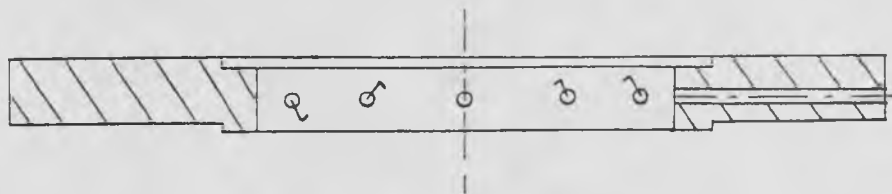


FIG 3.4

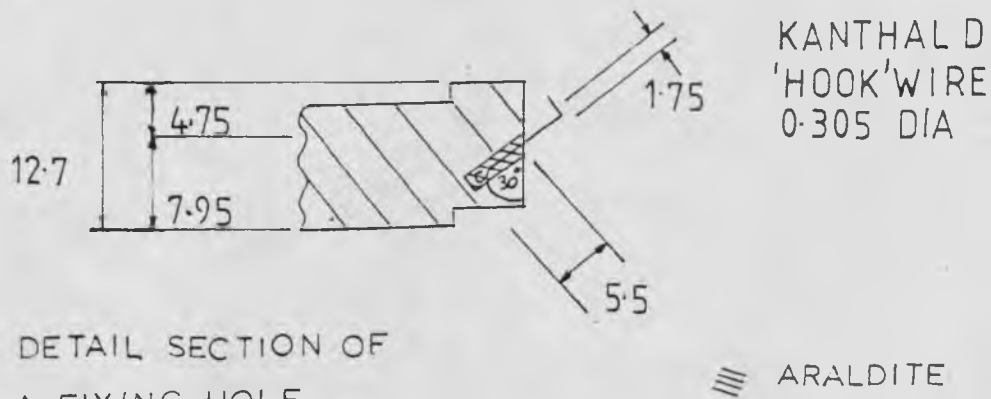
DETAIL OF HEATER WIRE POSITIONING



TUFNOL HOUSING (SEE FIG 3.3)
10 HOOKS PROTRUDING



SECTION BB



DETAIL SECTION OF
A FIXING HOLE
SCALE: TWICE FULL SIZE

into the horizontal bed and also allows 76.2mm inside diameter x 87.3mm outside diameter x 1.58mm thick rubber seals to be placed between the male and female union providing an adequate seal. Contact is made with the 0.006 inch (0.152mm) diameter Kanthal D heater wire of approximately 300mm length by two, 4 B.A. brass rods as can be seen in Fig. 3.3. The heater wire is contacted to the brass rods by soft solder.

The positioning of the heater wire is shown in Fig. 3.4 being held taught in position by Kanthal D 0.012 inch (0.305mm) hooks which are araldited into the Tufnol Carp. This heater element design allows rapid response for a step heat input. (The heater wire time constant is 8.9 milli-seconds at $2000 \text{ ft}^3/\text{h}$ ($0.016 \text{ m}^3/\text{s}$)). The heat distribution is over a wide cross-sectional area of flow, whilst the flowrate impedance is reduced to a minimum.

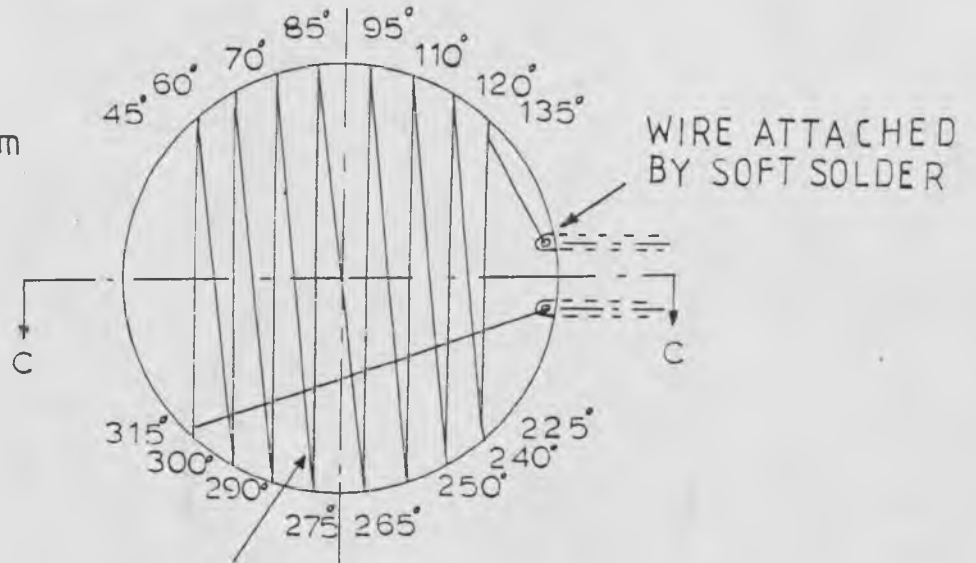
3.3.7 Temperature Indication

Considerable attention was focused on the method of indicating the air temperature. The temperature sensing element would have to fit into the horizontal bed, be of rapid response, impede the flowrate as little as possible and provide a representative air temperature over the whole test bed cross-sectional area. A resistance thermometer element is used similar to those designed by Price (1964) and Coombs (1970), which fulfills the design criterion.

FIG 3-5

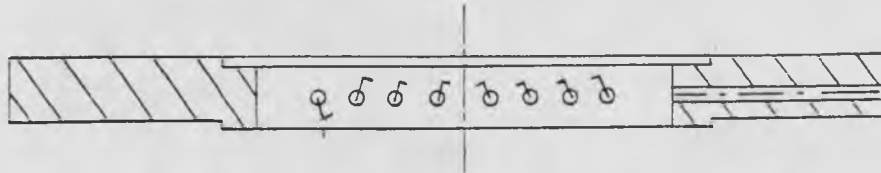
DETAIL OF RESISTANCE WIRE POSITIONING

ALL DIMENSIONS mm
SCALE FULL SIZE



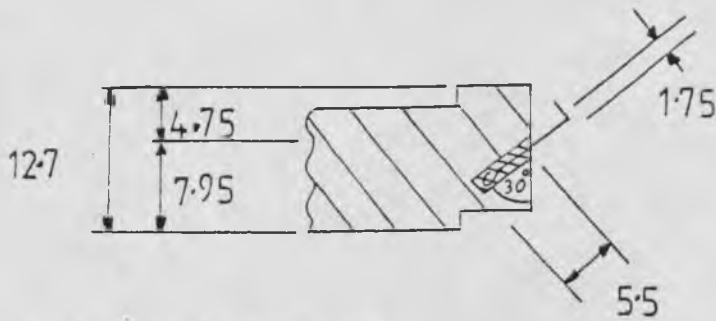
RESISTANCE WIRE
99.99% PLATINUM 0.0254 DIA

TUFNOL HOUSING (SEE FIG 3-3)
16 HOOKS PROTRUDING



SECTION CC

KANTHAL D
HOOK WIRE
0.305 DIA

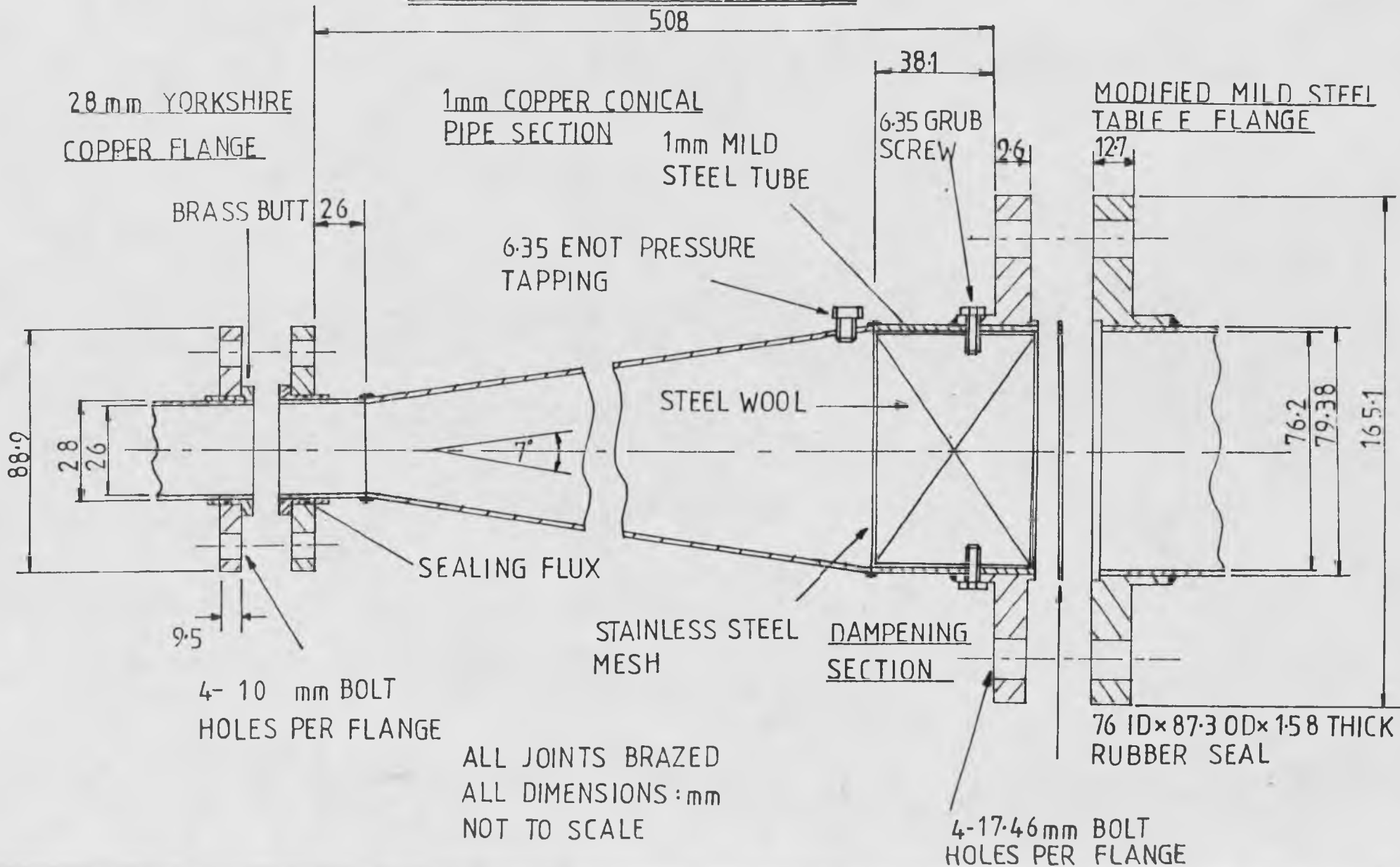


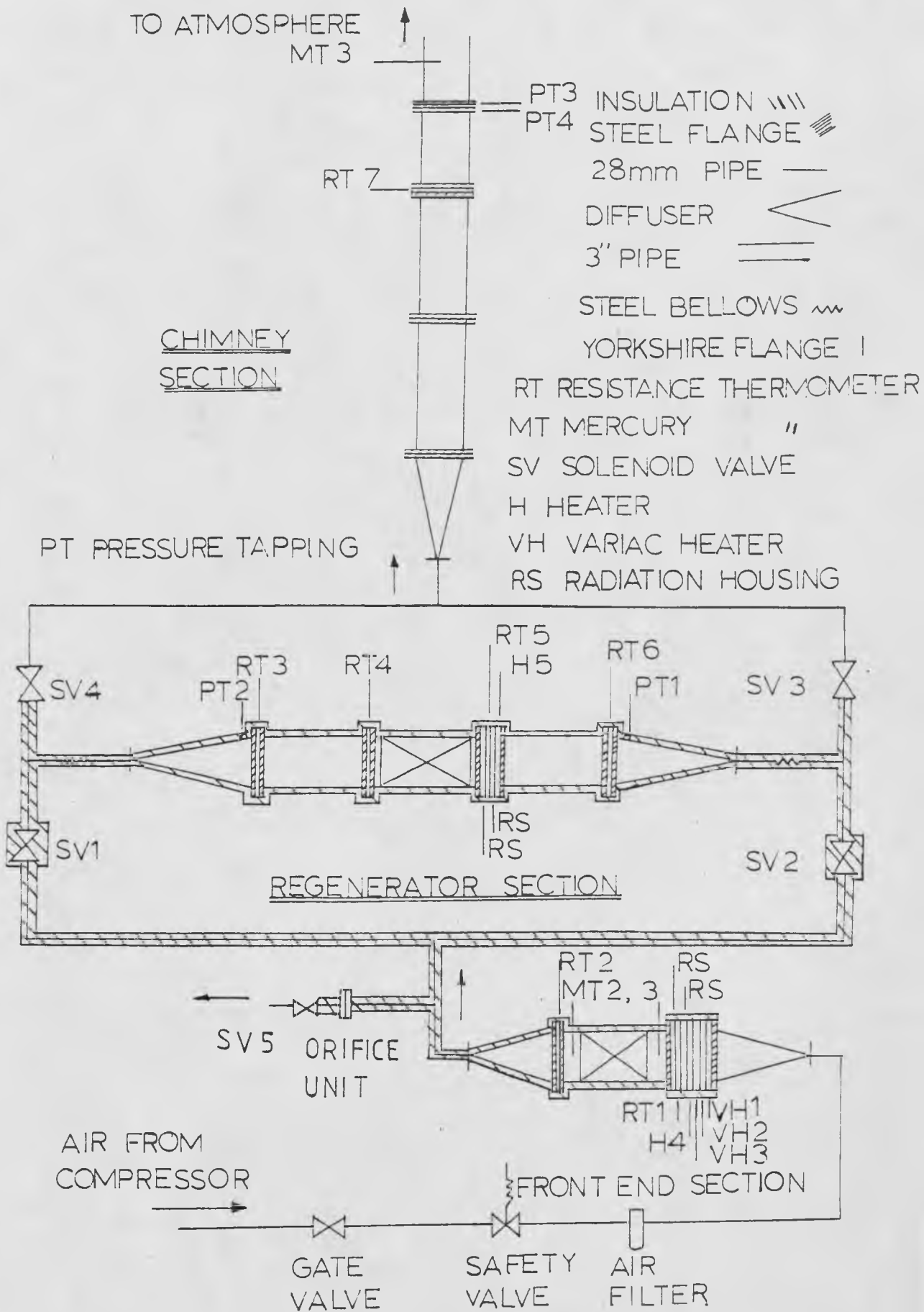
DETAIL SECTION OF
A FIXING HOLE
SCALE: TWICE FULL SIZE

≡≡≡ ARALDITE

FIG 3.6

REGENERATOR DIFFUSER CONTAINING A
TEMPERATURE DAMPENING SECTION





SCHEMATIC DIAGRAM OF THE REGENERATOR

The resistance thermometer uses the same Tufnol housing design as the heater, as shown in Fig. 3.3. The resistance wire is 99.999% platinum of 0.001 inch (0.025mm) diameter and one metre in length, to give an approximate resistance change of one ohm per degree centigrade. The wiring configuration is shown in Fig. 3.5.

3.3.8 Design for Plug Flow

One of the assumptions of regenerator modelling is that plug flow should exist within the packed bed section. Diffusers are employed to prevent jetting from the 26mm inside diameter peripheral pipework into the 3 inch (76.2mm) inside diameter regenerator section. The diffusers were constructed at an angle of 7° , as shown in Fig. 3.6, using a design method proposed by Simpson (1968).

3.4 Proposed Regenerator Operation

The regenerative apparatus comprises three main sections, as can be seen from Fig. 3.7. The front end, which provides a smooth inlet air temperature to the main test bed section which operates under CO and countercurrent flow and the chimney section which houses an orifice plate to indicate the flowrate through the apparatus.

3.4.1 Front End Section

This section produces a smooth air temperature input to the main regenerator section in three ways. Air from the

compressor is throttled by a gate valve, passes through a safety valve and air filter before entering a bank of three heaters HV1, HV2 and HV3, which are used to provide a step temperature rise. Downstream of these heaters is the control section, comprising an analog feedback control loop using resistance thermometer RT1 and heater H4. The analog control can be by-passed by computer control. Directly downstream of the controller section is an 8 inch (203.2mm) packed bed for Pettinos pebbles which dampens out any temperature fluctuations introduced by the controller.

Downstream of the packed bed is resistance thermometer RT2 which indicates the front end outlet temperature. Resistance thermometer temperature indication can be computer logged and recorded on a Kent MK3 multi-point recorder. Prior to the main regenerator test bed section is the Dewrance Asco bleed-off valve (SV5) which can be actuated for a given stroke. Directly upstream of this bleed off valve restriction is an orifice unit.

3.4.2 Main Regenerator Section

In this main regenerator section the air flow can be directed in a direction left to right, or vice versa, depending upon the actuated state of solenoid valves SV1, SV2, SV3 and SV4. The air temperature is increased by approximately 10°C when flowing right to left by the heater H5. The following valve settings allow countercurrent operation:

Hot stroke: SV1,3 closed SV2,4 open
heater 7 on.

Cold stroke: SV1,3 open, SV2,4 closed
heater 7 off.

For co current flow SV2 and 4 remain open, 1 and 3 remain closed as the heater is switched on and off according to the periods selected.

The test bed has been fitted with two pressure tapping points P1 and P2. These are linked to two manometers, one mercury and one water, for pressure drop data collection. The air temperatures are measured at points 2, 3, 4, 5, 6 and 7 by resistance thermometers. Electronic timing in the range 1 (1) 99 minutes and computer timing in the range 1 (1) ∞ seconds is available using continental series relays for the solenoid valve and test bed heater interfacing.

3.4.3 Chimney Section

This section houses various sharp edged orifice plates which are used to indicate the flow rate through the apparatus. The pressure drop over the orifice plate is tapped at points PT3 and PT4, is indicated by a water manometer and also computer logged using a Foxboro ME13DM differential pressure cell. The temperature upstream of the orifice plate is indicated by the resistance thermometer RT7.

3.5 Chapter Conclusion

An apparatus has been designed to examine the thermal characteristics of regenerative heat exchangers. Where possible the theoretical assumptions used in mathematical representations have been built into the design.

Chapter 4

Mechanical Construction and Analog Instrumentation Installation

4.1 Introduction

The regenerator was designed in three distinct sections; the front end, the regenerator test bed and the chimney section. The mechanical construction and inclusion of analog instrumentation for each of these sections will be dealt with separately. The apparatus is well positioned within the small laboratory room, affording a large control panel as shown in plate 4-1, behind which is all the necessary circuitry required for instrument operation. Single phase electricity is used, fused at 30 Amps at the mains contact breaker, shown in fig. 4.1. This arrangement allows a panic button situated near the entrance door and a panel switch.

4.2 Front End Section

Air from the Broom and Wade compressor 76.2 mm laboratory main pipe is removed by 28 mm copper pipe of 1 mm thickness. Air flowrate throttling is produced by a Conex 28 mm gate valve, shown schematically in fig. 3.7 and plate 4.1. The air line then passes behind the control panel where a Wilkerson Foo air filter removes oil droplets from the air flow. Further down stream is a Norgen pressure release valve set at 30 psig (2.068×10^5) N/m². Coupling to the 28 mm pipe is by 1 inch BSP male and 28 mm Conex female.

FIG 4.1

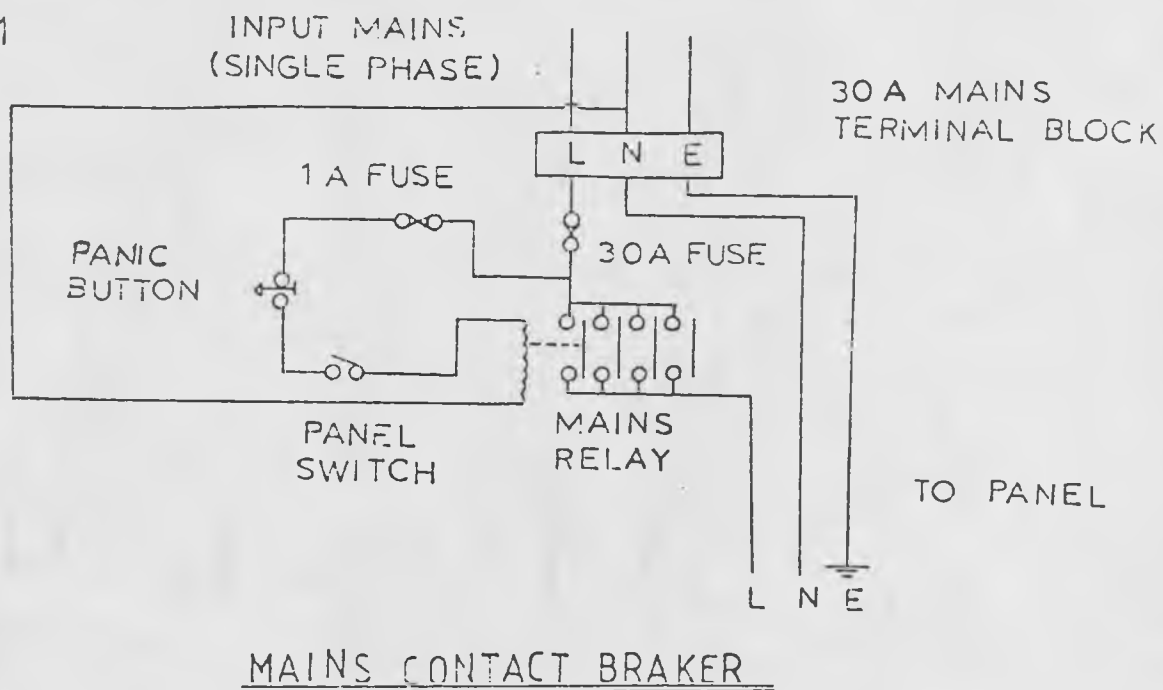
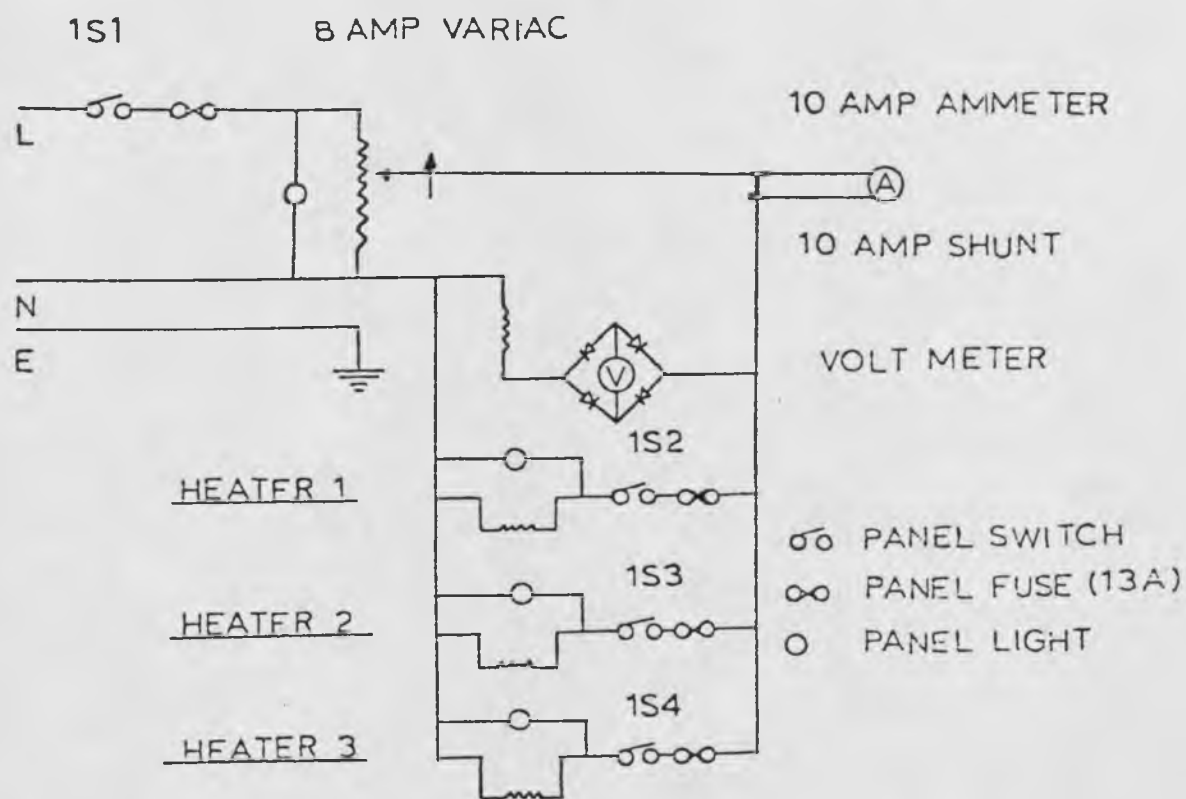


FIG 4.2

FRONT END STEP TEMPERATURE UNIT

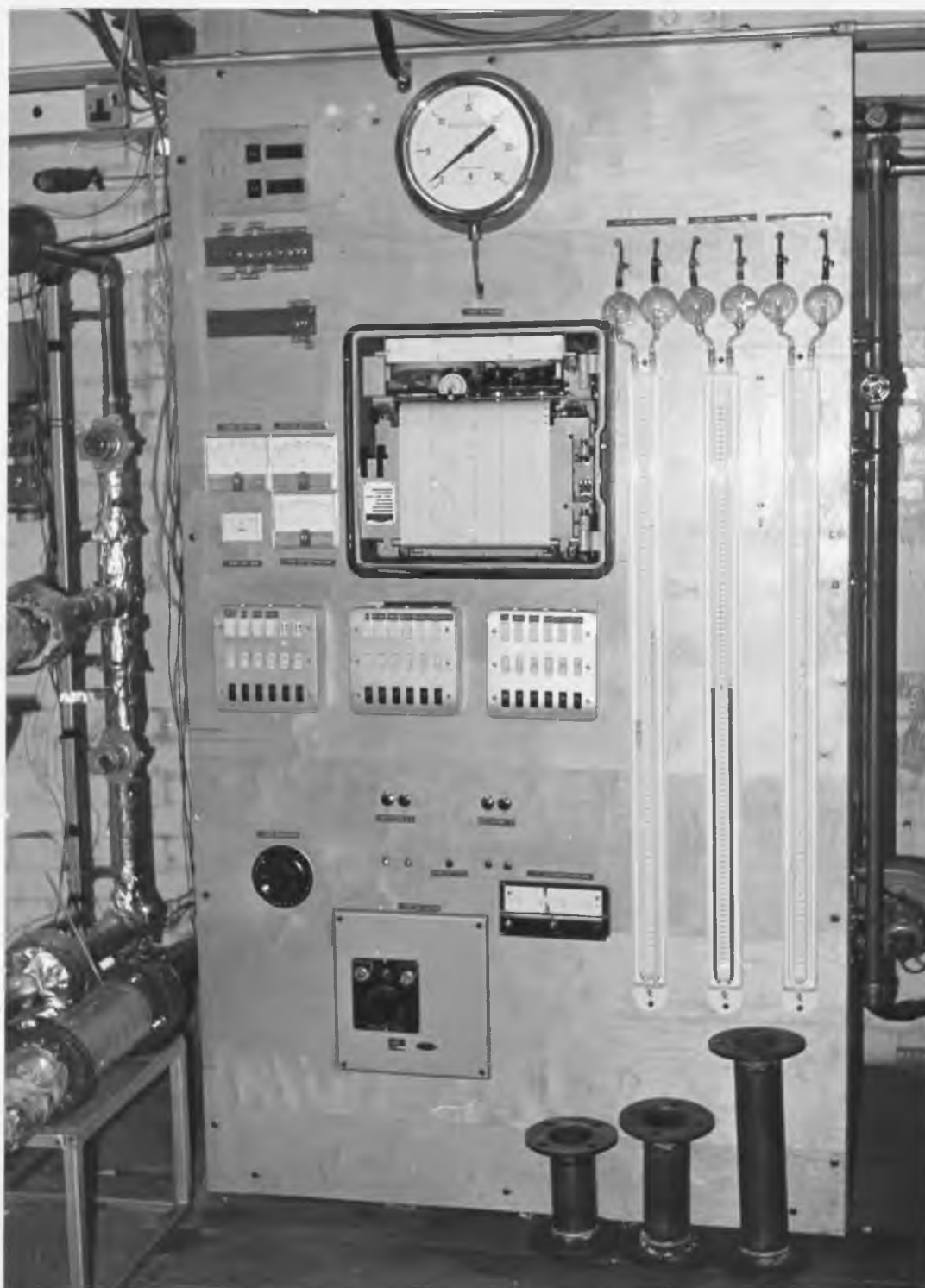


PLATE 4.1 CONTROL PANEL

The air pipe emerges from behind the control panel into the front end control section, with diffusers at either end. Fig. 3.6 shows the diffuser unit constructed of 1.59 mm copper plate, brazed down the centre with a 28 mm Yorkshire copper flange and a modified 63.5 mm table E stream flange, which provides the coupling between the peripheral and test bed pipework.

The control section comprises three variac heaters, downstream of which is the control heater and the control resistance thermometer. The design of the heater and resistance thermometer have been discussed in Chapter 3 and can be seen in figs. 3.4 and 3.5 respectively. The resistance thermometer wire was located by first soldering one end to the brass contact rod. The wire was kept in slight tension and carefully strung over the retention hooks according to fig. 3.5. The loose end was finally soldered to the other contacting rod. The heater wire is strung using a similar procedure. Each Tufnol Carp housing is separated by a 1.59 x 76.2 x 88.7 mm rubber ring which provides an air tight seal.

The main step temperature rise over the front end is obtained using three variac heaters. These are connected in parallel and wired to an 8 amp variac, as shown in fig. 4.2. This allows one, two or three heaters to be used according to the heat input requirements. The variac voltage is indicated by a rectified Radio Spares (R.S.) moving coil meter graduated 0(5)250V, for greater accuracy, whilst the

FIG 4-3

BACK OF CONTROLLER

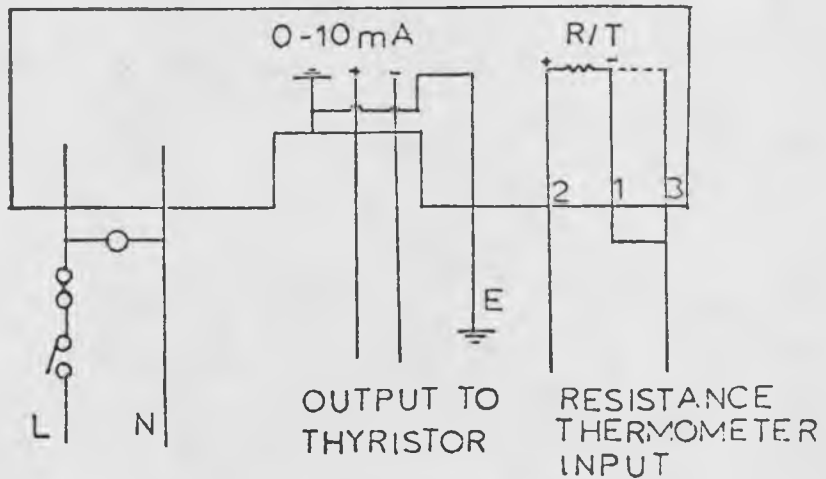
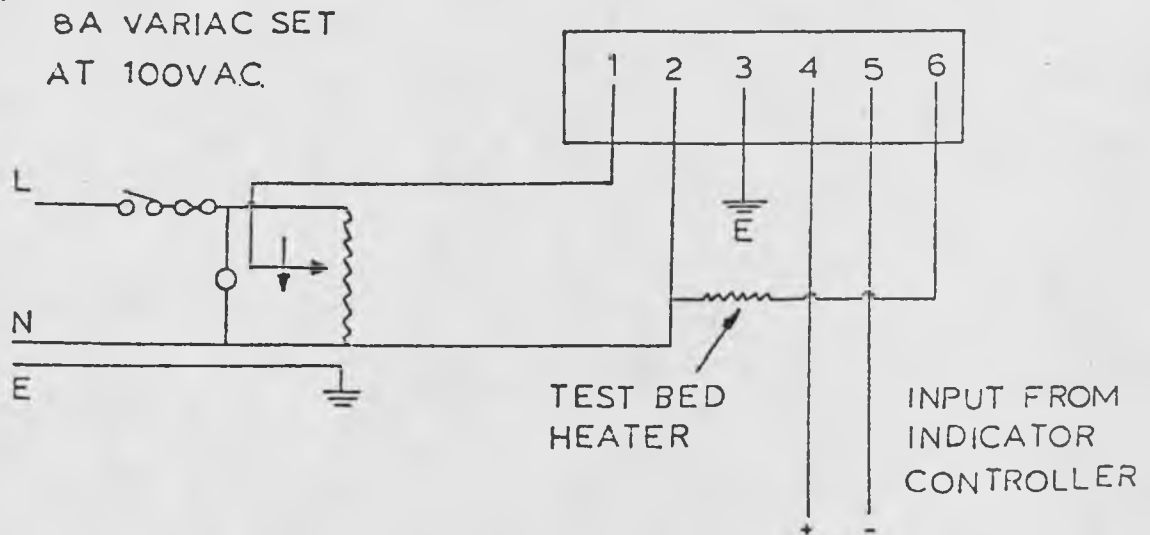
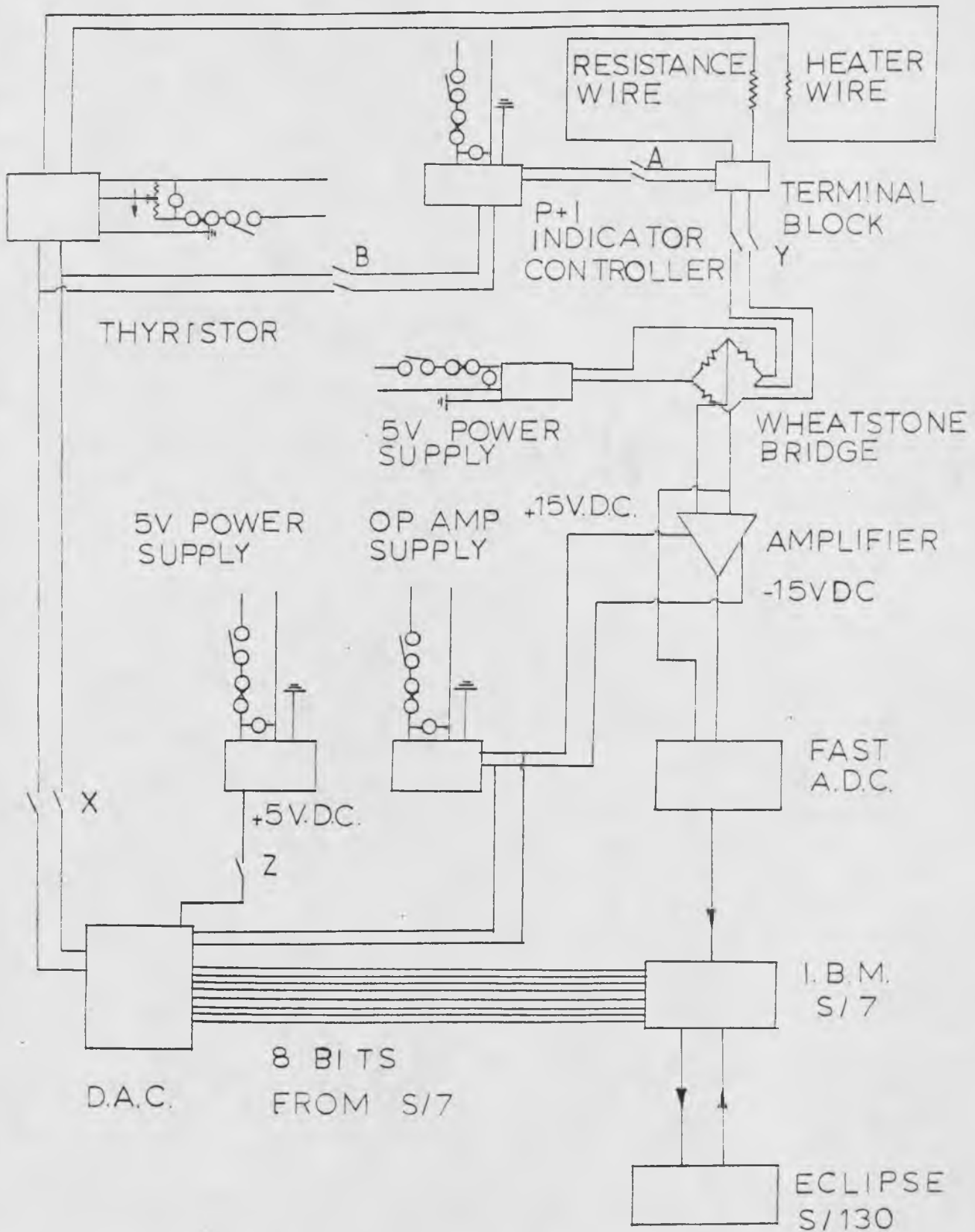
INDICATOR CONTROLLER WIRING

FIG 4-4

BACK OF THYRISTOR

C.S.R. THYRISTOR REGULATOR WIRING



FRONT END ANALOG AND COMPUTER CONTROL SET-UP

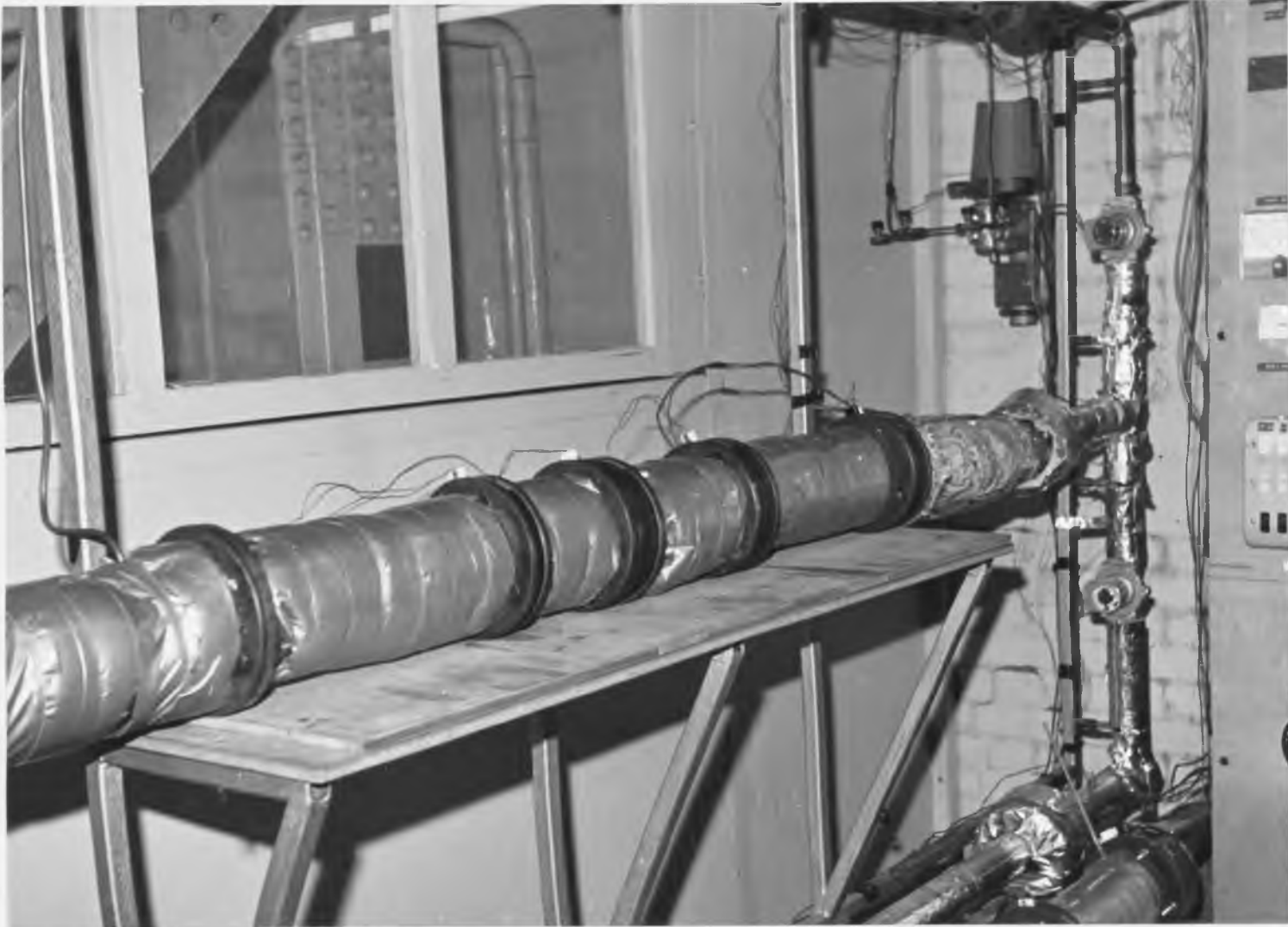
current is indicated by an R.S. moving iron meter shunted 10A and graduated 0(0.2) 10A. Downstream of the step temperature heaters is the feedback control section. The control resistance thermometer is wired to the back of the Foster Cambridge P130L P + I indicator controller as shown in fig. 4.3, the characteristics of which are given in Appendix A. The indicator controller temperature range is 10-40°C, pre-calibrated at the factory. However, on arrival the controller unit was re-calibrated as discussed in chapter 6. The proportional band range is 10-100% with an integral time constant of five minutes. This time constant was fixed at a 'works optimum', however being a basic R.C. circuit the capacitance rating can be reduced to allow a much smaller integral time constant.

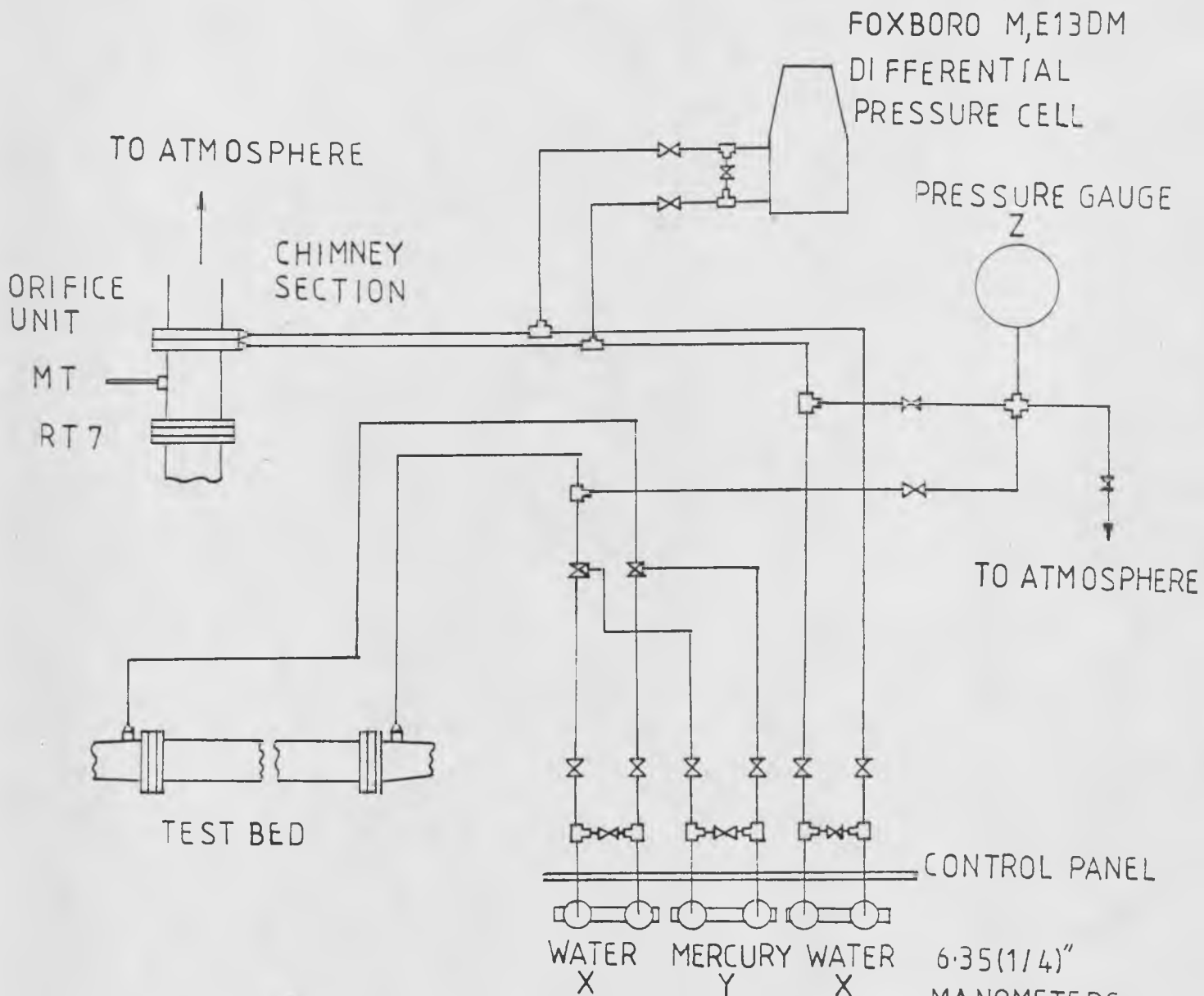
Analog output from the controller is 0-10 mA into 1 k Ω of the C.S.R. thyristor regulator i.e. 0-10 VDC; the external connections of which are shown in fig 4.4. The power requirement is 6 amps 100 V.A.C. maximum, supplied by an 8 amp variac set at 100 V.A.C. The analog control is isolated by opening the computer control circuit with miniature toggle switches X, Y and Z, whilst closing the analog control circuit with miniature toggle switches A and B as shown in fig. 4.5. The control resistance thermometer is connected to a junction terminal block and is in circuit with the analog controller, with toggle switches Y open and A closed. The 0 - 10 VDC output passes into the C.S.R. thyristor regulator circuit when toggle switch X is open and B is closed. The feedback control loop is completed by

connecting the C.S.R. thyristor regulator power output to the control heater.

Directly downstream of the controller section is the air temperature dampening section, constructed from 76.2 mm ID x 79.38 mm O.D. copper tube section 457.2 mm long. The central portion is packed with 6.35 mm diameter Pettinos pebbles to a length of 203.7 mm. This provides a smooth front end outlet temperature. The pebble bed is located in place using 6 mesh stainless steel gauze. Each gauze has three mild steel lugs brazed radially in position and all contain a 4 mm grub screw, which locate against the test bed wall. Either side of the pettinos pebble bed are access Enot connections for locating mercury in glass thermometers.

Downstream of the dampening section is resistance thermometer RT2, as shown in fig 3.7, which indicates the smooth outlet air temperature passing into the second diffuser. The front end is completed by the bleed off section. This comprises a Dewrance Asco 24 VDC solenoid valve described in Appendix A, located by a 1 inch (25.4 mm) tapered male thread with 28 mm conex connections, upstream of which is an orifice unit which can accommodate orifice plates up to 25 mm aperture. This restricts the air flow through the valve and correspondingly allows a decrease in the air flow through the main regenerator section.

PLATE 4.2 REGENERATOR TEST BED



□ ENOT 1/4" (6.35) STRAIGHT MALE ADAPTOR

▷ ENOT 1/4" (6.35) TUBING NUT

—⊗— 1/4" (6.35) WADE MINI VALVE

—⊗— 1/4" (6.35) WADE THREE WAY VALVE

⊞ ENOT 1/4" (6.35) TEE CONNECTION

⊕ ENOT 1/4" (6.35) 4 WAY CONNECTION

○ MANOMETER FLUID TRAP

— 1/4 (6.35) SOFT COPPER

X 0 (12.7) 1016 mm [0 (1/2) 40]"

Y 0 (1) 100 cm

Z 0- 2.068 × 10⁵ N/m² [0 (1) 30] P.S.I.G.

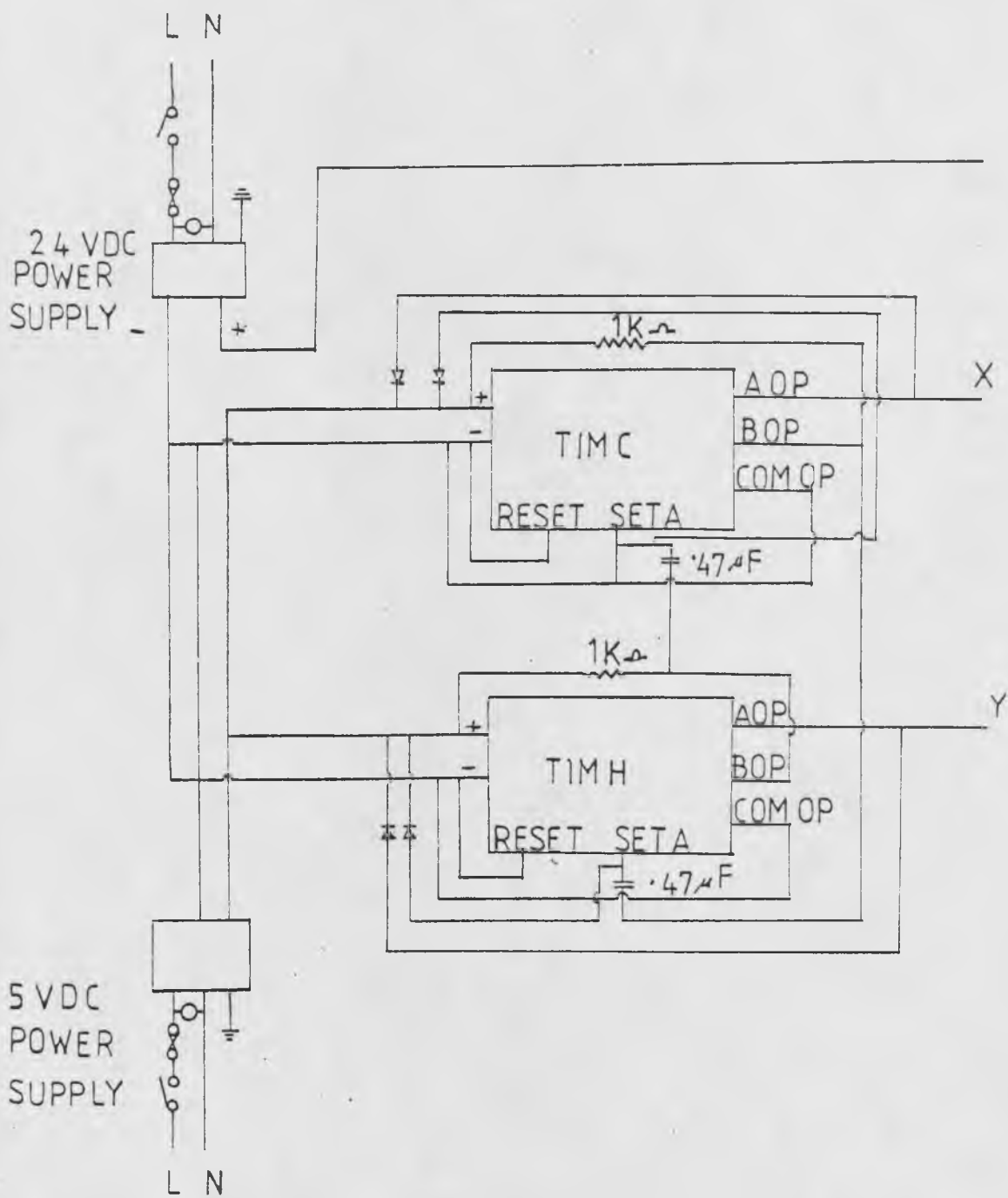
PRESSURE INDICATION LAYOUT

4.3 Main Regenerator Sections

The main regenerator body, as can be seen from the schematic diagram fig. 3.7, is basically a box section of height 1422 mm and width 3048 mm. The 28 mm peripheral pipework and Connex fittings are the same as those used in the front end section. The regenerator test bed is horizontal and 914.4 mm in length. This is supported by a wooden shelf, as shown in plate 4.2. Fig. 3.2 shows the various test bed combinations which will provide packed bed sections up to 304.8 mm in length. Each test bed unit comprises 76.2 mm diameter tubular section, with a modified 2½ inch (63.5 mm) table E steam flange at either end. The making and breaking of the test bed units is made possible by using two 28 mm stainless steel bellows located between the diffusers and the vertical solenoid valve pipework. The 28 mm stainless steel bellows are brazed in position, with a minimum and maximum length of 76.2 and 152.4 mm respectively.

Test bed pressure drop is indicated by a Negretti and Zambra O (12.7) 1016 mm O(½) 40 inch x 12.7 mm (½ inch) diameter water manometer, or a O(10) 1000 mm x 12 mm diameter mercury manometer. The 6.35 mm soft copper pressure pipework layout is shown in fig. 4.6, whilst the Enot connection to the diffuser sections are shown in fig. 3.6. Switchover between the water and mercury manometers is possible using Wade 6.35 mm three way valves. In addition 6.35 mm Wade mini valves are used for isolating and equalizing pipeline pressure. Absolute test bed pressure and pressure upstream of the orifice plate is obtained using a O - 2.068

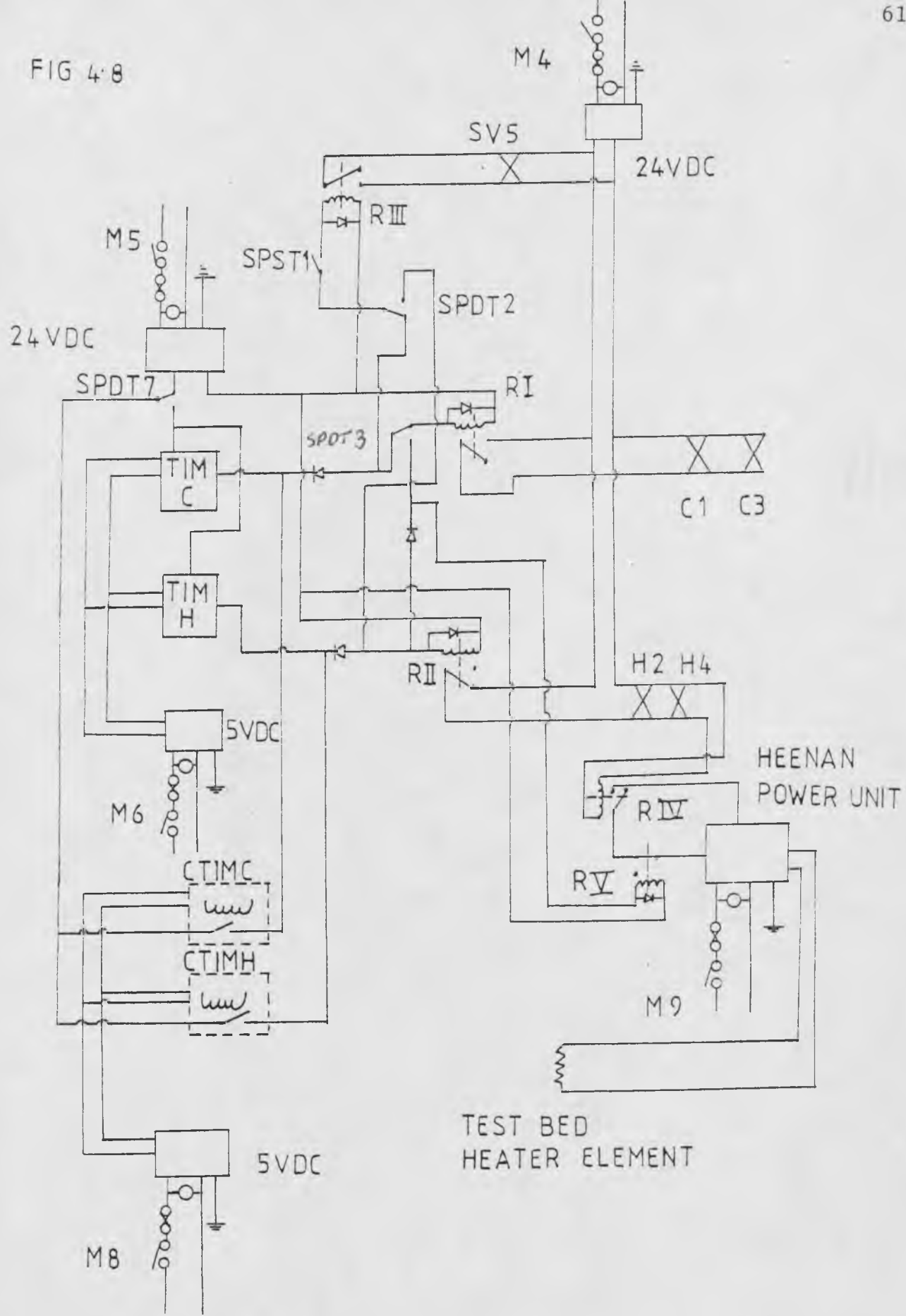
FIG 4.7



		HOT	COLD
STATE OF VOLTAGE	X	LOW	HIGH
	Y	HIGH	LOW

TWO P.042 LGM ELECTRONIC TIMERS WIRED FOR DISSIMILAR TIMING ACTIONS

FIG 4-8



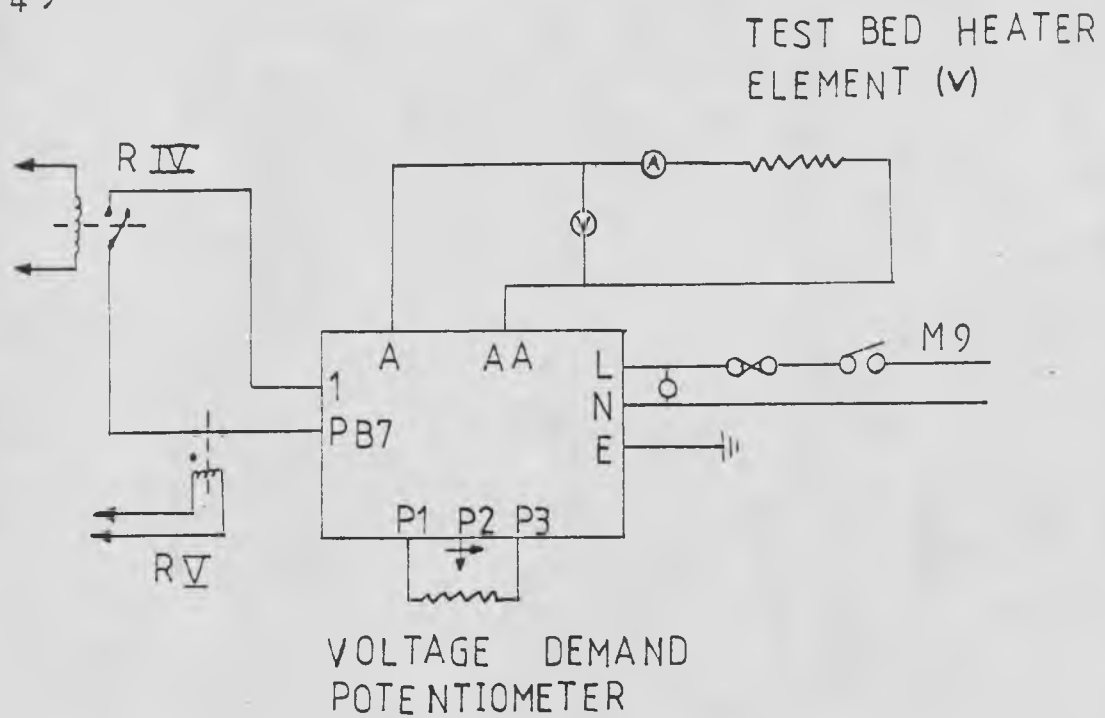
MANUAL AND COMPUTER TIMING INTERFACING
WITH TEST BED HEATER SET-UP.

$\times 10^5 \text{ N/m}^2$ O(1) 30 psig Negretti and Zambra pressure gauge. To prevent manometer liquid entering the pressure lines, 'liquid traps' have been placed at the top of each manometer limb. The test bed cylindrical sections are internally insulated using 1 mm Triton kaowool paper, externally insulated using 19.05 mm polyurethane and the steel flanges are insulated with fibre glass blankets.

The main electrical components of the regenerator test section comprises the timing, heating, switching interfacing and temperature indication circuitary. Two L.G.M. P.O.42 electronic timers are used, the properties of which are shown in Appendix A. These timers were chosen not only for accuracy and reliability but because they could be used together, to provide dissimilar timing periods over the range 1(1)99 minutes. Fig. 4.7 shows the two timers wired for separate timing actions, powered by an L.G.M. 5 V.D.C. stabilized voltage supply unit using a 24 V.D.C. stabilized voltage supply for the switching voltage. The timers act as primary relays, switching on and off the 24 V.D.C. supply required for the interfacing circuitry.

Fig. 4.8 shows the whole manual and computer timing interface and heating set up. The mains and toggle switch actions for this are in Appendix B. RS 1N 4000 series diodes are used in the timing interfacing circuitry to prevent back e.m.f.s, which were initially responsible for premature relay switching. Each solenoid valve action is indicated on the control panel as shown in plate 4.1.

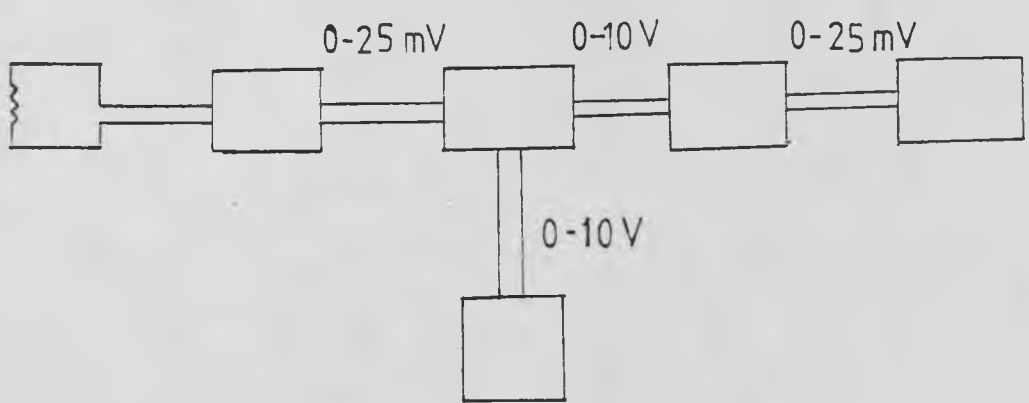
FIG 4.9



HEFNAN 180/6 (TEST BED HEATER UNIT) WIRING

FIG 4.10

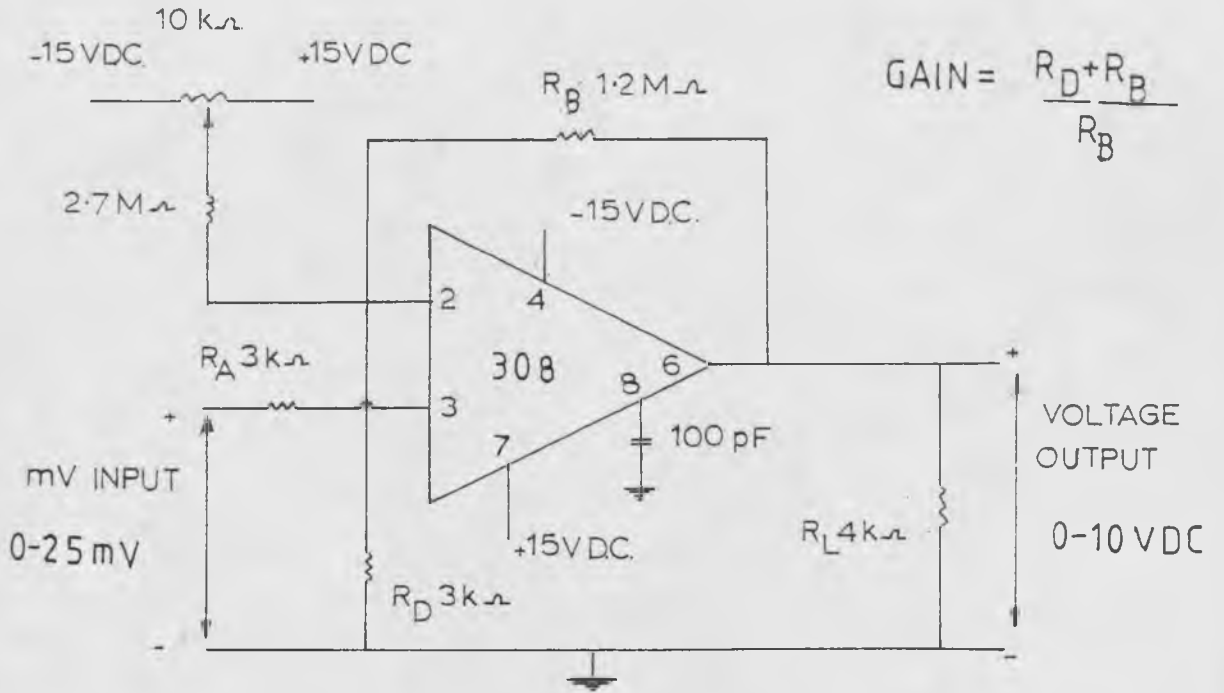
RESISTANCE THERMOMETER BRIDGE WHEATSTONE BRIDGE AMPLIFIER VOLTAGE REDUCER KENT RECORDER



FAST A/D CONVERTER

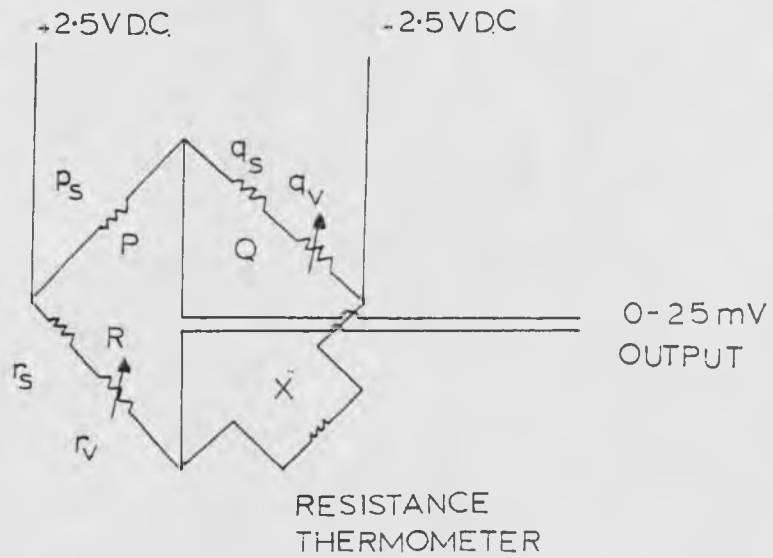
TEMPERATURE INDICATION PROCEDURE

FIG 4.12



308 AMPLIFIER IN THE NON INVERTING STATE

FIG 4.11



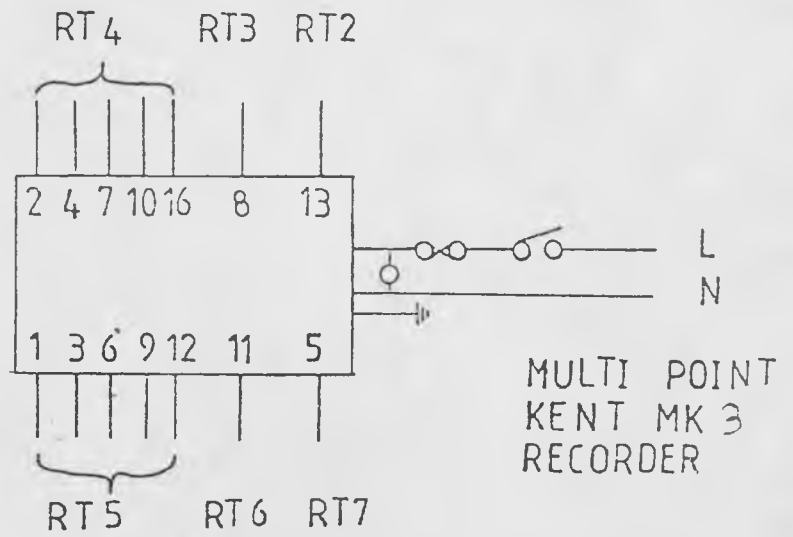
WHEATSTONE BRIDGE SET-UP

Temperature indication is provided as a mV output from a Wheatstone bridge circuit for a known resistance change, as shown in the block diagram 4.10. Each of the six resistance thermometers are connected to a Wheatstone bridge circuit as shown in fig 4.11. The Wheatstone bridges are designed for high accuracy using a constant stabilized voltage of 5VDC supplied by a Weir REG (5V1A) power unit, whilst resistance change with temperature is reduced to a minimum using R.S, thick film resistors with a temperature coefficient of ± 100 ppm/ $^{\circ}$ C and R.S. 10 turn ceramic potentiometers for the variable arms. The method of obtaining the resistance values for a known resistance thermometer change is discussed in Chapter 6. If a lower temperature range is to be examined the 0-25 mV output from the bridges can be achieved for a 5 - 25 $^{\circ}$ C range by reversing the input 5 VDC polarity using a double pole double throw toggle switch, located on the panel.

Initially the Wheatstone bridges mV output was fed to the 16 point Mark 3 Kent recorder then to the non-inverting 308 operational amplifier for the amplification within the range 0-10 VDC. However this method proved unsuccessful due to incorrect impedance matching. To avoid this the 0-25 mV output passes to a non-inverting 308 operational amplifier set at a gain of 400 to produce 0-10 VDC as shown in fig. 4.12. Contact is now made with the Fast Analog to Digital Converter (F.A.D.C.) and also to the voltage reduction resistors set to produce a range of 0-25 mV, for input to the 16 point Kent Mark 3 temperature

FIG 4-13
RT =
RESISTANCE
THERMOMETERS

INDICATOR
MARKERS

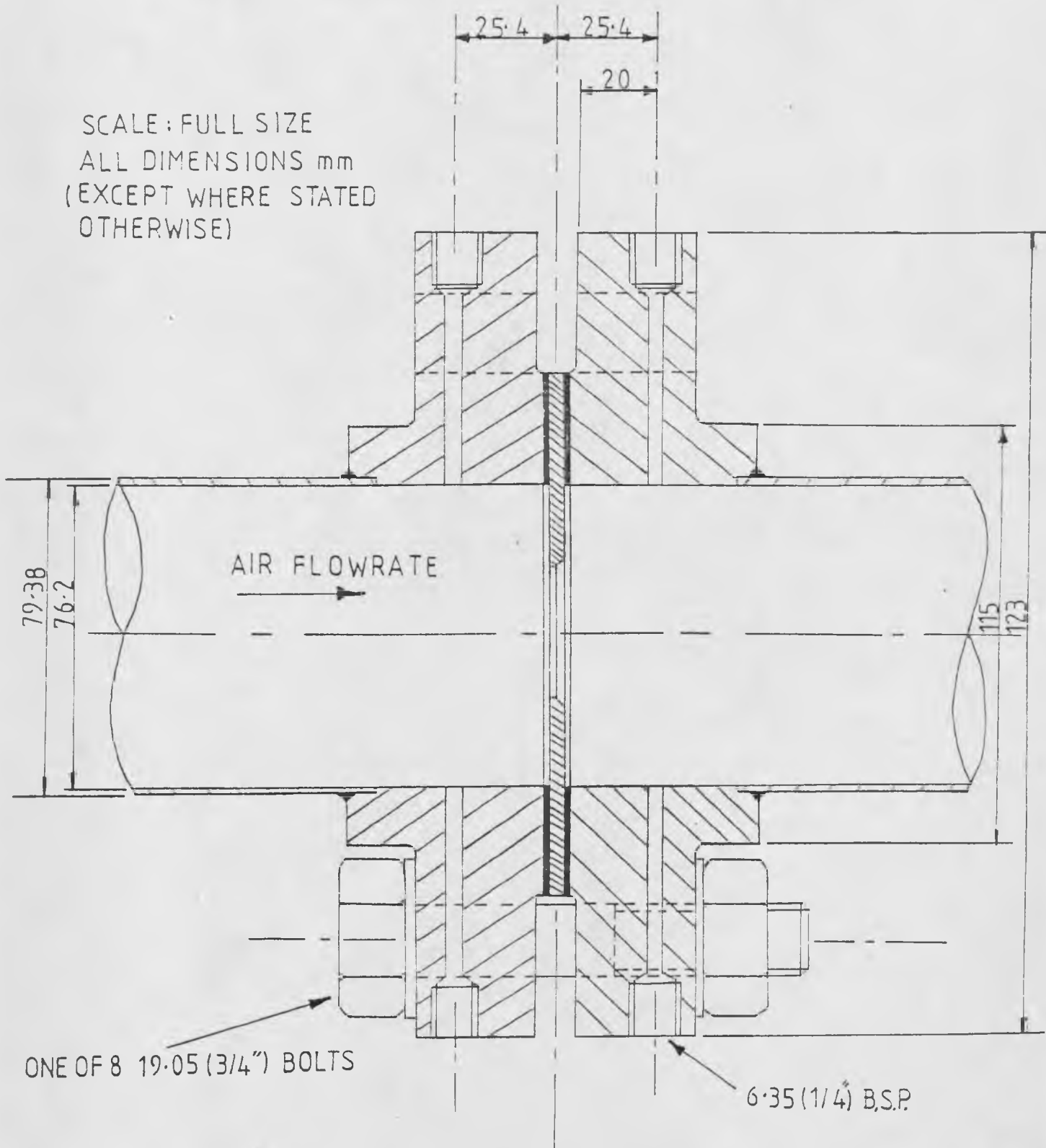


RESISTANCE THERMOMETER REPRESENTATION
ON THE MULTI POINT KENT MK 3 RECORDER

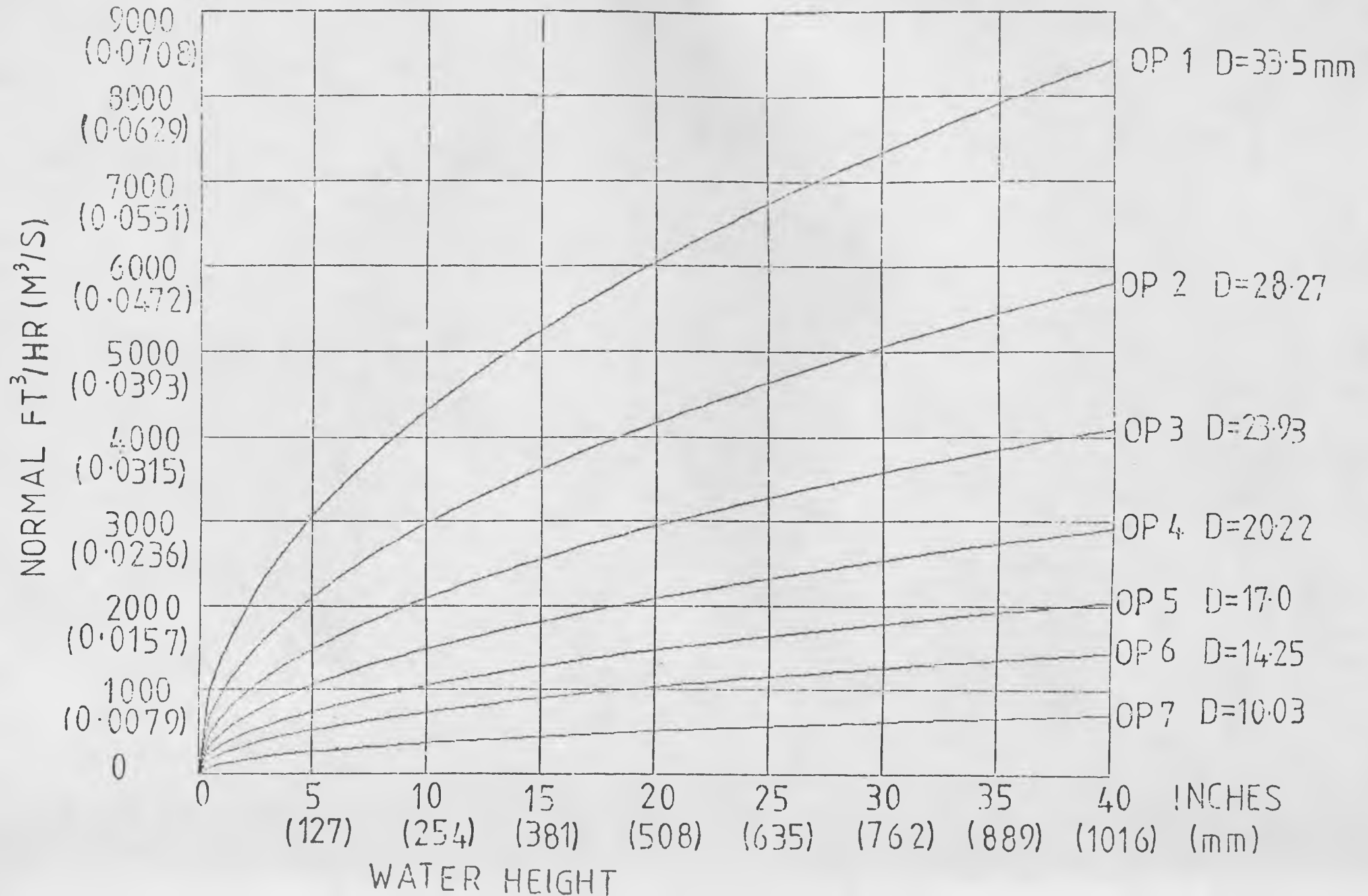
FIG 4.14

ORIFICE UNIT

SCALE: FULL SIZE
 ALL DIMENSIONS mm
 (EXCEPT WHERE STATED
 OTHERWISE)



-  MILD STEEL FLANGE
-  COPPER TUBING
-  STAINLESS STEEL SHARP EDGED ORIFICE PLATE
-  CORK SEAL

FIG 4.15 ORIFICE CALIBRATIONS

recorder, for full scale deflection. Out of the 16 indicator points two are ineffective, the rest representing the temperatures indicated by the resistance thermometers are shown in fig 4.13. The recorder has 6 chart speeds of which 381 mm per hour is regularly used. Initially the indicator marking speed was one point every four seconds, however, appropriate modification of the camming system reduced this to a reasonable one point every two seconds, which is barely minimal considering the response time of a resistance thermometer.

4.4 Chimney Section

The chimney section is used to obtain the air flowrate through the system by measuring pressure drop across a sharp edged orifice plate with one inch taps, shown in fig. 4.14, as proposed by Spink (1961). A comprehensive range of flowrates for the system is obtained by the use of seven orifice plates for a set pressure drop of 0 - 1016 mm (0-40 inches) water, as can be seen from fig. 4.15. Pressure drop across the orifice plate is indicated by a Negretti and Zambra 0(12.7) 1016 x 12.7 mm 0($\frac{1}{2}$) 40" x $\frac{1}{2}$ " water manometer and also computer logged with the aid of a Foxboro M E13 DM differential pressure cell, shown schematically in fig. 4.6, and described in Appendix A.

A schematic diagram of the chimney section is shown in fig 3.7, in relation to the whole apparatus. Unfortunately the apparatus is not housed near the top of the engineering

laboratory, so the chimney section is thus made long enough to pass through the experimental room above. Air from the 28 mm copper pipe of the main regenerator box section initially passes through a diffuser, then through a straightening vane unit comprising thirty 12.7mm ($\frac{1}{2}$ inch) x 16 S.W.G. x 127mm(5 inch) Acrylic plastic pipes Araldited in position, which are located 16 pipe diameters away from the orifice plate unit. 610 mm upstream of the orifice unit is resistance thermometer RT7 which is used to indicate the air outlet temperature. Additionally a mercury in glass thermometer is located in position by 6.35 mm Enot fittings. The process air then passes to the atmosphere.

4.5 Chapter Conclusions

A thermal regenerative apparatus has been constructed with the inclusion of manual instrumentation according to the design criteria discussed in Chapter 3. However the facility for computer control and data logging affording more concise and accurate data collection exists within the department. The inclusion of computer timing, temperature and flowrate logging and front end control will be discussed in Chapter 5.

Chapter 5

Computer Control and Data Logging Facilities

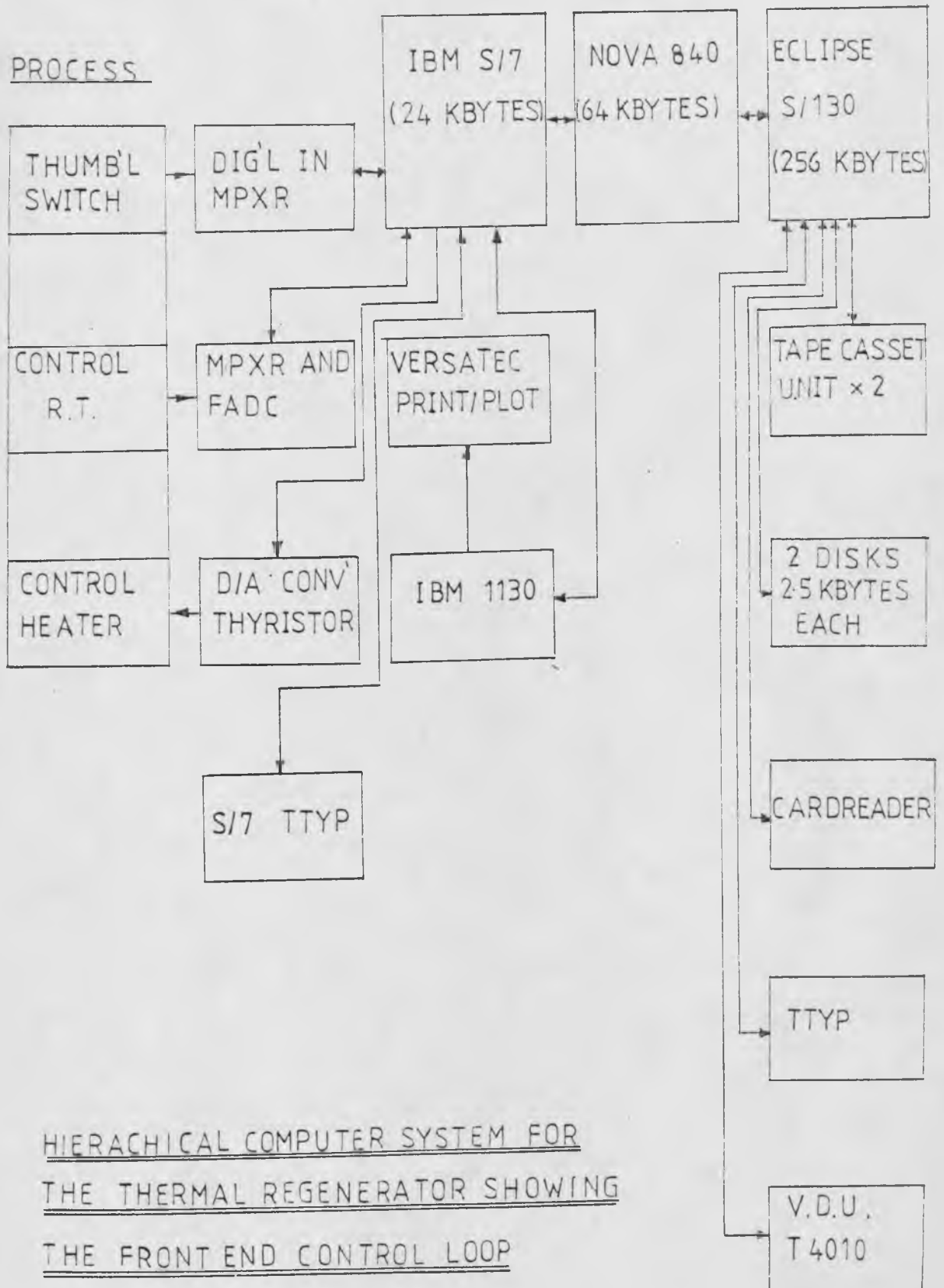
5.1 Introduction

Applications of computer control on industrial plants are well established and have been shown to have positive advantages over conventional analog techniques, as discussed by Adamopolis (1977). Apart from the initial equipment cost savings, the potentialities of the digital computer can offer additional benefits. Perhaps the most obvious is the increased control over the response which can be obtained. Higher accuracy and resolution often allow control actions to be based on smaller error signals, making possible better control. The repeatability of control settings and of controller performance which digital systems provide, is sometimes even more important than accuracy, since consistent control performance leads to a more uniform product and reduces the dependence on skilled operators. Digital systems provide flexibility; changes in control strategy can be made without corresponding changes in hardware.

The computer by-pass system devised, comprises four distinct parts, shown in Fig. 5.1.

1. The process.
2. Instrumentation
3. Interface.
4. Digital computers.

FIG 5.1



The instrumentation required is that by-passed from the analog (manual) state. Special attention has been paid to noise suppression and to signal conditioning so as to be compatible with the existing interfacing equipment housed in the data acquisition room. In particular, the multiplexer (MPXR) and the fast analog to digital converter (FADC). These devices are interfaced to and from the IBM S/7 (S/7) computer.

As described earlier, two main computers have been used in this work; the S/7 which acts as a front-end processor and a Data General Eclipse S/130 (Eclipse), which has enhanced general purpose capability compared with the S/7 to which it is linked. Such a configuration gives access to a greater range of peripheral equipment.

The S/7 is specially designed to operate as a sensor based machine in a host-satellite environment with the host in charge. It therefore functions quite naturally as part of the network, especially since more complex processing of data is called for. Basically the S/7 performs the role of a high speed data acquisition device, a digital filter, an output switch driver and a communications processor.

The link to the Eclipse provides real time communication with a multi-tasking system, which offers the possibility of direct interaction with the process. It also provides access to a large suite of general purpose scientific routines and the capability of developing complex algorithms in a high level language, ie. Fortran V. For the control

procedure (on line) and subsequent off line work this is an essential requirement.

5.2 Computer Interfacing

Plant instruments are usually adjusted to finally produce d.c. voltage signals in a standard range, as in this situation. The temperature signals are linear, but the flow measurements are not. Since these signals are analog an interface is necessary to convert them to digital form before they can be accepted by the S/7.

It is also necessary to provide some means of communications with the computers from the process end of the system, since the physical distance between the apparatus and the computer room is about 100m.

Using a purpose-built interface to the S/7, four thumbwheel switches have been used as process operator stations on the plant. The interface comprises TTL compatible digital in multiplexer, which has the capability to handle parallel transfer of data from different devices installed in the chemical engineering laboratory. It utilizes S/7 digital I/O functions under software control.

An interface is also necessary for the two banks of lights shown in plate 4.1 which display any two of the six fluid temperatures in the regenerator system. The interface

comprises TTL compatible digital de-multiplexer which has the capability to handle parallel data transfer to the chemical engineering laboratory.

It is convenient to define the terms used in describing the S/7 - thermal regenerator interface system.

1.	Measurement signals interface	AFØ1multiplexer (MPXR) and fast analog to digital converter (FADC)
2.	Communication devices interface to S/7	General purpose digital in multiplexer.
3.	Communication device interface from S/7	General purpose digital de-multiplexer.
4.	Thumbwheel switches	Description later
5.	L.E.D. lights	Description later

The units (1), (2) and (3) are located in a separately built data logging room, whilst units (4) and (5) are on the thermal regenerator control panel, shown in plate 4.1.

A brief description of the measurement signals interface, the digital multiplexer and the digital de-multiplexer are given in appendix C. A full description of these has already been undertaken by Adamopolis (1977).

5.3 Description of Digital Computers

The S/7 is a sensor based computer, initially installed to operate in a host satellite environment linked to an IBM 1130 computer. Using standard digital I/O equipment

and with the support of a multi-tasking programme, it is linked to the Eclipse S/130 via a Data General Nova computer. This link provides real-time communication in a multi-tasking environment.

It has been thought necessary to include a brief discussion of the main software facilities available on the S/7 and Eclipse, together with some details of the locally designed communications package. In general, each machine has its own standard software facilities plus the ones required for the present work. The former will be outlined in appendix D, IBM S/7 standard software facilities, IBM S/7 general purpose application programmes, A/D converter driving programme (ADCNX) and the Eclipse standard software facilities, whilst the latter will be described with the separate computer aspects.

With these departmental facilities available, it became possible to include on-line computer control and timing and computer temperature and flowrate logging. All of these functions have provided an extra dimension to the working of a regenerative apparatus, over manual operation. Each computer aided aspect of the process has specific advantages which will be discussed separately with each section.

5.4 Period Switching

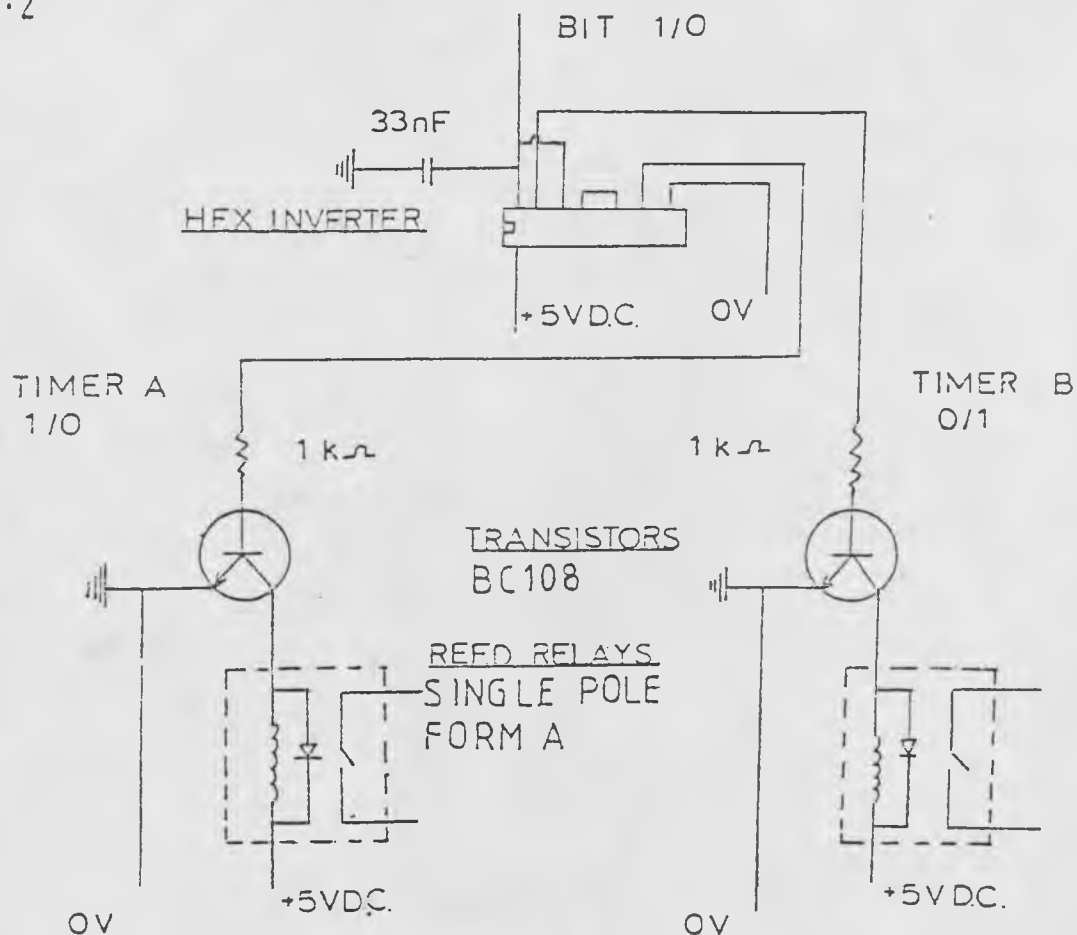
A full description of the manual timing has been given in chapter 4. This mode of operation is excellent for timing when the apparatus is run for long periods, when commissioning is being undertaken and frequent start-up and shut-down is required. However, for some experimental runs this mode of operation is restrictive because the minimum time between a period is one minute, and the timer range is 1 (1) 99 minutes. In order to examine regenerator behaviour efficiently a more comprehensive timing set up is required, which is solved using computer timing, operating with a minimum time interval of one second.

5.4.1 Timing Hardware

The manual electronic timers, as described in chapter 4, merely act as timing relays to the secondary solenoid valve relays RI and RII, given in Fig. 4.8. It was therefore conceivable to by-pass the electronic timers by a reed relay system controlled by S/7 output.

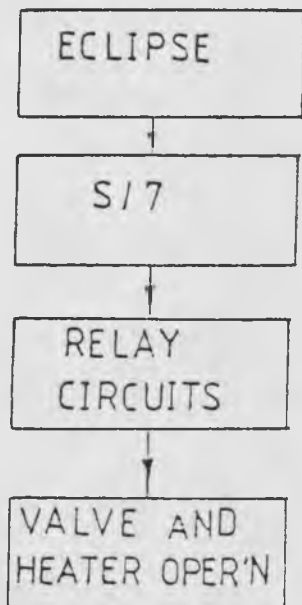
With the computer room over 100m away from the data acquisition room and that 40m away from the apparatus room, special screened 15 core 0.1mm cable of 314M Ω per metre is used for voltage transference. The reed relay circuitry is mounted in a special racked 'noise elimination box', containing all the process electronic circuitry and

FIG 5.2



COMPUTER REED RELAY TIMING CIRCUIT

FIG 5.3



BLOCK DIAGRAM OF THE COMPUTER TIMING

power supplies. Each power supply is separated from the next by a 3mm aluminium plate, whilst the whole power supply section is separated from the electronics by two 3mm aluminium plates.

The reed relay circuitry fulfilled the following design criterion:-

1. Suitable to fit into the existing timing interfacing with easy by-pass capability.
2. Only one Binary Transfer (BIT) input required for actuation.
3. Rapid switching with a long life span.
4. Relay contact ratings sufficient to switch the solenoid valve relays.
5. Reliability in operation using existing power supplies.

The following reed relay circuit developed, as shown in Fig. 5.2, encompasses all the above design features. The input BIT 1 (high) on entry after passing through the hex inverter will actuate reed relay A (+5V), but not reed relay B (0V), hence actuating the secondary relays RI, but not RII, as shown in Fig. 4.8 (and vice versa when the input BIT is 0 (low)).

The computer timing circuitry is placed in the overall timing set up, again as shown in Fig. 4.8, being connected to the interface circuitry by toggle switch SPDT7, which by-passes the manual electronic timers.

5.4.2 Overall Operational Procedure Software Programme

The overall software control programmes that actuate the apparatus are listed in appendix E.

These are SJH (REGEN, SWIT, FILDT and FIQUK) for the 'on-line' activation of the process in the Eclipse and STHRIG which is the S/7 assembler programme fired from the Eclipse. Flow diagrams of the relevant off-line programmes required to treat the logged temperature and measured data, ie. SJH (CYCT, CYCP) are also given in appendix E. The relevant thumbwheel switch and necessary data input will also be given.

5.4.3 Overall Timing Procedure

A schematic diagram of the timing procedure is shown in Fig. 5.3. The required multiple timing periods are typed into the Eclipse keyboard, along with the control data required. Subsequent activation of the S/7 programme SJHRIG activates the low power group output resulting with the timer BIT being initiated according to the timer period durations typed in at the Eclipse. The resulting BIT passes into the reed relay circuitry, activating the valve and, if required, the test bed heater operation.

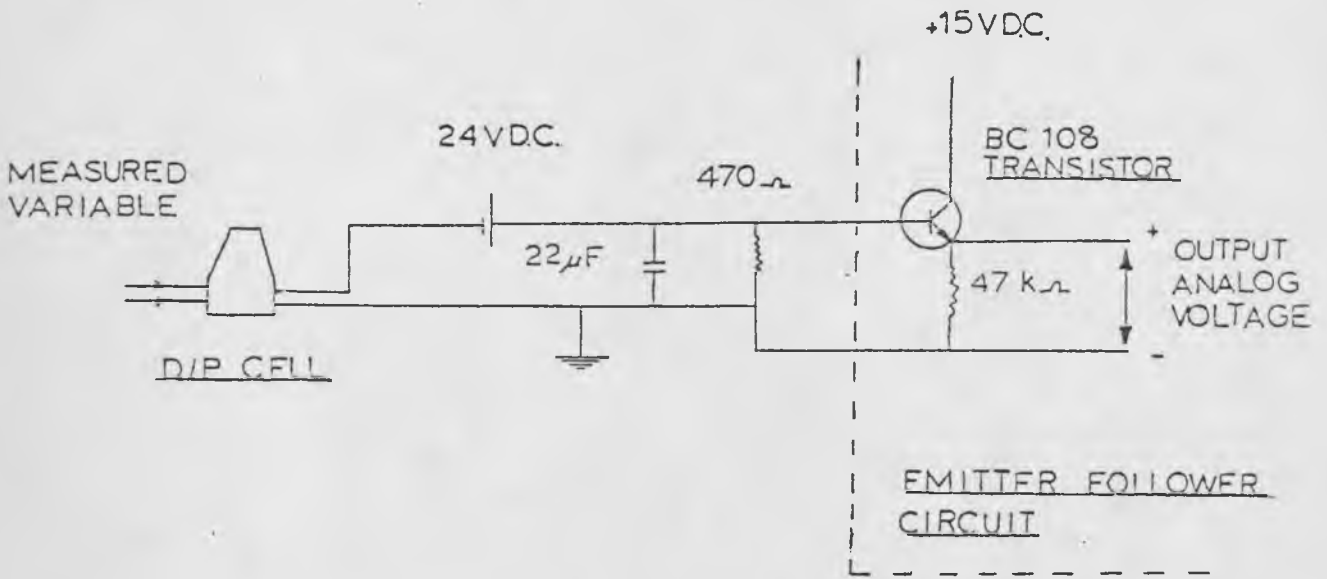
5.5 Flowrate Logging

Previous workers Price (1964), Heggs (1967) and Main (1978) when obtaining the flowrate of air through their apparatus used only a water manometer to indicate the pressure drop across the Foxboro orifice plates. However during commissioning when the flowrate manometer levels were examined it was found that due to the inadequacy of the Broom and Wade pressure controller, flowrate oscillations were present, particularly at high flowrates. With the manual approach it is impractical to constantly obtain pressure drop measurements over a whole set up of runs. However the average flowrate can be obtained by computer logging the pressure drop and then using the Spink (1961) correlation to obtain the flowrate.

5.5.1 Flowrate Logging Hardware

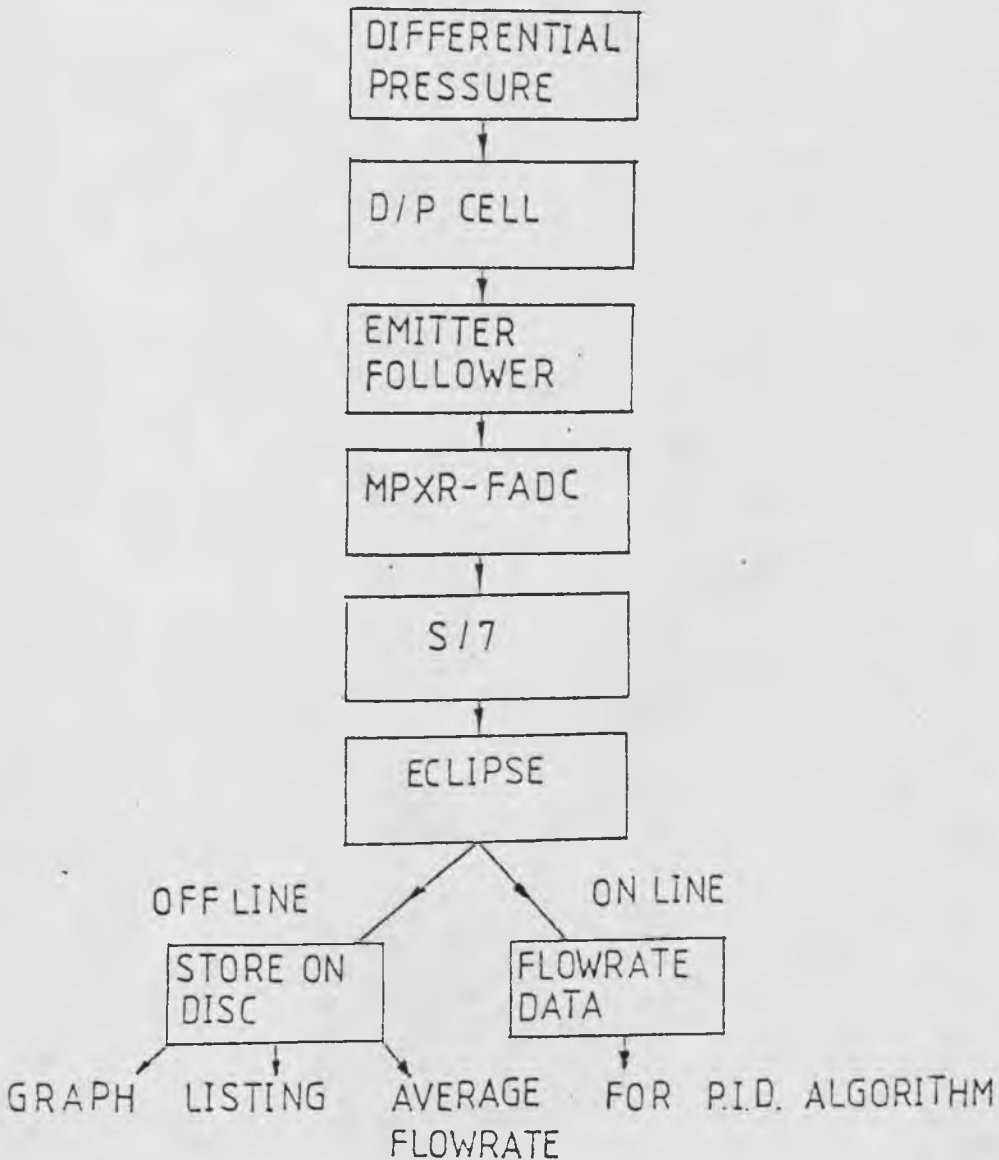
A Foxboro differential pressure (D/P) cell 0-40 inch (0-1016mm) water, the specification of which is given in appendix A, is placed in the manometer line, as shown in diagram 4.6. The D/P cell is protected from possible water surge into the 6.35mm ($\frac{1}{4}$ inch) pressure line by placing overflow bulbs onto each manometer limb.

In order to convert the 4 to 20m A current signal from the D/P transducer to a voltage, it is driven through a 470 ohm high stability thick film load resistor as proposed



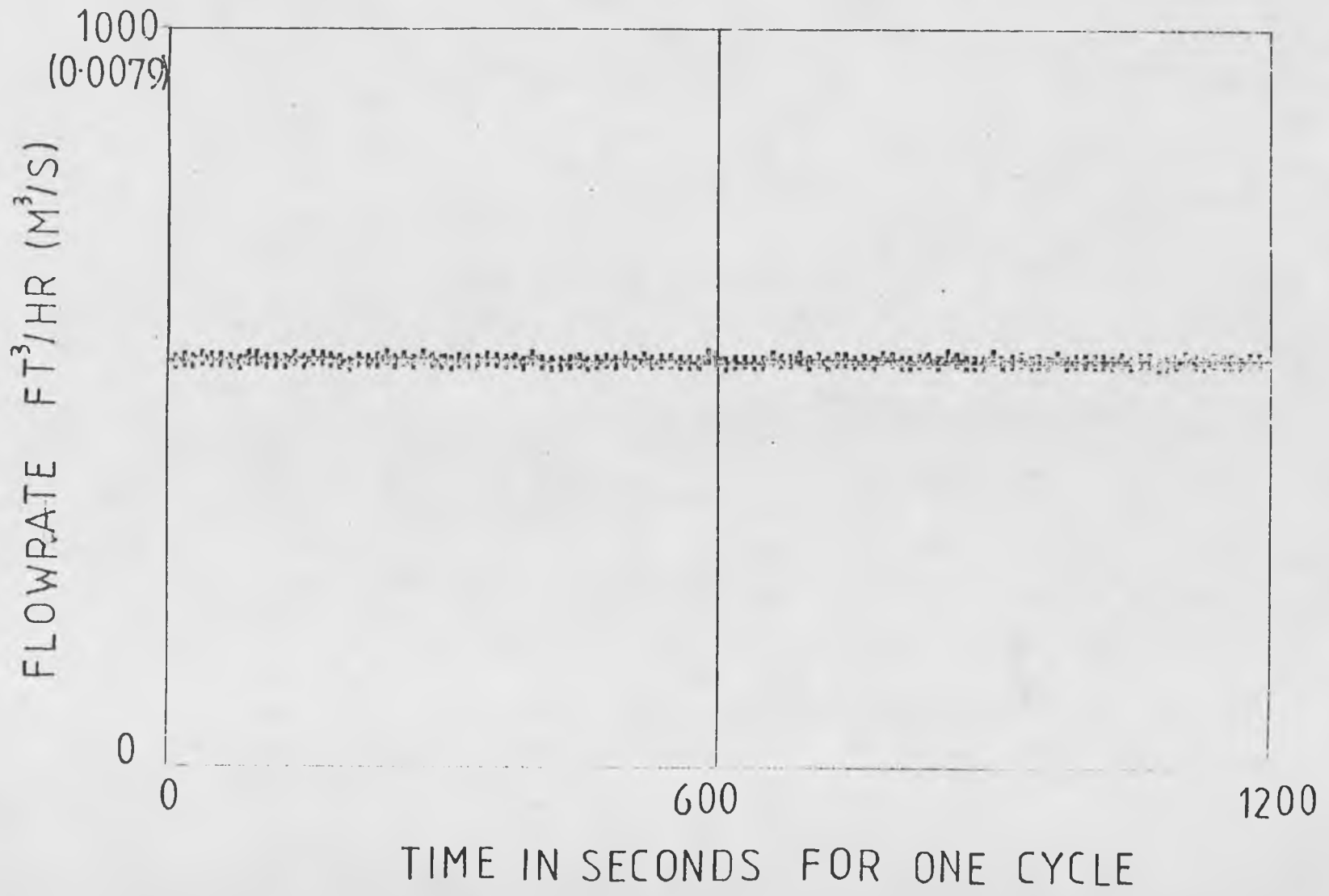
DIFFERENTIAL PRESSURE TO ANALOG VOLTAGE CIRCUIT

FIG 5.5



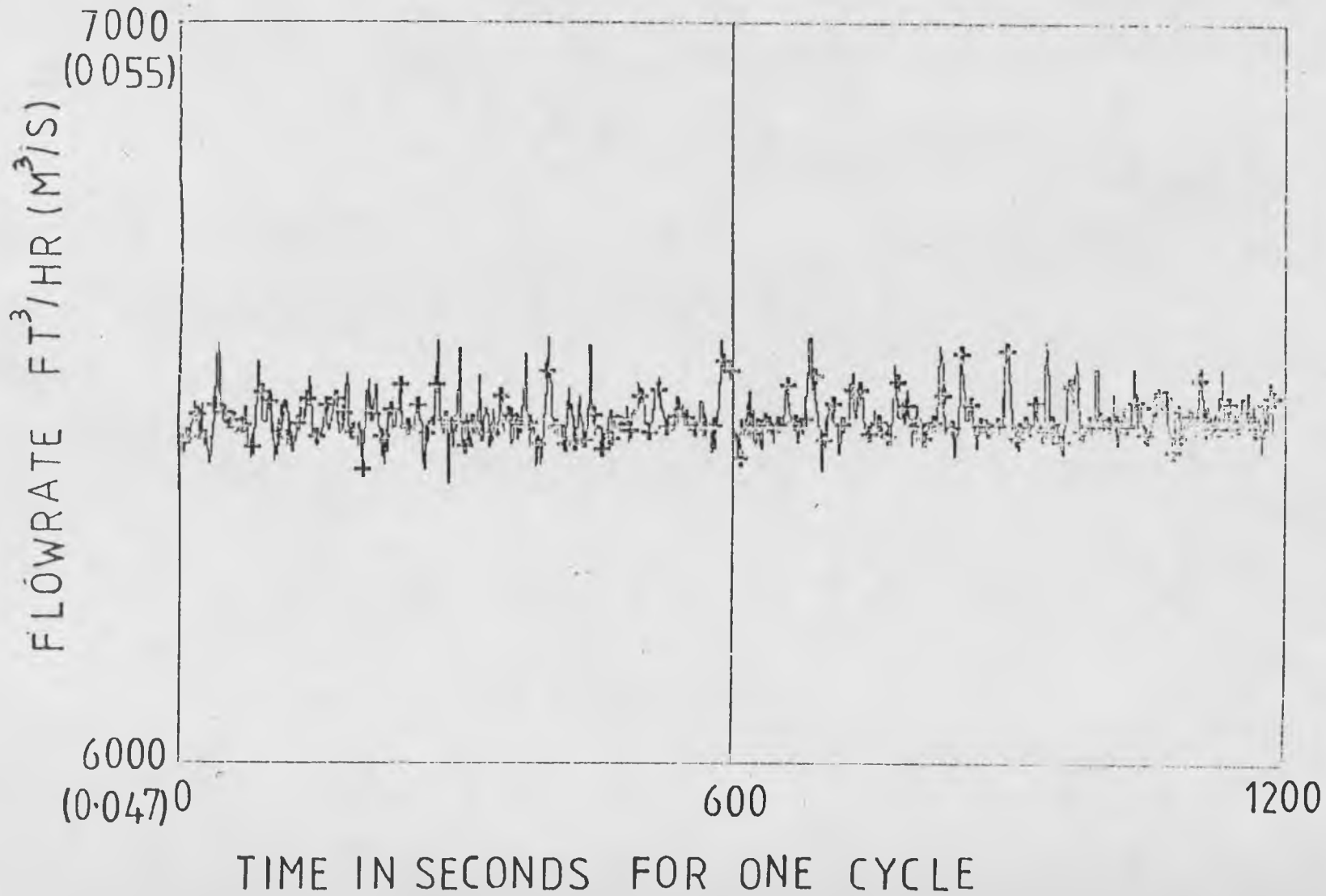
BLOCK DIAGRAM OF THE COMPUTER FLOWRATE LOGGING

FIG 5-6 FLOWRATE VS TIME FOR ONE CYCLE AT LOW FLOWRATE



84
FIG 5.7

FLOWRATE VS ONE ONE CYCLE AT HIGH FLOWRATE



by Foxboro in their D/P cell manual (1975). The voltage across this resistor, which is then proportional to the transmitted current signal and therefore the pressure measured, is passed to an emitter follower circuit, shown in Fig. 5.4, ensuring appropriate impedance matching with the FADC-MPXR.

5.5.2 Overall Flowrate Computer Logging

A schematic diagram of the flowrate logging set up is shown in Fig. 5.5. The differential pressure across the flow orifice plate is converted in a milli Amp range, using an M E13DM Foxboro differential pressure cell. The current range is then converted into the voltage range 0-10VDC. An emitter follower circuit then provides the correct impedance matching for input to the MPXR FADC. The subsequent BIT range is then fed into the S/7 and treated by the assembler programme ADCNX to smooth the input data before being passed to the Eclipse, where the data is stored on disc accordingly for each run.

The flowrate data is then treated off line by the software programme STHCYCP to give the average flowrate for a particular run, the flowrate profile plot for all cycles for one run and also an interactive flowrate plot of one cycle within a run. Figs 5.6 and 5.7 show the one cycle interactive plots for a low and comparatively high flowrate. This shows the inadequacy of the compressor pressure controller

FIG 5-8 REGENERATOR RESPONSE FOR FIVE
THIRTY MINUTE CYCLES
FOR RT POSITIONS SEE FIG 3-7

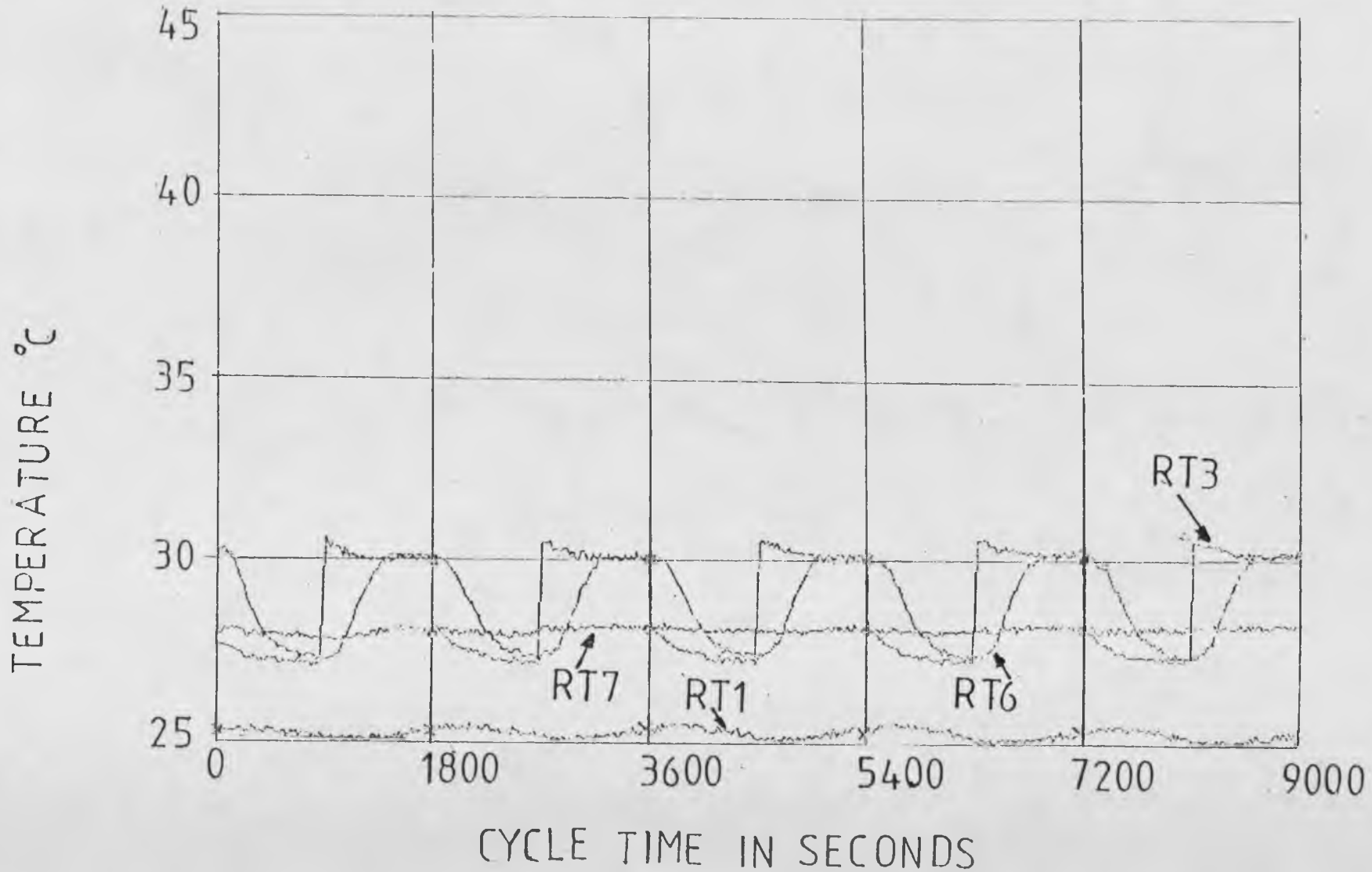


FIG 5-9 TWO CONSECUTIVE THIRTY MINUTE CYCLES
FOR RT POSITIONS SEE FIG 3-7

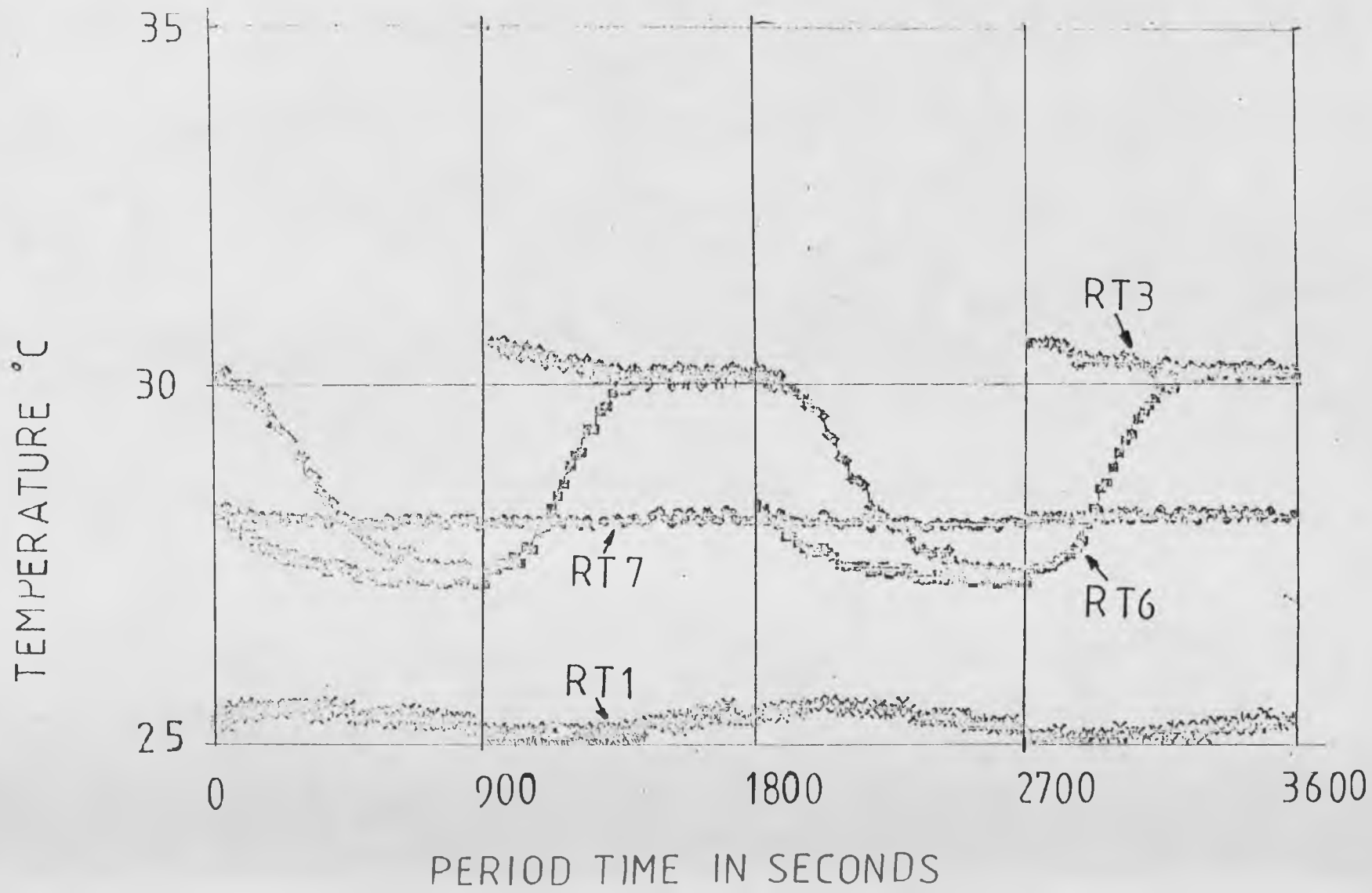
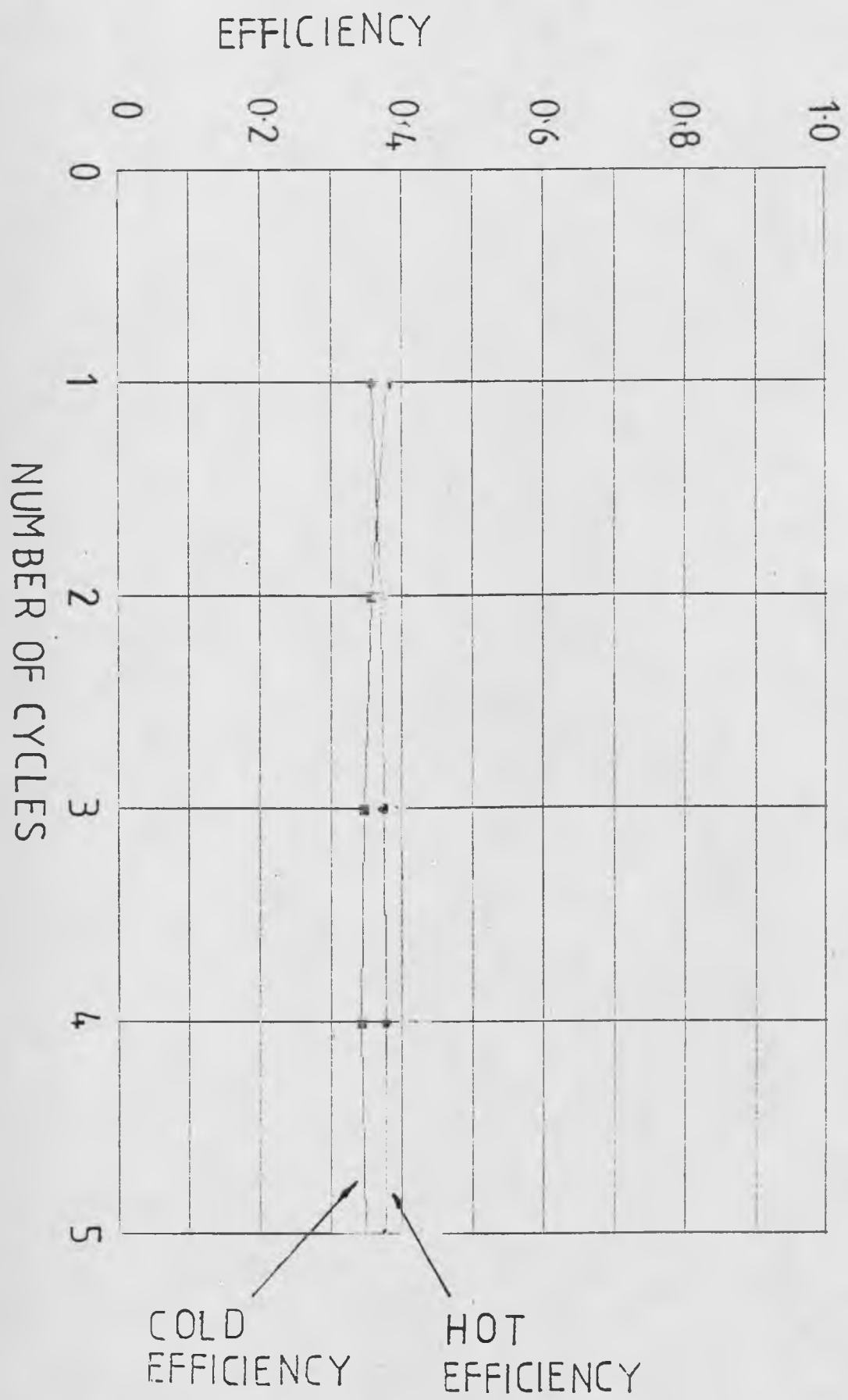


FIG 5-10 CYCLE EFFICIENCY VS TOTAL NUMBER
OF THIRTY MINUTE CYCLES



and how at high flowrates this would inevitably lead to errors in flowrate determination and also erratic heat transfer.

5.6 Computer Data Logging

Temperature logging on the computer has the following advantages over analog recording by the multi-point Kent recorder:

1. Provides temperature logging every second for every computer linked resistance thermometer.
2. When the data for a particular run has been logged it can be examined in concise form in the following manner:
 - a) Accurate determination of the average inlet and outlet temperatures, efficiencies and temperature swings for a chosen cycle.
 - b) Overall and interactive graphical output so particular cycles can be examined in detail as shown in Figs. 5.8 and 5.9 respectively.
 - c) The hot and cold efficiencies for every cycle within a run can be obtained as shown in Fig. 5.10, giving an overall indication of how the apparatus is progressing towards cyclic equilibrium.

3. The speed and ease of these operations prevents hours of tedious work obtaining efficiencies and temperature swings from the Kent recorder output.

4. The input temperature data can be processed on line to indicate cyclic equilibrium and the next run within the set up activated.

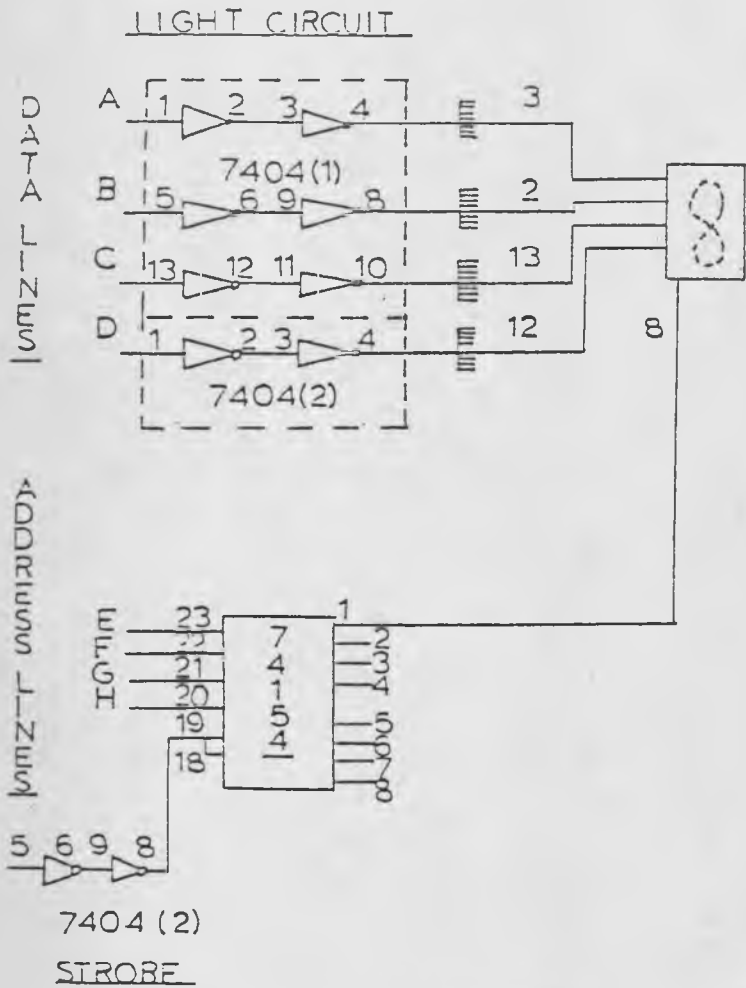
5.6.1 Temperature Logging Hardware

Initially the apparatus was designed to incorporate analog temperature logging and so the wheatstone bridge output voltages were designed for input to the Kent recorder as described in chapter 4. However, to allow temperature recording on the Kent recorder and the computer, the set-up was changed to that shown in Fig. 4.10, also described in chapter 4. The operational amplifiers used were 308's constructed non-inverting, as shown in Fig. 4.12. After the design and construction of the amplifiers commissioning work showed negligible noise pick up, and the drift characteristics were found excellent.

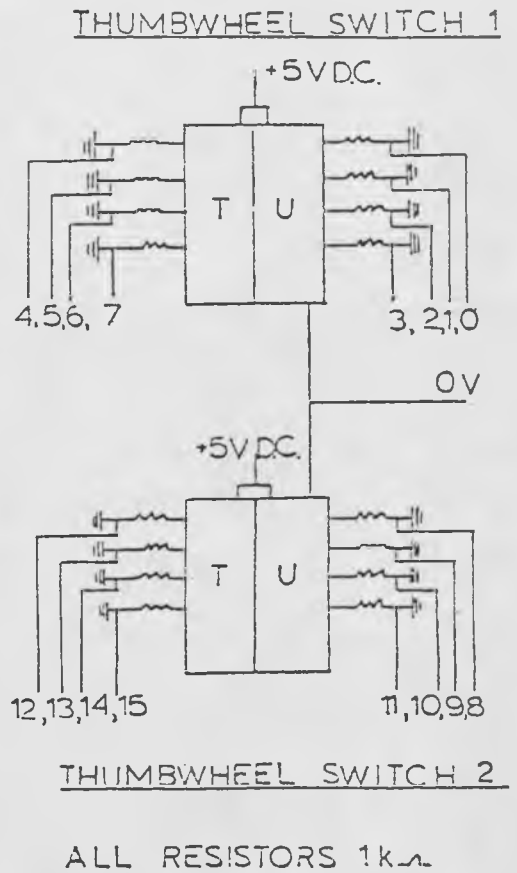
With the complexity of the computer control and data logging set-up, a need for communication to and from the computer room over 100M away became a necessity. Various Eclipse software logic could be actuated by digital communication using four thumbwheel switches, shown in Fig. 5.11, whilst any two of the six temperatures being logged could be

FIG 5-12

FIG 5-11

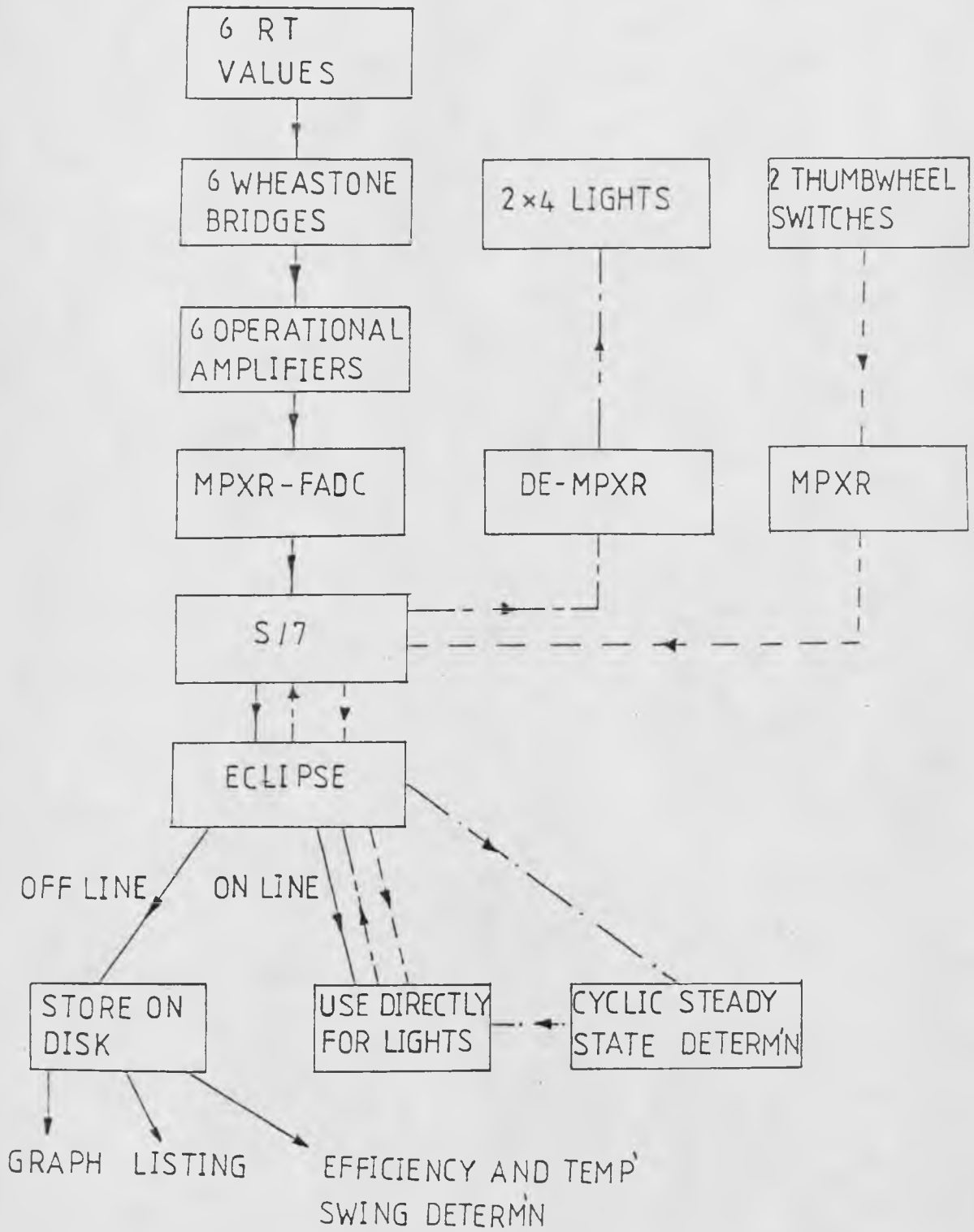


0.27 INCH LOGIC HEXIDECIMAL I.E.D. CIRCUIT



THUMBWHEEL SWITCH CIRCUIT

FIG 5.13



BLOCK DIAGRAM OF THE COMPUTER TEMPERATURE LOGGING PROCEDURE

represented by two banks of four L.E.D. 0.27 inch lights, a circuit diagram being shown in Fig. 5.12. The lights could also register the completion of one run and represent the number of cycles required to do this.

5.6.2 Computer Temperature Logging Procedure

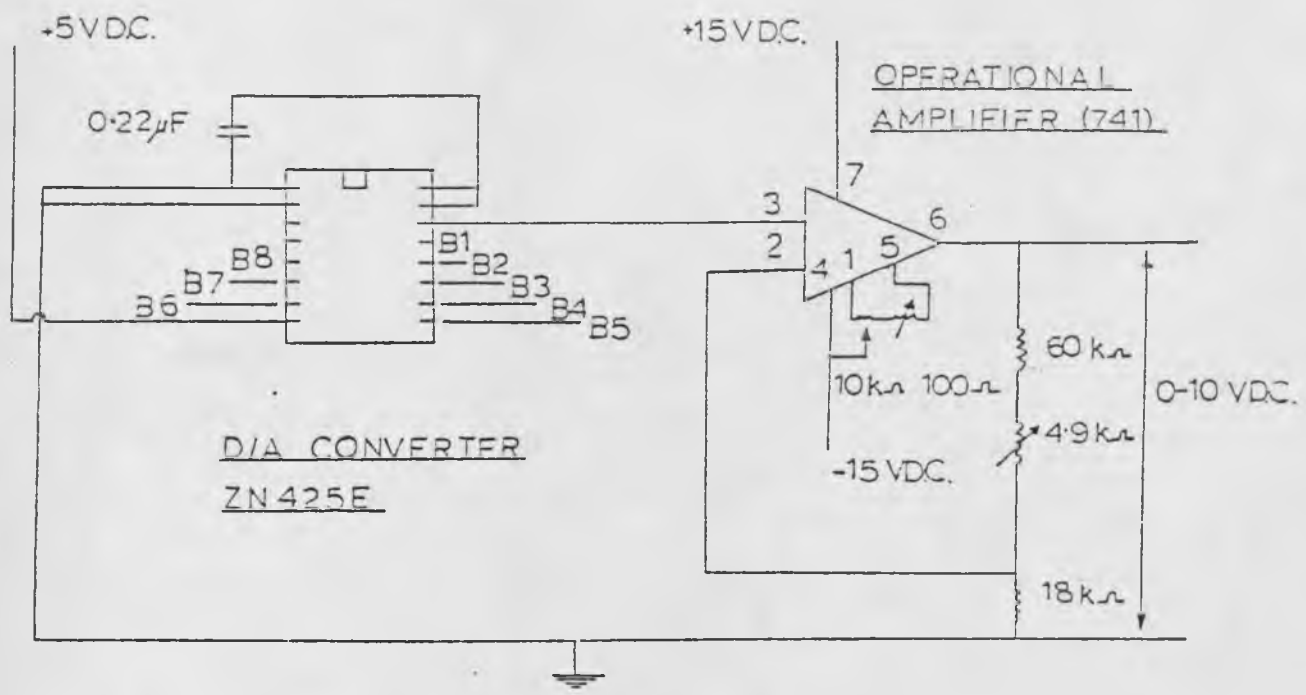
A block diagram showing the temperature logging procedure is shown in Fig. 5.13. The resistance change associated with a temperature change of 20°C is converted to the voltage range 0-25mV. This is converted by non-inverting 308 amplifiers into the range +0-10VDC, which is then fed into the MPXR FADC, which is shipped as binary to the S/7. The input data is processed by the filter programme ADCNX, then shipped every second to the Eclipse, where it is stored on disc. The temperature data is then utilised in two ways.

1. As 'on-line' temperature representation to 2 decimal places, using the two banks of 4 L.E.D. lights.
2. Treated 'off-line' by the programme SJHCYCT, as described in 5.6.1 section 2.

5.7 Front End Computer Control

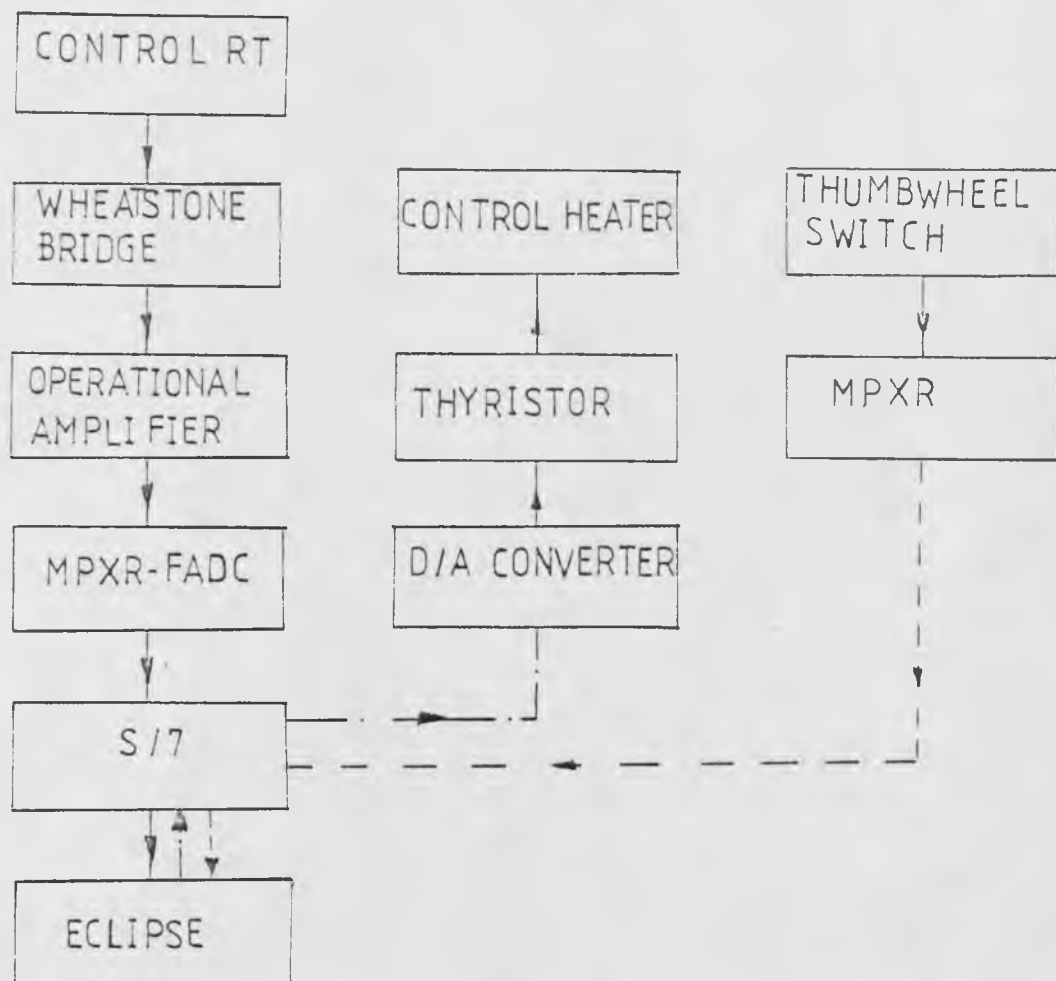
Computer control for this apparatus, over analog control, offers a greater variable flexibility and, if required, additional derivative action.

FIG 5.14



DIGITAL TO ANALOG CONVERTER

FIG 5-15



BLOCK DIAGRAM OF THE FRONT END
COMPUTER CONTROL LOOP

5.7.1 Control Hardware

The analog control set-up, as shown in Fig. 4.5, can easily be by-passed by closing X, Y and Z and opening A and B toggle switches respectively. The control resistance thermometer wheatstone bridge is calibrated in the range 20-40°C to produce 0-25mV, which is amplified within the range 0-10VDC for input to the MPXR FADC, similar to the temperature logging circuit. The binary input data is smoothed using the S/7 programme ADCNX before being shipped to the Eclipse, where the data is converted to engineering units and processed by a PID algorithm. The resulting temperature in the range 20-40°C is converted back to binary in the range 0-255 ($(8)^2$) and shipped back to the S/7, where the 0-255 BITS are converted to 8 BITS low voltage (+5VDC) output. These 8 BITS are then converted into the analog range +0-10VDC using a specially designed digital to analog (D/A) converter, shown in Fig. 5.14, for input to the C.S.R. thyristor regulator, which completes the feedback **CONTROL** loop by connection to the heater. A block diagram of the computer control procedure is shown in Fig. 5.15.

5.8 Conclusion

Computer timing, control and temperature and flowrate logging have been included into the regenerator design. This has been achieved using the departmental interfacing and computer system.

Chapter 6

Apparatus Commissioning

6.1 Introduction

This chapter discusses instrument calibration, initial equipment break down, individual item commissioning and leads up to full manual and computer operation. However during these routine commissioning procedures two phenomena were discovered: inconsistent errors in certain temperature measurements caused by radiation effects from the resistance heaters, and varying inlet temperatures to the test bed section caused by thermal inertia of the common pipework.

6.2 Radiation Effects on the Resistance Thermometers

Initially the front end section was used to calibrate the resistance thermometers by noting the resistance change using the departmental Digital Volt Meter (D.V.M.), to the nearest ohm for a step temperature rise produced by the banks of three variac heaters, for a known flowrate.

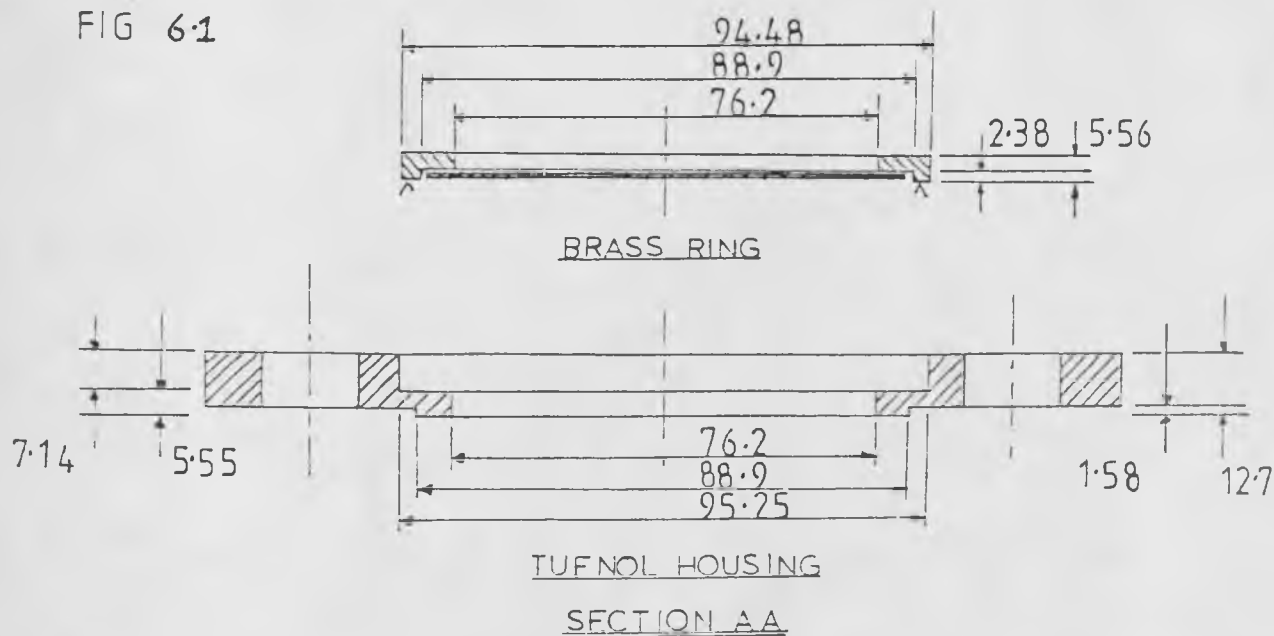
The steady state temperature was attained to the nearest 0.1°C , by two mercury thermometers MT1 and MT2 shown in Fig. 3.7. However it was discovered that MT2 (downstream of the packed bed) was always indicating a temperature 2°C less

than MT1 upstream of the packed bed for a flowrate of $0.0314 \text{ M}^3/\text{S}$. Initially this discrepancy in temperature was thought due to the two thermometers not being calibrated accurately. Two new (pre calibrated) thermometers were used and the same temperature discrepancy was seen. Heat loss along the front end section was then suggested, but a steady state calculation was performed and suggested that if this was the case then the temperature discrepancy should only be $1/10$ th of that seen. The resistance thermometers were then calibrated downstream of the front end packed bed and the slopes of the calibration curves were noted to be different to those taken upstream of the packed bed.

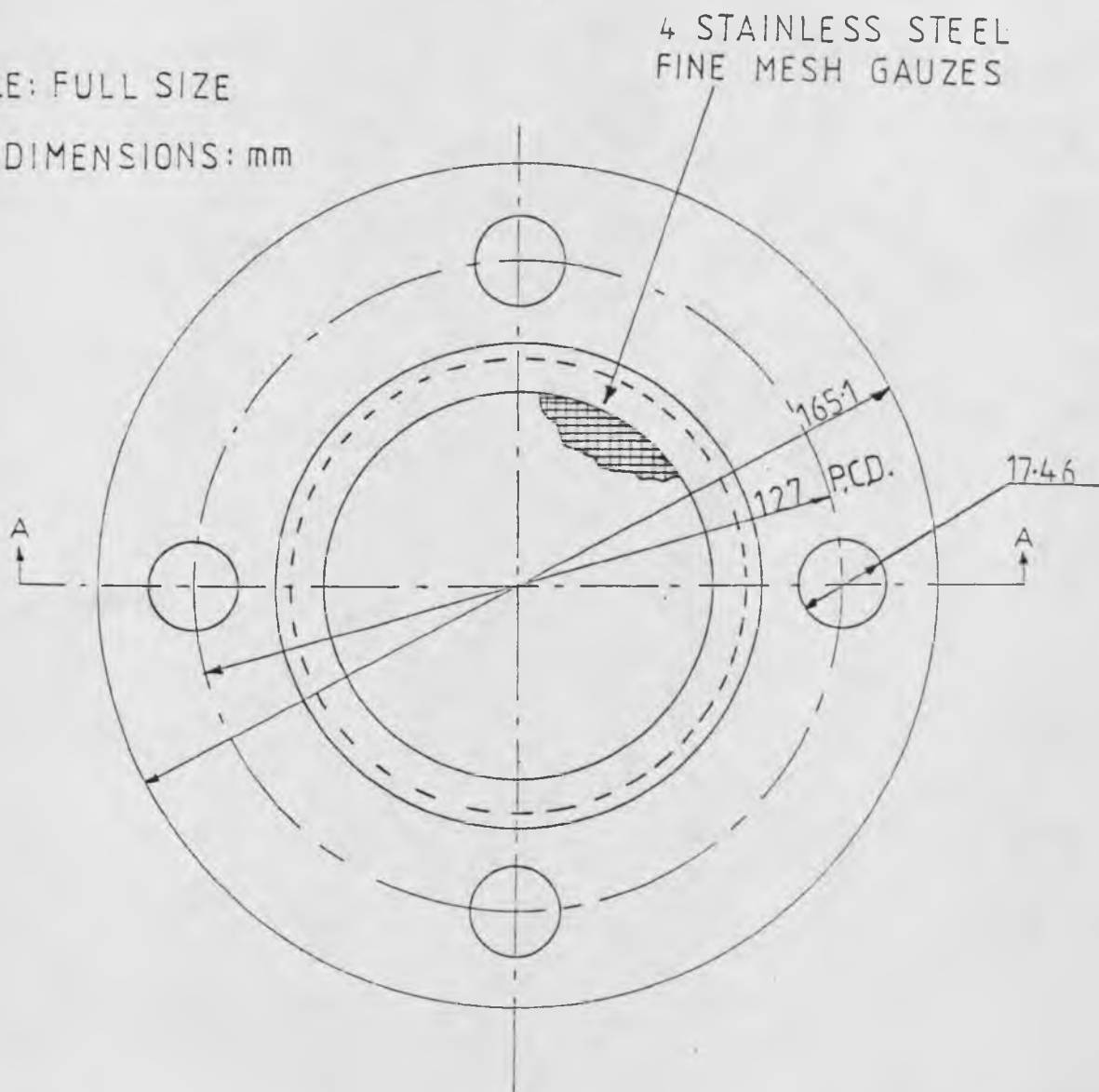
The heater elements were removed from the front end section and observed for a small voltage increase by the Variac. At only 15V the heater wires were seen to start to glow red. This suggested a radiation effect upon the resistance thermometers inevitably raising the temperature indicated by them above that predicted by convective heat transfer. This effect was validated by a steady state heat balance, including convective and radiative heat transfer as shown in Appendix F.

Calibration of the resistance thermometers could be undertaken downstream of the packed bed, where heater radiation effects were not present. However when the apparatus is in running condition heater radiation effects are prominent. To try and eliminate this effect

FIG 6-1

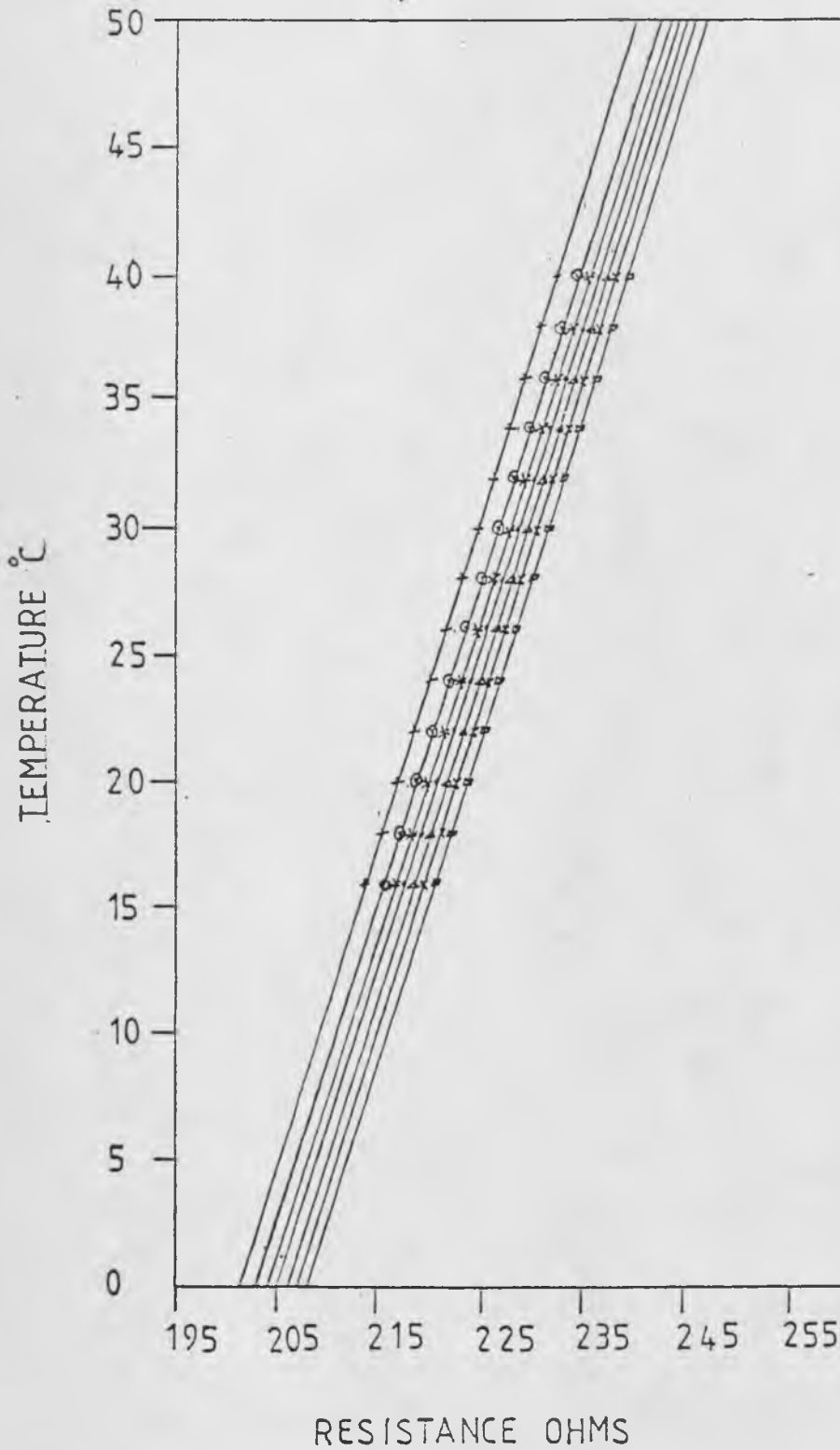


SCALE: FULL SIZE
ALL DIMENSIONS: mm



RADIATION SHIELD AND TUFNOL HOUSING

FIG 6.2 GRAPH OF TEMPERATURE Vs RESISTANCE FOR ALL SEVEN RESISTANCE THERMOMETERS (RT)



R.T. SEE FIG 3.7	SYMBOLS
1	□
2	△
3	.
4	*
5	+
6	x
7	○

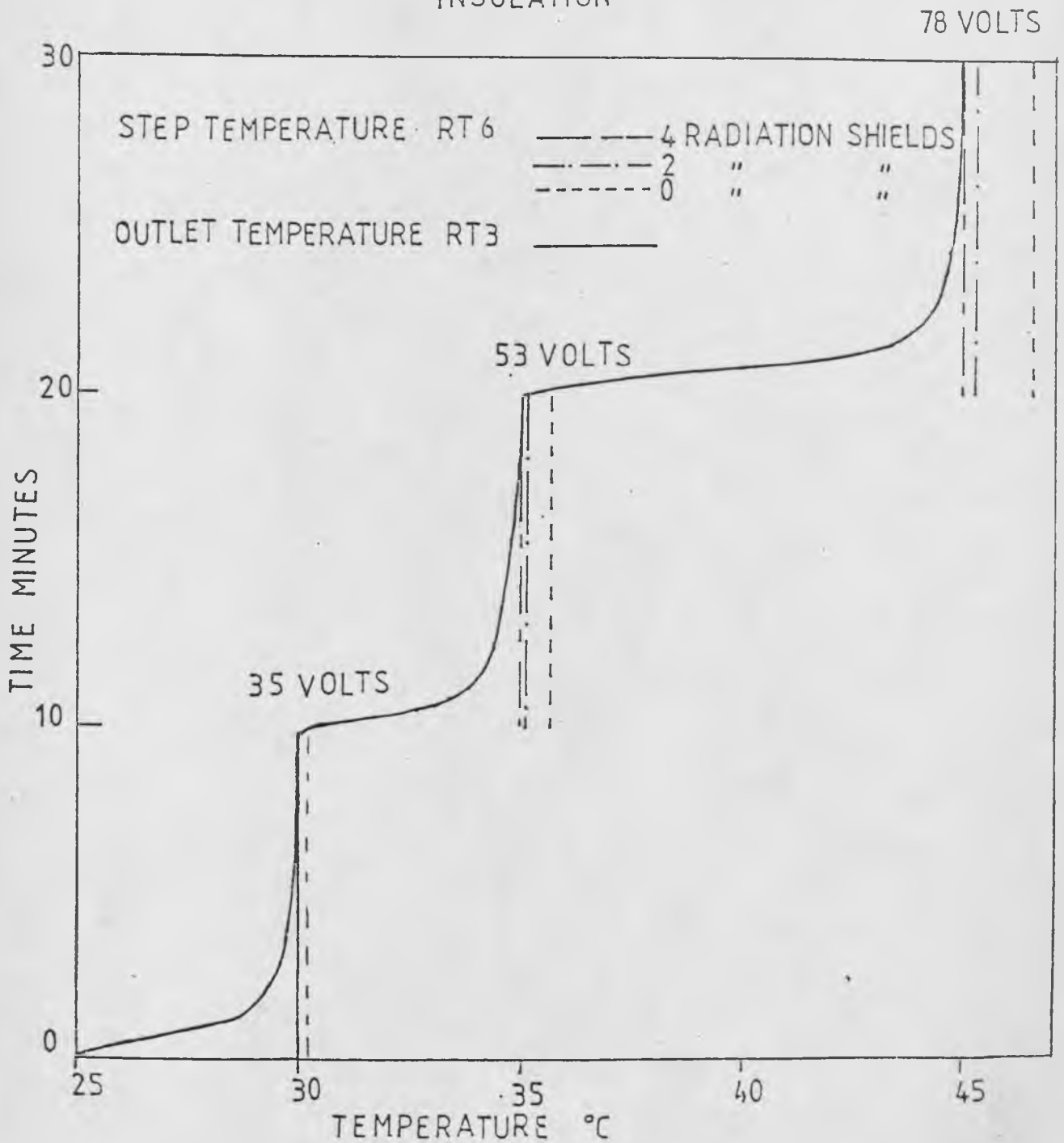
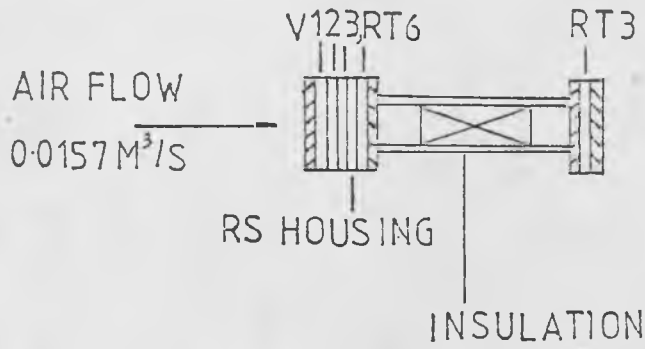
Table 6.1Wheatstone Bridge Resistance Values

Temperature Range : 25 - 45°C

Resistance Thermometer	(Resistance Ω)						
	Ps	Q	qs	qv	R	rs	rv
1	33	333	270	63	22.9	18	4.9
2	33	322	270	52	24.38	18	6.38
3	33	318	270	48	24.4	18	6.4
4	33	315	270	45	24.7	18	6.7
5	33	331	270	61	23.1	18	5.1
6	33	335	270	65	23.5	18	5.5
7	33	335	270	75	23.3	18	5.3

Resistance values correspond to Fig. 4.11

FIG 6-3 RADIATION SHIELD TEST RUNS
ANALYSIS OF RECORDED TEMPERATURES FOR
A STEP HEAT INPUT



a specially designed radiation shield and housing was constructed, as shown in Fig. 6.1. This provides easy location into the horizontal front end and test bed and the capability of housing up to four 60 mesh stainless steel shields in each housing.

The resistance thermometer calibrations were repeated, but this time using a Wheatstone bridge, balanced by a Decade resistor box capable of producing resistance change down to 0.01 ohm. The actual resistance of the thermometer can then be obtained by simple multiplication. This method produces a 0.05% error in resistance determination rather than the 5% error introduced by the D.V.M. because it can only indicate resistance to the nearest ohm over the resistance thermometer range. A graph of the thermometer resistance change over a set temperature range is given in fig. 6.2. All seven resistance thermometers were located in the front end for calibration and the resistance values were taken prior to the input to the wheatstone bridges, to allow for the finite resistance of the 1 mm Farnell circuit wire. The final resistance values of the calibrated wheatstone bridges are shown in Table 6.1. The individually constructed thermometers resulted in slightly dissimilar resistances, consequently each wheatstone bridge circuit is unique.

To examine the effect of heater radiation on a resistance thermometer the front end was set up as shown in fig. 6.3, with a resistance thermometer (RT 6) separated from 3

variac heaters by a radiation shield housing. With 0, 2 and 4 stainless steel meshes within the housing three step temperature changes were performed, for an air flowrate of $0.0157 \text{ M}^3/\text{S}$. The resulting temperatures were indicated by resistance thermometers RT6 and RT3. Fig. 6.3 clearly shows how the presence of radiation shields can eliminate the effect of radiation. Resistance thermometer RT6 with no gauzes present is always indicating a temperature greater than RT3, which is assumed to be the correct temperature. However with 4 gauzes present RT6 approximately indicates the same temperature as RT3. Consequently, a radiation shield housing containing 4, 60 mesh gauzes is always placed between a heater and resistance thermometer.

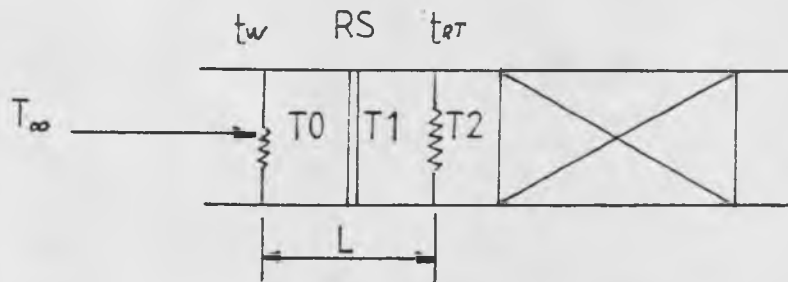
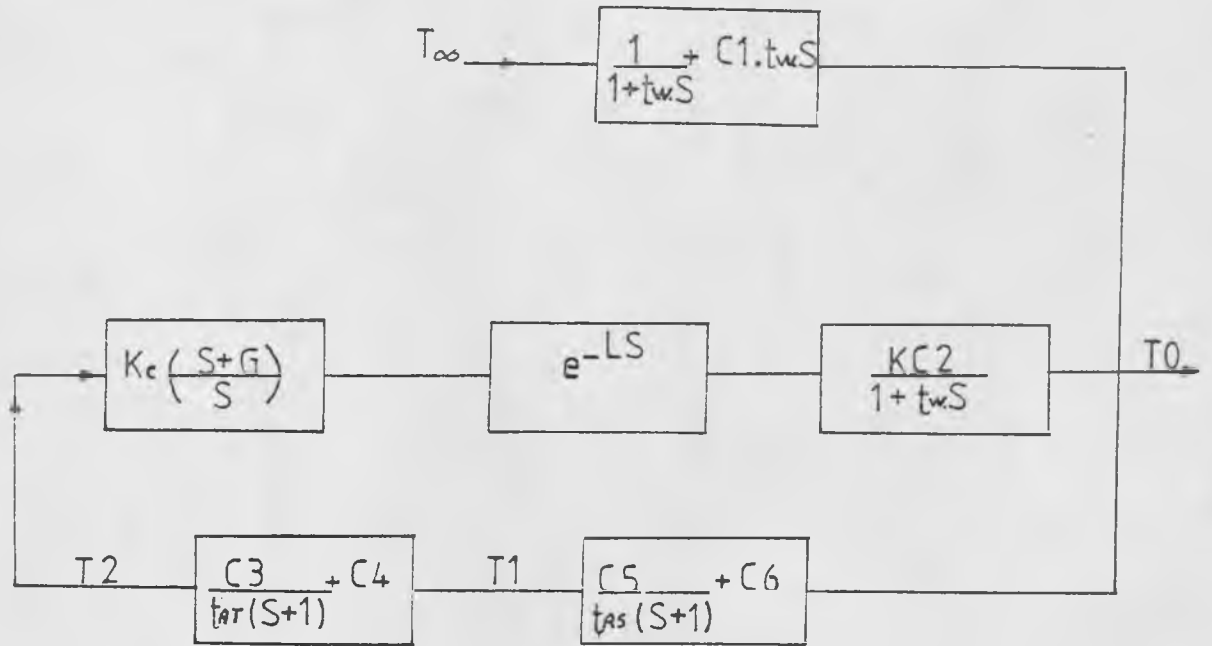
6.3 Control of the Inlet Temperature to the Test Bed Section

As discussed earlier, the proposed method of air temperature control prior to the front end packed bed is by either analog PI or computer PID control. Each method has been fully commissioned.

6.3.1 Computer Control

The required hardware circuitry has been discussed in Chapter 5. In order to obtain a true representation of the front end control section, especially with the heater and resistance thermometers of such low time constant

FIG 6.4



$$C2 = \frac{h_w A'_w}{\rho_g C_g V_g} \quad C1 = 1 - C2$$

$$C4 = \frac{h_{RT} A'_{RT}}{\rho_g C_g V_g} \quad C3 = 1 - C4$$

$$C5 = \frac{h_{AS} A'_{AS}}{\rho_g C_g V_g} \quad C6 = 1 - C5$$

CONTROL BLOCK DIAGRAM REPRESENTING
THE FRONT END

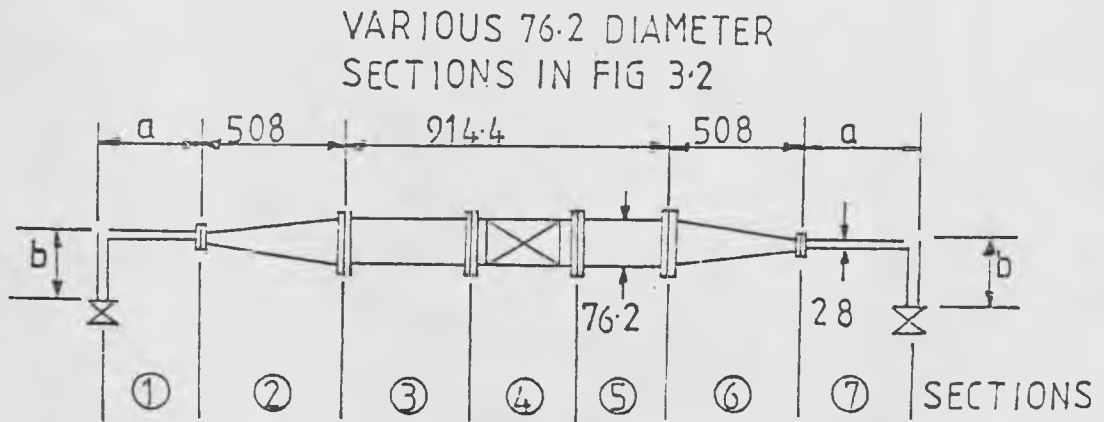
(19 and 6.2 milli seconds respectively at $0.0157 \text{ m}^3/\text{S}$ ($2000 \text{ ft}^3/\text{h}$)) the following block diagram of the system was produced as shown in fig. 6.4. This representation of the control section would produce a 5th order system very difficult to analyse using normal control procedures as shown by Pollard (1971). However using the Runge Kutta Merson technique obtained from Lance (1960) to solve the ordinary differential equations representing the heat balances over the control section, as shown in Appendix G, the response of the system can easily be produced for a known flowrate and step temperature. The Ziegler Nichols (1942) method was then applied to the theoretical response to provide the proportional constant (k_c), integral time (T_i) and derivative time (t_d) values for input to the PID algorithm, equation 6.1, used in SJHREGEN and shown in Appendix G.

$$q = k_c e + K_c T_d \left(\frac{de}{dt} \right) + \left(\frac{k_s}{T_i} \right) \int e dt + q_0 \quad (6.1)$$

6.3.2 Analog Control

The analog controller arrived with an integral time constant of 5 minutes as discussed in Chapter 4. The original capacitance within the R.C. circuit was replaced by one of value $0.0333 \mu\text{F}$ which provides an integral time constant of one second. With this fixed capacitance, runs over the required flowrate range were used to find the appropriate proportional band setting of 80%.

FIG 6.5



$$a+b = 736.6 = \textcircled{1} = \textcircled{7}$$

ALL DIMENSIONS : mm

NOT TO SCALE

TEST BED SECTIONS USED IN THE
MISP PROGRAM

Table 6.2

Data Required for a MISP Program Run to Examine a 4 inch (101.6 mm) packed bed section with internal insulation and a flowrate of 0.001 and 0.0463 M³/S

Sections According to Fig. 6.5

Units	1	2	3	4	5	6	7	Variable
kg/sm ²	27.86	0.707	0.299	0.276	0.299	0.707	27.86	G min
kg/sm ²	125.03	31.796	6.647	12.37	6.647	31.796	125.09	G max
w/m ²⁰ C	15.81	3.578	2.417	50.82	2.417	3.578	15.81	Laminar h
w/m ²⁰ C	319.24	100.39	50.19	637.23	50.19	100.39	319.24	Turbulent h
J/kg ⁰ K	1004.8	1004.8	1004.8	1004.8	1004.8	1004.8	1004.8	Cg
mm	4.511	6.0	12.192	3.17	12.192	6.0	4.511	Tube thickness
*w/m ⁰ C	119.4	194.23	88.65	45.52	88.65	194.23	119.4	Thermal conductivity
m ² /s	3.51x10 ⁻⁵	5.77x10 ⁻⁵	2.58x10 ⁻⁵	1.26x10 ⁻⁵	2.58x10 ⁻⁵	5.77x10 ⁻⁵	3.5x10 ⁻⁵	Diffusivity
m ² /m ³	59.05	33.41	39.18	1192.43	389.18	33.41	59.03	Area/unit volume
m ²	6.13x10 ⁻⁴	2.28x10 ⁻³	4.94x10 ⁻³	4.56x10 ⁻³	4.94x10 ⁻³	2.28x10 ⁻³	6.13x10 ⁻⁴	X sectional area
-	0.852	0.894	0.742	0.37	0.742	0.894	0.852	Voidage
m	0.444	0.508	0.6096	0.1015	0.406	0.508	0.444	Length

* The conductivity values allow for the mild steel flanges used for coupling

Minimum superficial flowrate = 0.0011 M³/S; Re = 100

Maximum superficial flowrate = 0.0463 M³/S; Re = 4,500

where $Re = \frac{G D}{\mu}$ and $Pv = 0.37$

6.4 Thermal Inertia

During the initial counter current test runs on the apparatus, it was discovered that the hot and cold inlet temperature profiles were not constant as expected, but varied with time. The common peripheral pipework to the counter-current flows were acting as additional heat sinks and sources, as shown by Heggs and Hollins (1978). A copy of this paper is shown in Appendix H. The pipework and the test bed section were simulated by the MISP program (1977). In the simulation the apparatus was split into seven sections, as shown in fig. 6.5. The program uses a finite difference technique to process the thermal response of up to sixteen different regenerator sections, subject to Schumann assumptions. Table 6.2 lists the data for a 4 inch (101.6 mm) bed for superficial flowrates of 0.0011 and 0.0463 M³/S. The heat transfer coefficients for the pipe sections 1 to 3 and 5 to 7 were obtained using equation 6.2, taken from Krieth (1973)

$$Nu = 0.023 \left(1 + (D/L)^{0.7} \right) / Re_D^{0.2} * Pr^{0.67} \quad 6.2$$

Heggs (1967) equation for spheres shown in table 3.1, was used to obtain the overall convective heat transfer coefficient for a packed bed of $\frac{1}{8}$ inch (3.18 mm) steel spheres. The MISP program was used to simulate a 12" and 4" bed section comprising $\frac{1}{8}$ inch diameter steel spheres with 1 mm and 3 mm internal insulation and switching times of 1 and 10 minutes for flowrates of 0.0011 and 0.0463 M³/S.

FIG 6.6 GRAPH OF MISP OUTPUT
REGENERATOR BED TEMPERATURE Vs DISTANCE

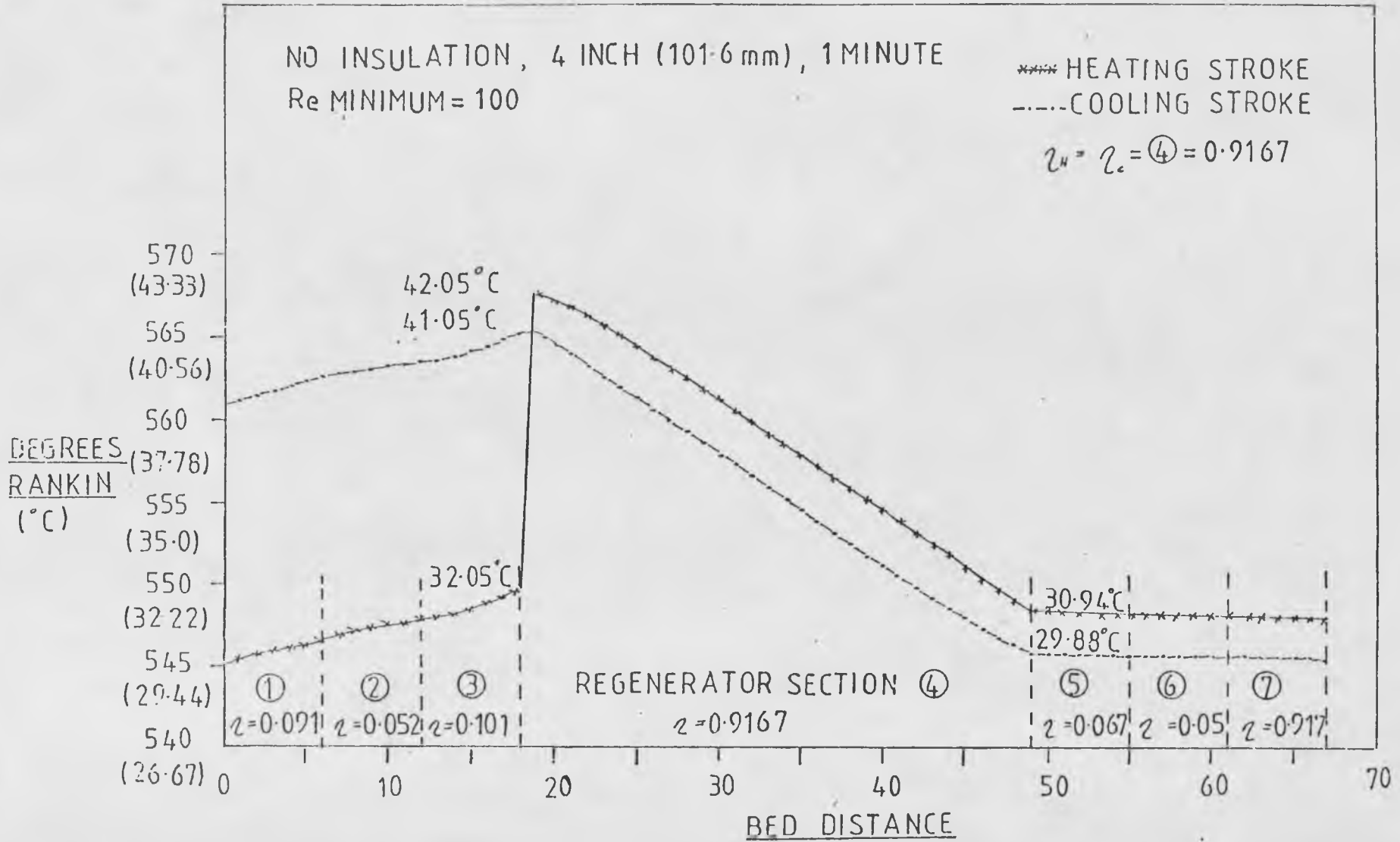


Table 6.3

MISP Output for the Seven Regenerator Sections

The MISP program was used to examine the following system, using a convergence factor of 0.0001

No insulation in the Apparatus

1 mm " " " "

3 mm " " " "

Time periods of 1 and 10 minutes

Reynold numbers : Re MIN = 100, Re Max = 4,500

Bed Section lengths 4 inch and 12 inch (i.e. section 4)

$\frac{1}{8}$ inch (3.17 mm) steel ball bearings are used as the regenerator packing.

Six runs, including all seven section efficiencies will be tabulated first. The remaining runs will just include the efficiencies for the packed bed section.

Time = 1 minute, bed length = 101.6 mm, Re = 100

Efficiencies for the heat stroke, according to the
section in Fig. 6.5

Run	Insulation State	1	2	3	4	5	6	7
1	No	0.0913	0.052	0.1005	0.9167	0.0678	0.0521	0.0971
2	1 mm	0.0913	0.0479	0.0952	0.9167	0.0633	0.048	0.0918
3	3 mm	0.0913	0.0415	0.0877	0.9164	0.0482	0.0412	0.0917

Time = 10 minutes, bed length = 101.6 mm, Re = 100

4	No	0.0819	0.0516	0.1011	0.8717	0.0767	0.540	0.1008
5	1 mm	0.0819	0.0476	0.0959	0.8718	0.0667	0.0496	0.101
6	3 mm	0.0818	0.0412	0.0869	0.8719	0.0517	0.0427	0.1022

Run	Insulation State	Time Minutes	Length mm	Re	η_H	η_C
7	No	1	304.8	100	0.9736	0.9681
8	1	1	304.8	100	0.9736	0.9681
9	3	1	304.8	100	0.9777	0.9681
10	No	10	304.8	100	0.9653	0.9663
11	1	10	304.8	100	0.9664	0.9664
12	3	10	304.8	100	0.9668	0.9666
13	No	1	101.6	4,500	0.3116	0.3116
14	1	1	101.6	4,500	0.3116	0.3117
15	3	1	101.6	4,500	0.3117	0.3118
16	No	$\frac{1}{2}$	101.6	4,500	0.5564	0.5565
17	1	$\frac{1}{2}$	101.6	4,500	0.5565	0.5566
18	3	$\frac{1}{2}$	101.6	4,500	0.5565	0.5566

Table 6.4

Regenerator Section Time Constants

Time = 10 minutes

Re = 100 packed bed superficial velocity = $0.0011\text{M}^3/\text{s}$

Insulation state = None

Packing length = 101.6 mm

Section	Π	A	$(\rho_s C_s)$	h	$\frac{\rho_s C_s}{hA}$
1	1.11	59	504	15.8	0.541
2	0.20	33	357	3.6	3.00
3	0.064	39	887	2.41	9.437
4	16	1192	2276	50.8	0.0376
5	0.064	39	887	2.4	9.437
6	0.20	33	357	3.6	3.00
7	1.11	59	504	15.8	0.541

Initial temperature profiles of 30°C were used with a step temperature on the hot stroke of 10°C. A typical system temperature response at cyclic steady state for one of the runs is tabulated in table 6.3 and shown in figure 6.6

The pipework heat capacity causes the design temperature change from 30 to 40°C within the regenerator to be exceeded. The inlet cold temperature remains at approximately 30°C, however the inlet hot temperature starts above 40°C. This extra temperature rise emanates from the pipework heat capacity upstream of the heater. When calculating the hot and cold efficiencies not only has the mean hot and cold outlet temperatures, with time to be found, but the mean inlet temperatures with time have also to be evaluated. This being a consequence of the peripheral pipework. In theoretical modelling however, it is assumed that the hot and cold inlet temperatures are constant. Each peripheral pipe section acts as a small regenerative system and therefore has an associated efficiency, as shown in fig 6.6 and table 6.3. In comparison to the packed bed efficiencies, around 90%, the peripheral pipework sections produce efficiencies in the range 4 to 10%.

Apart from the graphs obtained using the MISP program, a rough indication of the magnitude of the affect of the peripheral pipework can be found by examining the time constant of each section, as shown in table 6.4.

$$\text{where time constant} = \tau = \frac{\rho C_s}{h A} \quad 6.3$$

Table 6.5MISP Output for Just a 4 inch (101.6 mm) Packed Bed

Run	Insulation State	Time Minutes	Length mm	Re	η_H	η_C
1	1	1	101.6	100	0.9169	0.9164
2	1	10	101.6	100	0.8732	0.8732

Intuitively one would expect the pipework to reach cyclic steady state first, however the controlling factor of the whole regenerative system is the peripheral pipework. This is clearly shown by comparing the time constants for sections 3 and 5 (9.437 seconds) with the packed bed section (0.0376 seconds).

The effect of the extra heat capacity by the peripheral pipework on the temperature profiles could not be changed, however it was necessary to examine whether the pipework significantly affected the efficiency of the packed bed section in comparison to a single regenerator section without peripheral pipework. The MISP program was rerun for a single packed bed section, i.e. section 4. Tables 6.3 and 6.5 clearly show that the efficiencies between the seven sections set up and single unit are within measurable accuracy for the data used. This was true over the whole range of possible practical investigations. However the number of cycles ^{REQUIRED} to reach cyclic steady state is vastly increased from 4 for the single packed bed section to 16 for the seven section system.

6.5 Further Rig Commissioning

The commissioning of the apparatus was carried out in three distinct phases; analog, mechanical, and then computer aspects.

6.5.1 Analog Commissioning

The timing circuitry, as discussed in Chapter 4, after design and construction suffered from premature switching caused by back e.m.f.s. These effects were prevented by correct positioning of R.S. diodes 1N1004. When the timing procedure was fully operational the internal R.C. circuit was adjusted to produce repeatable time periods accurate to the nearest $1/10$ th of a second (0.33% error in one minute period). All three power supply voltage outputs were checked to be in the correct range. The Kent mark 3 recorder was initially calibrated in the range 0 - 25 mv by a decade voltage source capable of producing 10 - 0.001 mvs. The subsequent temperature indication in the range 25 - 45°C was $\pm 0.05^\circ\text{C}$ i.e. 0.5% error. The Kent mark 3 recorder performance was initially acceptable but began to deteriorate over the numerous commissioning and set up runs. Eventually a major overhaul was required replacing many integral parts.

6.5.2 Mechanical Commissioning

Pressure testing of the apparatus was carried out in three distinct sections, up to 30 psig. This was undertaken

in order to isolate precisely any leaks from the apparatus. The front end was the first section tested, with solenoid valves SV1 and SV2 closed according to fig. 3.7 and the pressure indicated by a Norgren 2 inch (50.8 mm) O (1) 30 psig pressure gauge mounted on the pressure release valve. The regenerator section was then tested up to 30 psig using the Negretti and Zambra pressure gauge, by blocking off at the 28 mm pipe prior to the chimney diffuser, whilst opening the hot solenoid valves. Finally the whole regenerator section was pressure tested 'blocking off' the air at the orifice plate unit. The whole apparatus, after attending to minor leaks around welded points and applying P.T.F.E. tape to screwed fittings was then pressurized up to 30 psig and attained a half life of 10 hours. During running conditions whenever the test bed was broken to allow installation of different packings, the appropriate rubber seals were examined and where found faulty were replaced and the whole apparatus re-pressure tested.

Initial runs on the apparatus were concerned with attaining a cyclic steady state according to the temperature set by the front end. With the additional peripheral pipework this action took considerable time depending on the set point temperature of the front end, even though the highest flowrate possible for the installed orifice was used. During these runs when initial cyclic steady state had been reached it was discovered that although resistance thermometers RT4 and RT5, with reference to fig 3.7, should have been recording the same temperature they were about 0.3°C dissimilar. Co and countercurrent

operation was used with varying degrees of heat input and flowrate to examine this discrepancy, and it was discovered that this temperature difference was a factor of flowrate only. The lower the flowrate the greater the temperature difference. This difference in temperature was reduced somewhat by placing turbulent promoters in each of the diffuser sections. These were canisters 3 inch (76.2 mm) inside diameter by $2\frac{1}{2}$ inch (63.5 mm) long, containing compact steel wool held in position by stainless steel 6 mesh and located in the straight section of the test bed diffusers. Test runs carried out after the installation of these two additional heat capacity sections showed that the jetting effect was significantly reduced but not eliminated.

6.5.3 Computer Commissioning

The 308 non-inverting operational amplifiers exhibited excellent drift characteristics and the noise effect was reduced to a minimum using an R.S. circuit design offering an improved noise reduction. Calibration for hardcopy and graphical output was performed on the Eclipse S/130 by logging the temperature change over the full 20°C range for all six resistance thermometers. This was necessary because the Fast Analog to Digital converter uses emitter follower circuitry of which the gain is always just greater than one. The front end control temperature indications were treated in the same way.

FIG 6.7

GRAPH OF WATER MANOMETER HEIGHT Vs
VOLTAGE FOR CALIBRATION OF THE D/P-
EMITTER FOLLOWER CIRCUIT

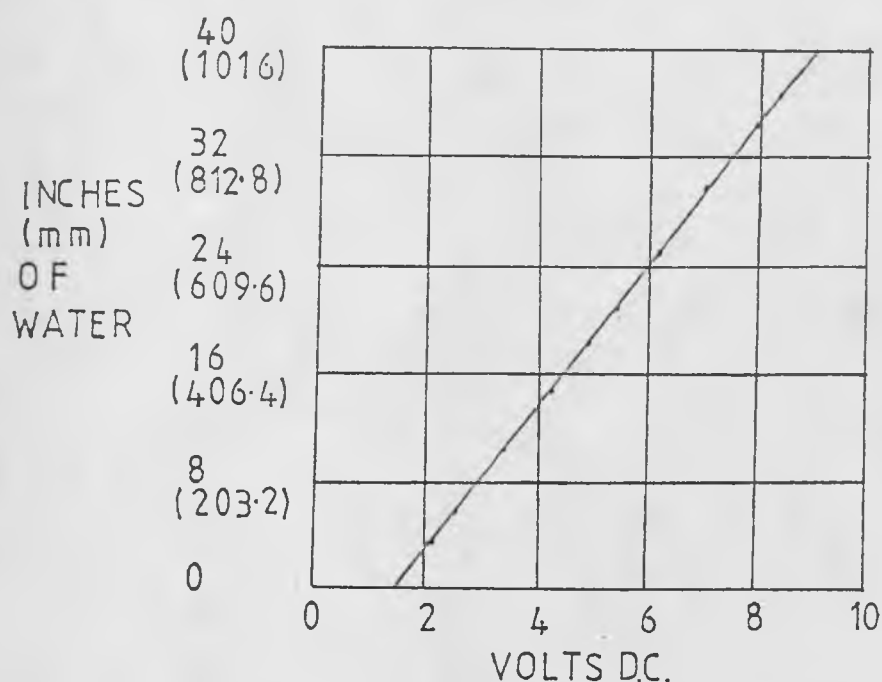
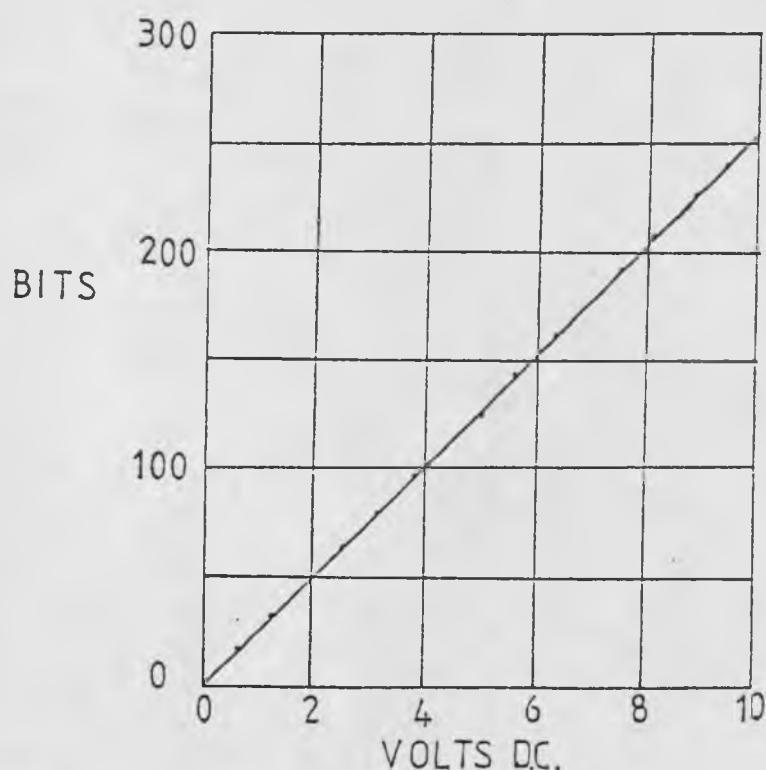


FIG 6.8

GRAPH OF BITS Vs VOLTAGE OUTPUT
FOR THE D/A CONVERTER



BCD	BITS
00	0
04	64
08	128
0C	192
FF	256

Calibration of the ME13DM Foxboro differential pressure cell was carried out according to the Foxboro manual (1975). The differential pressure cell was originally calibrated to produce 4 to 20 mA for a differential pressure of 0-40 inches (1016 mm). However due to the additional emitter follower circuit required after the voltage resistor, see fig. 5.4., and the emitter follower circuit present in the F.A.D.C. a differential pressure input was applied 0-40 inches (0 - 1016 mm), for the smallest orifice plate, measured on the Negretti and Zambra 0(1)40 inch water manometer. The resulting binary output was printed out on the S/7 teletype station. This was then reduced to a voltage range as shown in fig 6.7 and plotted against the differential pressure. The slope of this curve was then used to produce inches of water for a known binary, hence voltage range in SJHREGEN on the Eclipse.

The timer circuitry before contact with the S/7 was initially activated by a 5 volt source. After contact with S/7, timing was activated primarily by the S/7 and then by SJHREGEN on the Eclipse.

The final item of computer commissioning was the feed back control loop incorporating the Digital to Analog (D/A) converter. This was designed to change 0-255 (2^8) bits representing a 20°C range into the voltage range 0-10 VDC for input to the CSR Thyristor regulator. After construction the unit was connected up to the S/7 and the above bit range was fed to the A/D convertor by the S/7

producing the following voltage output as shown in fig. 6.8, which was satisfactory.

All the necessary data acquisition room connections are given in the departmental computer users log book (1978). 15 core 0.1 mm screened cable is used throughout, with 3 amp terminal blocks used for necessary connections. To help with the commissioning a telephone link was installed from the apparatus room to the computer room. During the initial stages of the computer commissioning De multiplexer and Digital in multiplexer breakdown was common, but was eventually rectified as shown in the departmental computer users log book (1978).

6.6 Chapter Conclusions

The apparatus was fully commissioned, as discussed above. However the formulation of a running procedure and technique to produce heat transfer coefficients was required. The derivation of these two concepts will be discussed in Chapter 7.

Chapter 7

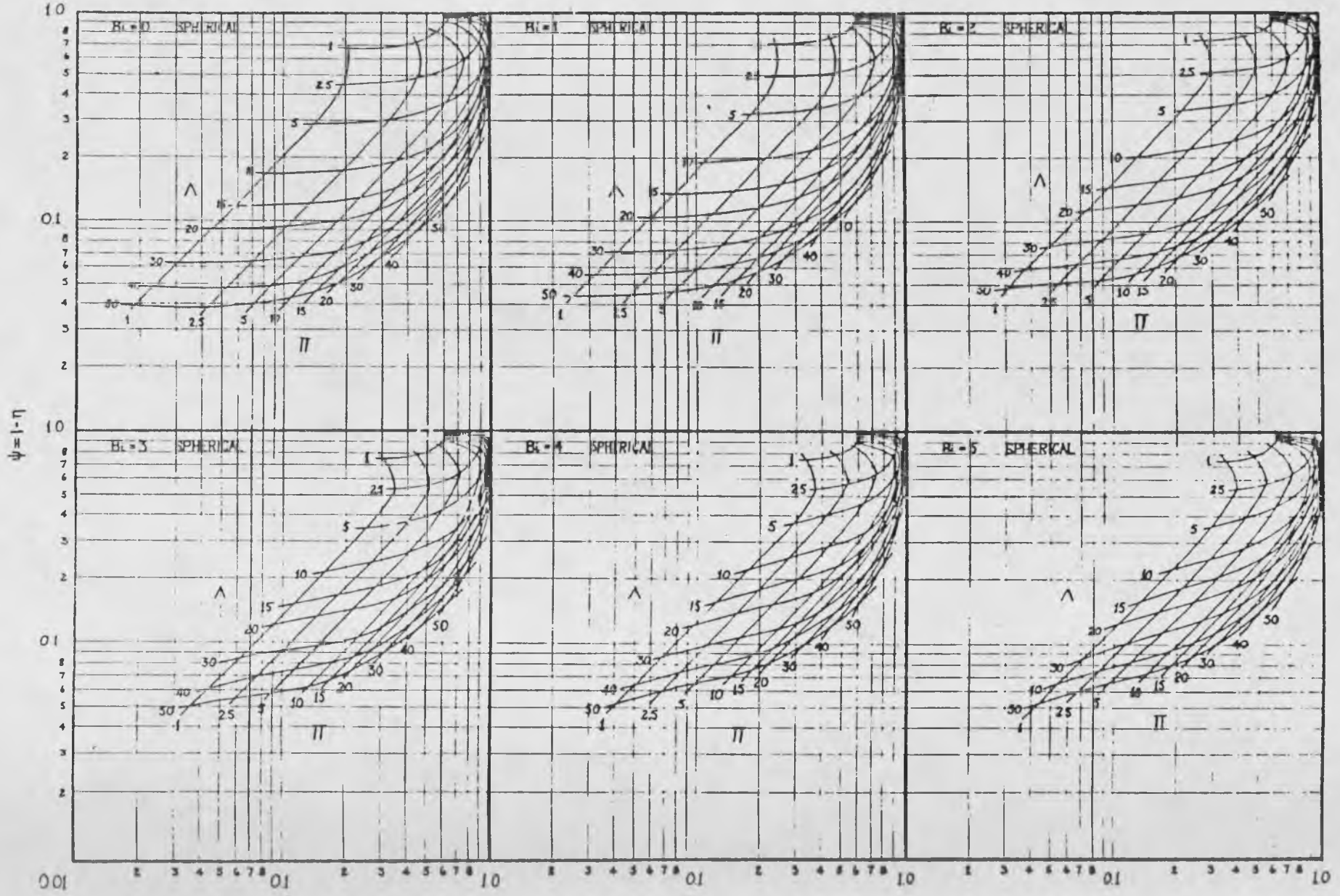
Experimental Programme

7.1 Introduction

A theoretical examination of thermal regenerator design has been recently conducted by Carpenter (1976). Attention focused around thermal regenerator characteristics for the Schumann assumptions, discussed in chapter 1, and intraconduction effects experienced in low thermal conductivity packings. The severity of intraconduction is represented by the Biot number (hD/k) as shown by Heggs et al (1980). Fig. 7.1 shows one of Heggs et al's graphs of log inefficiency against log dimensionless temperature swing for Λ and Π , for various values of Biot number. This graph is for spheres only and shows how a gradual increase in intraconduction (Biot number $0 \rightarrow 5$) increases the dimensionless temperature swing whilst decreasing the efficiency for a fixed Π and Λ . Carpenter also concluded that practical packing to fluid heat transfer coefficient data is inadequate, and correlations that do exist are only specific to certain areas and types of regenerator operation.

However, experimental data from any regenerator apparatus will include the efficiencies and the arrangement parameters, e.g. flowrate, period, bed length, fluid heat capacity, solid heat capacity and total surface area. The heat transfer

FIG 7-1 HEGGS ET AL INTRA CONDUCTION DESIGN CHART FOR SPHERICAL PACKINGS



coefficient must then be obtained from the charts of Hausen (1929) or Pieser and Leiner (1953). Such a procedure would require iteration because the parameters Λ and Π , each include the heat transfer coefficient. The ratio of Π to Λ however does not include the heat transfer coefficient and in fact only includes measurable regenerator parameters, as shown below:-

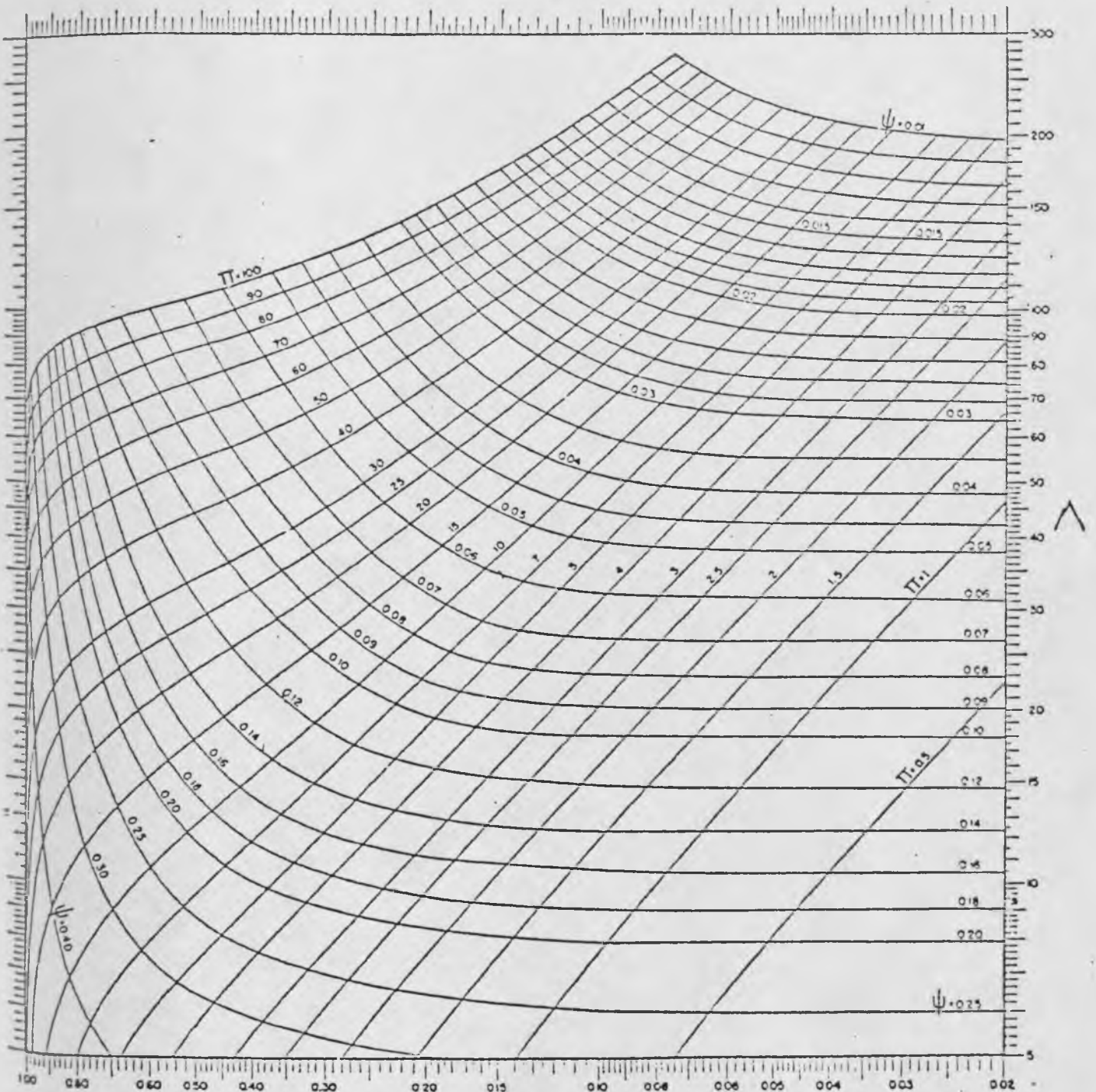
$$\frac{\Pi}{\Lambda} = \frac{w \cdot C_g \cdot P}{M \cdot C_s} \quad (7.1)$$

where: w = superficial mass flowrate (kg/s)
 C_g = Specific heat of the fluid (kj/kgK)
 P = Time period (s)
 M = Mass of packing (kg)
 C_s = Specific heat of the packing (kj/kgK)

This ratio is called the utilisation factor, and if charts of η versus utilisation factor for a range of Λ values are available, then iteration for the heat transfer coefficient determination is avoided.

An experimental programme was therefore designed to use a simple, quick and accurate method of obtaining convective heat transfer coefficients for various values of Λ (5 \rightarrow 25) and utilisation factor Π/Λ (0 \rightarrow 2.0) and to examine spherical packings of various thermal conductivity, as Π changes. This would perform the following functions:

FIG 7.2 PEISER AND LEHNER'S DESIGN CHART FOR SYMMETRIC REGENERATORS



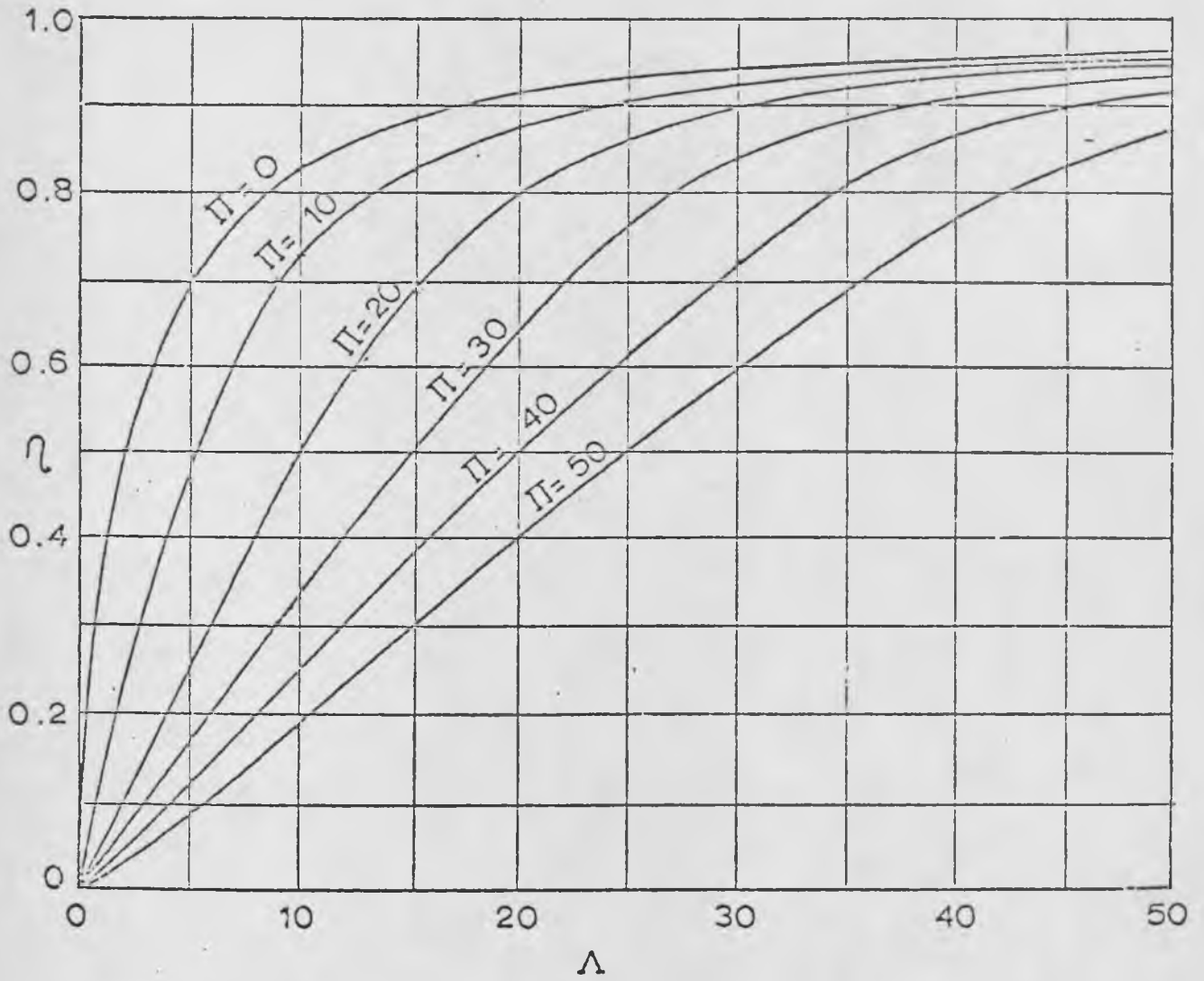
δT
 DIMENSIONLESS EXIT TEMPERATURE SWING
 $\psi = 1 - \eta =$ INEFFICIENCY

Produce a technique to provide overall heat transfer coefficients for the majority of thermal regenerator packings, obtain and provide data for producing correlations of overall heat transfer coefficients and show the practical effect on regenerator efficiency as Π , Λ and Bi are changed. Previous MISP programme runs and examinations of the Heggs et al chart at Bi = 0, Fig. 7.1, and the Peiser and Lehner design chart Fig. 7.2, showed that provided Π/Λ was ≤ 2.0 the regenerator efficiency would always be in the range $0.45 \leq \eta \leq 0.91$ for $\Lambda = 5$ to 25. The concept of a number of runs, ie. real time changes for a known set-up (regenerator arrangement) would therefore need simulating in order to predict values for the actual number of cycles required to reach equilibrium.

7.2 Choice of Packing

In order to highlight intraconduction effects it was decided to use spherical packings of different thermal conductivity. This geometrical shape was used to approach as close as possible remaining Schumann assumptions. Three types of materials have been examined:-

Steel ($\frac{1}{4}$ inch, 6.35mm) $K_{st} = 45.7$ (w/mk)
 $\rho_{st} = 7849.1$ (kg/m³)
 $C_{st} = 0.461$ (kj/kgK)
 $\alpha_{st} = 1.263 \times 10^{-5}$ (m²/s)

FIG 7.3 HAUSEN'S EFFECTIVENESS CHART

Lead glass (6 mm)

$$K_{g1} = 3.116$$

$$R_{g1} = 2948.6$$

$$C_{g1} = 0.287$$

$$\alpha_{g1} = 3.682 \times 10^{-6}$$

$$\frac{K_{g1}}{K_{st}} = 0.068$$

$$\frac{(R_{g1} C_{g1})}{(R_{st} C_{st})} = 0.234$$

Alumina ($\frac{1}{2}$ inch 12.7mm)

$$K_a = 2.093$$

$$R_a = 1842.1$$

$$C_a = 0.8573$$

$$\alpha_a = 1.357 \times 10^{-6}$$

$$\frac{K_a}{K_{st}} = 0.046$$

$$\frac{(R_a C_a)}{(R_{st} C_{st})} = 0.426$$

The packing data was obtained from Krieth (1973), Englass (1976) and Alcoa (1969) respectively. These three types of packing should show the gradual departure from the Schumann assumptions, because of the thermal conductivity decrease from steel at 45.7 to lead glass 3.116 and finally alumina 2.095 w/mk.

7.3 Apparatus Simulation

A simulation of the apparatus was undertaken to define a practical operating range. Using Hausen's (Fig. 7.3) and

Peisher and Lehnert's (Fig. 7.2) design charts, and with the information obtained from the initial MISP runs, it was found that provided the utilisation factor Π/Λ does not exceed 2 the regenerator efficiency will remain above 45% for a dimensionless length range (Λ) of 5 to 25. To examine the regenerator properties over the range Π/Λ 0 to 2.0 the real time period would have to be changed, however, there was no previous work to show whether the real time period should be increased or decreased over the range to be investigated. To obtain a feel for the most efficient way of operating the apparatus a simple Schumann assumption model was produced based on the work done by Carpenter (1976).

7.3.1 Model Solution

Under Schumann (1929) assumptions, heat balances on the fluid and solid phases over a small element of the regenerator in Eulerian co-ordinates result in the following equations:

$$\rho_s C_s \frac{\partial t}{\partial \theta} = -hA (t-T) \quad (7.2)$$

$$\frac{GC_g}{u} \frac{\partial T}{\partial \theta} + GC_g \frac{\partial T}{\partial y} = hA (t-T) \quad (7.3)$$

The associated boundary and thermal equilibrium conditions are:-

$$T = T_{HI}, y = 0 \text{ and } \Theta \leq \Theta \leq \Theta + PH \quad (7.4)$$

$$T = T_{CI}, y = 0 \text{ for co current operation, } y = L \text{ for} \\ \text{countercurrent and } \Theta + PH \leq \Theta \leq \Theta + PH + PC \quad (7.5)$$

$$t = f(y), 0 \leq y \leq L \text{ at } \Theta = \Theta \text{ and } \Theta + PH + PC \quad (7.6)$$

$$\Theta = n(PH + PC) \text{ where } n \text{ is an integer}$$

These equations are usually simplified by changing to Lagrangian co-ordinates as proposed by Schumann. This is done by the following transformations:

$$sL = \frac{hA}{\rho s C_s} (\Theta - \frac{y}{u}) \quad (7.7)$$

$$x = \frac{y}{L} \quad (7.8)$$

The heat balances are reduced to the following:

$$\frac{\partial t}{\partial sL} = (T - t) \quad (7.9)$$

$$\frac{\partial T}{\partial x} = \Lambda (t - T) \quad (7.10)$$

where: dimensionless length, $\Lambda = \frac{hAL}{GC_g}$

At the end of the true time period, where $\Theta = P$, the value of sL varies from $hAP/\rho s C_s$ at the inlet, to $\frac{hA}{\rho s C_s} (P - \frac{L}{u})$

at the exit. To simplify this situation, therefore, the

assumption is made that the residence time of the fluid at any point within the regenerator may be neglected in comparison to the total period, which is valid for the real time periods used on the apparatus. Thus the Lagrangian dimensionless time and period become Eulerian dimensionless time and period respectively.

$$sL = S = \frac{hA\Theta}{\rho sCs} \quad (7.11)$$

$$\Pi_L = \Pi = \frac{hAP}{\rho sCs} \quad (7.12)$$

The boundary and cyclic equilibrium conditions are now:-

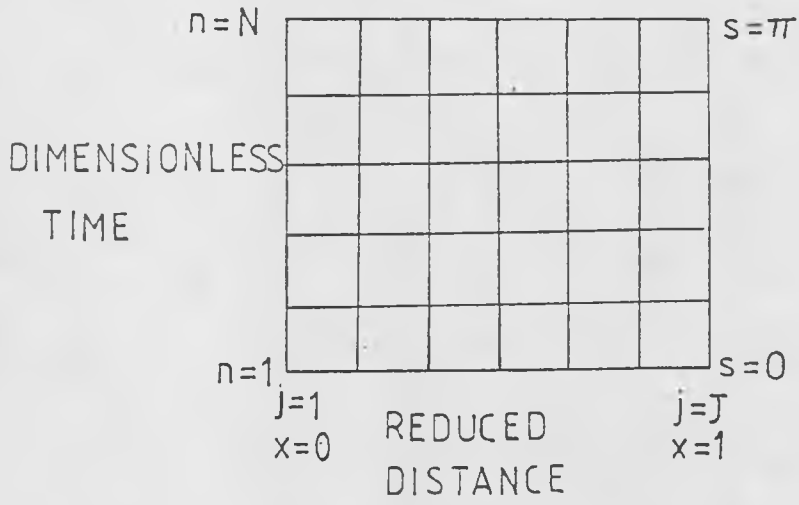
$$T = TH, \quad x = 0 \quad \text{and} \quad S \leq s \leq S + \Pi_H \quad (7.13)$$

$$T = TC, \quad x = 0 \quad \text{for co current and} \quad x = 1 \quad \text{for counter-current and} \quad S + \Pi_H \leq s \leq S + \Pi_H + \Pi_C \quad (7.14)$$

$$t = f(x), \quad 0 \leq x \leq 1 \quad \text{at} \quad s = S \quad \text{and} \quad s = S + \Pi_H + \Pi_C \quad (7.15)$$

The solution of the regenerator model is complicated by the boundary conditions representing the reversing method of operation. Finite difference techniques offer a very simple and easy solution, as discussed by Carpenter (1976).

FIG 7.4



NUMERICAL SCHEME FOR THE SCHUMANN MODEL

The convective heat transfer coefficient controlling model using Schumann assumptions is solved by the use of the central difference approximation, again described by Carpenter (1976).

The central difference approximation is applied to equations (7.9) and (7.10) resulting in a pair of simultaneous equations which apply at each point on a two-dimensional grid, in dimensionless time and space as shown in Fig 7.4. These equations are:-

$$T(n, j+1) = \frac{(1-a)}{(1+a)} T(n, j) + \frac{a}{1+a} (t(n, j+1) + t(n, j)) \quad (7.16)$$

$$t(n+1, j) = \frac{(1-b)}{1+b} t(n, j) + \frac{b}{(1+b)} (T(n+1, j) + T(n, j)) \quad (7.17)$$

$$\text{where: } a = \frac{\Delta \Delta x}{2} \text{ and } b = \frac{\Delta s}{2}$$

The model is solved by commencing the first period with an arbitrary solid temperature profile, each period thereafter commencing with the last evaluated solid profile. Where applicable, however, when cyclic equilibrium has been reached and a new run is started, it is done so with the solid temperature profile of the previous run. At the beginning of each period the 'new' fluid temperature profile is calculated from this solid profile by applying equation 7.16. This method means that the fluid residence

time is neglected. The equations 7.16 and 7.17 are then solved along the regenerator for each time increment.

The calculations are performed in this way until cyclic equilibrium is reached. This is discussed in chapter 1 and exists when the temperature time history of a cycle is identical to that of the previous and subsequent cycles. In the model this is described by equation 7.15. It is monitored in the computations by the percentage difference between solid temperature profiles at the end of the cold inlet period, which slowly reduces as equilibrium is approached. When the difference becomes reduced to 0.05% then most systems are within 0.2% of equilibrium as shown by Carpenter (1976), measured on the fluid outlet temperature for the cold inlet period. The equilibrium situation used in this determination exists when the cycle repeated itself exactly to five significant figures, for the final solid temperature over the whole regenerator length.

Once equilibrium has been achieved in the computations, Simpsons rule, obtained from B. Carnham, H.A. Luther and J.O Wilkes (1969) is used to determine the mean fluid exit temperatures required to calculate the effectiveness. Although there is no stringent stability criterion associated with the central difference approximation upon which the model is based, the approach to the true solution depends upon the step sizes employed, and the convergence tolerance. Carpenter's (1976) values of $\Delta s \leq 0.4$ and $\Delta x \leq 0.333$ were used, however, to ensure accuracy for small Δ and Δx a minimum of ten increments is set in both time and space.

FIG 7.5 NUMBER OF CYCLES REQUIRED TO OBTAIN EQUILIBRIUM
Vs π/Λ FOR LAMBDA 25(5)5 π/Λ DECREASING

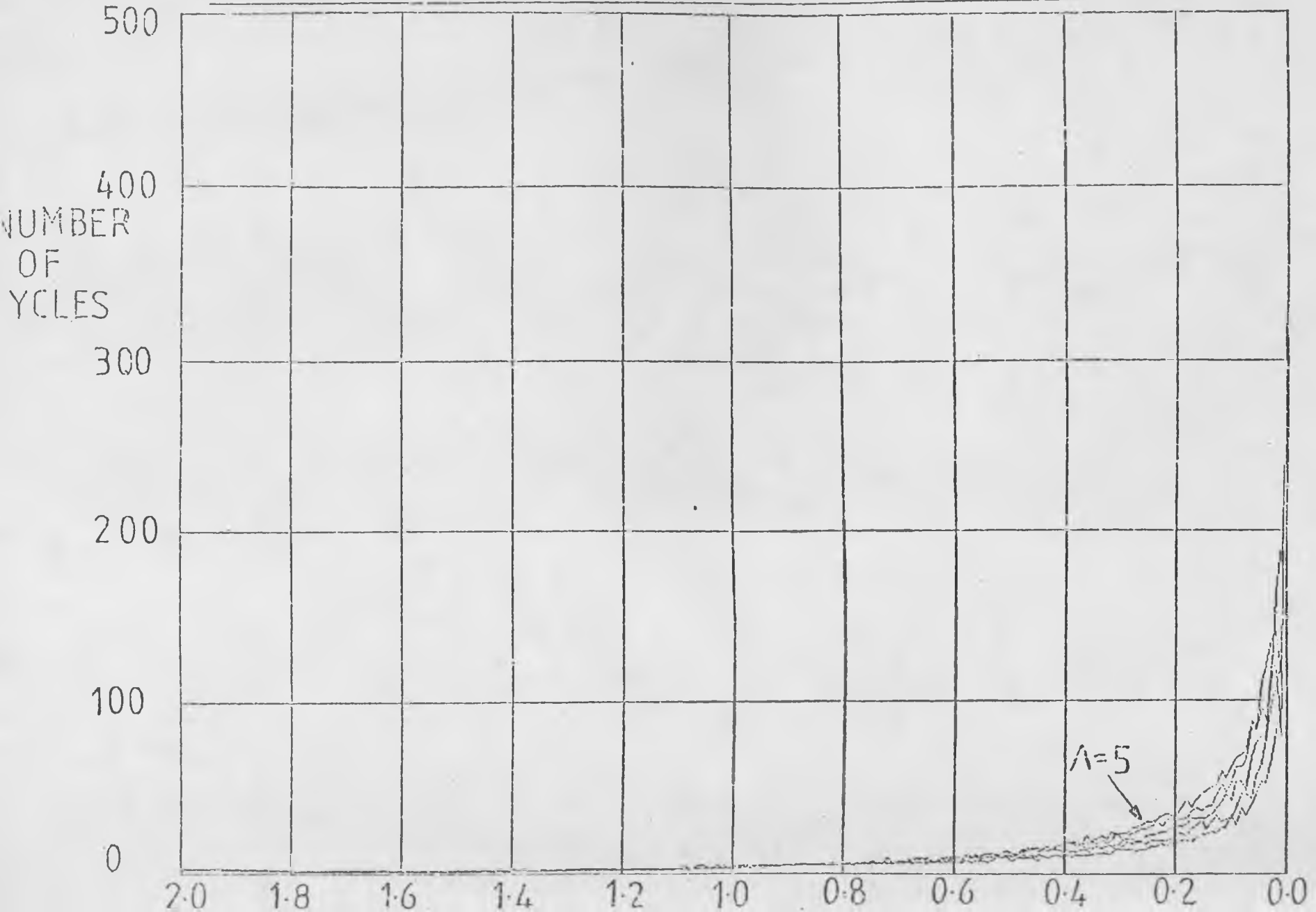


FIG 7-6 NUMBER OF CYCLES REQUIRED TO OBTAIN EQUILIBRIUM
Vs π/λ FOR LAMBDA 25(5) 5 π/λ INCREASING

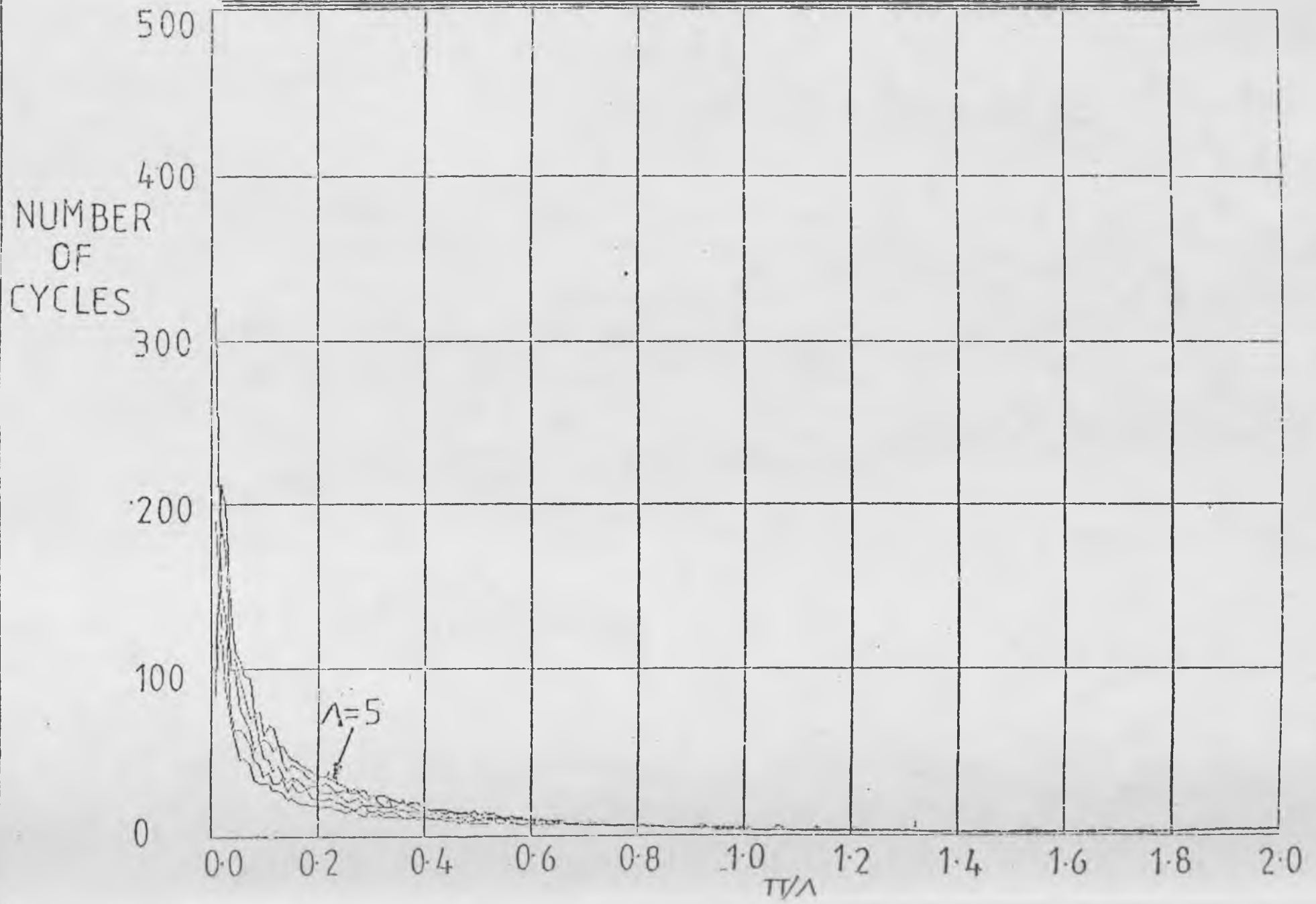


TABLE 7.1

Efficiency values at $\Lambda = 15$ and 20 for $\Pi/\Lambda \leq 2.0$ obtained using the Schumann model programme SJHEFF1.

$\Lambda = 15$ convergence = 0.0001

<u>Run No.</u>	<u>P Mins.</u>	<u>No. Cycles</u>	<u>$\eta_H = \eta_C$</u>	<u>Π/Λ</u>	<u>Total Time (hrs)</u>
1	12	2	0.521	1.906	0.8
2	11	2	0.565	1.746	0.734
3	10	2	0.613	1.586	0.666
4	9	3	0.664	1.426	0.90
5	8	3	0.714	1.266	0.80
6	7	4	0.759	1.11	0.934
7	6	4	0.796	0.946	0.80
8	5	5	0.825	0.786	0.834
9	4	7	0.846	0.626	0.934
10	3	9	0.861	0.466	0.90

$\Lambda = 20$

1	29	2	0.512	1.95	1.934
2	26	2	0.5683	1.75	1.734
3	23	2	0.6339	1.55	1.534
4	20	3	0.7046	1.35	2.0
5	17	3	0.7711	1.15	1.70
6	14	4	0.8236	0.949	1.866
7	11	6	0.8593	0.749	2.2
8	8	9	0.8823	0.549	1.4
9	5	15	0.8974	0.349	1.5
10	2	31	0.9074	0.149	2.066

7.4 Test Bed Simulation

The programme SJHEFFI, with a tolerance of 0.000001, enables a simple study into how the test bed only will behave as Π/Λ is changed. Initially the test bed simulation was used to show the number of cycles required to reach equilibrium, first decreasing Π/Λ , Fig. 7.5, and then increasing Π/Λ , Fig. 7.6, using the final temperature profile to start off the next run. No discernible difference could be found between the two approaches, so from a practical point of view it was decided to start Π/Λ large then reduce, consequently increasing the efficiency.

To critically examine the regeneration over a set-up, 10 values of Π/Λ will be used. The Schumann model programme SJHEFFI was modified to produce 10 steps of Π/Λ for each set-up of $\Lambda = 15$ and 20 for a tolerance of 0.0001. The resulting hot efficiencies and number of cycles required to reach equilibrium are shown in table 7.1. As expected, the number of cycles required to reach cyclic equilibrium increases as Π/Λ decreases. This method gives an indication how the test bed only will behave, however, as discussed in chapter 6, in cyclic operation the peripheral pipework has a significant effect. The MISP programme was therefore used to obtain a criterion by which the apparatus will be run. However, the programme requires an overall heat transfer coefficient for the packed bed section, as well as values for the various sections of empty pipework.

TABLE 7.2

MISP simulation results for steel and lead glass at
 $\Lambda = 25, 20, 15$ and 10 .

1. Steel
 $\Lambda = 25$

<u>Run No.</u>	<u>P Mins</u>	<u>Π/Λ</u>	<u>η_{Hot}</u>	<u>η_{Cold}</u>	<u>No.Cycles</u>	<u>Total Time (hours)</u>
1	55	1.87	0.5362	0.5359	12	22.0
2	50	1.70	0.5862	0.5863	4	6.66
3	45	1.53	0.6429	0.6431	6	9.0
4	40	1.36	0.706	0.707	4	5.334
5	35	1.19	0.7671	0.7681	8	9.334
6	30	1.02	0.8211	0.8214	6	6.0
7	25	0.85	0.8591	0.8592	10	8.334
8	20	0.68	0.8853	0.8849	6	4.0
9	15	0.51	0.9027	0.9017	8	4.0
10	10	0.34	0.9168	0.9123	6	2.0
Total Time:						76.66

$\Lambda = 20$

1	29	1.95	0.519	0.5187	12	11.6
2	26	1.75	0.5741	0.5742	4	3.466
3	23	1.55	0.6381	0.6354	4	3.066
4	20	1.35	0.707	0.7074	4	2.66
5	17	1.15	0.772	0.7723	4	2.266
6	14	0.95	0.8235	0.8237	8	3.734
7	11	0.75	0.8593	0.8595	6	2.2
8	8	0.55	0.8826	0.8814	6	1.6
9	5	0.34	0.9004	0.8940	6	1.0
10	2	0.14	0.9178	0.8967	6	0.4
Total Time:						31.992

$\Lambda = 15$

<u>Run No.</u>	<u>P Mins.</u>	<u>TTA</u>	<u>η Hot</u>	<u>η Cold</u>	<u>No. Cycles</u>	<u>Total Time (hours)</u>
1	12	1.91	0.562	0.5254	14	5.6
2	11	1.75	0.5628	0.5682	4	1.47
3	10	1.58	0.6145	0.6146	4	1.33
4	9	1.43	0.6631	0.6633	4	1.20
5	8	1.27	0.7112	0.7115	4	1.07
6	7	1.11	0.7552	0.7554	4	0.93
7	6	0.95	0.7923	0.7422	6	1.20
8	5	0.74	0.8216	0.8211	6	1.0
9	4	0.63	0.8433	0.8428	6	0.80
10	3	0.48	0.8598	0.8589	6	0.60

Total Time: 15.2

 $\Lambda = 10$

1	4	1.99	0.4695	0.4657	14	1.87
2	3.5	1.74	0.5245	0.5245	4	0.47
3	3	1.49	0.5914	0.5915	4	0.40
4	2.5	1.24	0.6609	0.6609	4	0.33
5	2	0.94	0.7236	0.7236	6	0.40
6	1.5	0.75	0.7722	0.7722	8	0.40
7	1	0.56	0.8059	0.8059	6	0.20

Total Time: 4.07

2. Lead Glass 6mm diameter

$\Lambda = 25$

<u>Run No.</u>	<u>P Mins.</u>	<u>π/Λ</u>	<u>η Hot</u>	<u>η Cold</u>	<u>No. Cycles</u>	<u>Total Tim (hours)</u>
1	35	1.96	0.5142	0.5139	14	16.33
2	30	1.68	0.5942	0.5942	4	4.0
3	25	1.40	0.6937	0.6940	6	5.0
4	20	1.12	0.794	0.7944	8	5.33
5	15	0.84	0.8627	0.8629	10	5.0
6	10	0.56	0.8996	0.898	6	2.0
7	5	0.28	0.922	0.9143	8	1.33

Total Time: 38.99

$\Lambda = 20$

1	18	1.98	0.5092	0.5090	16	9.60
2	16	1.76	0.5682	0.5682	4	2.13
3	14	1.54	0.6382	0.6383	4	1.87
4	12	1.32	0.7142	0.7144	4	1.60
5	10	1.10	0.754	0.7842	6	2.0
6	8	0.88	0.8367	0.8360	8	2.13
7	6	0.66	0.870	0.869	6	1.2
8	4	0.44	0.8918	0.8892	8	1.07
9	2	0.22	0.9084	0.8994	8	0.53

Total Time: 22.13

$\Lambda = 15$

1	7	1.82	0.5474	0.5471	16	3.73
2	6	1.56	0.6225	0.6228	4	0.8
3	5	1.30	0.7026	0.7027	4	0.67
4	4	1.04	0.7736	0.7735	8	1.07
5	3	0.78	0.8243	0.8240	8	0.80
6	2	0.52	0.8567	0.8557	6	0.40
7	1	0.26	0.8809	0.8698	6	0.20

Total Time: 7.67

$$\Lambda = 10$$

<u>Run No.</u>	<u>P Mins</u>	<u>Π/Λ</u>	<u>q Hot</u>	<u>q Cold</u>	<u>No. Cycles</u>	<u>Total Time</u> (hours)
1	2	1.74	0.5543	0.554	16	1.07
2	1.5	1.31	0.6671	0.6671	4	0.20
3	1	0.87	0.7608	0.7605	10	0.33
4	0.5	0.44	0.8756	0.8128	6	0.10
Total Time:						1.70

Heat Transfer Coefficient Data for the MISP Programme

<u>Λ</u>	mm	w/m^2k	kg/sm^2		m^3/s					
	<u>L</u>	<u>HTC4</u>	<u>G4</u>	<u>Q</u>	<u>G3</u>	<u>HTC3</u>	<u>G2</u>	<u>HTC2</u>	<u>G1</u>	<u>HTC1</u>
25	203.2	54.73	0.262	3.53	0.2413	2.186	0.518	1.725	1.938	12.525
20	203.2	85.44	0.512	6.91	0.472	3.742	1.014	6.927	3.796	21.46
15	203.2	151.41	1.214	16.37	1.119	7.455	2.402	13.81	8.99	42.69
10	203.2	338.6	4.074	54.93	3.08	19.64	8.064	36.39	30.1	112.6

where HTC (4,3,2,1) correspond to the heat transfer coefficients in the sections according to Fig. 6.5.

Assumed voidage = 0.37

7.5 MISP Simulation for Operational Procedure

The MISP programme was used to examine the response of the whole regenerator, the structure of which is given in chapter 6.4. A criterion for the efficient operation of the apparatus for 4 values of Λ per packing, a bed length with the corresponding flowrates and 10 real time periods within the Π/Λ range for one set up per packing with the corresponding number of cycles required to reach equilibrium is necessary. To economise on time, only $\frac{1}{4}$ inch steel and 6mm glass computer runs were carried out. It was assumed that the alumina and glass heat transfer properties would be approximately the same for this consideration. Heggs single blow correlation for spheres, shown in table 3.1, was used to determine the overall heat transfer coefficient required for a known packing by varying the flowrate until the correct Λ was produced for a fixed bed length of 8 inches. Π hence the real time switching values were then obtained.

If the Schumann assumptions used are correct, then Λ is independent of Π , that is the overall heat transfer coefficient should not change with decreasing Π/Λ but if intraconduction effects are prominent then Λ is a function of Π as shown by the intraconduction charts produced by Carpenter (1976) and Heggs et al (1980).

The MISP programme results for glass and steel spheres are shown in table 7.2, for $\Lambda = 10, 15, 20$ and 25. The initial temperature profile is 30°C with a 10°C step temperature

TABLE 7.3

MISP and Schumann model responses for steel at $\Lambda = 20$.

No. of Schumann Cycles	No. of MISP Cycles		Schumann $\eta^H = \eta^C$	MISP η		Π/Λ	Run Time Mins.	Run No.	Total Run Time Hours
	S	T		S	T				
2	2	78	0.5109	0.519	0.5188	1.95	29	1	37.7
2	2	158	0.5675	0.5735	0.5736	1.75	26	2	68.47
3	2	165	0.6313	0.6359	0.6355	1.55	23	3	63.25
4	2	138	0.7059	0.7075	0.7074	1.35	20	4	46.0
6	2	92	0.7739	0.7727	0.7725	1.15	17	5	26.07
8	2	38	0.8264	0.8249					
				0.8263	0.8237	0.95	14	6	8.87
11	2	92	0.8620	0.8646					
				0.8657	0.8595	0.75	11	7	16.87
20	2	58	0.8833	0.8947					
				0.8718	0.8814	0.55	8	8	7.73
35	2	60	0.8953	0.902					
				0.8731	0.894	0.34	5	9	5.0
119	2	66	0.8973	0.9453					
				0.849	0.897	0.14	2	10	2.2
									282.16 hours

S = MISP convergence using slack convergence of 0.004

T = MISP convergence using tight convergence of 0.000001

η^S = MISP efficiency using convergence = 0.004

η^T = MISP efficiency using convergence = 0.000001

Schumann η = efficiency from SJHEFF1: convergence = 0.000001

(MISP η^s values: Top = η^H , Bottom = η^C)

rise and subsequent runs use the previous temperature profiles for starting, with a convergence factor of 0.0001. It can be clearly seen that the number of cycles required to reach cyclic equilibrium follows a different pattern than just the test bed alone, although as expected, the efficiencies produced for Π/Λ are approximately the same. When the peripheral pipework is considered the number of cycles required for the first run, at high Π/Λ is large, there is then a substantial decrease, eventually rising again for the last Π/Λ 's. The final large run is explained by the additional pipework also having to come to equilibrium, which as discussed earlier in Chapter 6 is controlling factor.

Once a temperature state has been reached a change of period has initially little effect on the subsequent number of cycles required to reach the next steady state. Eventually as with just the packed bed section, shown in table 7.1, the number of cycles required to reach cyclic steady state increases, as the period of operation is substantially reduced. The MISP programme results provide the necessary criterion by which the apparatus is run, however, in actual running conditions the number of cycles were exceeded where possible, particularly on the first run and for overnight operation. The MISP programme data was found adequate for a total run time, as shown in table 7.2 by using a convergence factor of 0.0001. When considering two convergence extremes of 0.004 at $\Lambda = 20$ and 0.000001 at $\Lambda = 20$, shown in table 7.3, it is

clear that if a tight convergence is used a set up could last 1.68 weeks, but if a slack convergence is used a maximum of only two cycles per run are produced. A test bed simulation using SJHEFFI with a convergence of 0.000001 is shown for comparison in table 7.3. A compromise of a sufficiently tight convergence 0.0001 and a suitably long set up run time is therefore reached to produce a series of investigational set-ups. Apparatus running conditions have been effectively simulated for efficient operation. A suitably accurate, yet simple technique using minimum rig raw data has also been developed to produce convective heat transfer coefficients within the dimensionless length and utilisation factor range, 5 to 25 and 0 - 2 respectively.

7.6 Convective Heat Transfer Coefficient Prediction

7.6.1 Suitable Method

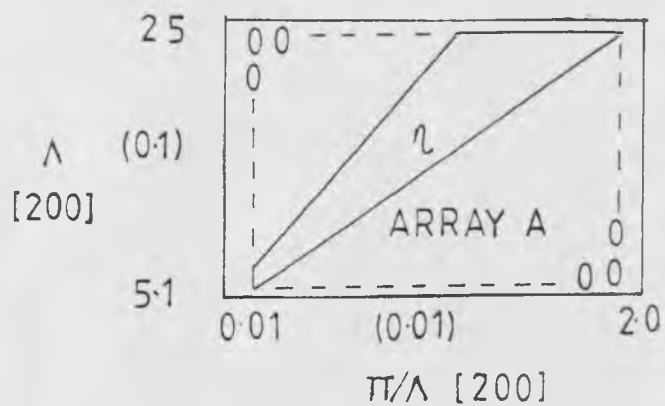
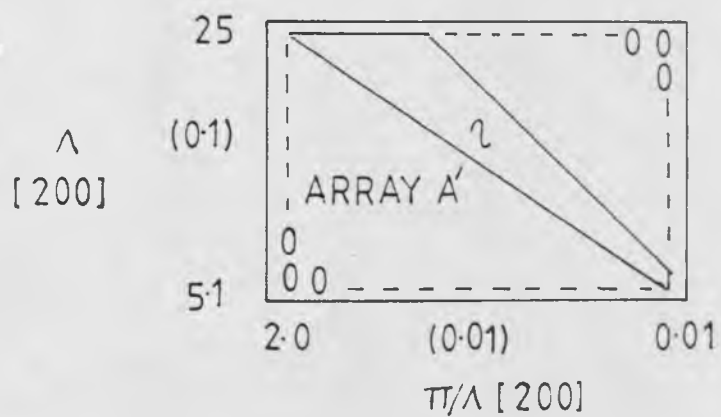
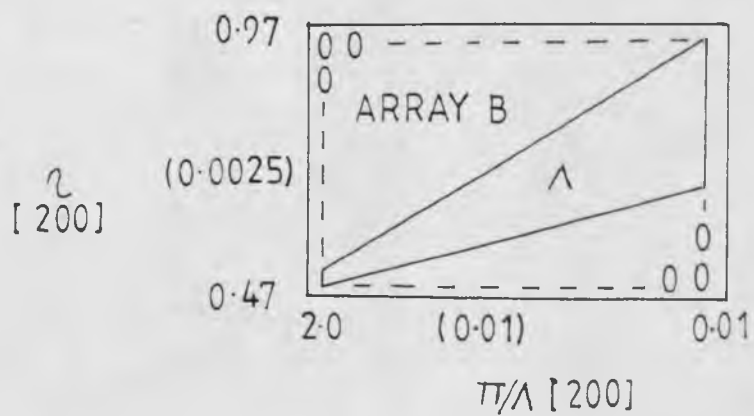
Previous workers when obtaining practical heat transfer coefficients either used approximate techniques; Ridgion and Kerrison (1964), Bretherton (1970) and McDonald (1966) or iterative techniques; Price (1964), Heggs (1967) and Main (1978). The former technique is usually a form of Tiplers (1947) approximate solution used in cyclic work, which assumes linear temperature profiles with respect to length producing an error of 4% in the final heat transfer coefficient for $\Lambda \geq 10$ as discussed by Carpenter (1976), whilst the latter

when used for single blow work assumes a starting heat transfer coefficient and iterates to a final value based on the apparatus data. If design graphical techniques are used, again a heat transfer coefficient must be assumed. Previous MISP simulation work and design chart study showed how effectiveness (η) is a function of Π/Λ for a given Λ . However, a suitable means had to be found to promote this concept based on raw data applicable to most types of balanced cyclic regenerators.

7.6.2 Convective Heat Transfer Coefficient Determination

Willmott (1964) initially produced a finite difference solution for a balanced cyclic regenerator, using Schumann assumptions. Since then this technique has been examined by many workers. Recently, Carpenter (1976) used this finite difference technique as an approach to examine thermal regenerator characteristics with Schumann assumptions, intraconduction and fluid hold up. Carpenter's Schumann model technique is extended in this work to produce the required dimensionless length and time manipulations necessary for the easy production of a convective heat transfer coefficient.

The basic form of the model mathematics and constraints are given in section 7.3.1. Carpenter's Schumann model programme SJHEFF2 was reproduced, however the efficiencies

FIG 7.7 REPRESENTATION OF ARRAY AFIG 7.10 REPRESENTATION OF ARRAY A'FIG 7.11 REPRESENTATION OF ARRAY B

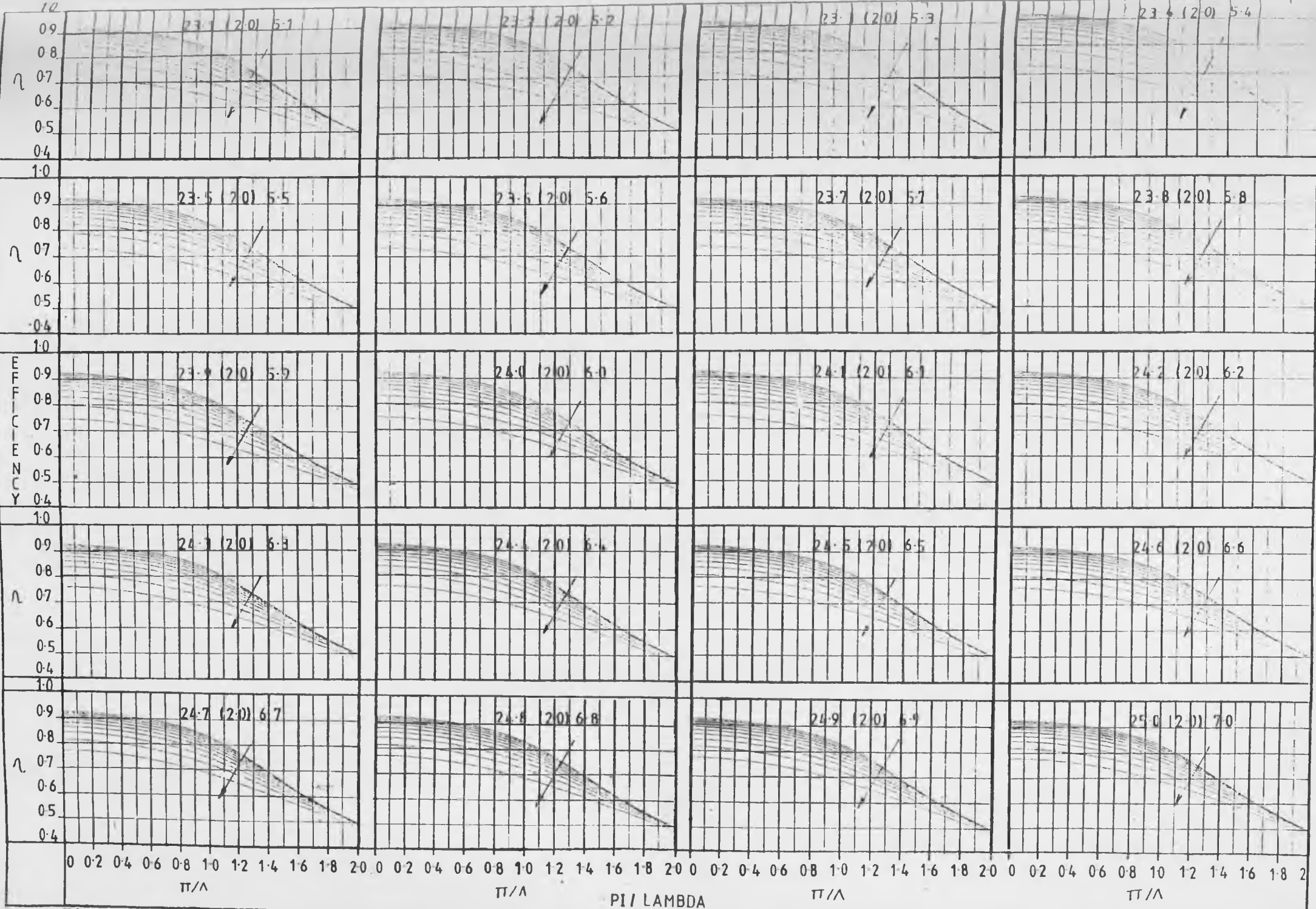


Fig 7.8 Matrix Method Linear Design Graph - η Versus $\frac{\pi}{\lambda}$ For λ

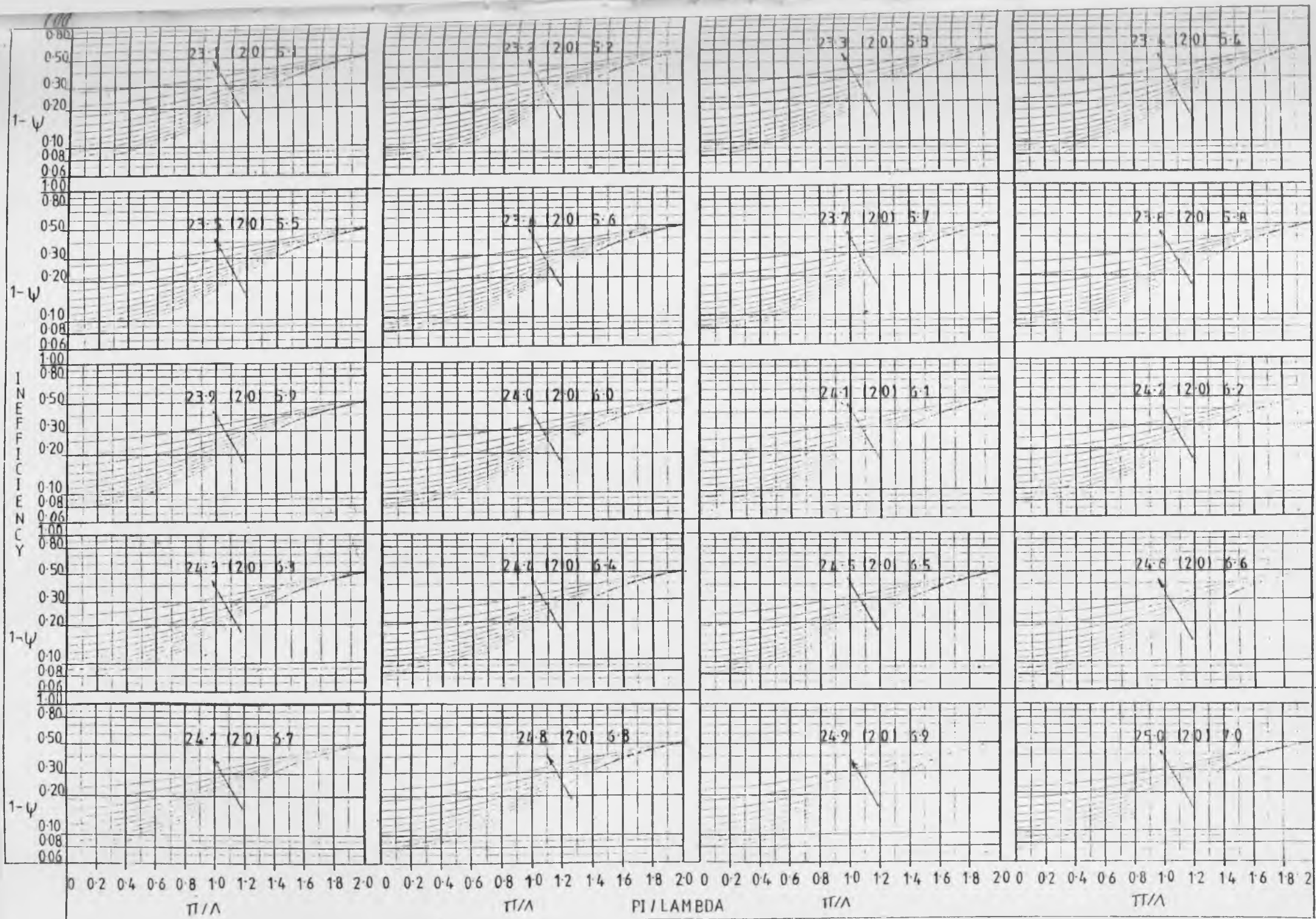


Fig 7.9 Matrix Method Semi Log Design Graph $-\log(1-\psi)$ Versus π/λ For λ

produced were not in a suitable form, so the programme was arranged, as shown in Appendix I in an iterative manner, producing values of efficiency to 5 decimal places for Λ (25 (0.1)5) and Π/Λ (0.01(0.01)2.0). The temperature range used was 0 to 10°C, starting the initial temperature profile for a given Λ at 0°C and thereafter with the final temperature profile of the previous run within the Π/Λ range. This approach was the same as that used by the MISP programme. The convergence factor used was 0.000001.

The resulting efficiencies obtained were checked at $\Lambda = 25, 20, 15, 10$ and 5 for $\Pi/\Lambda = 2, 1.5, 1$ and 0.5 with Carpenter's finite difference programme and agreed to 4 decimal places. The efficiency values were stored in array A (200 x 200), shown in Fig. 7.7.

This arrangement was transformed into graphical representation using programmes SJHEFF (3,4). The former with linear scales, Fig. 7.8, whilst the latter used a log 10 scale (2 cycles), Fig. 7.9, for greater accuracy. Twenty graphs each showing 20 Λ steps (5.1(0.1)25) are shown for the linear and log 10 scale respectively. This graphical method allows an easy but accurate estimation of the convective heat transfer coefficient. For a value of efficiency η and utilisation factor Π/Λ ($\frac{wv \cdot C_g \cdot P}{M \cdot C_s}$), Λ can be obtained with a reasonable degree of accuracy, hence the convective heat transfer coefficient since $\Lambda = \frac{hAL}{GCP}$. This

form of representation allows a rapid, but accurate first estimate on a balanced cyclic regenerator design. The Tipler (1947) equation has the inbuilt error of linear solid temperature profiles, whilst Hausens (1929) chart, shown in Fig. 7.3, requires a guess for either Π or Λ and the accuracy of the graphical reading is affected by the large range. Analysis of Fig. 7.8 indicates that values of Λ , for various Π/Λ 's could only be obtained with reasonable assurity if Π/Λ was ≤ 1.0 and not 2.0 as previously assumed. At $\Pi/\Lambda \leq 1.0$ the curves are horizontal with a large spread, however as Π/Λ approaches 2.0 this spread decreases and consequently a small change in Π/Λ results in a large Λ difference. The efficiency range is therefore restricted between 0.93 and 0.6. For computer analysis, however, the data in array A was transposed into array A', Fig. 7.10, suitable for final interpolation.

For three known values of efficiency η_1, η and $\eta_1 + 0.0025$ and two known values of Λ , Λ_1 at $\eta = \eta_1$ and Λ_2 at $\eta = \eta_1 + 0.0025$, the unknown value of Λ can be found at Π/Λ by linear interpolation and hence array B produced, shown in Fig. 7.11. To maintain an array of 200 x 200 the efficiency difference was set at 0.0025. Programme SJHEFF7 was used to perform the interpolation and the resulting array stored on a Data General S/130 disc.

The data is now in a suitable form for easy data access by the computer, knowing η and Π/Λ . Both variables can be found from the apparatus, however Π/Λ includes the bulk

density and length terms. Although the length can be accurately determined the bulk density is more difficult to obtain because of the Triton Koawool ceramic paper used as internal insulation. Data manipulation resulted in this Π/Λ form:-

$$\Pi/\Lambda = \frac{w.Cg.P}{M.Cs}$$

These variables can be obtained with a high degree of accuracy.

One final programme was required; SJHEFF8, to take the input values of η_{rig} and Π/Λ_{rig} and produce a value of Λ_{rig} by linear interpolation, ie. $\eta, \eta_{rig}, \eta + 0.0025$ and $\Pi/\Lambda, \Pi/\Lambda_{rig}, \Pi/\Lambda + 0.01$.

7.7 Experimental Start-up and Shut Down

The apparatus is capable of operation using analog instrumentation or computer data logging and control. However, the test bed set-ups require a large operating time for completion so ruling out total computer control and data logging, therefore, the apparatus is initiated using analog instrumentation then transferred to computer control and data logging. Appendix J describes how the apparatus is started up and shut down, using analog instrumentation and computer aspects and also describes the necessary operations for analog through to computer control and data logging.

7.8 Data Collection

The experimental investigation comprised the examination of steel $\frac{1}{4}$ inch (6.35mm), glass (6mm) and alumina $\frac{1}{2}$ inch (12.7mm) for values of $\Lambda = 15$ and 20. The set-ups are categorised as steel A, B glass C, D and alumina E, F respectively. Runs within a set-up are numbered 1 to 10 corresponding to Π/Λ decreasing. The actual rig operating criterion is taken from the MISP data simulations for steel and glass at $\Lambda = 15$ and 20, shown in table 7.2. The experimental data obtained, therefore comprised two distinct sections. The data required for a set-up and the runs within a set-up. Π/Λ and η for a run could be found, then the corresponding value of Λ , hence the convective heat transfer coefficient.

Finally, because a single shot convective heat transfer coefficient correlation was used to predict the response of the cyclic runs, the first hot period of the first run each set-up was lengthened to allow a single shot breakthrough curve. Λ_{SS} (single shot) was obtained for each set-up using Darabis (1981) graphical method, derived using finite difference techniques for Schumann assumptions specific to single shot applications.

7.8.1 Set Up Data Collection

The following procedure was used for each packing set-up:- Consistant data values used were the specific heat of air (1004), density of air (1.294) and Prandtl number (0.72) taken from Kreith (1973).

<u>Variable</u>	<u>Comment</u>	<u>Estimated Measurement Error</u>
Set up letter		
packing material		
Particle diameter (PD) mm		
Packing Specific Heat (CS) $\text{kJ/kg}^\circ\text{C}$		
Packing density (DS) kg/m^3		
Bed length (LSEC) mm	a maximum of 203.2mm (8 inches)	0.5%
Bed mass (M) kg	measured on the school balance Gross (kg) Tare (kg) $M = \text{Gross} - \text{Tare}$	maximum of 0.05%
Bed diameter (BD) mm		1.3%

<u>Variable</u>	<u>Comment</u>	<u>Estimated Measurement Error</u>
Number of layers of 1mm internal insulation (INSU)		
Thermal conductivity of the packing (KPACK)	w/mk	
Dimensionless length (Λ)	Estimated for an 8 inch bed by Heggs correlation for spheres given in table 3.1	

The apparatus data for six set-ups is shown in appendix K.

7.8.2 Run Data for a Set-Up

<u>Variable</u>	<u>Comment</u>	<u>Estimated Measurement Error</u>
Runs for set-up		
Run Number (N)	Maximum of 10 runs	
Orifice plate use (Fo)	Indicates the number of the orifice plate used corresponding to a diameter given in Fig. 4.15.	
Temperature leaving the front end (TFEND) °C		0.33%
Step temperature prior to the test bed section (REGSTEP) °C	Not greater than 10°C	0.25%
Ambient temperature (AMB) °C	Measured by a mercury thermometer mounted on the control panel. Used in the Spink (1961) equation to calculate G	0.25%
Temperature downstream of the orifice plate (TG2) °C	Indicated by the Kent recorder and computer logged; also measured by the mercury thermometer MT3. Used in the Spink equation to calculate G.	0.25%

<u>Variable</u>	<u>Comment</u>	<u>Estimated Measurement Error</u>
Differential water pressure over orifice plate. (MANO) inches of water.	Used in the Spink equation to calculate G from either the computer logged raw data or one MANO value	0.8%
Gauge pressure upstream of the orifice plate (PO2) psig	Measured by the Negrette and Zambra pressure gauge. Value used in the Spink equation to calculate G.	0.3%
Atmospheric pressure (BARO) mm Hg	Measured by the departmental mercury manometer located in the laboratory. Used in the Spink equation to calculate G.	0.1%
Time for hot period (PH) minutes	Computer or manual selection	
Time for cold period (Pc) minutes	Computer or manual selection	
Minimum number of cycles required to reach equilibrium (NCYCM)	Taken from MISP runs shown in table 7.2.	
Actual number of cycles required to reach equilibrium (NCYCA)	Where possible the MISP number was exceeded	
Efficiency hot stroke (η_H)	Calculated using Simpson's rule by hand for the manual runs, otherwise by the computer programme SJHCYCT. = $\frac{THIM - THOM}{THIM - TCIM}$	
Efficiency cold stroke (η_C)	= $\frac{TCOM - TCIM}{THIM - TCIM}$ by hand or SJHCYCT	
Mean efficiency (η_m)	= $\frac{\eta_H + \eta_C}{2}$	

The run data for each set up is shown in appendix L.

For each run:-

$$\Pi/\Lambda = \frac{W.Cg.P}{M.Cs}$$

and knowing η a value of Λ can be obtained from array B using SJHCYC8. The convective heat transfer coefficient is found knowing $\Lambda = \frac{hAL}{GCg}$

7.9 Chapter Conclusions

A simple non-iterative technique has been produced to obtain values of Λ for balance cyclic regenerators, in the range $\Pi/\Lambda \leq 2.0$ for $5.1 < \Lambda < 25$. The only data required is Π/Λ and η . Prior to any experimentation the operating parameters required for steel, lead glass and alumina were estimated by computer simulation using the MISP programme. Analysis of the subsequent practical runs are given in chapter 8.

Chapter 8

Analysis of Results

8.1 Introduction

The experimental data for the regenerator set-ups, A through to F comprises both the single shot and cyclic regenerator recordings. The single shot data is analysed first, using a technique developed by Darabi (1981). The cyclic data is then analysed by the matrix method, developed in Chapter 7.

8.2 Single Shot Analysis

The single shot run data was obtained by extending the first hot period of each of the first runs for the air regenerator set-ups. The single shot period of operation was taken as 1.5 times the MISP program prediction, enabling the regenerator packing to become saturated and a complete breakthrough outlet temperature profile to be obtained, as shown in Fig. 8.1. These breakthrough curves provide the time period P_{SS} , between the 20% and 80% breakthrough temperature points, which uniquely defines the value of the heat transfer coefficient for each set up, as shown by Darabi (1981).

The non iterative single shot analysis used is an extension of the iterative technique developed by Price (1964). Under Schumann assumptions theory predicts that each complete breakthrough curve uniquely defines the single shot

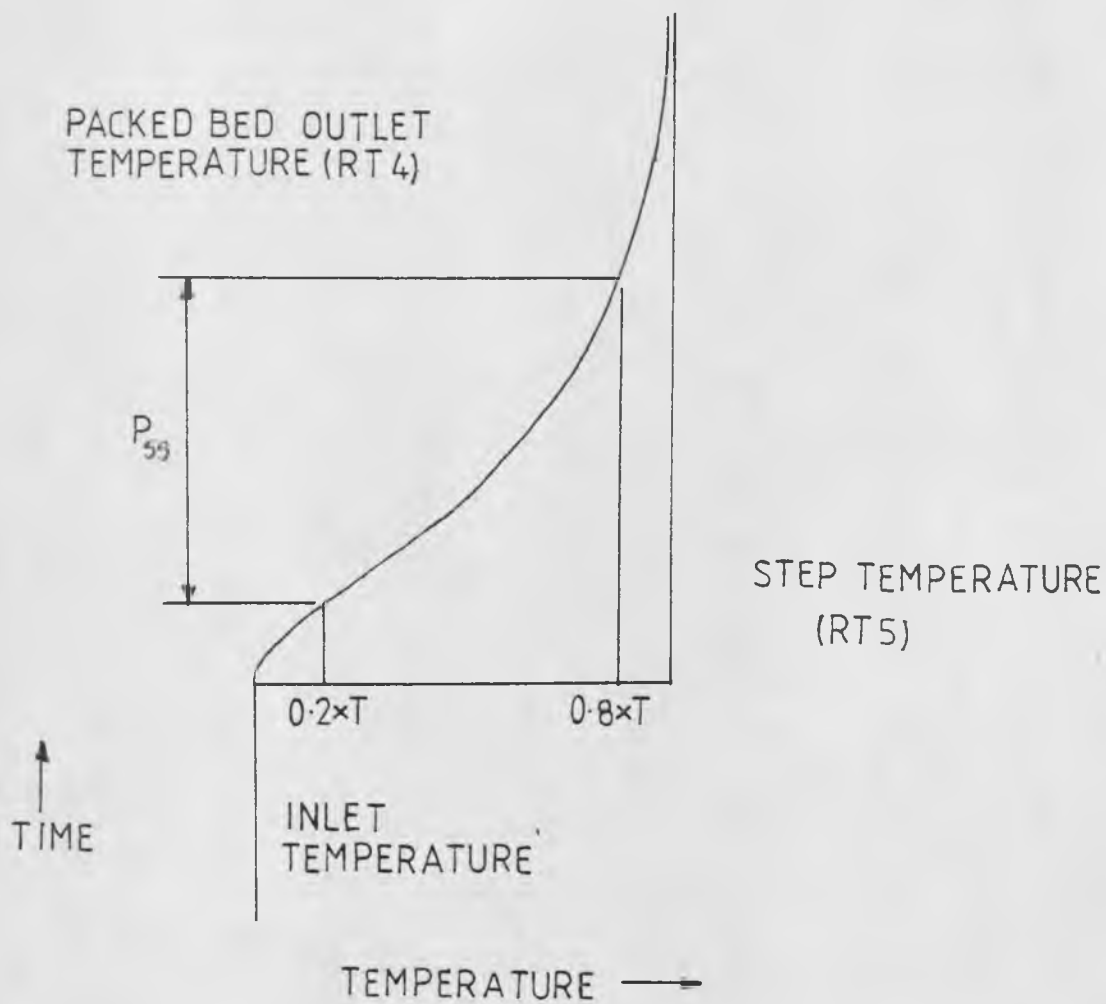
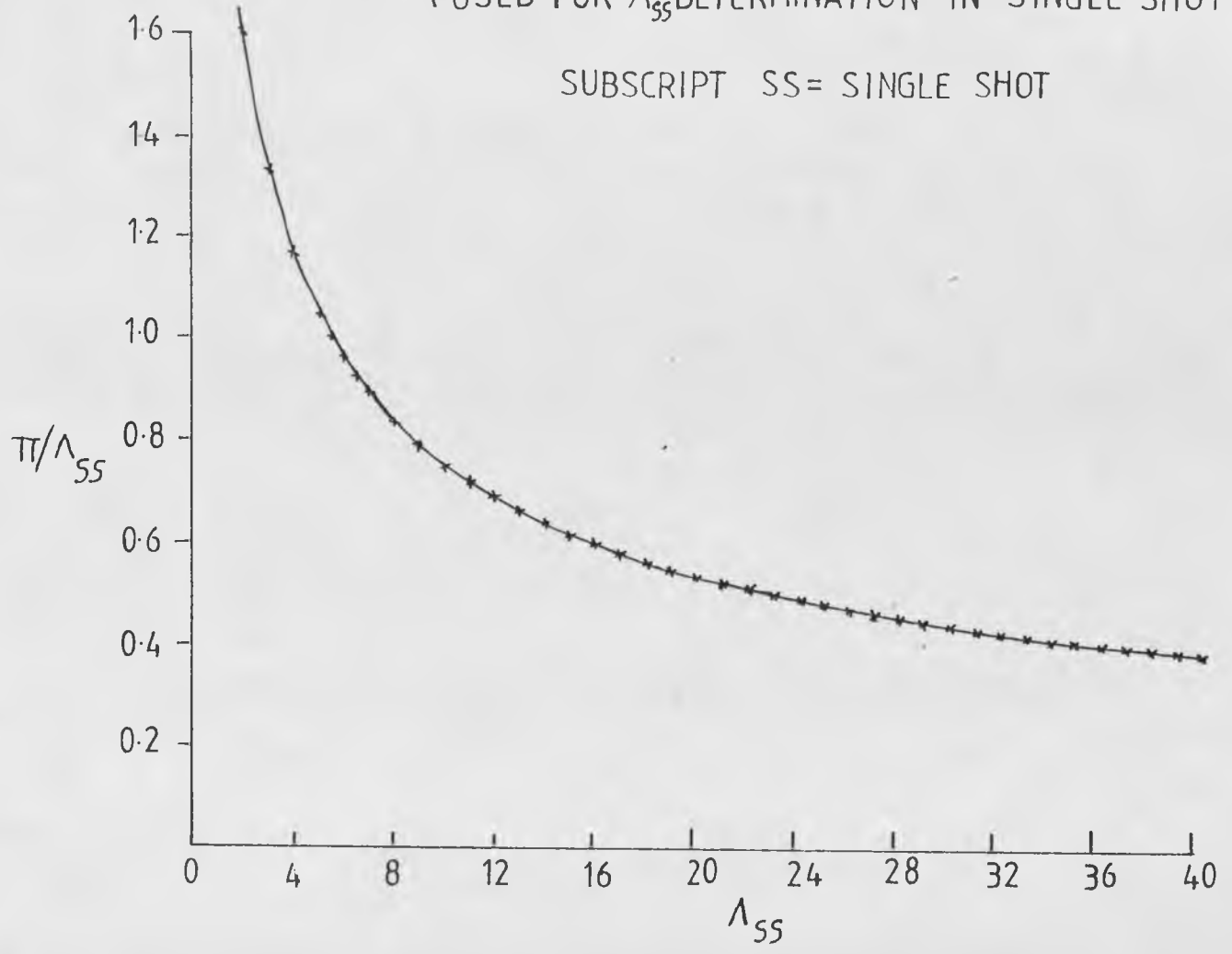


FIG 8.1 TEMPERATURE RESPONSE FOR A SINGLE SHOT RUN

FIG 82 DARABI'S GRAPH OF π/Λ_{SS} VERSUS Λ_{SS}
(USED FOR Λ_{SS} DETERMINATION IN SINGLE SHOT WORK)



dimensionless length Λ_{SS} Darabi (1981), has shown that the value of the single shot dimensionless time Π_{SS} between the 20% and 80% breakthrough temperature points divided by Λ_{SS} is solely dependent on Λ_{SS} . The resulting graph is shown in Fig 8.2. The ratio of Π_{SS} to $\Lambda_{SS} = \left(\frac{w \cdot C_g R_s}{M \cdot C_s} \right)$ is similar to the utilisation factor used in the matrix method and does not contain the convective heat transfer coefficient. Knowing Π_{SS}/Λ_{SS} , which can easily be obtained from rig raw data, Λ_{SS} can be obtained from fig. 8.2, hence the convective heat transfer coefficient since $h_{SS} = \frac{\Lambda_{SS} \cdot G \cdot C_g}{A \cdot L}$.

This technique coupled with the matrix method discussed in Chapter 7.6, gives a clear indication of the cyclic and single shot heat transfer coefficients which can be obtained under Schumann type assumptions. This particular apparatus offers a unique opportunity to produce cyclic and single shot heat transfer coefficients for the same physical set-up.

The rig raw data and derived values of Π_{SS}/Λ_{SS} , Λ_{SS} and h_{SS} are shown in table 8.1 for each set-up. The derived values of Λ , obtained by Heggs (1967) correlation and used in the MISP program simulation are 20 and 15 corresponding to the lower and higher flowrates respectively, for each packing set-up. For each packing the lowest flowrate produced the largest value of Λ_{SS} as expected since the heat transfer coefficient is proportional to a fractional power of the flowrate. For a fixed flowrate the values of Λ_{SS} decrease in the order $\Lambda_{SS} \text{ steel} > \Lambda_{SS} \text{ glass} > \Lambda_{SS} \text{ alumina}$, due to the intraconduction effects present in the packing. Consequently the convective heat transfer coefficient becomes less

FIG 8.3 Bi VERSUS π_{ss} FOR THE SIX SINGLE SHOT RUNS MADE PRIOR TO EACH SET UP

HEGGS CRITERION FOR INTRACONDUCTION: $\lambda/\beta_i \leq 60$

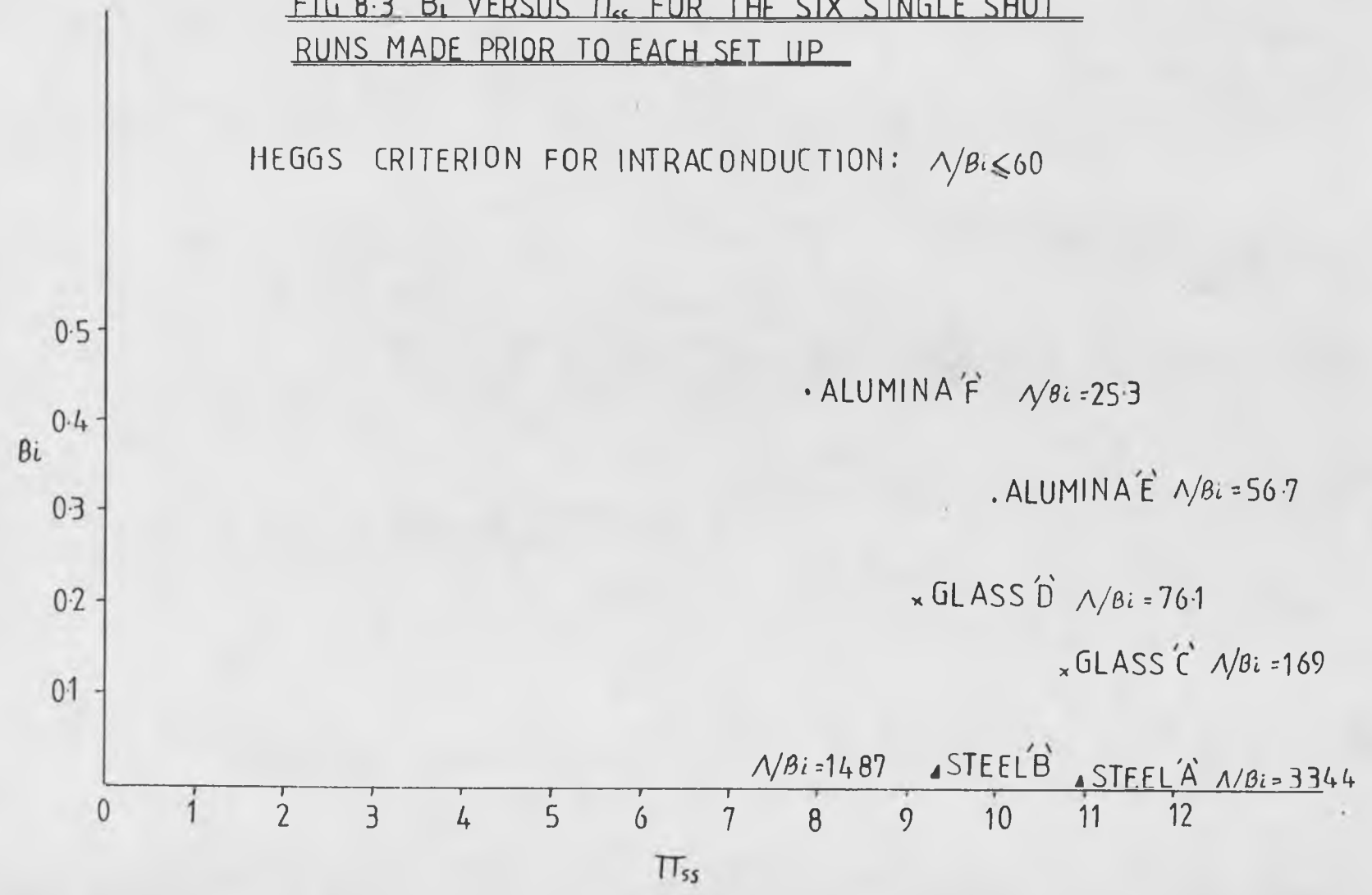


TABLE 8.1

Single Shot Set-up Data

Variable	Packing Set-Up					
	Steel		Lead Glass		Alumina	
	A	B	C	D	E	F
W	3.18	3.18	3.0	3.0	6.35	6.35
G	0.525	1.176	0.525	1.176	0.525	1.176
K	45.7	45.7	3.116	3.116	2.093	2.093
C _S kJ/kgk	0.461	0.461	0.287	0.287	0.837	0.837
C _g J/kgk	1004	1004	1004	1004	1004	1004
P (minutes)	6.89	5.52	3.76	2.00	6.60	3.72
Re	1712	3836	1615	3618	3419	7659
Π/Λ_{SS}	0.49	0.52	0.51	0.59	0.56	0.70
Λ_{SS}	22.41	17.85	21.0	15.45	17.8	11.15
Π_{SS}	10.98	9.28	10.71	9.12	9.97	7.81
L (m)	0.203					
h	97.56	137.7	86.22	142.1	164.6	231.0
Bi	0.0067	0.012	0.124	0.203	0.314	0.441
Λ/Bi	3344	1487	169	76.1	56.7	25.3
n	0.719		0.634		0.430	

important. The values of Λ_{SS} for the higher flowrate were 17.85, 15.45 and 11.15 and for the lower flowrate were 22.41, 21.0, and 17.8 for steel, lead glass and alumina respectively. The steel and lead glass values are close to each other with the lead glass Λ_{SS} values approximating to the design values of 15 and 20. The Λ_{SS} difference for each packing is 4.56, 5.55 and 6.65 for steel, lead glass and alumina respectively, which shows the gradual effect of intraconduction as the theoretically design Λ difference of 5 is exceeded.

The intraconduction effects are highlighted by plotting Bi versus Π_{SS} for Λ/Bi as shown in fig. 8.3. The associated data is shown in Table 8.1. Heggs (1967) Criterion of Λ/Bi for intraconduction within spherical packings is used to show the relative effect of intraconduction. Again as expected the steel results show a finite intraconduction effect with a small value of Bi and a high value of Λ/Bi . Glass shows an increasing intraconduction effect whilst alumina produces large values of Bi and small values of Λ/Bi , exceeding Heggs (1967) criterion. The large intraconduction effect associated with alumina is produced because the spheres are $\frac{1}{2}$ inch (12.7 mm) diameter compared to steel and glass which are $\frac{1}{4}$ inch (6.35 mm) and 6 mm diameter respectively.

It can also be seen from fig. 8.3 that intraconduction becomes more significant as Λ_{SS} is reduced for each type of packing. This corresponds to increasing the mass flowrate which also causes an increase in the heat transfer coefficient. The heat transfer coefficient is usually proportional to a

fractional power of the flowrate, therefore an increase in flowrate causes a decrease in Λ_{SS} . A decrease in Λ_{SS} therefore, causes an effective reduction in surface resistance, as the increased flowrate facilitates surface heat transfer by effectively increasing the driving temperature.

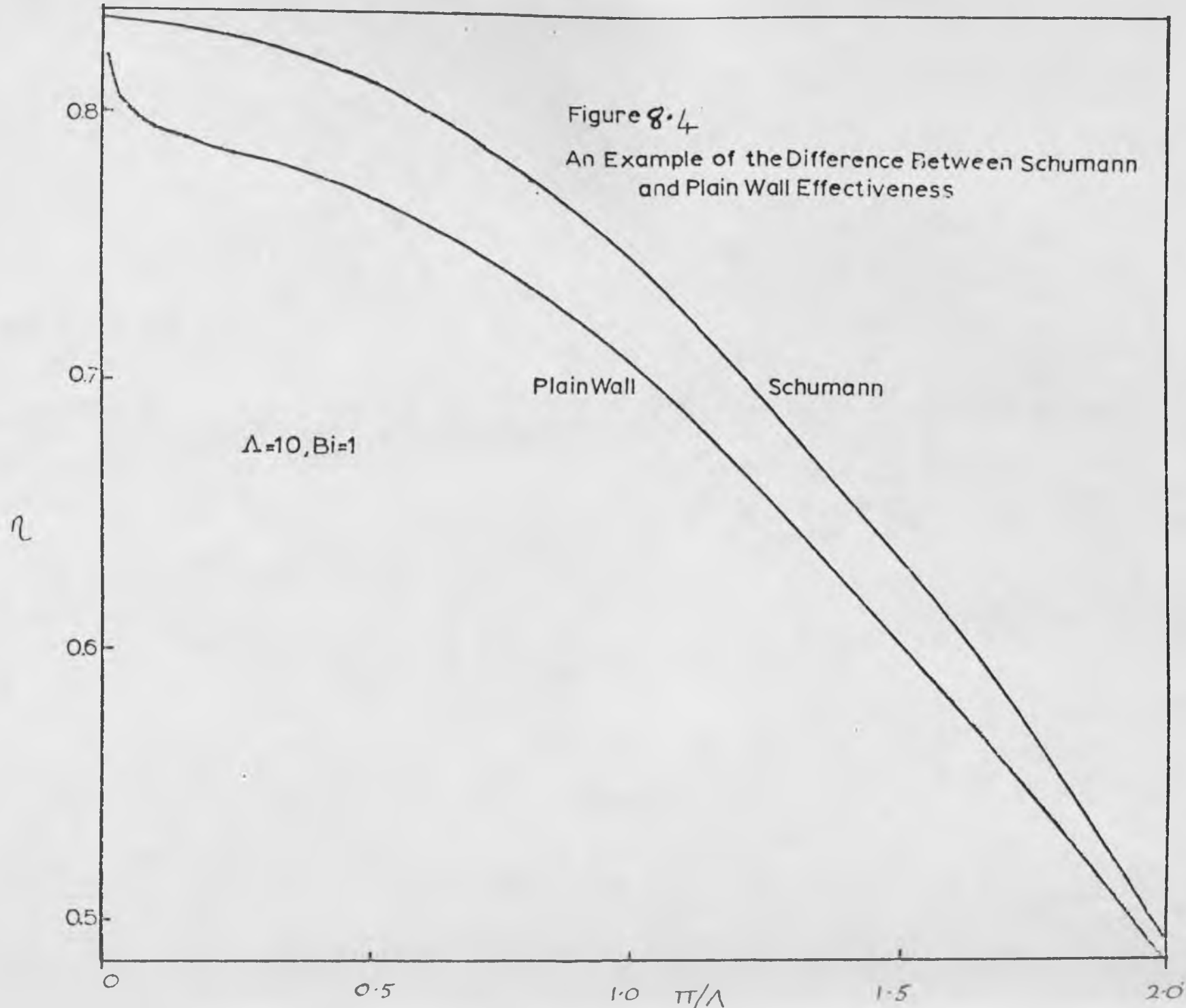
Decreasing Λ_{SS} , as shown in the alumina set-ups, therefore causes internal resistance to control. This effect can be quantitatively examined by obtaining values of the exponents for all three packings,

$$\text{since } hA \propto GA^n \quad (8.2)$$

$$\text{therefore } \frac{\Lambda_{SS A}}{\Lambda_{SS B}} = \left(\frac{GA}{GB} \right)^n \quad (8.3)$$

where subscripts A and B denote set ups A and B respectively, for each packing.

Table 8.1 shows the exponent values obtained for superficial gas mass velocity (G) values of 0.525 and 1.176. As expected $n_{\text{steel}} > n_{\text{glass}} > n_{\text{alumina}}$ which indicates the relative effect of intraconduction significantly increasing as the thermal conductivities are reduced and in the case of alumina the diameter is increased. The steel value of n (0.719) approximates to that of the Jh integer value of 0.665, shown in table 3.1, for metallic spheres. This verifies that the Darabi's (1981) graphical technique for single shot analysis is adequate for obtaining convective heat transfer coefficients for high conductivity packings. The lead glass integer value (0.634) is less than that of steel. However a Jh correlation was not available for the alumina and glass spheres, but



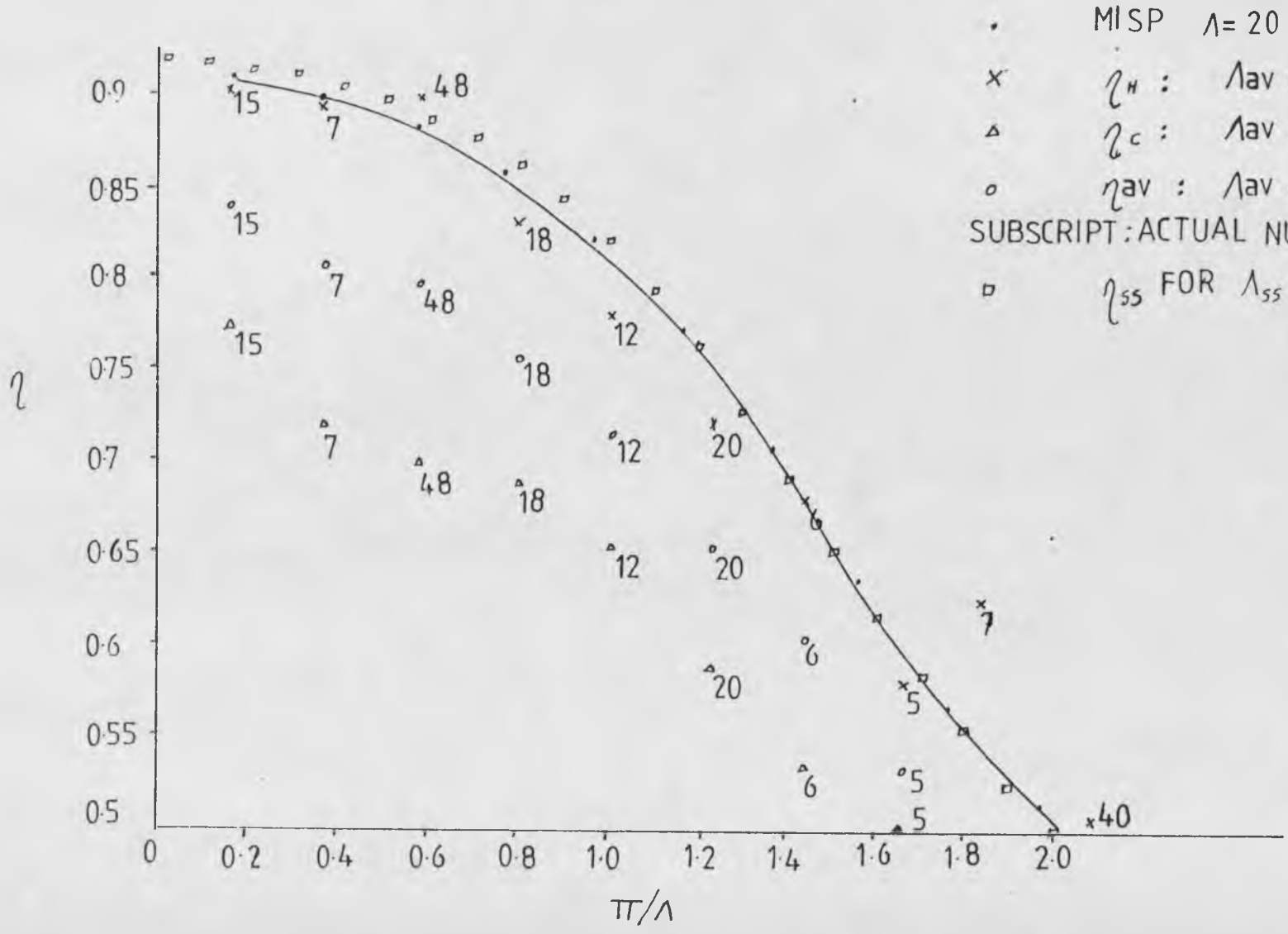
considerable work has been carried out on alumina plate configurations by Heggs (1967), see table 3.1. The integer values are considerably less than those for steel packings and approximate to the integer (0.43) value obtained for alumina spheres.

The single shot work undertaken can only show the trend for intraconduction upon the overall heat transfer coefficient and any type of J_h correlation similar to those proposed by Price (1964), Heggs (1967), and Main (1978) cannot be produced because only two data points per set-up are available. This is due to the limited number of set-ups specific to the cyclic operation of the apparatus. However, the single shot work carried out, in addition to the cyclic work, clearly shows that convective heat transfer coefficients can be simply obtained without need for iteration using rig raw data.

8.3 Cyclic Analysis

A reasonable comparison of how close the practical results are to the theoretical simulation is to plot η versus Γ/Λ for Λ , as shown in fig. 7.12. This concept was used in the derivation of the matrix method. Carpenter used a similar method to show the comparison between the Schumann and intraconduction plain wall system efficiencies for $\Lambda_H = \Lambda_C = 10$ and $Bi_H = Bi_C = 1$, shown in fig 8.4. The intraconduction effect is significant over the entire range of Γ/Λ and reduces the efficiency as expected, consequently reducing Λ . Graphs of η versus Γ/Λ for steel set-ups A and B, lead glass

FIG 8.5 η VERSUS π/λ FOR STEEL SFT-IIP \ddot{A}



• MISP $\lambda = 20$ ———
 x η_H : $\lambda_{av} = 15.86$
 Δ η_C : $\lambda_{av} = 5.83$
 ° η_{av} : $\lambda_{av} = 8.26$
 SUBSCRIPT: ACTUAL NUMBER OF CYCLES
 □ η_{ss} FOR $\lambda_{ss} = 22.41$

FIG 8.6 η VERSUS π/λ FOR STEEL SET-UP 'B'

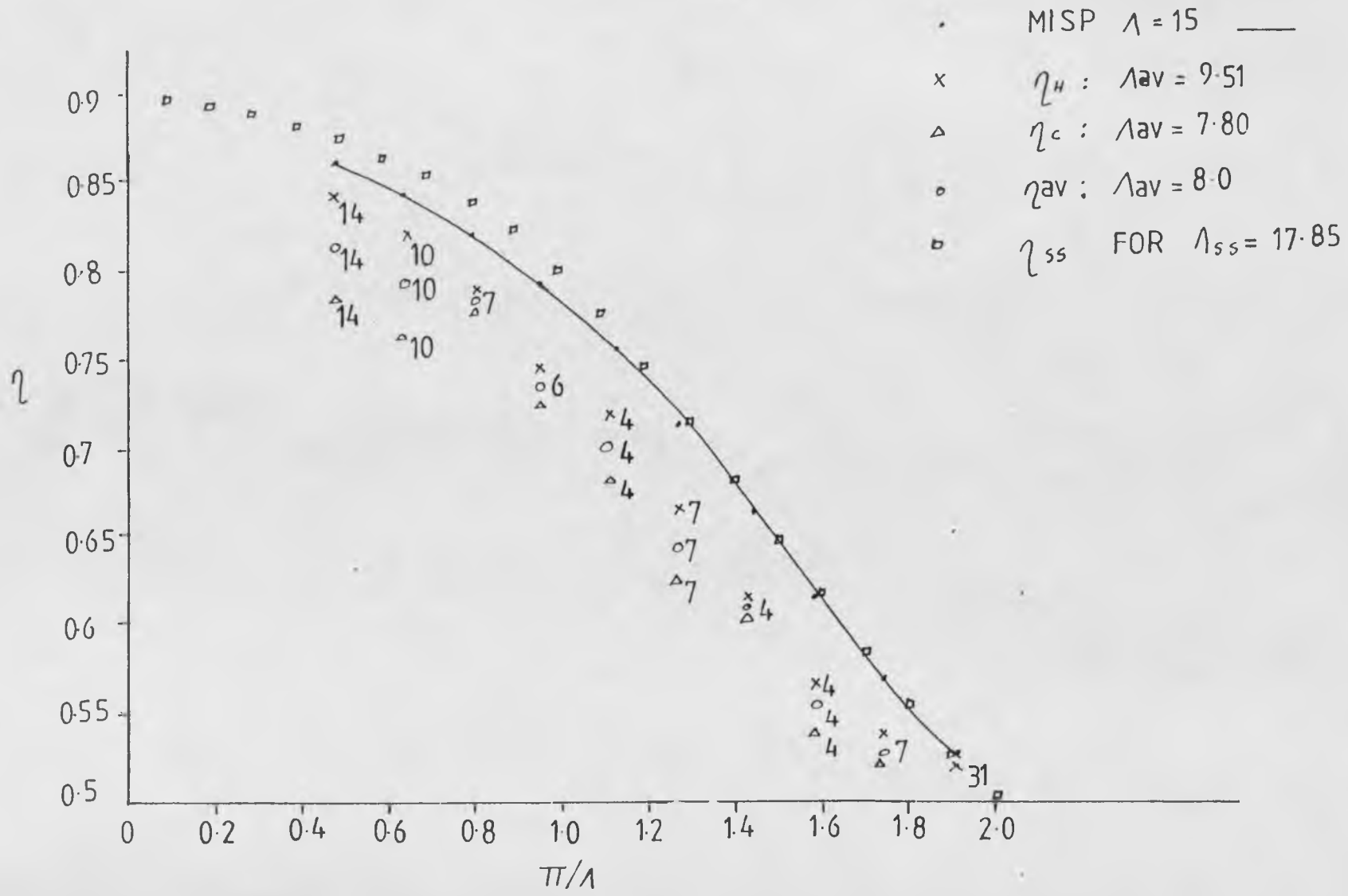


FIG 8-8 η VERSUS π/λ FOR LEAD GLASS SET-UP 'D'

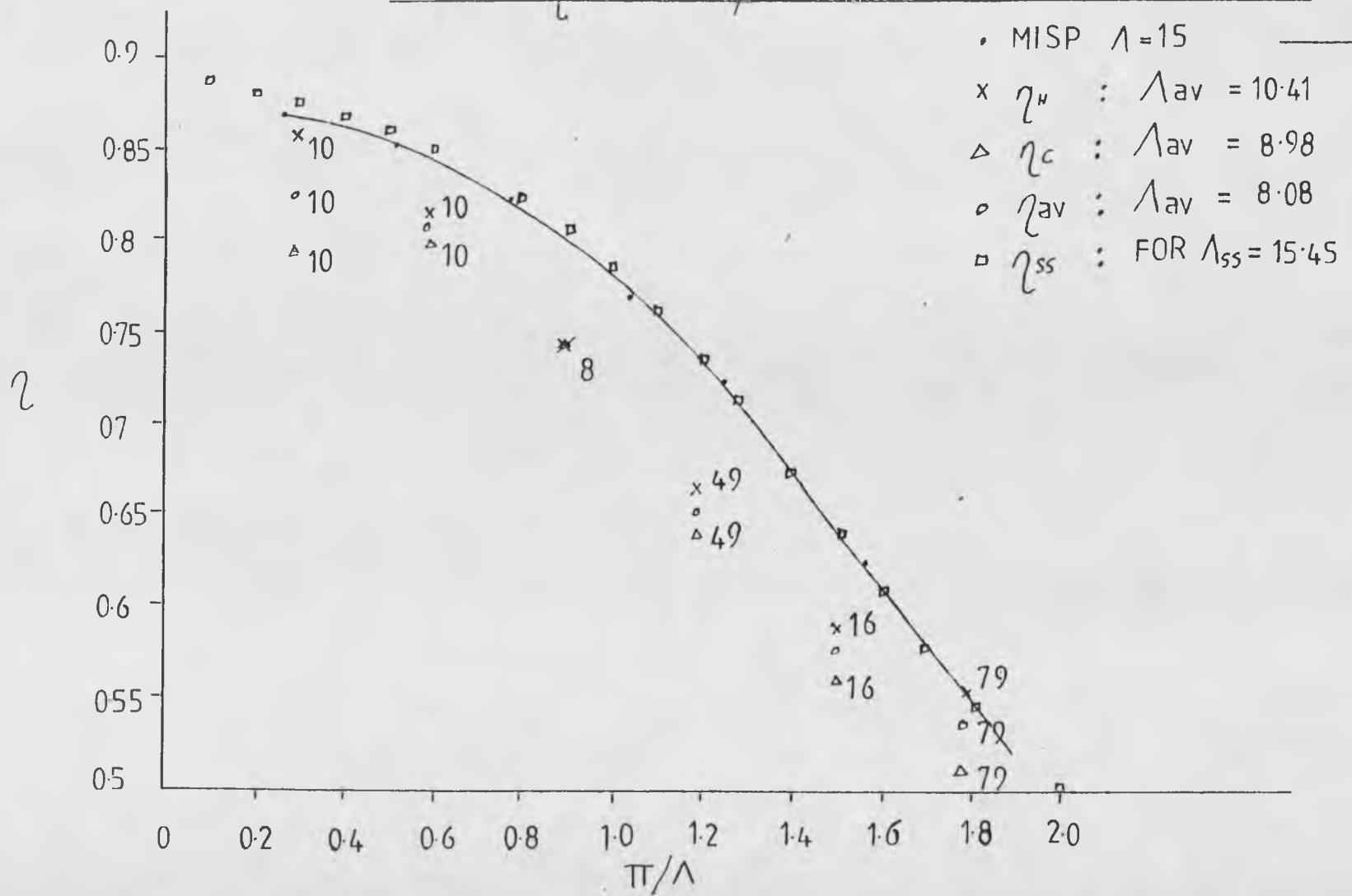


FIG 8.9 η VERSUS π/Λ FOR ALUMINA SET-UP 'E'

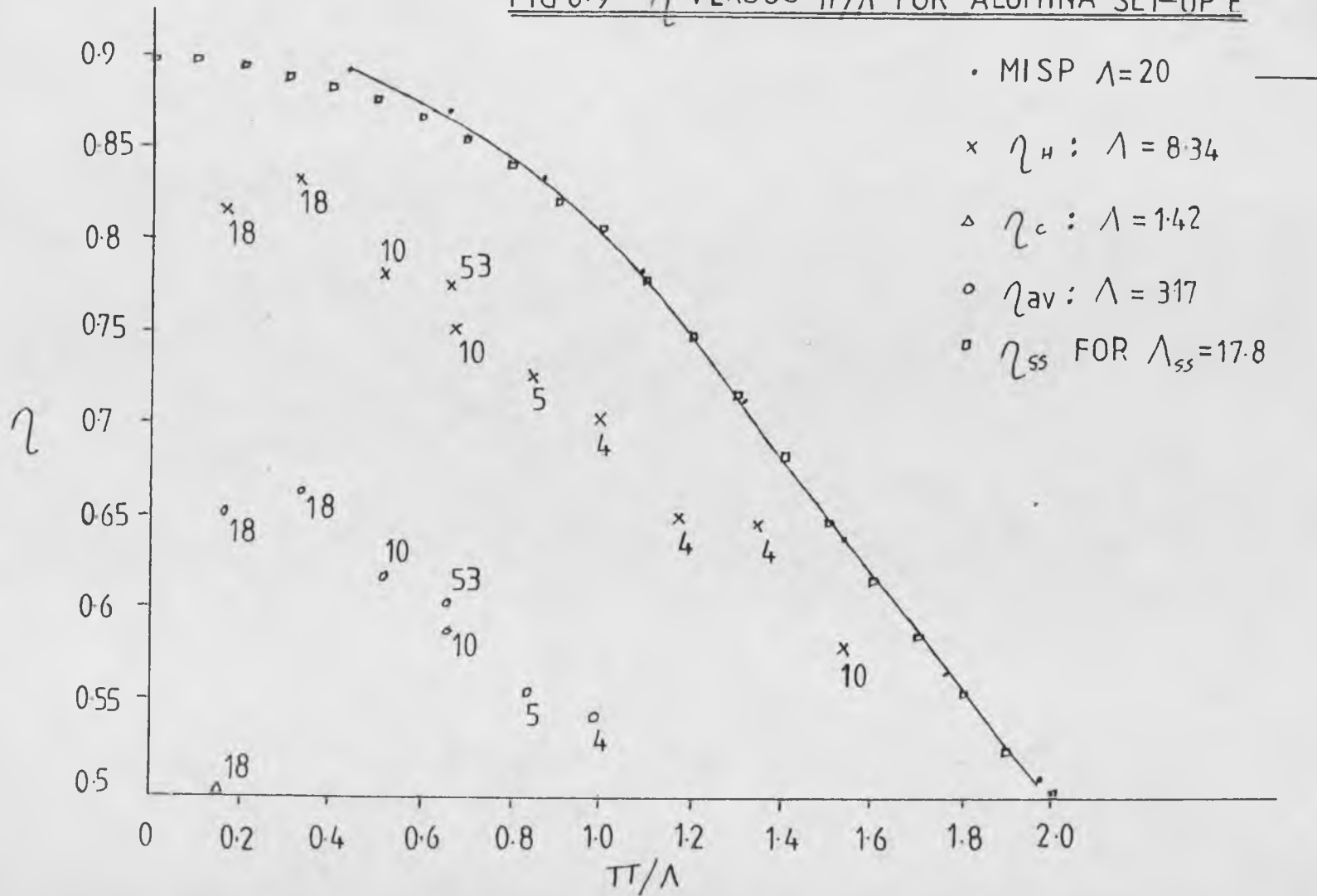
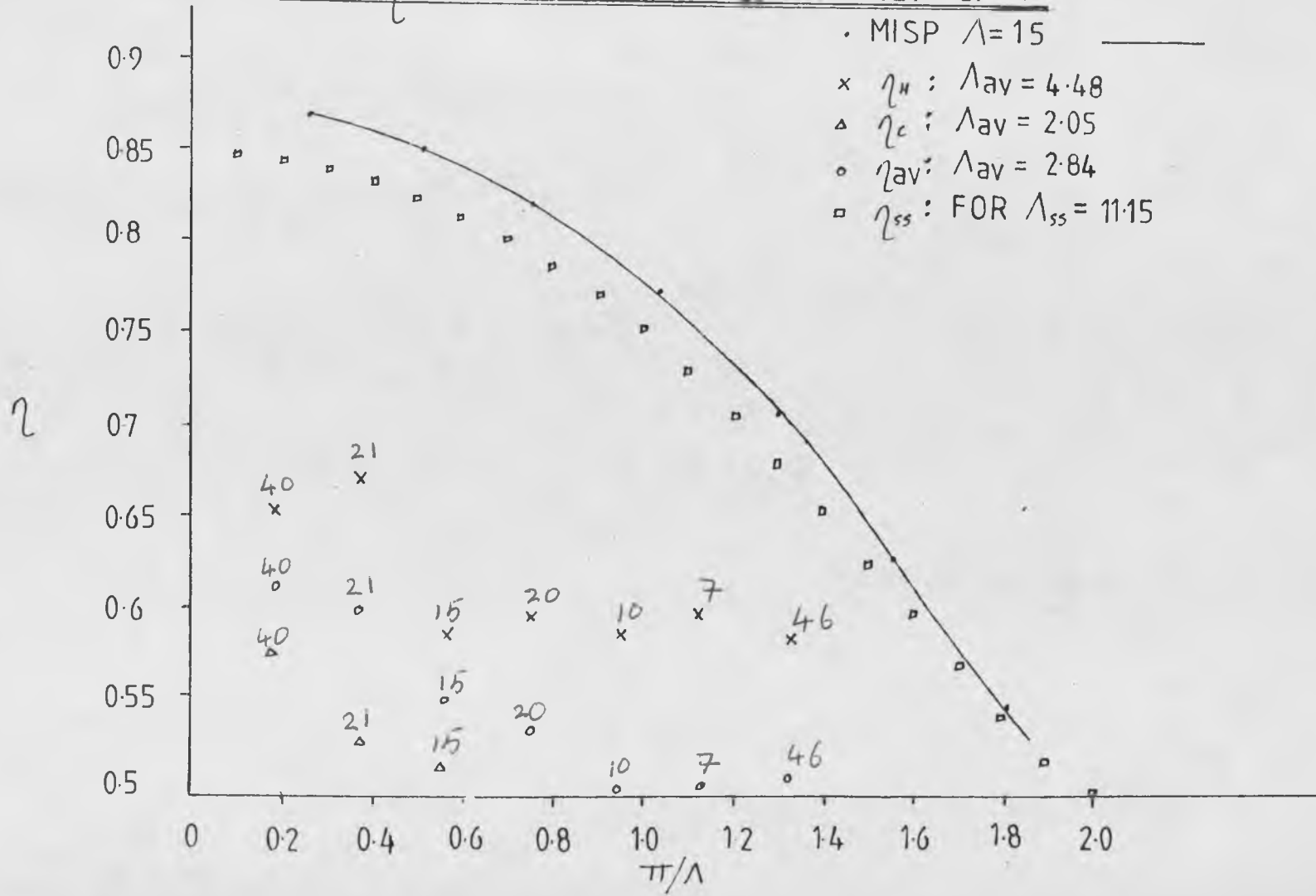


FIG 8.10 η VERSUS π/Λ FOR ALUMINA SET-UP 'F'



set-ups C and D and alumina set-ups E and F are shown in figs. 8.5 to 8.10 respectively. Each graph contains the associated MISP program simulation results, listed in Table 7.2, for $\Lambda = 20$ and 15, the plots for the single shot results shown in table 8.2, and the cyclic practical results which comprise hot, cold and average efficiencies and are listed in Table 8.4.

The steel results in Figs. 8.5 and 8.6 show that $\eta_H > \eta_{av} > \eta_C$ with the associated curves having the same shape as the MISP prediction, but at a lower level. However, theory suggests that at equilibrium $\eta_H = \eta_C$. This shows that the hot and cold strokes have a lower value of Λ than that predicted by the MISP program. It is also evident that as the air flowrate increases, the gap between the hot and cold efficiency curves becomes less.

The lead glass results show a similar trend to that of the steel packing. However the alumina runs are very distinctive in that for each set up the cold efficiency values are so low that they fall below the 50% level. The η_{av} and η^H values, for set up E are wider apart than the steel and glass results, but do follow the same shape as the MISP simulation. However, the results for set up F, at the higher flowrate, do not adhere to any of the experimental results and simulations previously obtained. The η_H and η_{av} curves follow a horizontal trend.

For comparison with the cyclic data the lambda values obtained from the single shot runs were plotted with

the corresponding cyclic data. The cyclic values of η were obtained at various Π/Λ_S for the known single shot lambda value (Λ_{SS}) by using a numerical print out used in the formulation of array A, shown in fig 7.7. The resulting values of η for all six single shot set-ups are shown in table 8.2. The resulting curves are higher than the MISP and practical results of η_H , η_{av} and η_C for the steel and lead glass set ups, because the single shot values of lambda are larger. However, the alumina single shot plots fall below the MISP simulation, as expected, because the values of Λ_{SS} are lower than those used in the MISP predictions.

The discrepancy between the cyclic and single shot results and MISP simulation is not a function of just one effect but a combination of many. Highlighted in this work are the combined effects of the number of cycles required to reach equilibrium, intraconduction within the ceramic packings and also heat leak from the test bed section causing the hot and cold efficiency profiles shown in figs. 8.5 to 8.10 to be dissimilar.

8.4 Effect of the Number of Cycles to Reach Equilibrium

The number of cycles required to reach cyclic equilibrium, which were predicted by the MISP program, are given in table 7.2, and were adhered to where possible for each run. However, for continuous overnight operation the number of cycles for a run were exceeded, particularly

Table 8.2

Values of Efficiency From the Cyclic Method Matrix Using
Single Shot Values of Lambda

Set Up Λ_{SS}	Steel		Lead Glass		Alumina	
	A	B	C	D	E	F
Π/Λ	22.41	17.85	21.0	15.45	17.8	11.15
	η	η	η	η	η	η
0.1	0.9167	0.8982	0.9117	0.8838	0.8974	0.8461
0.2	0.9135	0.8949	0.9085	0.8804	0.8944	0.8428
0.3	0.9090	0.8900	0.9038	0.8754	0.8895	0.8377
0.4	0.9033	0.8839	0.8980	0.8690	0.8333	0.8311
0.5	0.8960	0.8763	0.8906	0.8603	0.8758	0.8228
0.6	0.8871	0.8668	0.8815	0.8516	0.8662	0.8129
0.7	0.8759	0.8551	0.8702	0.8397	0.8546	0.8011
0.8	0.8619	0.8407	0.8561	0.8252	0.8402	0.7871
0.9	0.8441	0.8230	0.8383	0.8097	0.8225	0.7708
1.0	0.8218	0.8017	0.8163	0.7870	0.8012	0.7513
1.1	0.7948	0.7763	0.7896	0.7626	0.7758	0.7294
1.2	0.7632	0.7472	0.7588	0.7351	0.7467	0.7057
1.3	0.7282	0.7152	0.7247	0.7052	0.7149	0.6797
1.4	0.6914	0.6816	0.6888	0.6738	0.6813	0.6528
1.5	0.6545	0.6475	0.6527	0.6417	0.6473	0.6249
1.6	0.6188	0.6141	0.6176	0.6099	0.6140	0.5973
1.7	0.5851	0.5822	0.5844	0.5794	0.5821	0.5700
1.8	0.5541	0.5523	0.5537	0.5505	0.5522	0.5438
1.9	0.5256	0.5246	0.5254	0.5234	0.5246	0.5188
2.0	0.4997	0.4991	0.4995	0.4984	0.4991	0.4952

for the smaller time period runs. Run 8 for steel set up A, shown in Fig. 8.5, clearly indicates how increasing the number of cycles increases the hot efficiency, decreases the cold efficiency, but the average value tends to remain on the slope of average efficiency plot. The steel set up B, fig. 8.6 was run approximately to the MISP program predictions and the efficiency values are consistent, with the hot average and cold curves much closer together.

The lead glass values however show a vastly different trend. Lead glass values for set up C, fig. 8.7, commence at a high Π/Λ using the number of cycles predicted by the MISP program. However, the slope does not follow that of the MISP or single shot curve. On the sixth run the regenerator was left operational overnight and 58 cycles were achieved. This altered the slope of the hot cold and average efficiencies, to that of the MISP and Λ_{SS} plots, consequently altering the value of Λ . The tenth cycle efficiencies are also included for the sixth run and clearly shows how, if only 10 cycles were used the previous data slope would be followed. The remaining runs, however, do not recover from the 58 cycles and therefore follow the new slope.

The lead glass set-up C clearly shows that an inadequate number of cycles produces a curve not consistent with that of the MISP prediction. This suggests that the correct temperature profile with respect to length and time corresponding to cyclic equilibrium is not attained and this

consequently alters the slope of the efficiency curve, producing different values of Λ . However when an adequate number of cycles is used, in excess of those predicted by the MISP program, the correct slope is achieved as the correct temperature profiles for each stroke are produced.

The effect of too many cycles for a run is shown for the lead glass set up D, Fig. 8.8, where the results for the first run (high Π/Λ) were obtained after 79 cycles. The remaining efficiency values follow the slope of the MISP and single shot curve, but much lower, corresponding to a lower value of Λ .

The alumina plot for set up E, fig. 8.9 shows only the hot and average efficiency values which are wider apart than the corresponding steel and lead glass set ups, however the slopes do approximate to the MISP and single shot curves. A similar effect to the steel and lead glass set-ups are shown for the sixth run where 53 cycles were used. The hot efficiency for the tenth cycle is less than that of the 53rd cycle, as expected. The alumina plot for set up F, fig. 8.10 shows an inconsistency with the MISP and single shot curves. The hot and average efficiency curves are almost horizontal, but the two curves are closer together than set up E.

It is clear that the number of cycles required to reach equilibrium have a significant effect upon the response of a cyclic regenerator. The regenerator efficiencies (hot

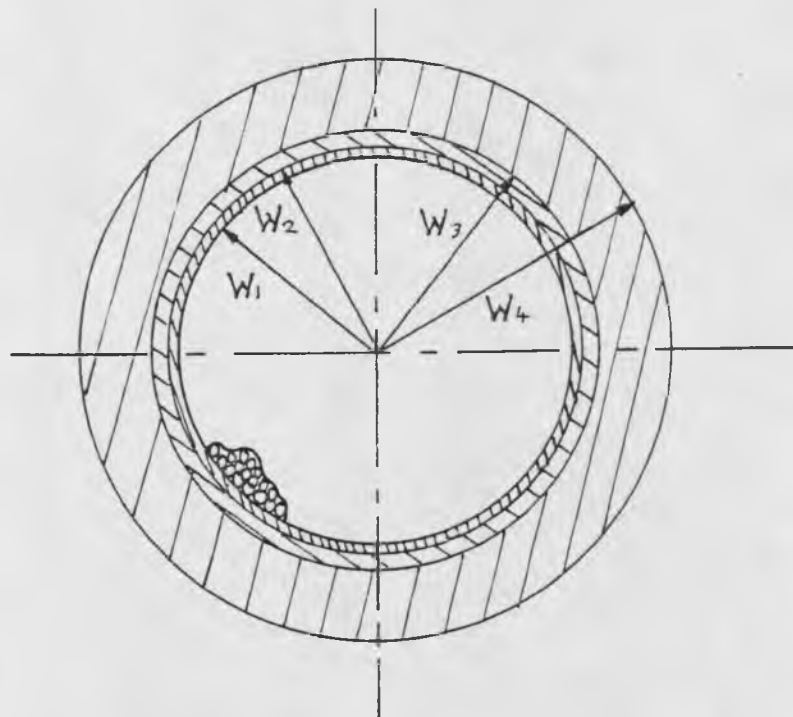
and cold) can be markedly affected by the number of cycles employed and when used in sequence with other runs it can significantly alter the slope of the efficiency versus Π/Λ curve. In operating the apparatus a significantly long set-up time in conjunction with a sufficiently tight convergence factor in the MISP program simulation had to be achieved. It is now clear that the number of cycles required to reach equilibrium was inadequate. Previous workers when operating regenerative apparatus paid little attention to this aspect, however with the advent of digital computers and the aid of finite difference techniques the actual number of cycles required to reach equilibrium can be examined in greater detail.

A further aspect arising from the graphs shown in figs. 8.5 to 8.10 is the discrepancy between the hot and cold efficiencies. This is caused by heat leak from the system.

8.5 Discrepancy Between Hot and Cold Efficiencies

The discrepancy between the hot and cold efficiencies for all the set-ups, which are shown in figs. 8.5 to 8.10, is considered to be partially due to heat leak from the test section. In all cases the hot efficiencies are greater than the cold efficiencies. In addition the closeness of the hot and cold efficiency curves is a function of the flowrate within the test section, for a fixed ambient and mean regenerator temperature. Observation of the steel and lead glass set up plots, figs. 8.5 to 8.8 respectively,

FIG 8.11 SECTION THROUGH THE REGENERATOR BED



- ≡ TRITON KAOWOOL: $K_{II} = 0.04 \text{ W/m}^2\text{K}$
 ≡≡ COPPER WALL: $K_w = 384.3 \text{ W/m}^2\text{K}$
 // POLYURATHENE: $K_{EI} = 0.033 \text{ W/m}^2\text{K}$

BED LENGTH = $L = 203 \text{ mm}$

INTERNAL AREA = $A_z = 0.0473 \text{ m}^2$

EXTERNAL AREA = $A_o = 0.075 \text{ m}^2$

CROSS SECTIONAL AREA OF FLOW = $A_x = 0.0046 \text{ m}^2$

$W_1 = 37.1 \text{ mm}$

$W_2 = 381 \text{ mm}$

$W_3 = 39.7 \text{ mm}$

$W_4 = 58.8 \text{ mm}$

TABLE 8.3

Heat Leak Calculation Data

Variable	Set up A	Set up B
G	0.525	1.176
w	3.18	3.18
C _g	1004	1004
Pr	0.72	0.72
μ	1.95×10^{-6}	1.95×10^{-6}
Re	1712	3836
Pv	0.37	0.37
h _I	80.35	157.4
h _o	1.82	1.82
UA'	0.0570	0.0576
T _{reg}	30	30
T _{amb}	15	15
T _{step}	5	5
q _{in}	54.81	122.8
q _{loss}	1.14	1.14
GB/GA	2.24	2.24
$\frac{q_{\text{loss}}/q_{\text{in}} \text{ in set-up B}}{q_{\text{loss}}/q_{\text{in}} \text{ in set-up A}}$		2.22

clearly shows that as the flowrate is increased the efficiency plots become closer.

Under Schumann type assumptions however, the regenerator walls are adiabatic. Heat from the rig was reduced to a minimum by insulating both internally and externally, as can be seen from the the schematic section through the test bed, fig. 8.11. The amount of heat that does escape is only fractionally altered by changing the internal air velocity, consequently the ratio of the heat loss to the heat input for the system falls for higher internal flowrates. The ratio of the heat loss, q_{loss} and the heat flow in q_{in} are listed in table 8.3.

Verification of the heat loss and heat input for the system can be simply examined by considering the regenerator bed at steady state and experiencing a step change in the inlet temperature.

Where heat loss = $q_{loss} = UA' (T_{reg} - T_{amb})$

and heat in = $q_{in} = G C_g \Delta T$

UA' = overall heat transfer coefficient x area

$$\text{and } \frac{1}{UA'} = \frac{1}{h_i A_i} + \frac{\ln \frac{w_0}{w_1}}{2\pi k_{II} L} + \frac{\ln \frac{w_1}{w_2}}{2\pi k_w L} + \frac{\ln \frac{w_2}{w_3}}{2\pi k_{EI} L} + \frac{1}{h_o A_o}$$

h_i = internal heat transfer coefficient obtained from table 3.1 for $\frac{1}{4}$ inch diameter steel shot.

h_o = natural convective heat transfer coefficient given by $Nu = 0.138 GR^{0.36} (Pr^{0.175} - 0.55)$

taken from Perry (1973)

where GR = Grashof number

The bed parameters $w_0, w_1, w_2, w_3, A'_1, A'_0, A'_x$, and L are given in fig. 8.11, along with the thermal conductivities,

polyurathane external insulation : k_{EI}

copper pipe : k_w

Triton Kaowoll internal insulation: k_{II}

The test bed gas mass velocities of 0.525 and 1.176 kg/sm^2 are used with an ambient temperature of 15°C and a regenerator input and step temperature of 30 and 5°C respectively. The data and calculated variables used to obtain the ratio of $q_{\text{in}}/q_{\text{loss}}$ for the two set up flowrates A and B are given in table 8.3. The heat in, to heat lost ($q_{\text{in}}/q_{\text{loss}}$) is 2.22 compared to 2.24 for the ratio of the flowrates. It can be clearly seen that the overall 'UA' is changed very little for a flowrate change by a factor of 2.24.

For an above ambient temperature regenerator the hot efficiency is always greater than the cold efficiency. This is because for a hot stroke the hot end is at maximum temperature, however the whole bed is heated with respect to time and heat is lost throughout this period. During the cold stroke the heat that is recovered is less than that theoretically imparted during the hot stroke, because of heat loss. Additionally there is also heat loss during the cold stroke. The end result is

$$\text{HIT} - \text{HOTM} \gg \text{COTM} - \text{CIT}$$

$$\text{i.e. } \eta_H = \frac{\text{HIT} - \text{HOTM}}{\text{HIT} - \text{CIT}} \gg \eta_C = \frac{\text{COTM} - \text{CIT}}{\text{HIT} - \text{CIT}}$$

The converse is true $\eta_C > \eta_H$ for a cryogenic system.

Verification of heat leak is upheld by plotting two of Bretherton's (1970) set ups, figs. 8.12 and 8.13 showing η versus Π/Λ for $\Lambda = 178$ at a flowrate of $0.001576 \text{ Nm}^3/\text{s}$ and $\Lambda = 250$ at a flowrate of $0.000643 \text{ Nm}^3/\text{s}$. The graphs show a similar trend to the steel and lead glass set ups with the efficiency curves apart, however the cold efficiency values are greater than those of the hot efficiency. This is due to the cryogenic nature of the apparatus with heat leak ingressing into the system. The efficiency plots are further apart for the lower flowrate of $0.000643 \text{ Nm}^3/\text{s}$, fig 8.13, but closer together for the higher flowrate of $0.001576 \text{ Nm}^3/\text{s}$, fig. 8.12, providing further evidence that the efficiency values obtained are a function of the flowrate within the test section.

This effect can be minimised and the Schumann type assumption of no heat leak approached if the regenerator is sufficiently insulated, it is run at a high flowrate, the ambient to mean regenerator temperature is low and the number of cycles to reach equilibrium are maximised to produce the correct temperature profiles within the regenerator test bed.

8.6 Dimensionless Length Prediction

Data from the six set-ups shown in table 8.4 was treated where possible by the cyclic regenerator matrix

FIG 8.12 BRETHERTON'S SET-UP AT $\Lambda = 178$ FOR 0.08 INCH (2.03mm) LEAD SHOT
 FLOWRATE = $0.001576 \text{ Nm}^3/\text{s}$

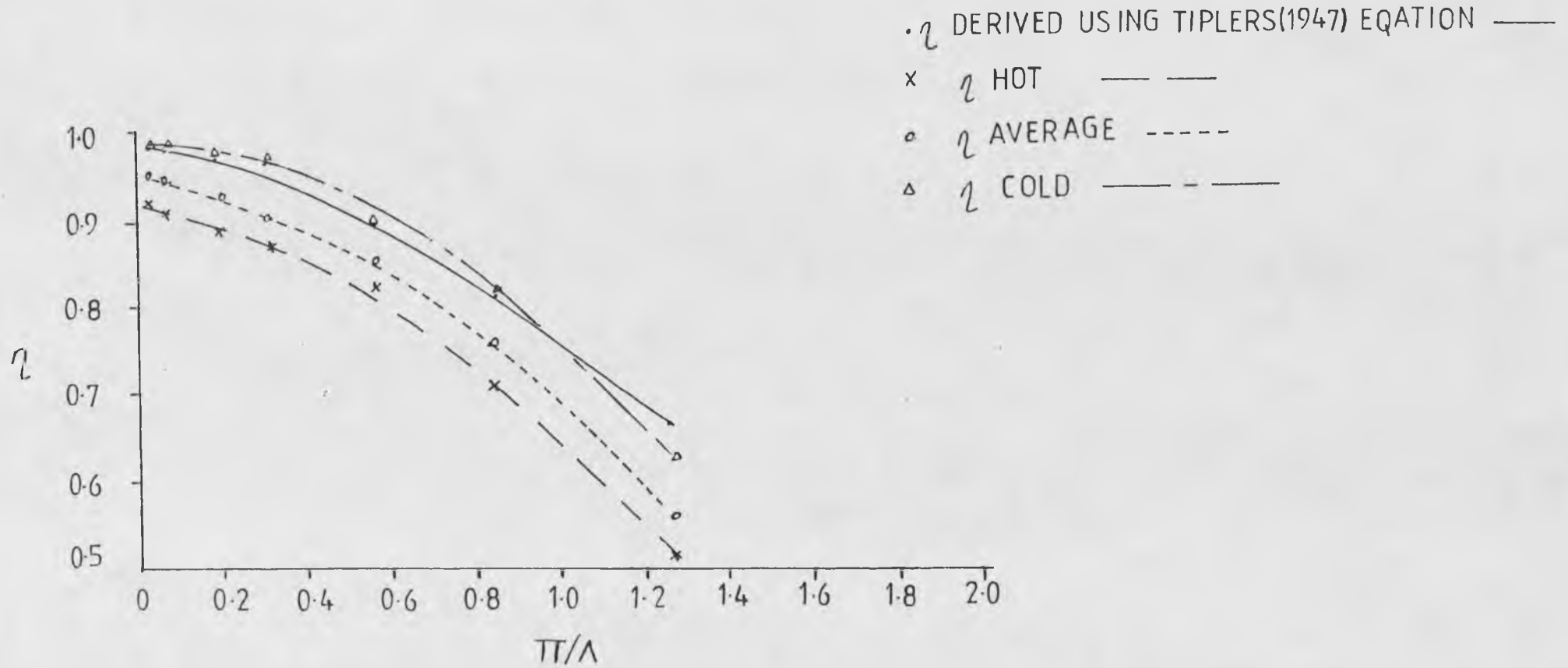


FIG 8.13 BRETHERTON'S SET-UP AT $\Lambda=250$ FOR 0.08 INCH (2.03) LEAD SHOT

FLOWRATE = 0.000643 Nm³/s

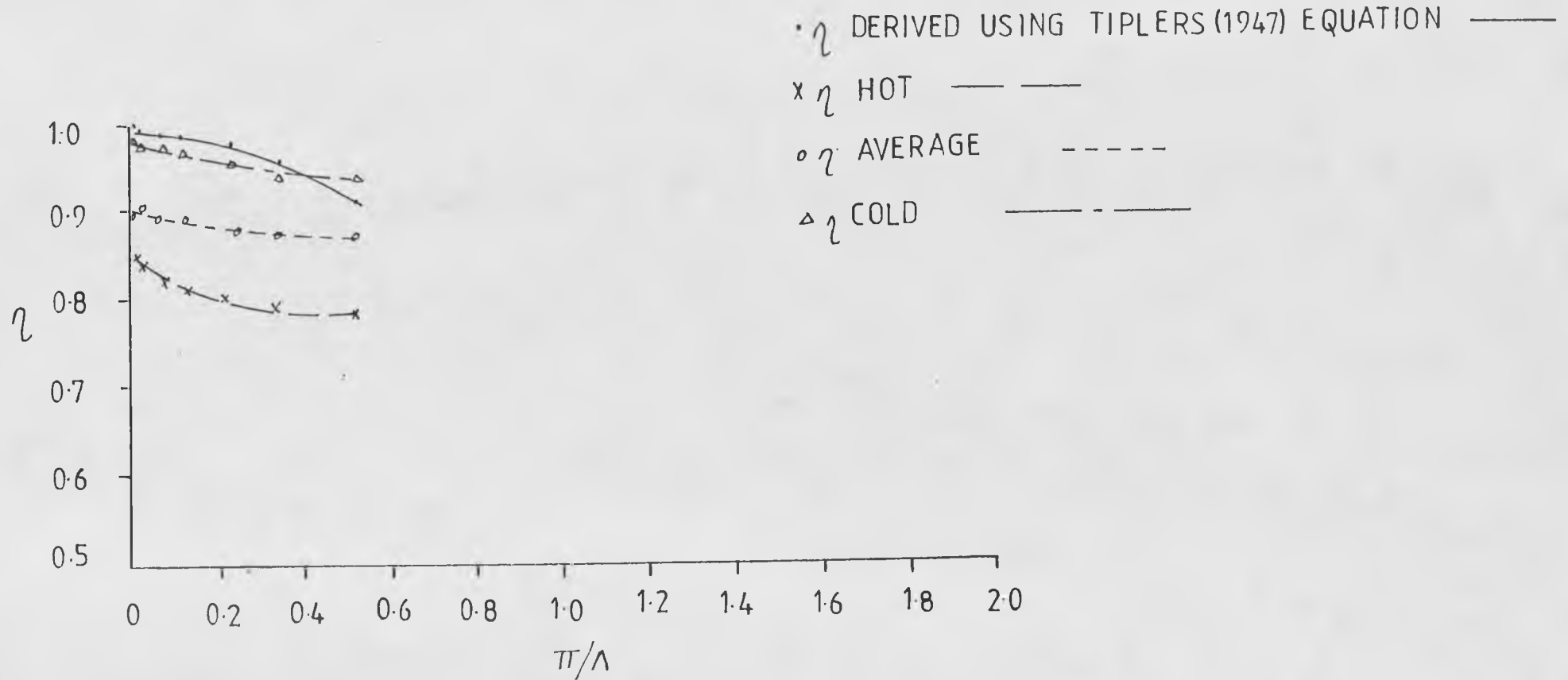


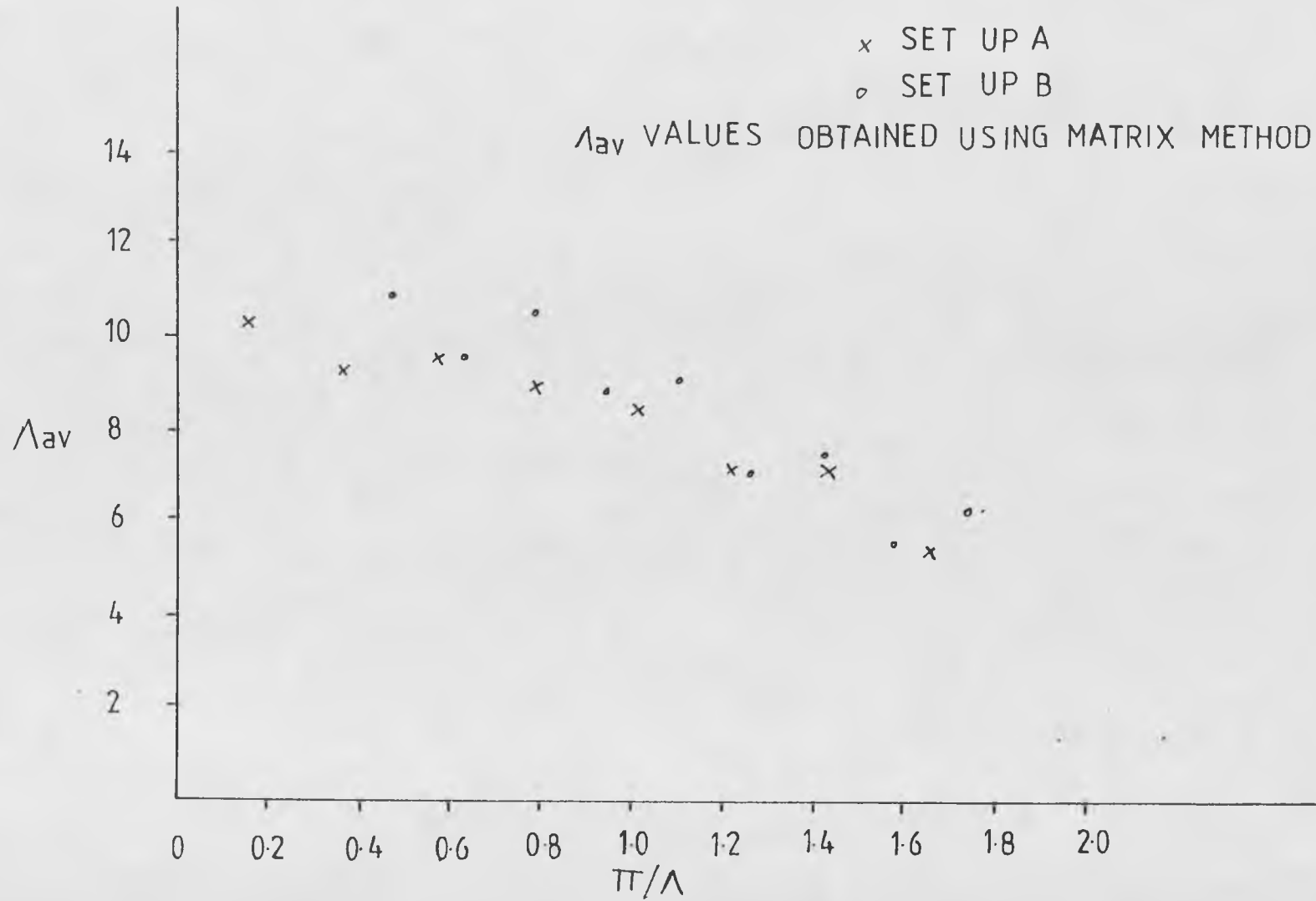
FIG 8.14 Λ_{av} VERSUS π/Λ FOR STEEL SET-UPS 'A' AND 'B'

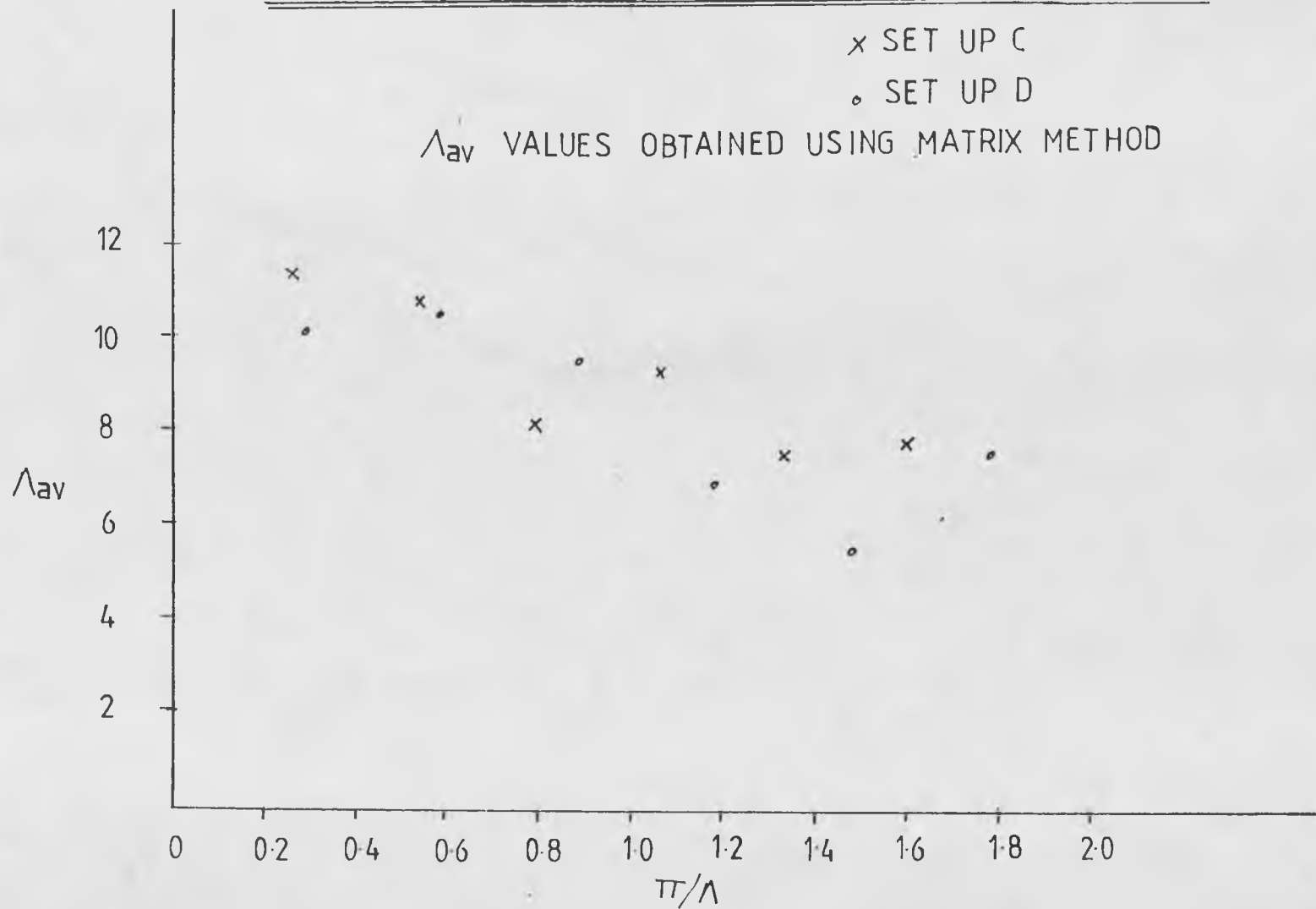
FIG 8.15 Λ_{av} VERSUS π/Λ LEAD GLASS SET-UPS C AND D

FIG 8.16 Λ_{av} VERSUS π/Λ FOR ALUMINA SET-UPS E AND F

x SET UP E

o SET UP F

Λ_{av} VALUES OBTAINED USING THE MODIFIED TIPLER EQUATION

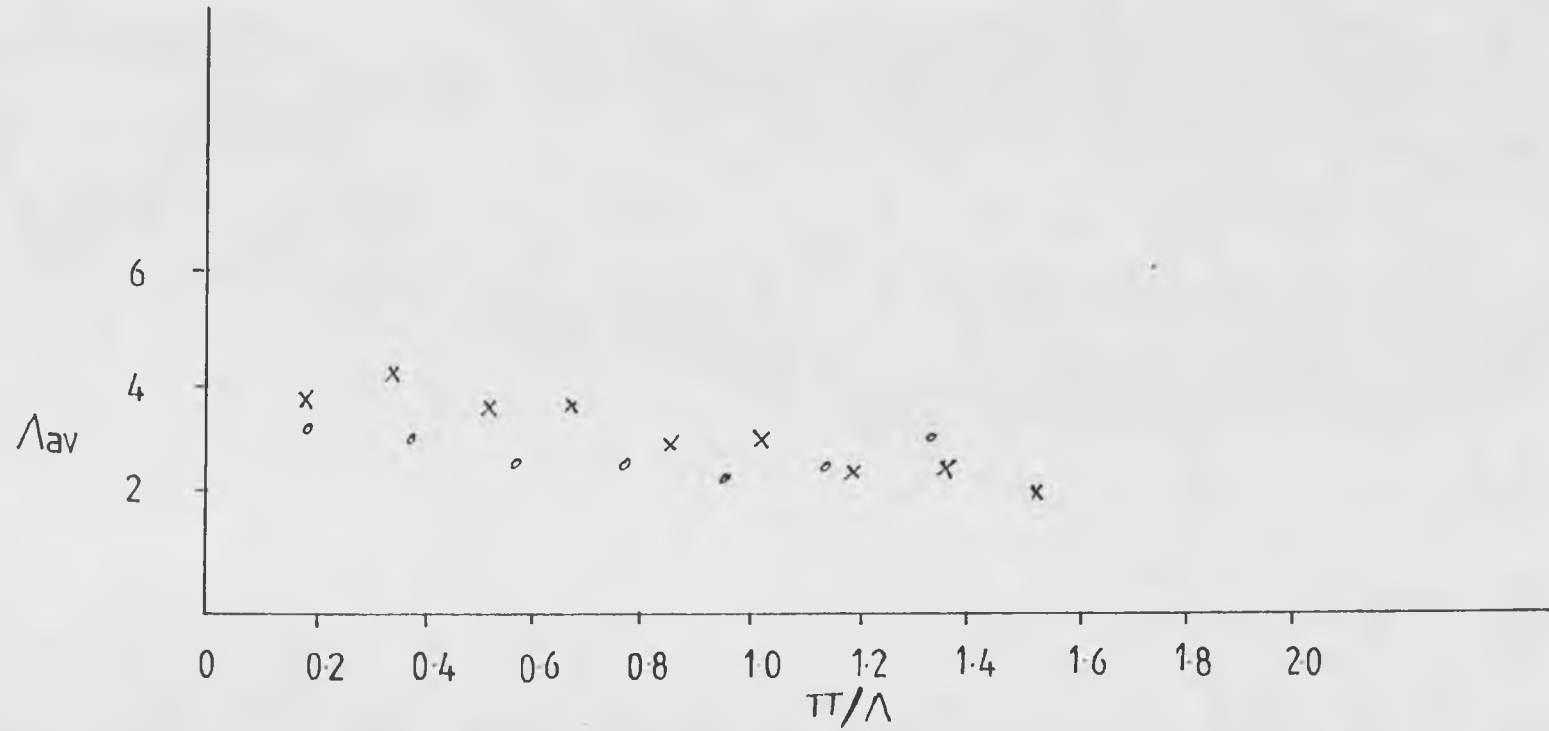


Table 8.4

Results From Set Ups A to F

Steel Data for Set Up A

Run	P	Π/Λ	η_H	Λ_H	Λ_T	η_C	Λ_C	Λ_T	η_{av}	Λ_{av}	Λ_T	Sequence Nos.
A1	2	0.1436	0.902	18.59	19.53	0.773	6.945	6.936	0.837	10.32	10.583	10
A2	5	0.359	0.897	19.78	26.61	0.721	5.478	5.627	0.809	9.21	9.974	9
A3	8	0.574	0.9	24.61	250.0	0.70	5.244	5.747	0.80	9.667	12.774	8
A4	11	0.79	0.824	15.911	119	0.6926	5.89	6.993	0.758	8.928	14.07	7
A5	14	1.01	0.777	14.1	U	0.657	5.586	7.581	0.717	8.451	19.57	6
A6	17	1.22	0.724	14.32	U	0.587	-	5.617	0.655	7.097	17.696	5
A7	20	1.44	0.681	9.994	U	0.533	-	4.764	0.607	7.074	30.0	4
A8	23	1.65	0.581	10.595	U	0.491	-	4.315	0.5353	5.30	10.71	3
A9	26	1.87	0.627	-	U	0.353	-	1.47	0.49	-	10.28	2
A10	29	2.27	0.507	-	U	0.391	-	3.281	0.449	-	-	1
Average				15.86	104		5.83	5.23		8.256	15.08	

Steel Data for Set Up B

Run	P	Π/Λ	η_H	Λ_H	Λ_T	η_C	Λ_C	Λ_T	η_{av}	Λ_{av}	Λ_T	Sequence Nos.
B1	3	0.475	0.841	12.717	16.278	0.782	8.125	9.19	0.812	10.917	13.578	10
B2	4	0.633	0.82	11.808	19.847	0.762	7.855	9.836	0.792	9.632	13.456	9
B3	5	0.792	0.785	10.793	22.674	0.784	10.67	22.19	0.784	10.67	22.19	8
B4	6	0.951	0.7436	9.648	25.274	0.726	8.47	16.57	0.735	8.852	20.142	7
B5	7	1.109	0.721	10.513	190.4	0.685	7.845	17.85	0.703	9.082	32.34	6
B6	8	1.267	0.664	8.633	59.1	0.624	6.076	11.065	0.644	7.162	18.7	5
B7	9	1.426	0.615	7.837	43.864	0.6128	7.618	35.11	0.614	7.521	48.9	4
B8	10	1.584	0.567	6.267	24.06	0.54	-	8.278	0.553	5.545	12.02	3
B9	11	1.743	0.5336	6.425	39.142	0.527	5.658	19.29	0.5303	6.261	25.73	2
B10	12	1.901	0.52	10.42	U	0.457	-	4.635	0.488	4.143	12.65	1
Average				9.506	48.96		7.789	15.4		7.89	20.98	

U = INDETERMINATE Using the modified Tipler (1947) equation

- = outside the matrix method $25.0 < \Lambda < 5.1$ bounds

Lead Glass Data For Set-up C

Run	P	π/Λ	η_H	Λ_H	Λ_T	η_C	Λ_C	Λ_T	η_{av}	Λ_{av}	Λ_T	Sequence Nos.
C1	2	0.266	0.932	-	39.52	0.755	6.478	6.533	0.8438	11.475	12.125	9
C2	4	0.532	0.938	-	U	0.701	5.259	U	0.82	10.881	14.516	8
C3	6	0.8	0.913	-	U	0.58	-	3.376	0.747	8.2	U	7
C4	8	1.065	0.823	-	U	0.631	-	6.50	0.727	9.269	U	6
C5	10	1.33	0.688	14.01	13.68	0.582	-	6.878	0.6356	7.604	27.43	5
C6	12	1.6	0.657	-	U	0.502	-	4.498	0.579	7.962	U	4
C7	14	1.865	0.673	-	U	0.4142	-	2.448	0.543	-	U	3
C8	16	2.13	0.598	-	U	0.335	-	1.447	0.465	-	U	2
C9	18	2.39	0.5658	-	U	0.349	-	2.041	0.458	-	U	-
Average				14.01	26.6		5.868	4.215		9.232	18.0	

Lead Glass Data for Set-up D

Run	P	π/Λ	η_H	Λ_H	Λ_T	η_C	Λ_C	Λ_T	η_{av}	Λ_{av}	Λ_T	Sequence Nos.
D1	1	0.296	0.794	8.127	8.478	0.86	13.05	U	0.827	10.116	U	7
D2	2	0.593	0.816	11.315	16.26	0.802	10.03	U	0.809	10.643	U	6
D3	3	0.89	0.743	8.971	16.75	0.744	8.906	U	0.745	7.614	U	5
D4	4	1.186	0.643	6.374	16.919	0.663	7.452	U	0.653	6.863	U	4
D5	5	1.48	0.591	6.629	21.24	0.558	-	7.702	0.574	5.515	U	3
D6	6	1.78	0.558	21.0	U	0.517	5.467	U	0.537	7.748	U	2
D7	7	2.07	0.464	-	33.1	0.428	-	4.205	0.446	-	7.0	1
Average				10.41	17.79		8.98			8.086		

Alumina Set Up Data E

Run	P	π/Λ	η_H	Λ_H	Λ_T	η_C	Λ_T	η_{av}	Λ_T	Sequence No.
E1	2	0.169	0.814	8.904	9.0616	0.497	1.985	0.655	3.8427	9
E2	4	0.3386	0.842	11.565	12.925	0.493	1.981	0.667	4.224	8
E3	6	0.508	0.781	8.323	9.517	0.459	1.756	0.62	3.584	7
E4	8	0.678	0.775	8.847	12.4	0.438	1.647	0.606	3.618	6
E5	10	0.846	0.728	7.73	11.256	0.379	1.294	0.553	2.995	5
E6	12	1.015	0.705	7.78	15.43	0.375	1.305	0.539	3.065	4
E7	14	1.18	0.649	6.479	11.894	0.324	1.076	0.487	2.49	3
E8	16	1.355	0.649	9.019	U	0.3	0.934	0.475	2.59	2
E9	18	1.523	0.578	6.375	18.87	0.279	0.8414	0.43	2.121	1
Average				8.336	12.67		1.42		3.17	

Alumina Set Up Data F

Run	P	π/Λ	η_H	Λ_T	η_C	Λ_T	η_{av}	Λ_T	Sequence No.
F1	1	0.189	0.6522	3.806	0.574	2.72	0.613	3.205	7
F2	2	0.379	0.672	4.392	0.527	2.296	0.60	3.137	6
F3	3	0.569	0.585	3.104	0.5168	2.278	0.551	2.653	5
F4	4	0.759	0.595	3.575	0.475	0.979	0.535	2.626	4
F5	5	0.948	0.589	3.971	0.4172	0.579	0.5033	2.422	3
F6	6	1.138	0.598	5.392	0.41	1.60	0.5043	2.696	2
F7	7	1.328	0.585	7.141	0.4295	1.906	0.507	3.195	1
Average				4.483		2.051		2.847	

method developed in Chapter 7.6. With three values of efficiency (η_H , η_{av} and η_C) corresponding to a Π/Λ value for each run the matrix bounds, shown in Fig. 7.11, for $0.47 < \eta < 0.9675$, $0.1 < \Pi/\Lambda < 2.0$ and $5.1 < \Lambda < 25$ were exceeded even though Heggs (1967) single shot correlation equation 3.1, was used to produce values of Λ equal to 15 and 20 for the steel, lead glass and alumina set ups. Exceeding the array bounds shows how intraconduction, the number of cycles to reach equilibrium and heat leak affect the value of heat transfer coefficient, hence Λ .

The Λ values which could not be obtained using the matrix technique were investigated using the modified Tipler (1947) method formulated by Willmott (1964). Unfortunately they were not consistent for steel and lead glass and in many cases were even unstable. The values of Λ obtained using the modified Tipler method (Λ_T) are shown with the matrix method values in Table 8.4 and can be seen to be inconsistent showing much higher values. Fortunately, however, complete treatment of the alumina set-ups E and F was possible giving consistent values of Λ_T , as shown in table 8.4. Examination of the average Λ values, will only be considered.

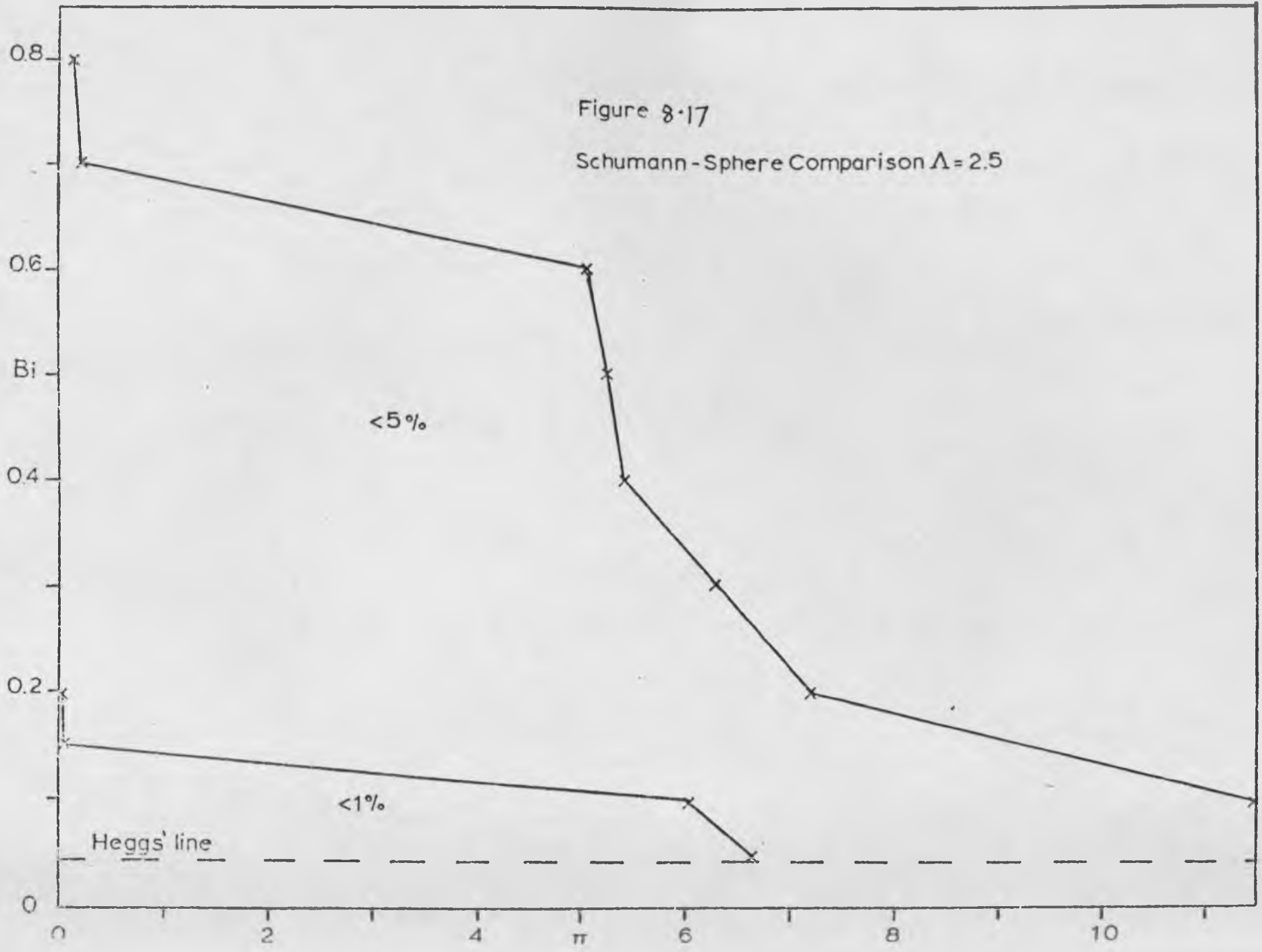
Figs. 8.14 to 8.16 show Λ_{av} values plotted against Π/Λ for the steel lead glass and alumina set-ups respectively. All the set ups show a tendency for Λ to decrease with increasing Π/Λ . This suggests that the convective heat transfer coefficient is dependent to some degree upon the

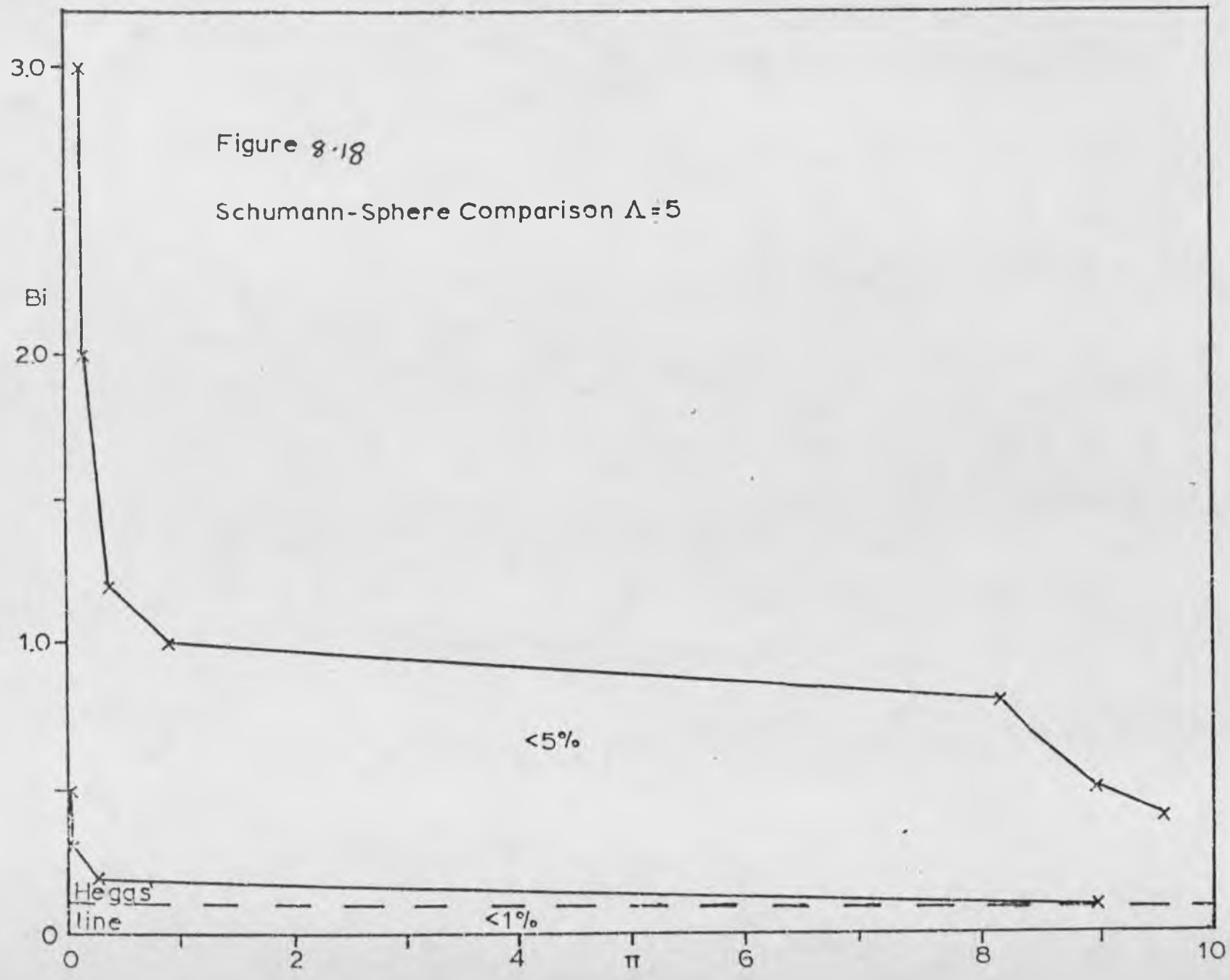
cycle time, increasing as time is reduced. This however is contrary to the theoretical results obtained by Carpenter (1976). Theoretical simulation of the practical runs predicted a difference of 5 for the set up Λ'_S . However, as can be seen from all three graphs the mean value difference for the Λ_{av} plots are not greater than 1.3, compared to a maximum value of 6.5 for the experimental single shot runs.

At high values of Π/Λ the efficiencies obtained did not fit into the Λ bound of 5.1 to 25 and consequently the practical data could not be evaluated. Inconsistent values of Λ for $\Pi/\Lambda > 1.0$ were obtained because the Λ nest of curves approached each other as Π/Λ increased beyond 1.0, as discussed in chapter 7.6.2, and only a fractional change in η causes a large change in Λ . Future experimental runs should therefore be restricted between $0 < \Pi/\Lambda < 1.5$, which has the automatic affect of producing bed efficiencies greater than 60 to 70%.

8.7 Intraconduction Analysis of the Cyclic Set-Ups

Intraconduction analysis of cyclic regenerator packings is well reported by Carpenter (1976), Bretherton (1970) and Hausen (1942). Hausen's Eigen function technique is used to obtain the packing heat transfer coefficient and subsequently the overall heat transfer coefficient. With the addition of intraconduction the regenerator efficiency is not only a function of Λ and Π but also Bi . Theoretically derived charts showing levels of intraconduction have been





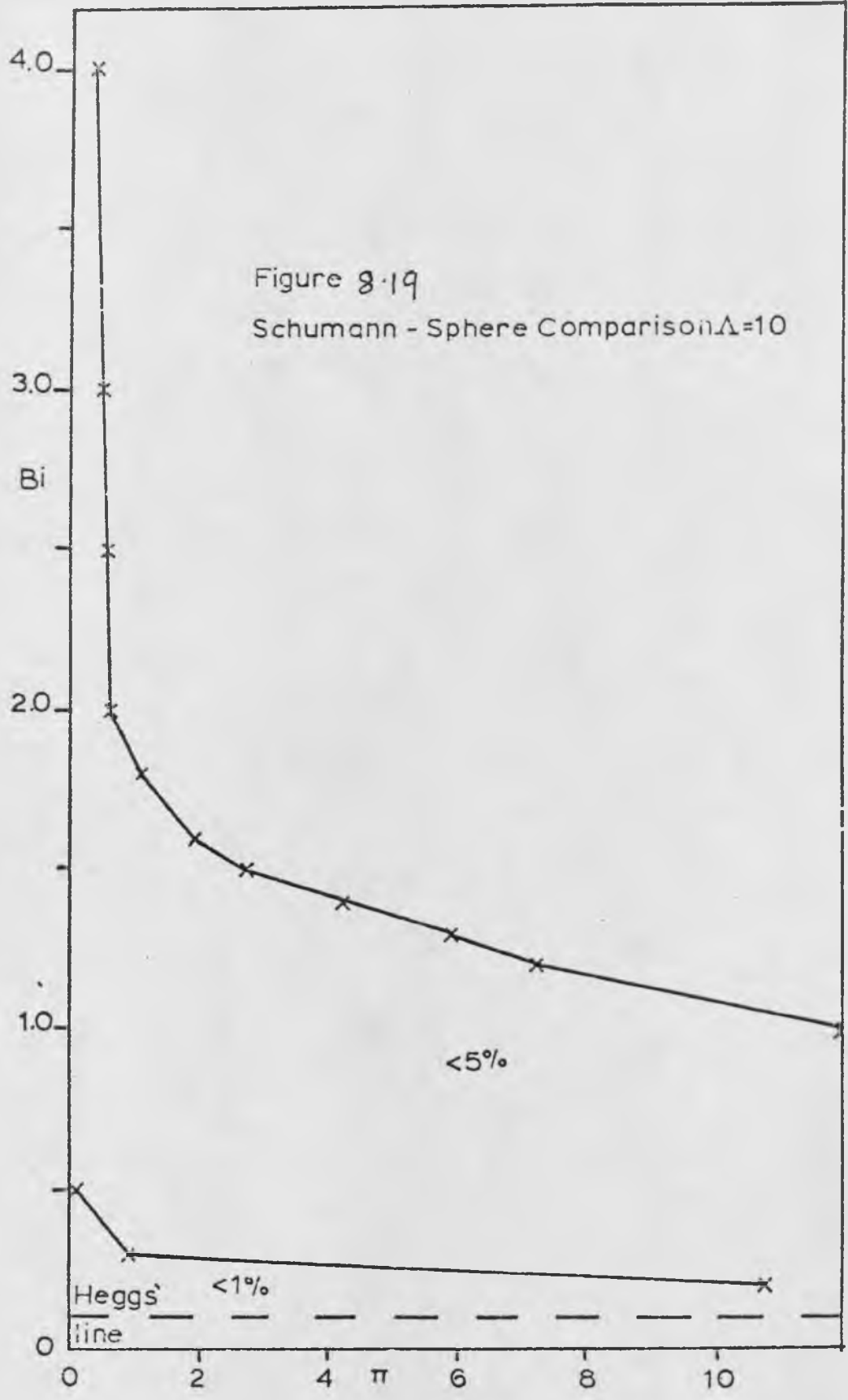


TABLE 8.5

Data Used in Intraconduction Analysis

$$Bi = \frac{h_c w}{K_s}$$

$$h_c = \frac{\Lambda_{av} \cdot G \cdot C_g}{A \cdot L}$$

$$h_s = \frac{3k}{\phi w}$$

$$Fo = \frac{\alpha \cdot p}{w^2}$$

$$\frac{1}{h_o} = \frac{1}{h_c} + \frac{1}{h_s}$$

$$PER = \frac{h_c - h_o}{h_c} \times 100$$

1. Steel Set-Up 'A'

$$w = 3.18 \text{ mm}, K_s = 44.7, G = 0.525, A = 595.3,$$

$$C_g = 1004 \quad C_s = 0.461, L = 0.203 \text{ m}, \alpha = 1.263 \times 10^{-5}$$

Run	P	Π/Λ	Π_{av}	Λ_{av}	hc	Bi	$(\frac{1}{Fo} + \frac{1}{Fo})$	ϕ	$\frac{\phi w}{3K_s}$	h_s	h_o	PER
A1	2	0.1436	0.482	10.32	45.01	0.00313	0.026	1	0.0000232	43155.8	44.96	0.105
A2	5	0.359	3.306	9.21	40.16	0.00363	0.0106	1	"	"	40.12	0.099
A3	8	0.574	5.549	9.667	42.16	0.00382	0.0066	1	"	"	42.11	0.098
A4	11	0.79	7.053	8.938	38.94	0.00352	0.00483	1	"	"	38.90	0.087
A5	14	1.01	8.535	8.45	36.85	0.00333	0.0038	1	"	"	36.82	0.092
A6	17	0.22	8.658	7.097	30.95	0.0028	0.0031	1	"	"	30.93	0.073
A7	20	1.44	10.187	7.074	30.85	0.0028	0.0026	1	"	"	30.83	0.055
A8	23	1.65	8.743	5.3	23.11	0.0021	0.0023	1	"	"	23.10	0.049
A9	26	1.87	-	-	-	-	-	-	-	-	-	-
A10	29	2.27	-	-	-	-	-	-	-	-	-	-
Average				8.26	36.0					43155.8	35.97	

2. Steel Set-up 'B'

$$w = 3.18 \text{ mm}, K_S = 45.7, G = 1.176, A = 595.3$$

$$C_g = 1004, C_S = 0.461, L = 0.203 \text{ m}, \alpha = 1.263 \times 10^{-5}$$

Run	P	Π/Λ	Π_{av}	Λ_{av}	hc	Bi	$(\frac{1}{Fo} + \frac{1}{Fo})$	ϕ	$\frac{\phi w}{3ks}$	h_s	h_c	PER
B1	3	0.475	5.186	10.92	106.7	0.007	0.017	1	0.0000232	43155.8	106.43	0.247
B2	4	0.673	6.097	9.63	94.15	0.0065	0.013	1	"	"	93.94	0.218
B3	5	0.792	8.451	10.67	104.26	0.0071	0.0106	1	"	"	104.0	0.242
B4	6	0.951	8.451	8.85	86.52	0.0059	0.0084	1	"	"	86.34	0.20
B5	7	1.109	10.07	9.08	88.75	0.0061	0.0076	1	"	"	88.57	0.206
B6	8	1.267	9.076	7.16	70.01	0.0048	0.0066	1	"	"	69.89	0.162
B7	9	1.426	10.725	7.52	73.51	0.0051	0.0059	1	"	"	73.38	0.171
B8	10	1.584	8.783	5.54	54.19	0.0037	0.0053	1	"	"	54.13	0.126
B9	11	1.743	10.91	6.26	61.16	0.0042	0.0048	1	"	"	61.06	0.142
B10	12	1.901	7.876	4.14	40.49	0.0027	0.0044	1	"	"	40.45	0.094
Average				<u>7.98</u>	<u>77.97</u>					<u>43155.8</u>	<u>77.82</u>	

3. Glass Set-Up 'C'

$$w = 3.00 \text{ mm} \quad K_S = 3.116 \quad G = 0.525 \quad A = 629.9$$

$$C_g = 1004 \quad C_S = 0.287 \quad L = 0.203\text{m} \quad \alpha = 3.682 \times 10^{-6}$$

Run	P	Π/Λ	Π_{av}	Λ_{av}	hc	Bi	$(\frac{1}{Fo} + \frac{1}{Fd})$	ϕ	$\frac{\phi W}{3K_S}$	h_s	h_o	PER
C1	2	0.266	3.053	11.475	47.29	0.067	0.136	0.991	0.00047	2126.7	44.26	2.175
C2	4	0.532	5.789	10.88	44.84	0.064	0.0684	0.995	0.00047	2118.8	43.91	2.072
C3	6	0.80	6.56	8.2	33.79	0.048	0.0456	0.997	0.00047	2110.1	33.26	1.576
C4	8	1.065	9.871	9.269	38.20	0.055	0.0342	0.998	0.00047	2108.6	37.52	1.78
C5	10	1.33	10.11	7.60	31.33	0.044	0.0273	0.998	0.00047	2107.7	30.87	1.464
C6	12	1.60	12.75	7.96	32.81	0.047	0.0228	0.998	0.00047	2107.7	32.36	1.532
Average				9.23	38.05					2113.3	37.35	

4. Glass Set-Up 'D'

$$w = 3.0 \text{ mm}, \quad K_S = 3.116, \quad G = 1.176, \quad A = 629.9$$

$$C_g = 1004, \quad C_S = 0.287, \quad L = 0.203, \quad \alpha = 3.682 \times 10^{-6}$$

Run	P	Π/Λ	Π_{av}	Λ_{av}	hc	Bi	$(\frac{1}{Fo} + \frac{1}{Fo})$	ϕ	$\phi \frac{w}{3k}$	h_s	h_o	PER
D1	1	0.296	2.99	10.11	93.43	0.133	0.274	0.982	.000467	2143.0	89.52	4.37
D2	2	0.593	6.31	10.64	98.29	0.14	0.137	0.991	.000471	2122.6	92.94	4.63
D3	3	0.89	6.77	7.61	70.32	0.1	0.0912	0.994	.000472	2116.3	68.05	3.34
D4	4	1.186	8.163	6.88	63.37	0.091	0.0684	0.995	.000473	2113.5	61.71	3.01
D5	5	1.48	8.162	5.52	50.94	0.081	0.0547	0.996	.000474	2110.7	49.73	2.43
D6	6	1.78	13.79	7.75	71.55	0.102	0.0456	0.997	.000474	2110.1	69.20	3.40
D7	7	2.07	14.51	7.01	64.72	0.092	0.0391	0.998	.000474	2108.6	62.79	3.07
Average				7.93	73.26					2117.8	70.71	

5. Alumina Set-Up 'E'

$$\begin{aligned}
 w &= 6.35 \text{ mm}, & k_s &= 2.093, & G &= 0.525, & A &= 279.6, \\
 C_g &= 1004, & C_s &= 0.837, & L &= 0.203\text{m}, & \alpha &= 1.357 \times 10^{-6}
 \end{aligned}$$

Run	P	Π/Λ	Π_{av}	Λ_{av}	h_c	Bi	$(\frac{1}{Fo} + \frac{1}{Fo})$	ϕ	$\frac{\phi_w}{3k}$	h_s	h_o	PER
E1	2	0.169	0.649	3.84	33.52	0.068	0.595	0.960	.00066	1516.1	32.80	2.14
E2	4	0.338	1.43	4.22	36.85	0.075	0.298	0.980	.00067	1501.9	35.97	2.395
E3	6	0.508	1.821	3.58	31.26	0.064	0.1986	0.987	.00067	1491.7	30.62	2.052
E4	8	0.678	2.453	3.62	31.55	0.064	0.149	0.99	.00067	1486.6	30.89	2.078
E5	10	0.846	2.534	2.99	26.12	0.053	0.119	0.992	.00067	1483.7	25.66	1.73
E6	12	1.015	3.11	3.06	26.73	0.054	0.099	0.993	.00068	1482	26.26	1.772
E7	14	1.18	2.94	2.49	21.72	0.044	0.085	0.994	.00068	1482.6	21.40	1.44
E8	16	1.355	3.51	2.59	22.57	0.046	0.074	0.995	.00068	1470.7	22.23	1.50
E9	18	1.523	3.23	2.17	18.50	0.038	0.066	0.996	.00068	1478.7	18.27	1.23
Average				3.17	27.65					1489	27.12	

6. Alumina Set-Up 'F'

$$\begin{aligned}
 w &= 6.35 \text{ mm}, & k_S &= 2.093, & G &= 1.176, & A &= 279.6, \\
 C_g &= 1004, & C_S &= 0.837, & L &= 0.203 \text{ m}, & \alpha &= 1.357 \times 10^{-6}
 \end{aligned}$$

Run	P	Π/Λ	Π_{av}	Λ_{av}	h_c	Bi	$(\frac{1}{Fo} + \frac{1}{Fo})$	ϕ	$\frac{\phi_w}{3K}$	h_s	h_o	PER
F1	1	0.189	0.606	3.205	62.65	0.127	1.191	0.920	.00062	1599	60.29	3.77
F2	2	0.379	1.189	3.137	61.33	0.124	0.595	0.960	.00065	1533	58.96	3.85
F3	3	0.569	1.51	2.653	51.86	0.105	0.397	0.973	.00066	1512	50.14	3.32
F4	4	0.759	1.993	2.626	51.53	0.104	0.298	0.98	.00067	1502	49.63	3.30
F5	5	0.948	2.296	2.422	47.36	0.096	0.238	0.984	.00067	1496	45.88	3.07
F6	6	1.138	3.067	2.695	52.68	0.107	0.198	0.987	.00067	1492	50.88	3.41
F7	7	1.328	4.243	3.195	62.42	0.127	0.170	0.989	.00067	1490	59.95	4.02
Average				2.85	55.67					1518	53.68	

produced by Carpenter (1976) and three graphs particular to this work are shown in figs. 8.17 to 8.19. These are for the Schumann sphere comparison of Bi versus Π for Λ equal to 2.5, 5 and 10 respectively and span the practical values of Λ obtained. Above the 1% dividing line intraconduction effects become prominent and as Λ is reduced a lower value of Bi, results in intraconduction which is indicative of a ceramic packing.

The data analysis for all six cyclic set-ups is shown in Table 8.5. Values of area per unit volume A, convective heat transfer coefficient, Biot number Bi, packing heat transfer coefficient h_p and overall heat transfer coefficient h_o were obtained as follows :

$$A = \frac{6 \cdot (1 - Pv)}{D} \quad 8.3$$

An assumed voidage of 0.37 was used which was obtained from Heggs (1967).

$$h_c = \frac{\Lambda \cdot G \cdot C_g}{A \cdot L} \quad 8.4$$

$$Bi = \frac{h_c \cdot w}{K_s} \quad 8.5$$

$$h_p = \frac{3K_s}{\phi \cdot w} \quad 8.6$$

$$\text{where } \phi = 1 - \frac{1}{15} \left(\frac{1}{Fo_H} + \frac{1}{Fo_C} \right) \quad \text{for } \frac{1}{Fo_H} + \frac{1}{Fo_C} \leq 5 \quad 8.7$$

$$\text{and } \phi = \sqrt{0.3 + 2 \frac{2.142}{\left(\frac{1}{Fo_H} + \frac{1}{Fo_C} \right)}} \quad \text{for } \frac{1}{Fo_H} + \frac{1}{Fo_C} \geq 5$$

$$Fo = \frac{\alpha P}{w^2}$$

FIG 8.20 Bi VERSUS π FOR STEEL SET-UPS 'A' AND 'B'

• SET UP A, $\Lambda_{av} = 8256$
x SET UP B, $\Lambda_{av} = 8.0$

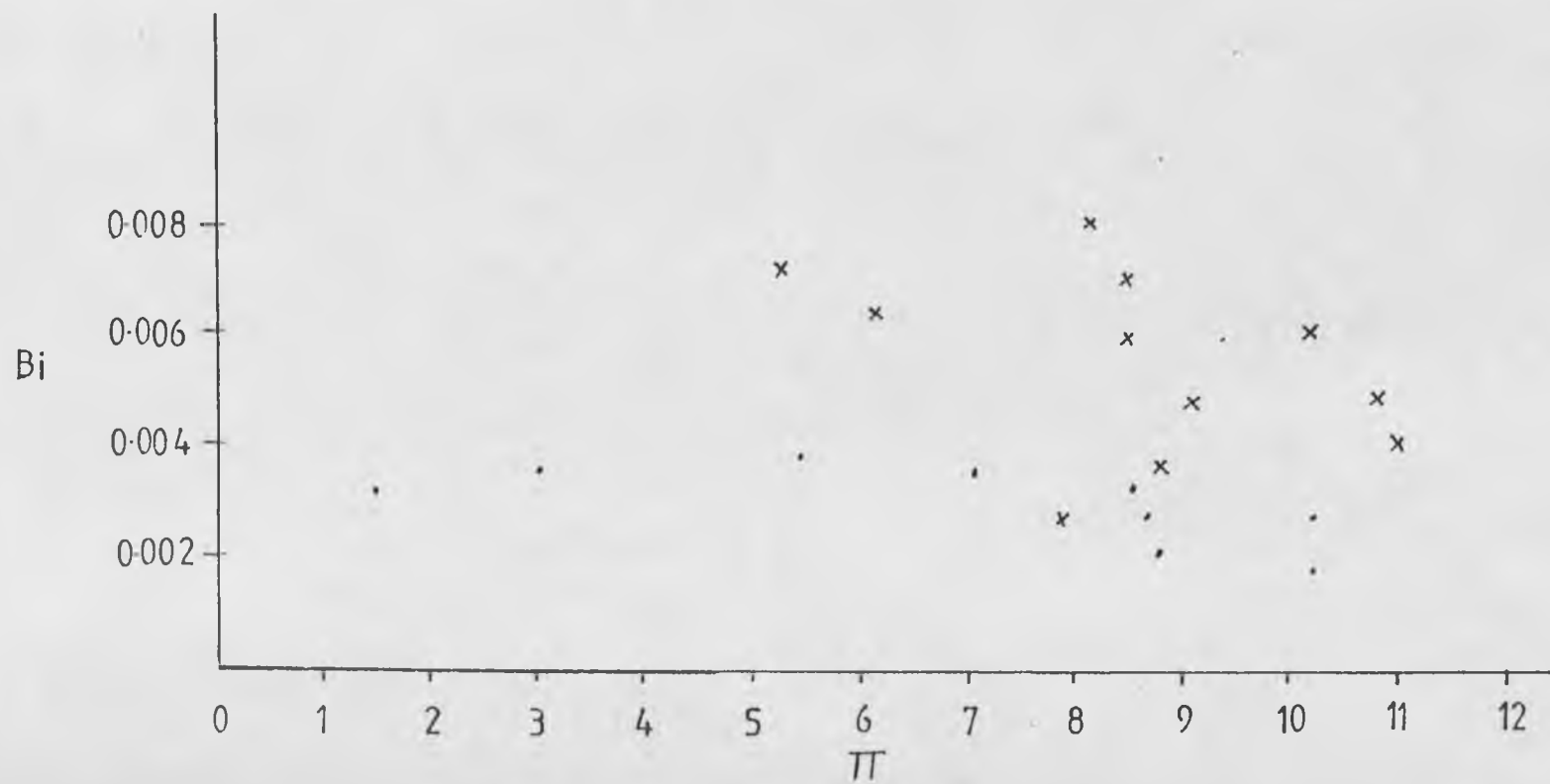


FIG821 Bi VERSUS π FOR LEAD GLASS SET-UPS 'C' AND 'D'

• SET UP C ; $\Lambda_{av} = 9.23$
x SET UP D ; $\Lambda_{av} = 8.08$

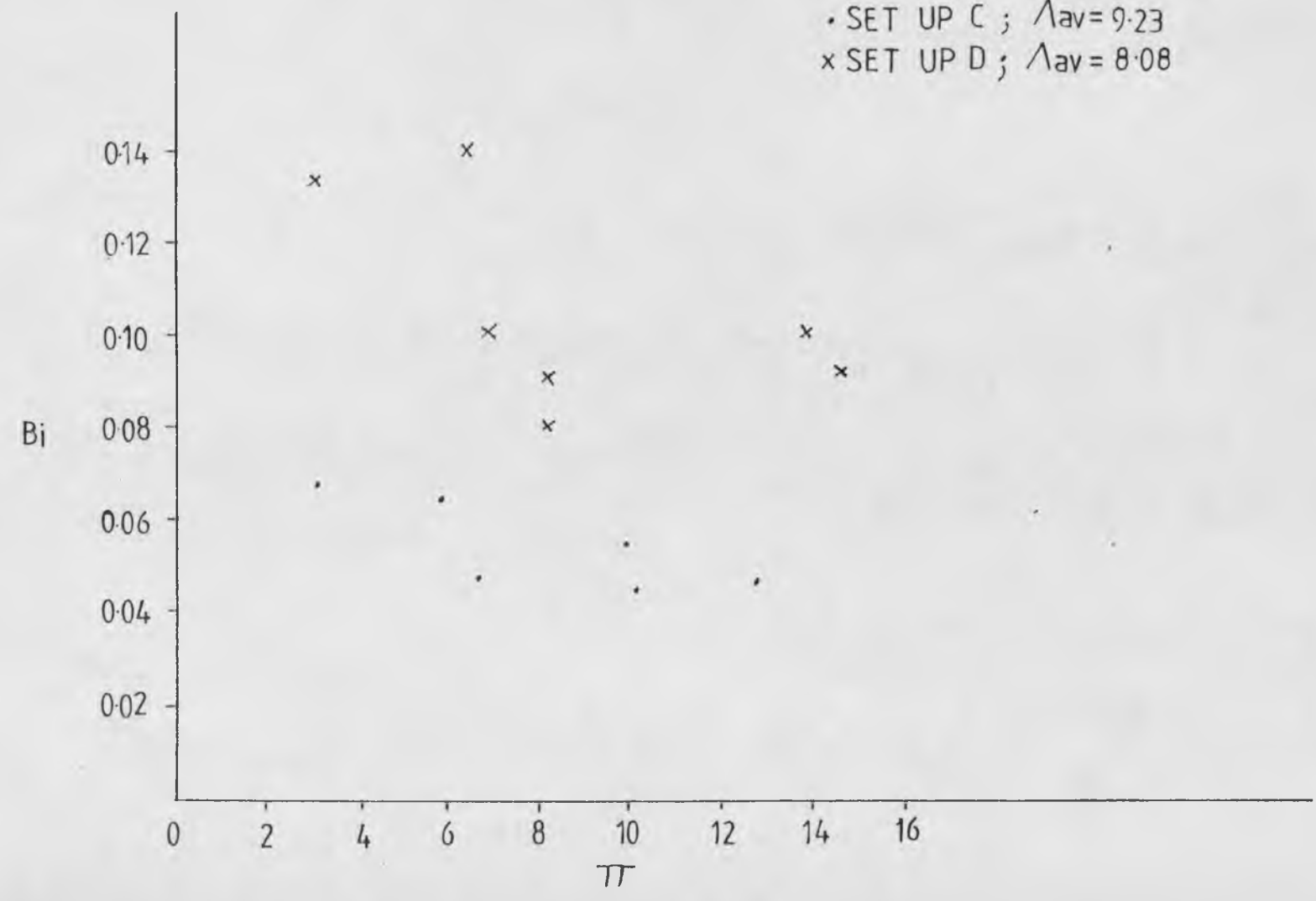
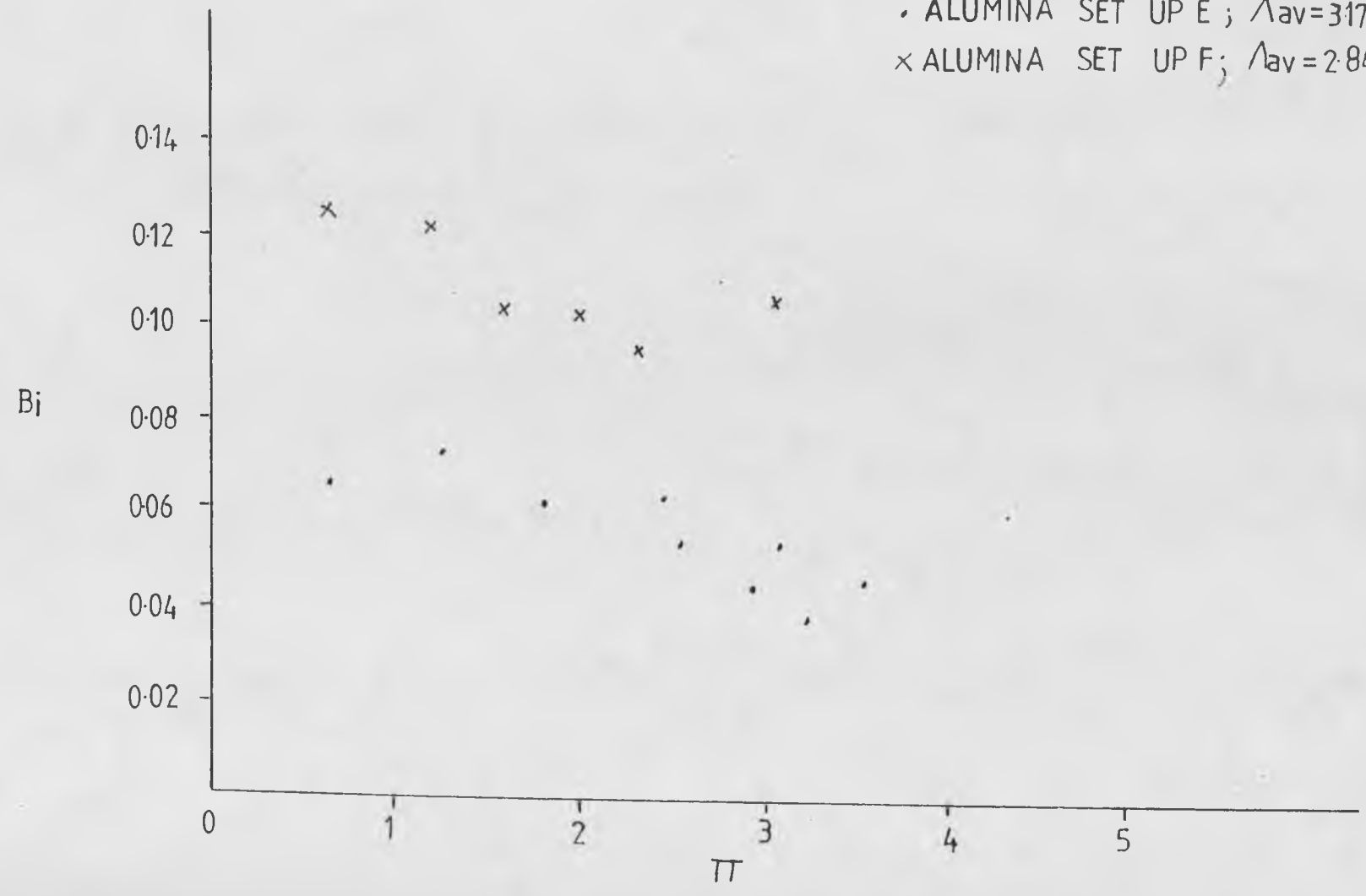


FIG 8.22 Bi VERSUS π FOR ALUMINA SET-UPS 'E' AND 'F'

• ALUMINA SET UP E ; $\Lambda_{av}=317$
x ALUMINA SET UP F ; $\Lambda_{av}=284$



$$\frac{1}{h_o} = \frac{1}{hc} + \frac{1}{hs} \quad 8.8$$

For the packings considered it can be seen from figs. 8.20 to 8.22, for small values of Bi the Schumann model predictions approach that of the results. The reduction in Bi represents an increase in the thermal conductivity of the solid material e.g. steel, or a decrease in radius. This corresponds to a decreasing internal resistance of heat transfer in relation to the surface resistance. Hence the temperature distribution within the solid becomes less important with this relative decrease in resistance, and convective heat transfer becomes the controlling mechanism. This is highlighted by examining the percentage ratio of $\frac{hc-h_o}{h_o}$, shown in table 8.5. The effect of packing resistance on the steel results is minimal but is increased significantly for the ceramic packings. This is evident in the lead glass and alumina plots, where the Biot number Bi increases as Π approaches zero, which supports Carpenters theoretically derived curves shown in figs. 8.17 to 8.19.

It can also be seen from figs. 8.20 to 8.22 that intraconduction becomes more significant as Δ is reduced, as shown in the single shot runs, which corresponds to increasing the mass flowrate which also causes an increase in heat transfer coefficient. A decrease in Δ therefore, causes an effective reduction in surface resistance, as the increased flowrate facilitates surface heat transfer by effectively increasing the driving temperature. Decreasing Δ , as shown in the alumina set ups, therefore facilitates

Table 8.6

Comparison for the Cyclic and Single Shot Set-Ups

Set-Up	$\hat{\Lambda}_{\text{Cyc}}$ Average	$\hat{\Lambda}_{\text{Cyc}}$ Difference	$\hat{\Lambda}_{\text{ss}}$	$\hat{\Lambda}_{\text{ss}}$ Difference
A	8.26	0.28	22.41	4.56
B	7.98		17.85	
C	9.23	1.30	21	5.55
D	7.93		15.45	
E	3.17	0.32	17.8	6.65
F	2.85		11.15	

intraconduction. Only the alumina set-up data exceeds Carpenters 1% design limits and intraconduction should therefore be allowed for, as in the single shot analysis.

8.8 Comparison of Cyclic and Single Shot Heat Transfer Coefficients

The apparatus was designed for cyclic operation by a single shot correlation. Cyclic operation is periodic heating and cooling of the packing whilst single shot is complete temperature saturation of the packed bed until the outlet temperature approaches that of the inlet temperature. These two separate regenerator actions were performed for the same set-up conditions, i.e. packing length and air flowrate. Table 8.6 shows Λ_{SS} , and the mean values of Λ for the Λ_{av} runs (denoted as Λ_M), obtained for the single shot and cyclic set ups respectively. The Λ_M values are much less than the Λ_{SS} values for each set-up, and in each case the values of Λ are greater for the lower air flowrate, as expected. The Λ_M difference for each packing is remarkable low (0.28, 1.3 and 0.32 for steel lead glass and alumina) however the Λ_{SS} values are roughly in accordance with the MISP simulation difference of 5 (4.56, 5.55 and 6.65 for a steel, lead glass and alumina). The severity of intraconduction for the single shot set up increases as the Λ_{SS} values fall, such that $\Lambda_{set\ up\ A} > \Lambda_{set\ up\ C} > \Lambda_{set\ up\ E}$. This corresponds to an increasing influence of the packing intraconduction transfer over that of the convective transfer at the packing surface. This trend is also true for set up B D and F. The difference

between the Λ_{SS} values for each packing also increases as intraconduction increases. The Λ_M values approximately follow the same difference pattern as the Λ_{SS} values, however the difference for the lead glass set ups is particularly high. This discrepancy is caused by the effect of the number of cycles required to reach equilibrium, raising the Λ_{av} value, as discussed in 8.4.

8.9 Chapter Conclusions

Analysis of the regenerator data has been in two distinct sections, single shot and cyclic. Values of Λ_{SS} were obtained using Darabi's (1981) simple graphical technique and the packings were examined for intraconduction by Heggs (1967) $\Lambda/Bi < 60$ criterion and producing integer values for comparison with the Jh correlations previously obtained. In both cases intraconduction was found to be negligible in the steel, evident in the lead glass and considerable in the alumina spheres.

Analysis of the cyclic runs clearly showed that heat leak from the apparatus and the number of cycles required to reach equilibrium are important factors and should be carefully considered during the design stages, and operation of a thermal regenerator. The steel and lead glass convective heat transfer coefficients were obtained using the matrix method. However, due to the combination of heat leak, the number of cycles required to reach equilibrium and packing intraconductions the apparatus results for the

alumina set ups fell below the bounds of the matrix method. Consequently Willmotts (1964) modified Tipler (1947) equation was used to obtain the alumina Λ values. This equation, however, became unstable when it was used on the steel and lead glass results.

Analysis of the packing intraconduction effects showed a similar trend to the single shot work and verified Carpenters (1976) theoretical intraconduction studies. Comparison of the single shot and cyclic results clearly show that single shot heat transfer correlations can be used with confidence to design single shot apparatus but should only be used to design cyclic regenerators when the cyclic design assumptions of cyclic equilibrium, no heat leak and minimal intraparticle conduction can be practically achieved.

Chapter 9

Summary of Conclusions and Proposals for Future Work

9.1 Conclusions

An apparatus has been designed and built to examine thermal regenerator characteristics. The apparatus was designed using existing 'schumann type' assumptions and a single shot heat transfer correlation to calculate the air flowrate and bed length for known dimensionless length. The analog control of the apparatus was significantly enhanced by employing four modes of computer operation, allowing more concise and accurate values of flow and temperature to be logged.

A computer simulation of the apparatus was undertaken using the MISP program. This simulation included the peripheral pipework common to the packed bed and showed that the number of cycles required to reach cyclic equilibrium is significantly increased by this pipework. The common pipework acts as a small thermal regenerator, but has little affect upon the packed bed efficiency. During the routine commissioning of the apparatus it was discovered that two effects specific to the apparatus were affecting the temperature indicated by the platinum resistance thermometers. These were radiation effects from the heater wires and a velocity effect as the air entering the packed bed was not significantly dispersed by the diffusers. The radiation and velocity effects were reduced considerably by employing

radiation shields and a flowrate dampening device.

Three different types of spherical packing, steel (6.35 mm), lead glass (6 mm) and alumina (12.7 mm) were employed to examine intraconduction effects. However a more accurate concise and non iterative method of obtaining packing to fluid heat transfer coefficients had to be found. From the MISP simulations of the apparatus and observations of previous work it was conceivable to produce a nest of curves of dimensionless length Λ for efficiency η versus utilisation factor Π/Λ . So for a known efficiency and utilisation factor the dimensionless length, hence convective heat transfer coefficient can be found. This concept was developed using finite difference techniques and produced in two forms. One is present on the Departmental Eclipse computer Disc, whilst the other representation is a design graph.

A series of MISP simulations were undertaken to examine the response of the apparatus, particularly the number cycles required to reach equilibrium for a run within a set-up. These simulations included the peripheral pipework and the heat transfer coefficient derived from Heggs (1967) single shot correlation for metallic spheres. The apparatus was operated under the MISP simulation Criterion.

At the beginning of each cyclic set-up the first run corresponding to the largest time period was extended to enable a single shot breakthrough curve. Using Darabis (1981) graphical technique the single shot response was analysed to

produce Λ hence a convective heat transfer coefficient. This provided the unique opportunity to examine both single shot and cyclic regenerator characteristics for the same set up. For each packing the lowest flowrate produced the largest value of Λ_{SS} and for a fixed flowrate the values of Λ_{SS} decreased in the order $\Lambda_{SS} \text{ steel} > \Lambda_{SS} \text{ glass} > \Lambda_{SS} \text{ alumina}$ due to the intraconduction effect in the packing. The intraconduction effect for each packing was examined by comparing the fractional power of the flowrate with the dimensionless length and further checked using Heggs (1967) criterion $\Lambda/Bi \leq 60$ for spherical packings. In both cases intraconduction was negligible in the steel, finite in the glass and considerable in the alumina.

The cyclic raw data was represented as η versus Π/Λ for each set-up, and showed that the hot and cold efficiency values were dissimilar for the entire set up. However the curves produced approximately followed the same slope of the MISP simulations and the Λ_H and Λ_C values were much lower than those predicted by the MISP program. The MISP program successfully simulated the single shot set ups giving approximately the correct values of Λ compared with those obtained using Darabi's (1981) graphical method. The number of cycles required for each practical run within a set up was obtained from the MISP program using a tolerance of 0.0001. When the number of cycles predicted were exceeded the slope of the η curves changed, approaching the MISP simulation curves. The predicted number of cycles required to reach equilibrium were insufficient and a much

tighter tolerance must be used during the computer simulation to attain the correct packed bed temperature profiles for each run.

Observation of the raw data plots of η versus Π/Λ for each set-up clearly showed the trend $\eta_H > \eta_C$ and the η_H and η_C curves approached each other as the flowrate increased. Heat was leaving the apparatus and the η_H and η_C curves could approach each other for a significantly high flowrate and adequate insulation, so approaching the Schumann type assumption of no heat leak.

Dimensionless length prediction of the raw data gave values much lower than the MISP prediction. The dimensionless length values for each set up showed a tendency to decrease with increasing Π/Λ suggesting that the convective heat transfer coefficient is dependent to some degree upon the cycle time, i.e. the amount of time required for heat soakage. With the additional characteristic of intraconduction the regenerator efficiency is not only a function of Λ and Π but also Bi . Analysis of the set up data by Hausen's Eigen function technique showed how the steel results approached the Schumann model prediction, with negligible intraconduction, whilst intraconduction heat transfer increased for the lead glass and alumina packings.

Examination of the single shot and cyclic results obtained during this research showed that single shot heat transfer correlations should only be used to design cyclic regenerators if the Schumann type assumptions of cyclic

equilibrium, no heat leak and negligible packing intraconduction can be practically achieved.

9.2 Future Work

It is evident from the extensive work carried out in this research project that in the conception, design, construction simulation, operation and treatment of results many fundamental regenerator characteristics are being overlooked. It is therefore necessary to accelerate practical research, because it is only during simulation and associated practical operation that regenerator characteristics can be fully examined. Prior to commencing any new projects it is necessary to further examine the effects of heat leak and the number of cycles required to reach equilibrium. The matrix method bounds of $5.1 < \Lambda < 25$ should be extended to $0.1 < \Lambda < 50$, and set ups that are examined should have a utilisation factor less than 1.5.

The MISP program should be used to determine the number of cycles required to reach equilibrium for the regenerator and common pipework using the convective heat transfer coefficients derived from the matrix method. A tighter tolerance of 0.000001 should be used, then the correct temperature profiles with respect to length should be achieved. This simulation should be in conjunction with a proper heat leak analysis. Consequently the apparatus hot and cold efficiencies should approach each other producing the same dimensionless lengths for each stroke.

Further regenerator research can be carried out on the apparatus after these fundamental characteristics have been fully examined. Various types of packing can be employed to examine intraconduction as well as longitudinal conduction. Fluid hold-up under computer control as well as imbalanced operation, i.e. $\Pi_H \neq \Pi_C$ or $\Lambda_H \neq \Lambda_C$ can also be examined. Variable mass flow through the test bed can also be achieved by replacing the bleed off solenoid valve with a stepping motor valve allowing variable air bleed off for individual strokes.

Appendix A

Instrument Characteristics

1. Foster Cambridge Clearspan P130L P + I Indicator Controller

Input resistance forms the fourth arm of a Wheatstone bridge within the controller.

Accuracy : $\pm 0.5\%$ span maximum

Total response time : 1 second maximum to 95% of final reading.

Temperature Coefficient : 0.05% span/ $^{\circ}\text{C}$

Warm up time : 10 minutes

Error due to power supply voltage variation $\pm 0.15\%$ span maximum for +10% to -20% variation.

Current output for thyristor drive 0-10mA into 1,000 ohms max.

Proportional band 10 - 100% span, nominal adjustable.

Integral action time from factory, 5 minutes.

2. Dewrance Asco Solenoid Valves

Supply voltage : 24 VDC (operating range 15 - 30 VDC)

Closing time : 4 - 20 mS

Operation : two way

Normally closed when not energised.

Valve body aluminium

Temperature of operation : maximum 150°F

3. Electronic Timer Unit P.042

Time period selection : Selectable in one minute steps from 1 - 99 minutes by two ten position switches giving a digital display of the time selected.

Principle and Accuracy : A Cermet preset in a pulse, generator circuit is adjusted so that the generator gives an output every 3 seconds. These pulses are counted and decoded. The timer resets when the selected time is reached.

TTL integrated circuitry

Output : Absolute maximum switching capability, 1 amp at 60 Volts.

Power supply required : 5V/250 mA.

4. Heenan 180/6 Stabilised Power (Motor Control) Unit

Mains supply : 200 - 240v, single phase A.C 50-60 HZ.

Stable to with $\pm 6\%$ of nominal voltage

Supply voltage : 0-180 VDC at 240 V mains

Current limit overload, protection : 2 - 8 amps

Speed Holding : $\pm 1\%$ of maximum speed for 100%

Load change, $\pm 6\%$ change of supply voltage and 20°C change in ambient temperature.

Current held to $\pm 5\%$ of set valve over the range maximum speed to stall.

5. Foxboro Yoxall Differential Pressure Cell

Type : ME13DM electronic

Span limits : minimum : 20 inches water

maximum : 205 inches water

Range limits 0-20 to 0-205 inches water

Span : fully adjusted between range limits

Transmitter output : 4 - 20 mA into 0 - 470 ohms

Nominal power supply voltage : 24 VDC

Repeatability : 0.1. of span

Accuracy : \pm 0.5% of span.

Appendix BManual and Computer Interface Switching Actions

The following mains and miniature toggle switch action, referring to fig. 4.8, is undertaken for manual co or countercurrent timing, with or without test bed heating.

<u>Unit</u>	<u>Position</u>	<u>Function</u>
M4 (Mains Switch Box)	Up off Down on	provides the 24 VDC required to actuate the five solenoid valves.
M5 (MSB)	Up off Down on	Provides the 24 VDC required for the electronic timers to actuate the continental series relays RI and RII.
M6 (MSB)	Up off Down on	Provides the 5 VDC stabilised voltage required for the TTL compatible circuitry of the electronic timers.

(Single Pole Single Throw 1) SPST1	Miniature toggle switch located on panel up open circuit down closed circuit	Allows the Solenoid Valve 5 'bleed off' valve to be actuated
(Single Pole Double Throw 2) SPDT2	Located on panel up hot stroke down cold stroke	with SPST1 down SPDT2 allows SV5 to be opened for a given stroke
SPDT3	Located on panel up countercurrent switching down cocurrent switching	This enables the cold timer 24 VDC output to be diverted for co or countercurrent switching
SPDT7	Located on panel up computer timing down manual timing	This enables easy bypass for manual or computer timing, by diverting the 24 VDC supplies required for interface switching.

M6 (MSB)	up off down on	Provides the 5 VDC stabilised voltage supply required for the computer timing electronic circuits, CTIMC and CTIMH (discussed in chapter 5).
M9 (MSB)	up off down on	Actuates the Heenon 180/6 stabilised voltage power unit described in Appendix A. The wiring of this unit, with respect to the RIV and RV continental series relays is shown in fig. 4.9. Direct current voltage output is regulated by a demand potentiometer graduated 0(1)100. The voltage and current are indicated by R.S. moving coil D.C. meters graduated 0(5)200 and 0(.2)10 respectively.

R.S. Continental Series Relay 1 (R1)	Cold solenoid valve Relay, Normally open, open circuit. Actuated, closed circuit	Secondary relay : Cold timer 24 VDC actuates RI, which closes the cold solenoid valve circuit, hence opening valves C1 and C3.
RII	Hot solenoid valve relay, Normally open, open circuit. Actuated, closed circuit	Secondary relay : Hot timer 24 VDC actuates RII, which closes the hot solenoid valve circuit, hence opening H2 and H4.
RIII	bleed valve relay. Normally open, open circuit. Actuated, closed circuit	Secondary relay switching required for 'bleed off' solenoid valve 5.
RIV	Countercurrent heater activation relay. Normally open, open circuit. Actuated, Heenen unit activated.	For countercurrent operation RIV is activated every hot stroke, so closing the heater circuit.

RV	Co-current heater activation relay. Normally open, closed circuit. Actuated open circuit. (always closed circuit for countercurrent operation).	For co-current mode RIV is always activated i.e. closed circuit. However RV when actuated during a cold stroke opens the heater circuit and closes it during the hot stroke, hence co-current operation.
----	---	--

Appendix CComputer Interfacing Equipment1. Measurement Signals Interface

The measurement signals interface serves to translate plant signals from analog to digital form. Generally the analog to digital conversion is one of the most important processes in any data acquisition or control system, and it forms a big link between the physical variables (temperature and differential pressure) which are essentially analog by nature, and the computer.

The measurement instruments of the thermal regenerator have been adjusted to finally produce d.c. voltage signals in the standard range 0 volts to +10 volts. Special attention has been given to achieving satisfactory impedance matching. A model AF01 MPX/ADC of digital equipment corporation 'instruction manual for AF01 A → D → C and MPXR document DEC-00-16AA-D (1969)' is used. The MPXR section can handle up to 64 analog input channels and uses solid state switching buffered through an operational amplifier to the ADC. The ADC is of the successive approximation type, with a manual selectable conversion accuracy of 6 up to 12 bits. For the present work the word length is always set to 12 bits in order to obtain the maximum possible resolution.

The digital output of the ADC appears in parallel form as 1's and 0's stored in an array of register cells, one

for each bit of the 12 bit digital word. Once the conversion is completed the number is transmitted to the S/7 and the next conversion starts. The combined MPX/ADC interface system is operated under the S/7 software control, with a specially written assembler programme. Generally it can be operated in either a random or sequential channel addressing mode, but for this application the hardware random mode of application is adopted, although the channels are actually scanned in sequence by the controller assembly programme. For the detailed specifications of both the MPXR and the ADC with the corresponding block and timing diagrams, see Brooks (1978).

2. Communications Device Interface (Digital MPXR)

The communication devices interface built within the department is essentially a 16 bit wide digital multiplexer (MPXR) so that up to 16 simple parallel peripheral devices can be connected to the S/7 computer through a common data bus. Again, the operation of this unit is under S/7 software control through a specially written assembler programme.

3. Digital Demultiplexer (DEMPXR)

The digital demultiplexer can be used to drive any low speed devices, relays, lights etc; two banks of four lights in this case. The digital demultiplexer is driven from the S/7 output group 2 in module 1; the board address is to

identify each individual user. The board address is used in conjunction with the 'strobe bit' by the de-multiplexer to produce a user strobe, or user device select. Other signals, data bits, device address and decimal point are repowered and reshaped by the de-multiplexer before being passed to the lights. A technical description of the MPXR and DEMPXR is given by Brooks (1978).

Appendix D

S/7 and Eclipse Software Facilities

1. IBM S/7 Standard Software facilities

Traditionally, programme operation on small control computers has been both inconvenient and inefficient. Severe limitations in system facilities, such as memory size, and standard input/output devices, make programme preparation more difficult and more expensive. However, availability of a host computer can simplify the problem significantly, given that the larger computer can be used for programme preparation and debugging and approximate use made of its greater machine facilities. Nevertheless, despite these extra facilities writing programmes for the S/7 is a time consuming operation. The control programme used, SJHRIG, was written in assembler language which in this case is a memoric language, having a one to one correspondence with the hardware instruction set. However, by programming in assembler language the programmer has greater control over the system hardware than with a high level language. Comprehensive literature about the S/7 software can be found in the computer manufacturer's manual (1971).

2. IBM S/7 General Purpose Application Programme

COMF5 is the S/7 part of a general purpose multi-tasking communication package that serves the Nova and Eclipse. It has been developed locally and provides the following

real time communication procedures.

1. Transmit a variable length record to the Eclipse and optionally execute a task in the Eclipse on completion of the data transfer.
2. Request transmission of a variable length record from the Eclipse, and optionally execute a task on the Eclipse on completion of the data transfer.
3. Execute a task in the Eclipse.
3. A/D Converter Driving Programme (ADCNX)

ADCNX is the general purpose assembler programme driving the MPXR and FADC unit. Every active channel is scanned 10 times per second. The activation of each channel is achieved by inserting the channel number value into a specially reserved table in the S/7 storage. Each channel reading is maintained in a second table. The stored values are automatically updated as new readings become available, thus the S/7 acts as a zero order hold device.

Another very important feature incorporated into the ADCNX programme is the exponentially smoothing which is performed on every active channel. The algorithm applied has been derived from Adamopolis (1977). The computer values of the exponentially smoother measurements are stored in a third S/7 table and are updated as soon as the new ones become available.

The structure of the overall programme is very convenient as it allows the user to utilise, according to requirements, either the current or the exponentially smoothed values of the measurements. Given that the conversion accuracy of the FADC corresponds to 12 bits, the S/7 range for all measurements is 0 up to 4096_{10} (2^{12}) corresponding to a converter analog input range of 0 up to 10,000mV.

4. Eclipse Standard Software Facilities

The computer operates under the Data General real time operating system ZRDOS (1978). This is a real time, disc based, software support system supervising file management, peripheral device handling and scheduling in a multitask environment. ZRDOS is file oriented in that most commands either use or operate on files, where a file may be a collection of information on any device receiving or providing the information. Generally ZRDOS combines the advantages of a disc operating system with the fast response provided by a core only real time system. It is real time oriented, since it can schedule and allocate programme control to many tasks in a multi-task environment. In such an environment, several tasks compete for C.P.U. control, giving an optimum utilization of the resources. The tasks operate asynchronously and in real time, with C.P.U. control being allocated by the task scheduler to the highest priority task which is ready.

The major advantage of this type of computer control is the possibility of programming in a high level language, such as Fortron V, as ZRDOS supports the system development software (high level languages, macro assembler, editors debugging aides, a library of utility programmes and a large suite of general purpose scientific routines). Thus ideal background facilities are provided for developing the software programmes needed to obtain and process temperature data from the apparatus as well as operate parts of the apparatus.

APPENDIX EFlow Diagrams Showing the ON and OFF Line Programs Required
For Computer Operating of the ApparatusOn Line Programs

- E1 Program Listing of the Main Eclipse On Line Program
SJHREGEN.
- E2 Program Listing of the Apparatus Switching Subroutine
SJHSWIT
- E3 Program Listing of the Subroutine Required to File the
Pressure and Temperature Data SJHFILDT
- E4 Program Listing of the Subroutine Required to Rapidly
Store the Data SJHFIQK
- E5 Thumbwheel Switch and Eclipse Data Input Listing
- E6 Flow Diagram of the S/7 Assembler Programme Required to
Activate the Apparatus.

Off Line Eclipse Programs

- E7 Flow Diagram of SJHCYCT, the off Line Temperature
Processing Program
- E8 Flow Diagram of SJHCYCP, the Off Line Pressure
Processing Program

E5. Thumbwheel Switch and Eclipse Data Input Listing

Thumbwheel Switch A

(TOP)

00 No action
 01 Start default timing
 02 Start control action
 03 Start data logging
 04 Start a new run
 The number of cycles required
 in the previous run will be
 displayed on the top lights
 31 display RT 2
 32 display RT 3
 33 display RT 4

Thumbwheel Switch B

(BOTTOM)

00 No action
 *02 Bypass control action
 *03 Temperature and pressure
 data will not be starred
 *04 will end a run i.e. impose
 cyclic steady state
 *05 will allow the previous run
 time period to remain until
 a new number is dialed.
 * The above actions will only
 be activated while the
 thumbwheel switch is on
 that number.

Eclipse Input Data

- a) The hot and cold time periods, in seconds, for up to 10 runs
- b) The letter for the set-up, e.g. giving SJHRUNAO to SJHRUNA9 for a set-up of 10 runs
- c) The set point temperature required on the front end.
- d) The proportional constant
- e) The integral time constant
- f) The derivative time constant.

S/7 and Eclipse Interface ChannellsData From S/7 to Eclipse : Channel 11

A/D	TSW1	TSW2							
30	31	32	33	34	35	36	37	38	39
RT2	RT3	RT4	RT5	RT6	RT7	RT1	PT1	LHS	RHS

Data From Eclipse to S/7 : Channel 12

A	B	C	D	E	F	G	H
0	D/A	0	Timer	Timer	0	Light	Light
1	value	1	on time	off time	1	top	Bottom
		2				value	value

A 0 No control required
 1 Control required; execute

C 0 Timer function unchanged
 1 Start timer
 2 Stop timer

F 0 NO L.E.D. light display
 1 L.E.D. light display

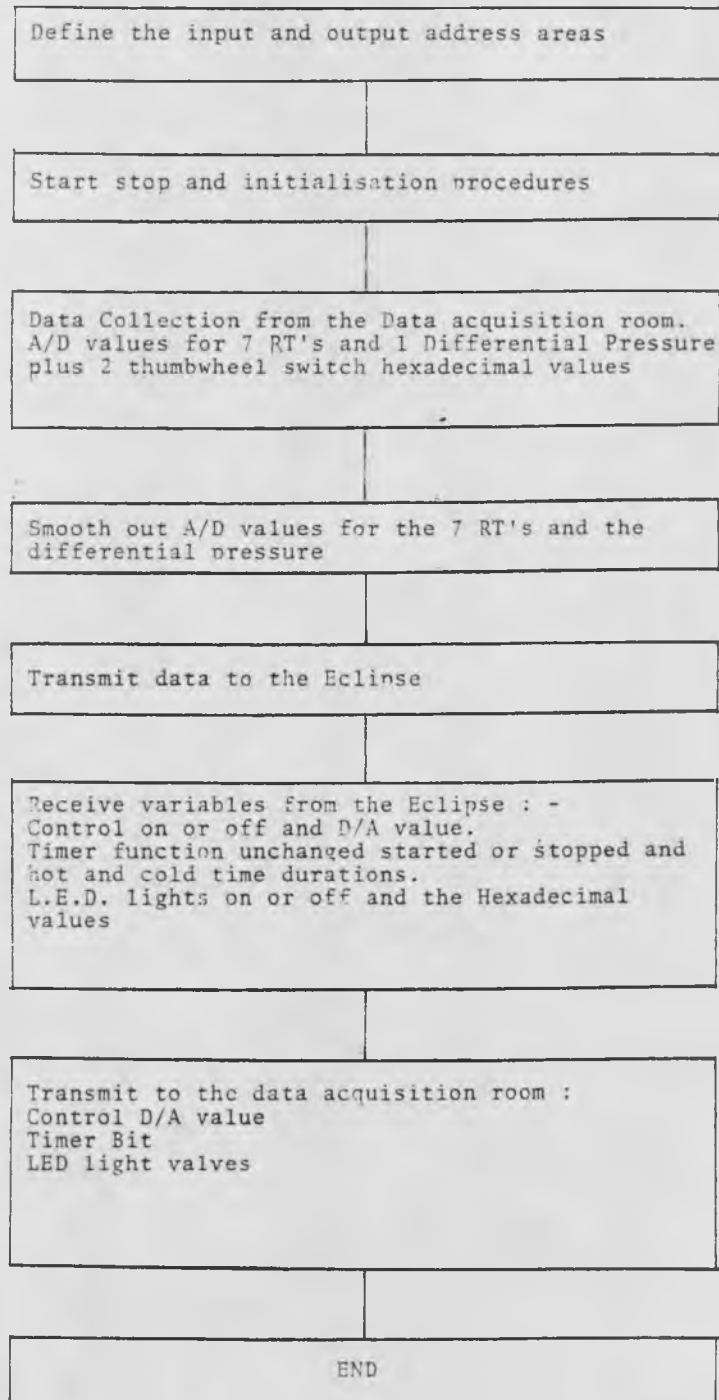
Timer durations to the nearest $\frac{1}{10}$ th sec.

D/A values in the range 0 - 255

LED light displays in the range (0 - 4095)

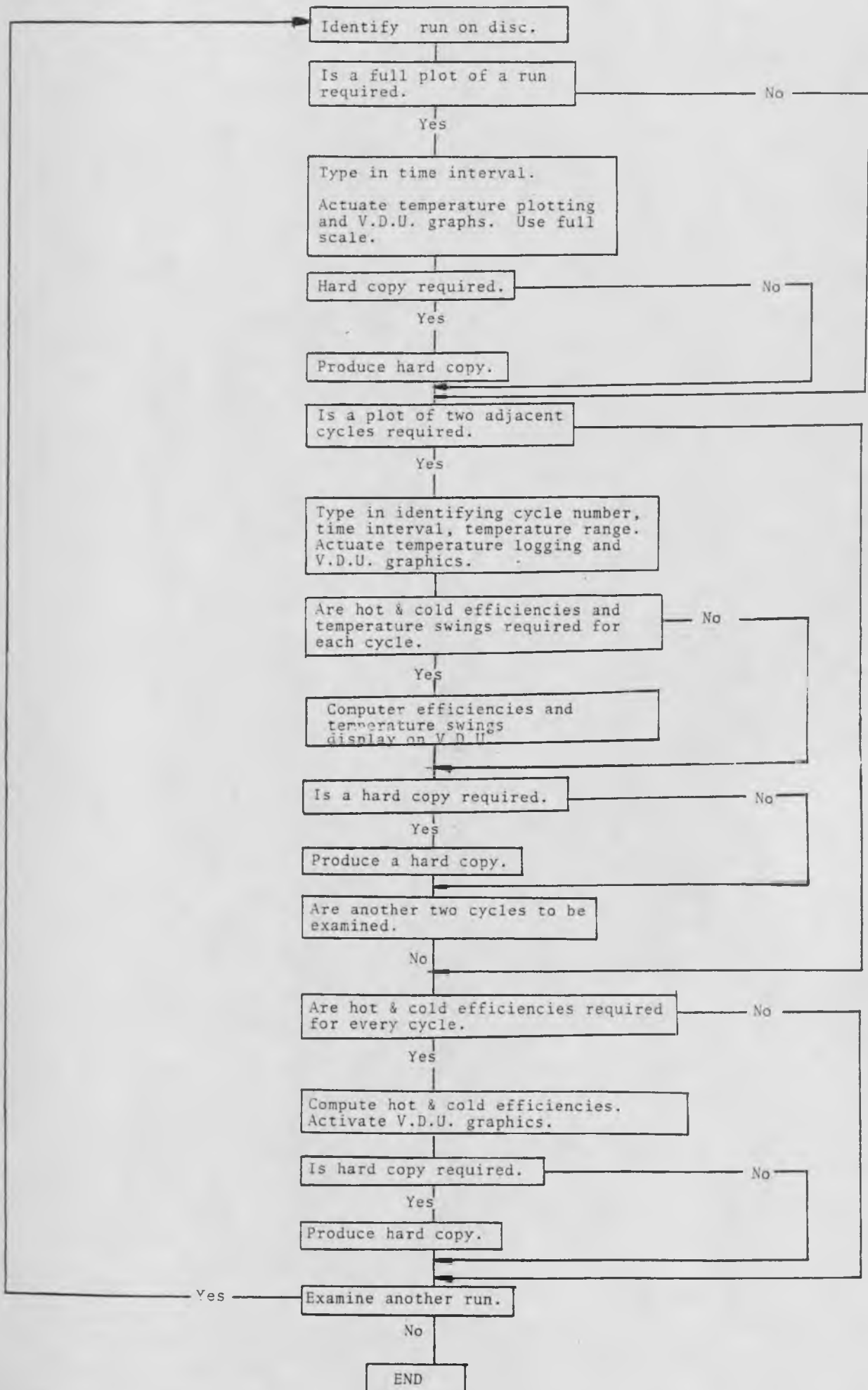
where PT = Pressure tapping
RT = Resistance Thermometer
D/A = Digital to Analog
A/D = Analog to Digital
TSW = Thumbwheel switch

Flow Diagram of the S/7 Assembler Program SJHRIG



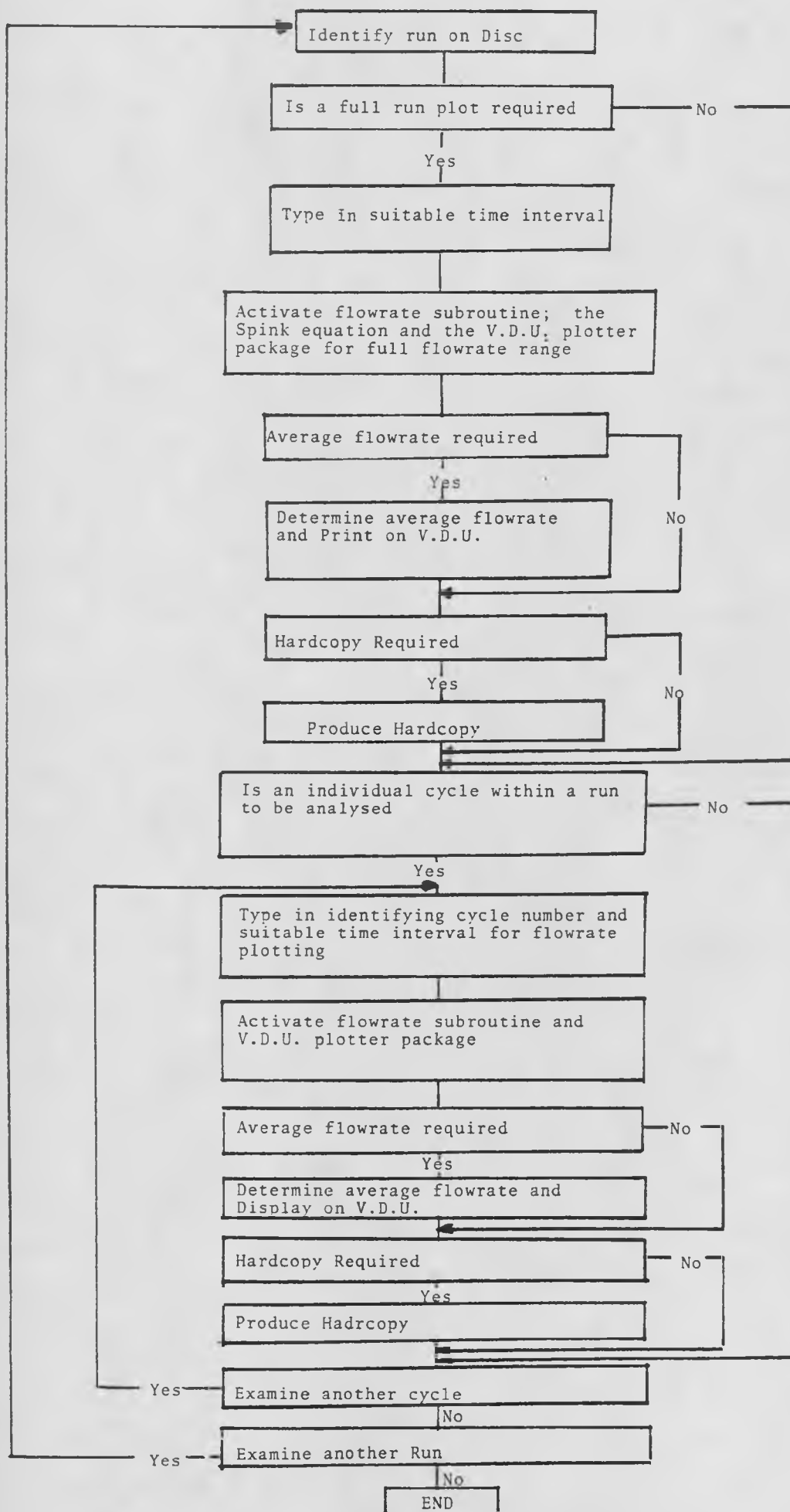
E7

SJHCYCT Off Line Temperature Processing Program



E8

STHCYCP Off-Line Pressure Processing Program



Appendix F

Front End Steady State Radiation Calculations

To represent the radiation effect, a steady state heat balance was carried out over the front end section, corresponding to an experimental run. The simulation and experimental run confirmed the presence of significant radiation effects. The experimental run Fig. F1, shows how the resistance thermometer upstream of the packed bed indicates a temperature higher than the resistance thermometer positioned downstream of the packed bed. This suggests that radiation from the heater wires is causing this difference in temperature, as shown by the run data in Fig. F1.

The simplified theoretical simulation diagram is shown in Fig. F2. The variac and control heater wire temperatures are obtained from the electrical input during the experimental run. A heat balance on the resistance thermometer should produce a temperature approximately equal to that obtained from the experimental run for RTB. The following assumptions were used :

1. Variac heaters 1, 2 and 3 are represented as one heater tw.
2. The heat balance is in the steady state.
3. The temperature of the packing face and inner tube wall are equal to the surrounding air.

4. There is no heat loss.
5. In order to find the temperature of both heaters the mode of heat transfer is convective.

Steady State Heat Balance on the Temperature Sensing Element

Assuming the resistance thermometer is at a higher temperature than the surrounding air, the heat balance according to Fig. F2, is given by :

$$\begin{aligned}
 & h_{RT} A_{RT} (t_{RT} - T_A) + \int_{RT \rightarrow TPIP} A_{RT} \sigma (t_{RT}^4 - t_{PIP}^4) \\
 & + \int_{t_{RT} \rightarrow t_{PAC}} \frac{A_{RT}}{2} \sigma (t_{RT}^4 - t_{PAC}^4) \\
 & = \int_{t_W \rightarrow t_{RT}} \frac{A_{tW}}{2} \sigma (t_W^4 - t_{RT}^4) \\
 & + \int_{t_{CH} \rightarrow t_{RT}} \frac{A_{CH}}{2} \sigma (t_{CH}^4 - t_{RT}^4)
 \end{aligned}$$

where RT = Resistance Thermometer

A = Surface Area

h = Convective heat transfer coefficient

σ = Stefan - Boltzman constant

T_A = Air Temperature

t_{RT} = Resistance thermometer temperature

t_{PIP} = Pipe wall temperature

t_{PAC} = Packing face temperature

t_W = Variac heater wire temperature

t_{CH} = Control heater wire temperature

Knowing the electrical power from the experimental run the Variac and control heater wire temperatures are given by :

$$q_{\text{electrical}} = h_W \cdot A_W (t_W - T_A)$$

$$q_{\text{electrical}} = h_{CH} \cdot A_{CH} (t_{CH} - T_A)$$

The heat transfer coefficients h_{RT} , h_W and h_{CH} were obtained from the formula taken from Krieth (1973) for circular cylinders in crossflow air.

$$\text{where } \frac{hD}{k} = 0.821 \frac{(u \cdot \text{C.D.})^{0.385}}{\mu} \quad (\text{F2})$$

$$\text{and } \mathcal{L}_{1 \rightarrow 2} = \frac{1}{F_{12} + \left(\frac{1}{\epsilon_1} - 1\right) + \frac{A_1}{A_2} \left(\frac{1}{\epsilon_2} - 1\right)}$$

The emissivity constants were taken from Perry (1973)

$$\text{Platinum wire} = 0.073$$

$$\text{Chromonickel wire (oxide)} = 0.98$$

$$\text{marble packing} = 0.93$$

$$\text{Copper tube (oxide)} = 0.66$$

Calculation of the resistance thermometer temperature RT , by equation E1 gave a value of 22.65°C . This is slightly in excess of that obtained during the practical run by RTB and the discrepancy is thought due to heat leak. This experimental run and simulation clearly shows that the resistance thermometer temperature indication can be clearly affected by radiation from the heater wires.

FIG F1

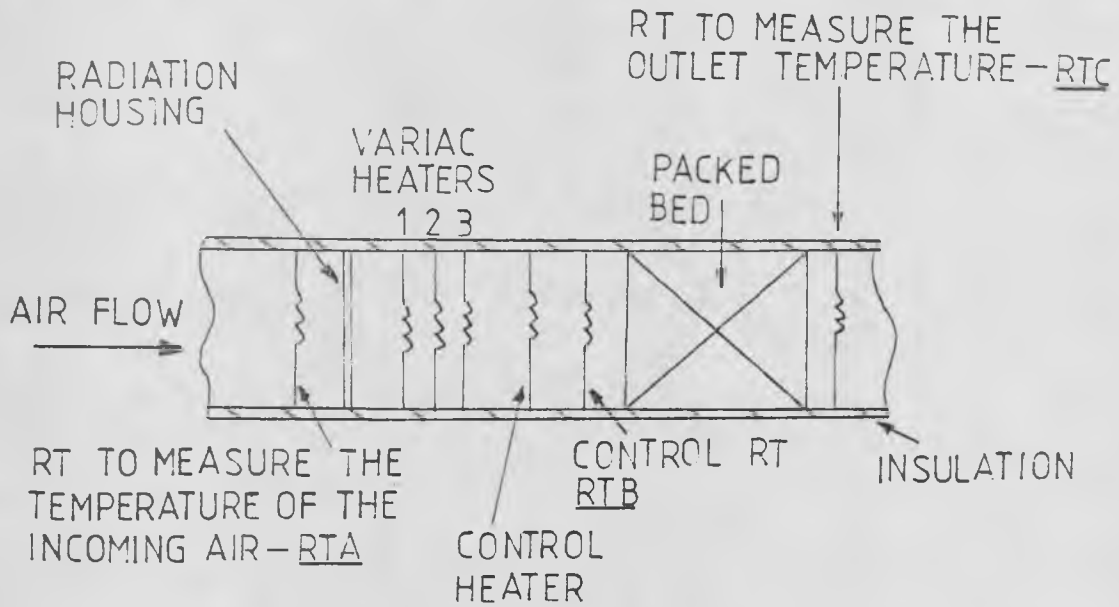
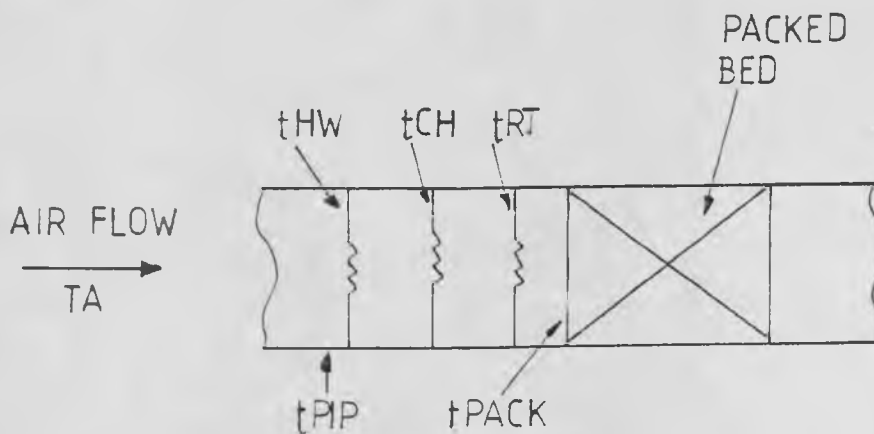
DIAGRAM OF THE FRONT END EXPERIMENTAL RUNEXPERIMENTAL RUN CONDITIONSAIR FLOWRATE = $0.0157 \text{ M}^3/\text{s}$ RTA = 17.5°C RTB = 22.5°C RTC = 22.0°C

FIG F2

DIAGRAM OF THE FRONT END SIMULATION

Appendix G

Prediction of the Temperature Response Within the Front End Section For a Known Step Heat Input

In order to predict the response for a step heat input to the front end control system, hence obtain the necessary outlet temperature and so determine the necessary control constants, the following unsteady state balance was solved using the Runge Kutter Merson technique.

This method was taken from Lance (1960) and used because of the very small time constants associated with the heater and resistance thermometer wire. The following procedure was incorporated into a computer program enabling a graphical production of the air temperature downstream of the heater wire and resistance thermometer, i.e. T_0 and T_2 respectively, as shown in Fig. G1.

Runge Kutter Merson Technique

This technique was used to solve the ordinary differential equations produced from the heat balance derived from fig. G1.

$$y_{n+1} = y_n + \frac{1}{5} (k_1 + 4k_4 + k_5) + O(h^5)$$

$$\text{where } k_1 = \frac{1}{3} h f(x_n, y_n)$$

$$k_2 = \frac{1}{3} h f(x_n + \frac{1}{3} h, y_n + k_1)$$

$$k_3 = \frac{1}{3} h f(x_n + \frac{1}{3} h, y_n + \frac{1}{2} k_1 + \frac{1}{2} k_2)$$

$$k_4 = \frac{1}{3} h f(x_n + \frac{1}{2} h, y_n + \frac{5}{8} k_1 + \frac{9}{8} k_3)$$

$$k_5 = \frac{1}{3} h f(x_n + h, y_n + \frac{3}{2} k_1, -\frac{9}{2} k_3 + 6k_4)$$

Heat Balance

An unsteady state heat balance was performed over the three elements present in the front end, i.e. the heater wire, the radiation shields and finally the resistance thermometer. Knowing the air inlet temperature (T_∞) and for a known electrical input (q), to the heater wire the air downstream of the heater can be computed (T_o). The radiation shield temperature, hence the air downstream of the shield (T_1), can be calculated. Similarly the resistance thermometer temperature, hence the air temperature (T_2) upstream of the packed bed is obtained.

Heater wire heat balance knowing T_∞ and q electric =

$$\frac{d t_{HW}}{d \theta} = \frac{q_{elec}}{C_{HW} \rho_{HW}} - \frac{h_{HW} A_{HW}}{C_{HW} \rho_{HW} V_{HW}} (t_{HW} - T_\infty) \\ - L_{HW \rightarrow RS} \frac{A_{HW} \sigma}{2 C_{HW} \rho_{HW} V_{HW}} (t_{HW}^4 - t_{RS}^4) \\ - L_{HW \rightarrow TUBE} \frac{A_{HW} \sigma}{2 C_{HW} \rho_{HW} V_{HW}} (t_{HW}^4 - t_{TUBE}^4)$$

solving for t_{HW} assuming t_{TUBE} and $t_{RS} = T_\infty$

$$\text{then : } T_o = T_\infty + \frac{h_{HW} A_{HW}}{C_g \rho_g Q} (t_{HW} - T_\infty)$$

solve for T_o

The heat transfer coefficient correlation for flow over cylindrical rods was taken from Krieth (1977), as used in Appendix F.

Radiation shield heat balance knowing T_o and T_{HW} :-

$$\frac{dt_{RS}}{d\theta} = - \frac{h_{RS} A_{RS} (t_{RS} - T_o)}{C_{RS} V_{RS}}$$

$$- \dot{Q}_{RS \rightarrow HW} = \frac{A_{RS} \sigma}{2} \frac{(t_{RS}^4 - t_{HW}^4)}{C_{RS} V_{RS}}$$

$$- \dot{Q}_{RS \rightarrow TUBE} = \frac{A_{RS} \sigma (t_{RS}^4 - t_{TUBE}^4)}{C_{RS} V_{RS}}$$

$$- \dot{Q}_{RS \rightarrow RT} = \frac{A_{RS} \sigma (t_{RS}^4 - t_{RT}^4)}{2 C_{RS} V_{RS}}$$

Solving for t_{RS} assuming t_{TUBE} and $t_{RT} = T_o$

$$\text{Then } T_1 = T_o + \frac{h_{RS} A_{RS}}{C_g \rho_g Q} (t_{RS} - T_o)$$

solve for T_1

Resistance Thermometer heat balance knowing T_1 and t_{RS}

$$\frac{dt_{RT}}{d\theta} = - \frac{h_{RT} A_{RT} (t_{RT} - T_1)}{C_{RT} V_{RT}}$$

$$- \dot{Q}_{RT \rightarrow RS} = \frac{A_{RT} \sigma (t_{RT}^4 - t_{RS}^4)}{2 C_{RT} V_{RT}}$$

$$- \dot{Q}_{RT \rightarrow TUBE} = \frac{A_{RT} \sigma (t_{RT}^4 - t_{TUBE}^4)}{C_{RT} V_{RT}}$$

$$- \dot{Q}_{RT \rightarrow PACK} = \frac{A_{RT} \sigma (t_{RT}^4 - t_{PACK}^4)}{2 C_{RT} V_{RT}}$$

Solving for t_{RT} assuming t_{TUBE} and $t_{PACK} = T_1$

$$\text{Then } T_2 = T_1 + \frac{h_{RT} A_{RT} (t_{RT} - T_1)}{G_g c_g Q}$$

solve for T_2

For a flowrate of $0.0157 \text{ M}^3/\text{s}$ and an electrical input corresponding to an air temperature rise of 2°C , the computer graphical output representing T_0 and T_2 is shown in fig.G2. This representation of the air temperatures allows the control constants, K_c , T_i and T_d to be found by the Ziegler Nichols (1942) technique and used in the PID algorithm (6.1)

where

- q elec = electrical power
- C = specific heat
- e = density
- h = convective heat transfer coefficient
- A = surface area
- T = gas temperature
- σ = Steffan Boltzman constant
- v = volume
- Θ = time
- t = solid temperature
- Q = volumetric flowrate

Subscripts :

- HW = Heater wire
- RS = Radiation shield
- TUBE = Copper tube
- RT = Resistance Thermometer
- PACK = Pebble Packing Face
- g = air

FIG G1

DIAGRAM OF THE CONTROL SET-UP

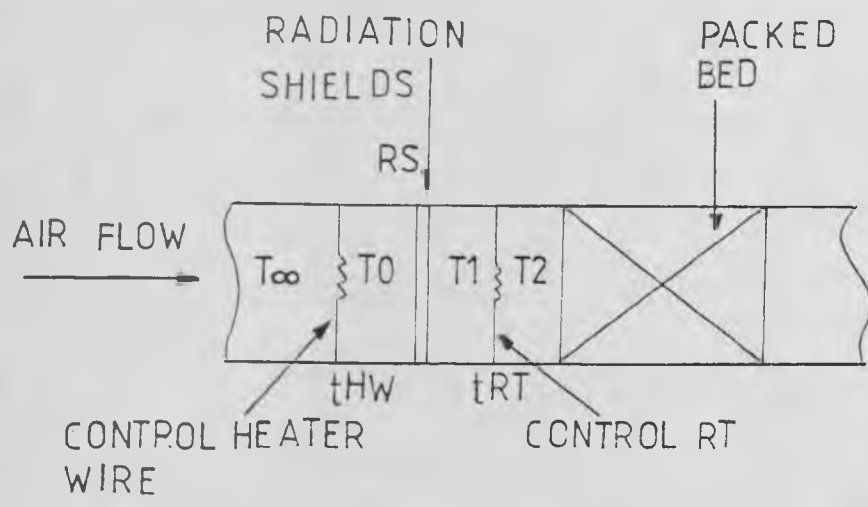
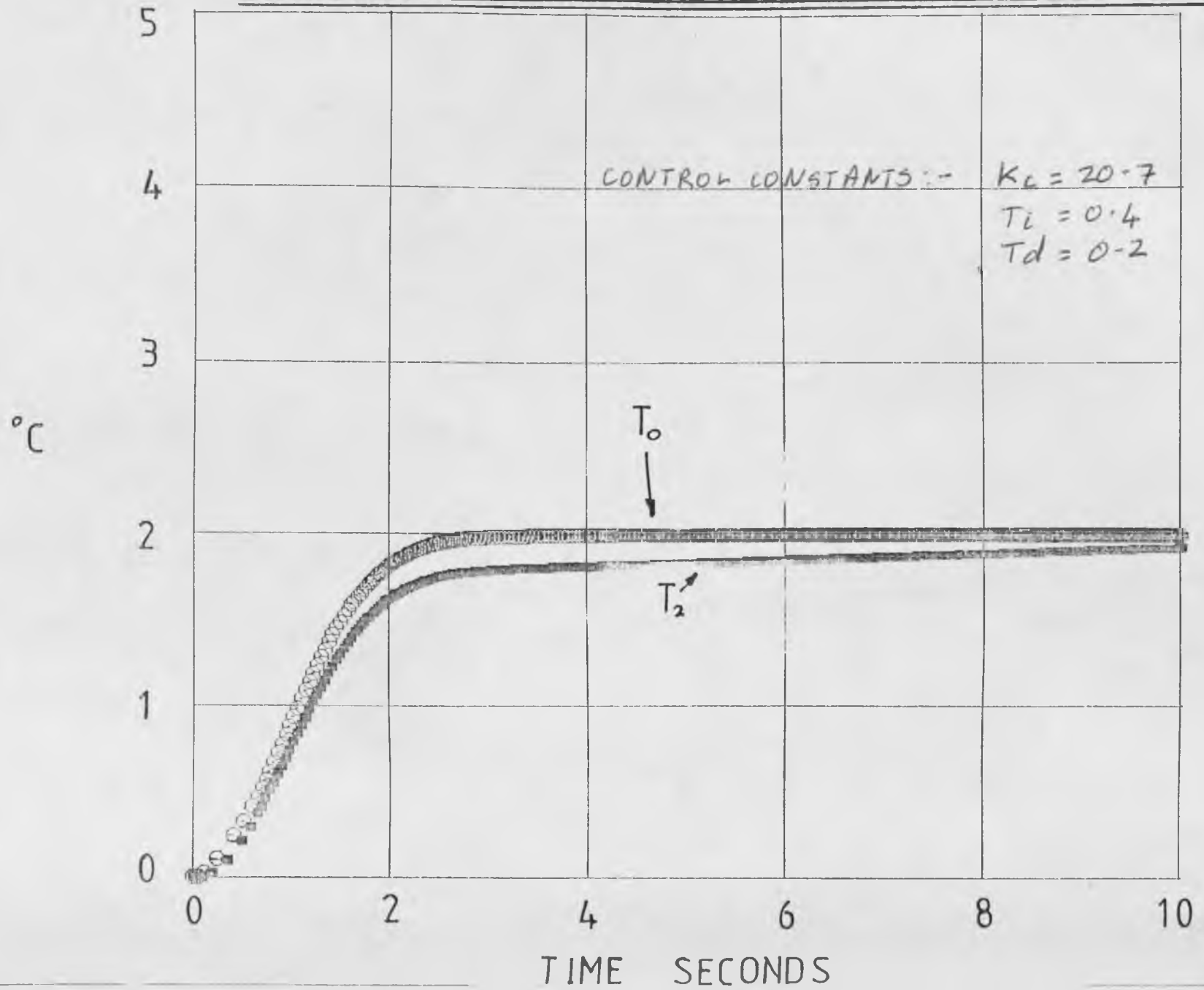


FIG G2

SIMULATED TEMPERATURE RESPONSE ACCORDING TO FIG G1



DEVELOPMENT OF AN APPARATUS TO INVESTIGATE THE THERMAL CHARACTERISTICS OF REGENERATOR HEAT EXCHANGERS

by P.J. Heggs and S.J. Hollins

Department of Chemical Engineering, University of Leeds, Leeds LS2 9JT

Before the advent of computers, thermal regenerators were designed by analogy with recuperators. Heat capacity, cycle times and conduction effects were incorporated in a modified heat transfer coefficient.

Computation techniques now allow a more thorough analysis and design of such systems. The following are some of the factors which can influence regenerator design and operation: surface heat transfer data, intraconduction and axial conduction in the packing material, axial dispersion in the fluid phase, fluid residence time at switch over and zones of different packing shape, size and material.

A number of mathematical models have been used to describe regenerator performance. The simplest is the Schumann model which assumes the heat transfer is solely convective. The efficiency η and temperature swings ΔT are functions of (π, π_1, A, A_1) . However in copper stoves in the steel industry and in pre-heat regenerators in the glass industry the transfer of heat is a combination of convection and intraconduction. Hence the efficiency η is now a function of $(A, A_1, \pi, \pi_1, B_1, B_{11})$ in situations where metallic packings are employed e.g. Fränkel packings and Lungström rotary regenerators, the effects of longitudinal conduction become important and here η and ΔT are functions of $(A, A_1, \pi, \pi_1, k_L, k_{L1})$. In some cryogenic regenerators the switch over times are very short and can lead to a plug of gas being captured in the regenerator voids. Carpenter/2/ has shown that the efficiency η increases for these situations. To obtain the best design efficiency and lowest temperature swings, not only will the above aspects have to be considered, but different packing materials, sizes, shapes and arrangements should also be considered. Zoned packing has been shown/2/ to provide more economic regenerator size.

An apparatus has been designed and is currently being commissioned to investigate the thermal characteristics of regenerator heat exchangers. This apparatus complements ongoing theoretical studies.

Design of regenerator apparatus

The design considerations were as follows:

1. Only one regenerator, which avoids the difficulties of assembling two identical units.
2. Co- and counter- current flow.
3. A wide range of equal and unequal cycle periods
 - (a) $\pi_1 = \pi_2$ FOR $\pi_1 = 1$ TO 10
 - (b) $\pi_1 \neq \pi_2$ Due to the reduction of the air flowrate at chosen half cycles and also the capability of having dissimilar time periods.
4. A wide range of equal and unequal dimensionless lengths
 - (a) $A_1 = A_2$ FOR $A_1 = 1$ TO 20 .
 - (b) $A_1 \neq A_2$ Due to the reduction of air flowrate at chosen half cycles.
 It is therefore possible to have balanced and unbalanced regenerators.
5. Accurate temperature measurement [temperature data to be recorded by a Kent recorder and computer logged], using special platinum resistance thermometers.
6. Maldistribution of air in the regenerator test bed is reduced considerably by placing diffusers at either end.
7. There is an exact flowrate change-over, because DC solenoid valves, electronically timed are used. [closing time 20 m secs]
8. The test bed is copper tubing 3" ID 3 1/8" OD. The copper has a relatively low heat capacity so minimising the regenerator wall heat capacity effect. This type of bed is easily, internally and externally, insulated.

9. The test bed heat input is from a stabilised voltage supply. There is a temperature rise of 10°C over the regenerator bed from 30 to 40°C . The 30°C is maintained constant by a primary heating section incorporating P+I control.

Description of apparatus

A schematic diagram of the rig is shown in Fig.1. Air at $8.273 \times 10^5 \text{ n/m}^2$ is throttled by gatevalve A, passes through a filter and pressure release valve set at $2.068 \times 10^5 \text{ n/m}^2$. The air is then heated to 30°C by the series of heaters 1,2,3 and 4. Heaters 1, 2 and 3 provide the main temperature rise whilst heat 4 provides the desired set point temperature. Heater 4 and platinum resistance thermometer 5 are in a feedback control loop with a P+I indicator controller. The air temperature control is further augmented by a packed bed to dampen out any temperature fluctuations. The air temperature after the packed bed being measured by platinum resistance thermometer 6. The following valve and test bed heater operation can then be incorporated giving up to 10°C rise.

For counter current flow

Hot stroke	CD open	7 on	EF closed
Cold stroke	EF open	7 off	CD closed

For C current flow C and D remain open, E and F remain closed as the heater, 7 is switched on and off according to the periods selected. If required valve B will open for any required stroke so reducing the air flowrate in the test section for that particular period. The air flowrate valve will depend on the orifice plate size chosen. The air after passing through the test bed will pass through orifice plate P1 enabling the air flowrate to be indicated by a water manometer.

The test bed has also been fitted with pressure points P2 and P3. These are linked to two manometers, one mercury and one water. This is for any bed pressure drop data required. The air temperature being measured at points 5,6,8,9,10, 11 and 12.

The following computer aspects are being incorporated into the system

- (a) Temperature logging on the computer
- (b) Computer timing to take over from the electronic timers
- (c) A PID control loop to supplement the indicator controller.

Thermal inertia

As a consequence of the design, the diffusers and flow solenoid valves require a considerable length of peripheral pipework. The effects of the pipework heat capacity on the regenerator performance has been investigated prior to the commissioning of the rig. Preliminary calculations were made of the system using the MISIP¹³¹ program, using the following criteria

1. No insulation in the apparatus
2. 1mm " " "
3. 3mm " " "
4. Time periods of 1 and 10 minutes
5. Reynold numbers: $\text{Re Min} = 100$ $\text{Re Max} = 4,500$
6. Bed section lengths 4" and 12" see Fig.II
7. 1/8" diameter steel ball bearings for the regenerator packing

The output data from one of the computer runs; as shown by Fig.III.

Apart from feeding the above data into the program a rough indication of the magnitude of the effect of the peripheral pipework could be found by examining the time constant associated with the dimensionless time,

Time constant = $(hA/M_s) \text{ s}^{-1}$ See table I for the value of the section parameters for a period of 600 seconds.

Table I.

Section	π	A	$(M_s C_s)$	h	$(hA/M_s C_s) \times 10^4$
1	1.11	59	504	15.8	18.5
2	0.20	33	357	3.6	3.35
3	0.064	39	887	2.41	1.06
4	16.	1192	2274	50.8	2066.0
5	0.064	39	887	2.4	1.06
6	0.20	33	357	3.6	3.35
7	1.11	59	504	15.8	18.5

Conclusions:- The work being done at the moment is still in the initial stages, but so far the following conclusions have been obtained.

1. Intuitively one would expect the pipework to reach cyclic steady state first. However it can be seen from the time constants that the controlling factor for cyclic equilibrium is the peripheral pipework. This aspect of the rig has effected the convergence of the computer program, in that the regenerator will cycle to equilibrium very quickly, but the pipework will not.
2. When internal insulation is used, the overall heat transfer coefficient is decreased, as the time constants of the pipework move further away from the time constant of the regenerator test bed.
3. The pipework heat capacity causes the design temperature change from 30°C to 40°C within the regenerator to be exceeded. The inlet cold temperature remains at 30°C, however the inlet hot temperature starts at 41.6°C for the profiles shown in Fig.III. The extra 1.6°C rise emanates from the pipework heat capacity upstream of the heater.
4. When calculating η_H [hot stroke efficiency] not only has the mean hot outlet temperature, with time, to be found, but the mean inlet temperature with time, has also to be evaluated. This being a consequence of the peripheral pipework. In theory however, it is assumed that the hot inlet temperature is constant.
5. The efficiencies calculated from the program were:-

$$\eta_H = 81\% \quad \eta_c = 78\%$$

The efficiency obtained from the Hausen⁽⁴⁾ plot was found to be $\eta_H = \eta_c = 83\%$ which should be the case for $A_1 = A_2$, $\pi_1 = \pi_2$. The unequal efficiencies were because the program did not achieve adequate convergence, for the reason stated above.

References

1. K.J. Carpenter, An investigation of thermal regenerator designs Ph.D. thesis, Leeds, 1976.
2. Heggs P.J. and Carpenter K.J. "The effects of packing material size and arrangement of the performance of thermal regenerators" Accepted for the 6th Int. Heat Transfer Conference, Toronto, August 7 - 11, 1978.
3. Heggs, P.J. Department of Chemical Engineering, Leeds University.
4. Jakob, M. 'Heat Transfer' Vol.2, p.296, Wiley and Sons Ltd., New York, 1957.

Nomenclature

A	= hA/LC_p	$\pi = hAP/M_s C_s$
h	= heat transfer coefficient $W/M^2 k$	
A	= heat transfer area per unit bed volume m^2/m^3	
L	= bed length (height) m	
G	= superficial fluid mass velocity $kg/m^2 s$	
C_p	= specific heat (air) C_s = specific heat solid KJ/kgk	
P	= period (s)	
M_s	= bulk density g/m^3	
Bi	= h_w/k_s	
x_w	= semi thickness in wall of packing	
k_s	= thermal conductivity of solid W/km	
K_L	= $hA/C_s L$	

Subscripts

- 1 = hot period
2 = cold period

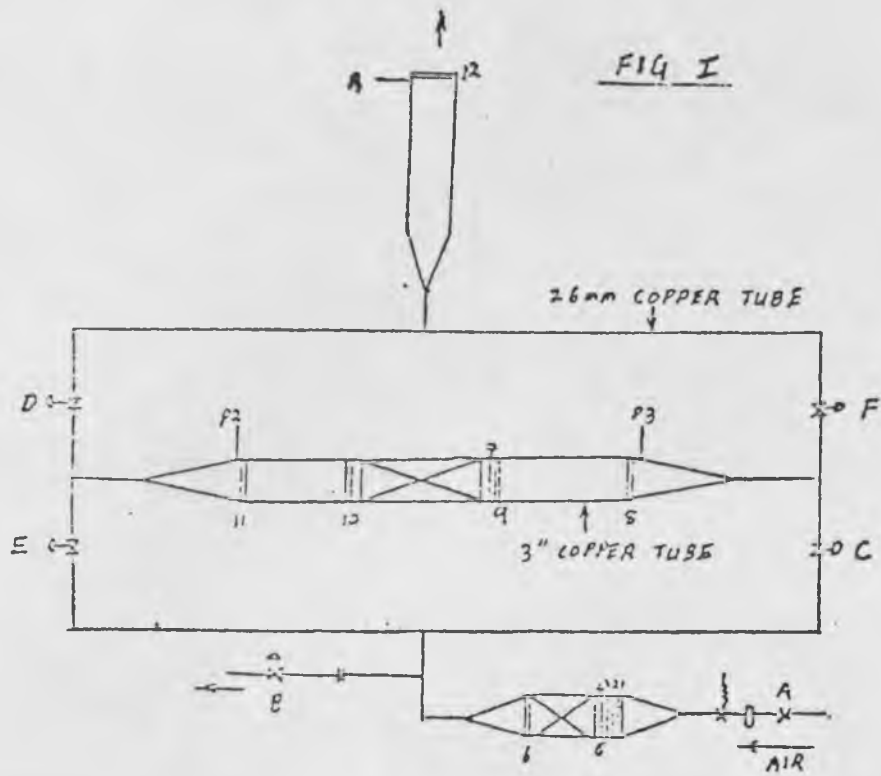


FIG I

FIG II (DIMENSIONS IN METERS)

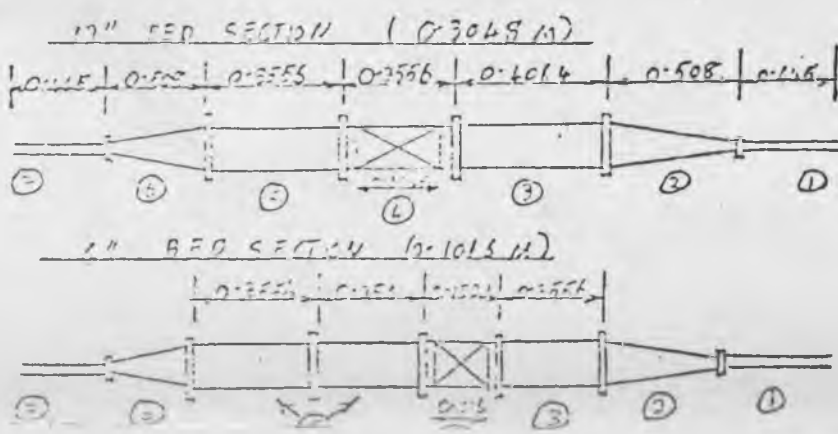
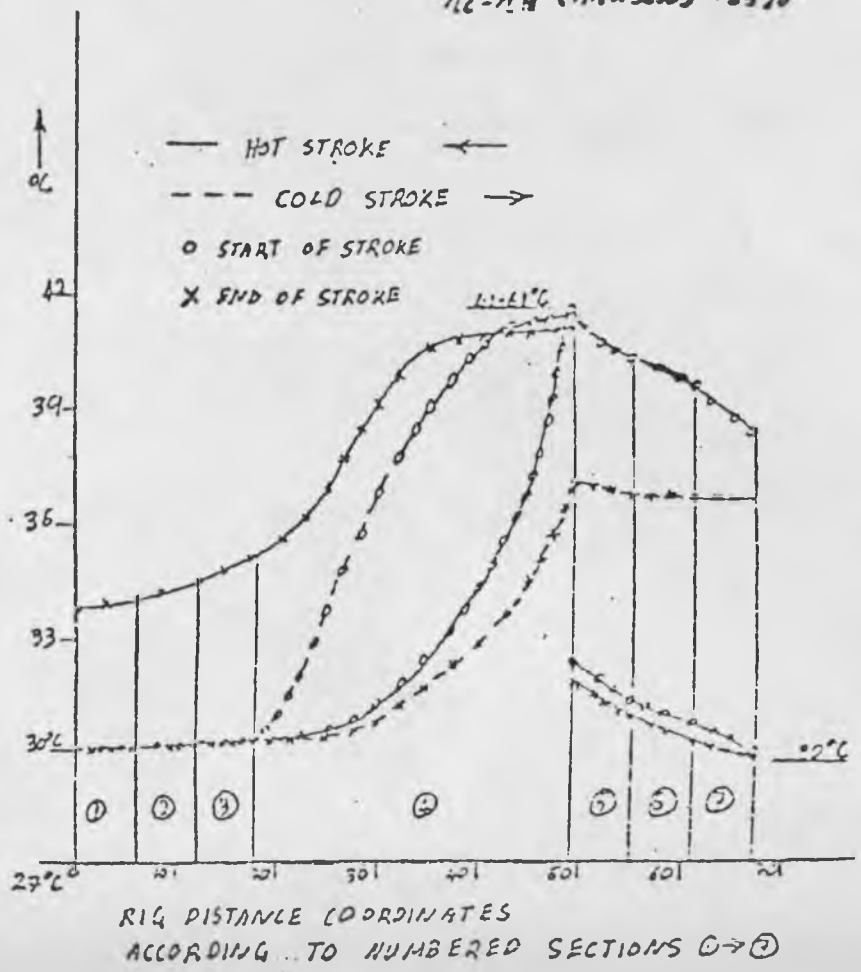


FIG III
GRAPH OF AIR TEMPERATURE vs LENGTH OF RIG [SEE FIG I]

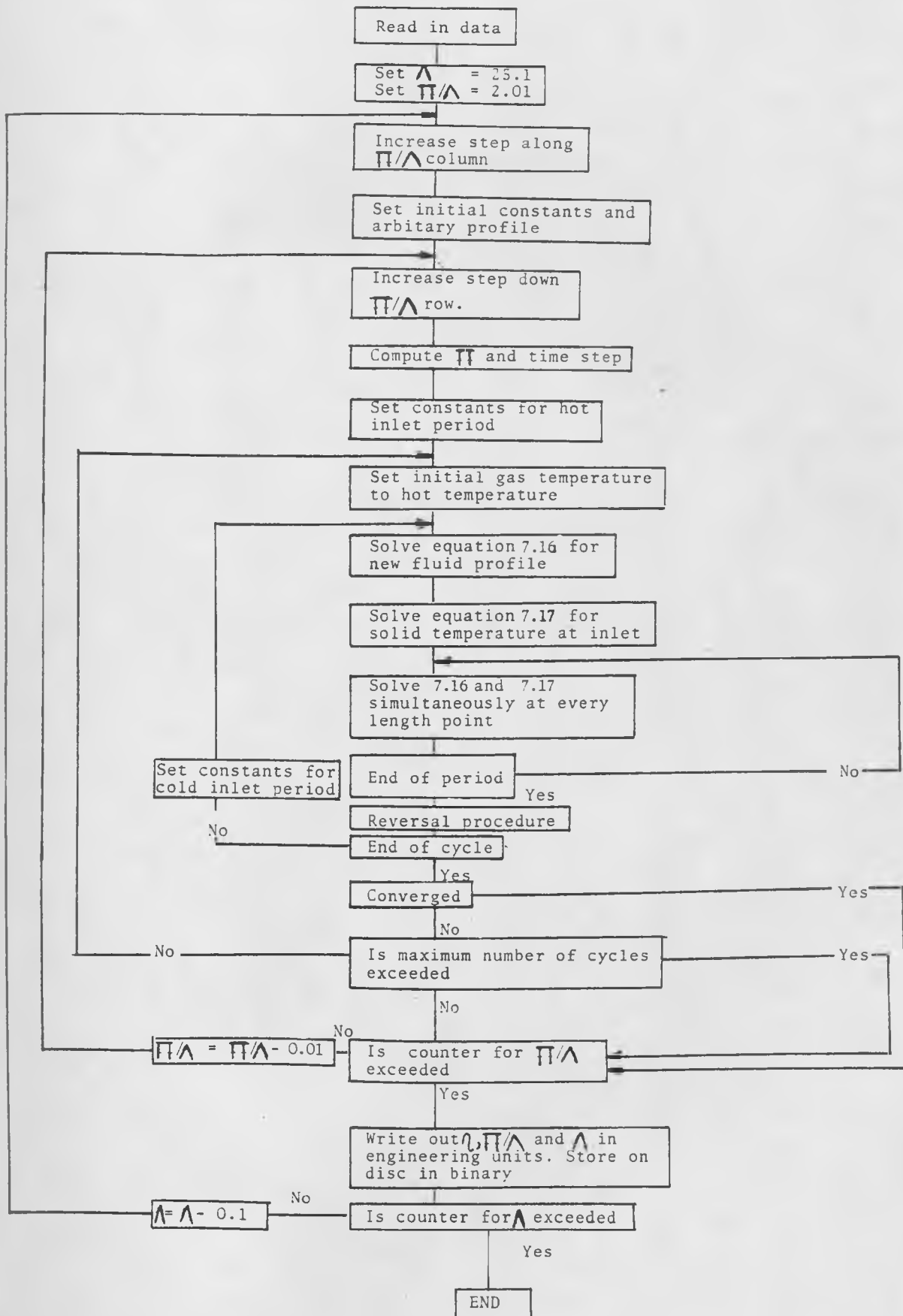
COLD OUTLET TEMPERATURE SWING $\Delta T = 5^\circ C$
HOT OUTLET TEMPERATURE SWING $\Delta T = 4.56^\circ C$

$\Pi_1 = \Pi_2 = 16$ η_H (PROG) = 81%
 $\Lambda_1 = \Lambda_2 = 22.2$ η_C (PROG) = 78%
 $\eta_C = \eta_H$ (HAUSEN) = 83%



RIG DISTANCE COORDINATES ACCORDING TO NUMBERED SECTIONS 1-7

LOGIC DIAGRAM FOR COMPUTER PROGRAM STHEFF2



Appendix JApparatus Start Up and Shut Down

- J.1 Introduction

- J.2 Analog Procedure
 - J.2.1 Start up
 - J.2.2 Shut down

- J.3 Computer Procedure
 - J.3.1 Start up
 - J.3.2 Shut down

- J.4 Analog Through to Computer Procedure
 - J.4.1 Changeover Procedure

J.1 Introduction

The apparatus running procedure is designed to include analog, computer and analog progressing to computer data logging and control. These procedures are therefore under three distinct sections and include the necessary information for apparatus running. Words spelt with capital letters represent the actual wording, identifying each toggle and mains switch on the panel.

J.2 Analog Procedure

J.2.1 Start Up

Primarily the toggle switch state is examined from right to left on the control panel. The underlined state gives analog operation.

<u>Switch</u>	<u>State</u>	<u>Operation</u>	<u>State Operation</u>
1	Down	Co-current	Up counter current
2	Down	25→45°C range	Up 5→25°C range
3	Down	Bleed off valve to actuate on cold stroke	Up bleed off valve to actuate on hot stroke
4	Down	Bleed off valve to be actuated	Up bleed off valve not to be actuated
5	Down	DIA→ Thyristor open circuit	<u>Up</u> DIA→ Thyristor closed circuit
6	<u>Down</u>	P+I→ Thyristor closed circuit	Up P+I→Thyristor open circuit

<u>Switch</u>	<u>State</u>	<u>Operation</u>	<u>State Operation</u>
7	Down	Wheatstone bridge to RT1 closed circuit	<u>Up</u> WB → RT1 open circuit
8	<u>Down</u>	P+I → RT1 closed circuit	Up P+I → RT1 open circuit
9	<u>Down</u>	Timing - manual	Up timing computer
10	Down	DIA → 5V supply closed circuit	<u>Up</u> DIA → 5V supply open circuit

The following mains switching sequence and equipment operation must then be followed after the mains electricity in the rig is switched on. All switch 'on' operation is down.

11 If the variac is required:-

- a) VP on
- b) H1)
- c) H12) closed circuit
- d) H123)

with the voltage demand potentiometer set at zero.

12 FAN switch on.

13 The temperature logging circuitry is then actuated

- a) K: mains for Kent recorder on.
- b) WBT5V: power supply for the wheatstone bridge circuit on.
- c) AMP: amplifier ± 15 VDC supply on.

The Kent recorder will take about two minutes to warm up. At this stage temperature indication is not necessary.

14 Front end feed back control:-

- a) Set the indicator pointer on 10°C .
- b) Set the proportional band width required.
- c) IC: Activate the indicator controller, and leave this for about 5 minutes to warm up.
- d) THY: Switch on the thyristor unit.

15 TBH240V: Activate the test bed heater (Heenon 180/6) heater unit with the voltage demand potentiometer set at zero.

16 Select the hot and cold time periods required.

17 Activate the LGM electronic timers by switching on the power supply units in this order:

SV24V: Solenoid valve 24 VDC

T24V: The 24VDC used for switching the secondary relays.

WT5V: The 5VDC power supply to the timers.

The timer circuitry has been designed so that the cold (SV's 1 and 3 according to Fig. 3.7) will open first indicated by the red lights directly under the cold time period selectors. The bleed off valve actuation is indicated by the green light located between the cold and hot red indicator lights. If co-current flow is required start the timing off under counter current flow, then change to the co-current mode.

- 18 Turn on the compressor and open the throttling valve to obtain the required flowrate indicated by the Negretti and Zambra $0(\frac{1}{2})40$ inch water monometer.
- 19 If required turn up the variac to obtain the required step temperature.
- 20 Move the red set pointer of the indicator controller to the required temperature point.
- 21 Start temperature recording until initial cyclic steady state has been reached by the rig. This is indicated by the test bed resistance thermometers approximately indicating the same temperature. Usually this is after 2 hours.
- 22 During a cold stroke turn the Heenon 180/6 voltage demand potentiometer to the required voltage for a step temperature input.
- 23 When cyclic steady state has been determined, switch to the next time period run in the set up. Cyclic steady state determination has been investigated using the MISP programme and is discussed in chapter 7.

J.2.2 Shut Down

- 1 Return the Heenon 180/6 voltage demand potentiometer to zero.

- 2 Move the controller set pointer to the 10⁰C point.
- 3 Return the variac demand potentiometer to zero.
- 4 Close the throttling valve.
- 5 Wait until the cold valves are activated, then turn off TBH240V.
- 6 Turn off the thyristor unit. THY.
- 7 Turn off the indicator controller, IC.
- 8 De activate the solenoid valves by switching off the timer unit power supplies in this order:
 - a) SV24V
 - b) T 24V
 - c) WT5V
- 9 Turn off the variac unit and make the heaters open circuit in this order:
 - a) VPON
 - b) H123
 - c) H12
 - d) H1

10 Turn off the temperature logging equipment

- a) K
- b) WBT5V
- c) AMP

11 Turn off the mains to the rig, located near the throttling valve.

After a very long run examine the Wilkinson F00 air filter unit and remove any oil collected.

J.3 Computer Procedure

J.3.1 Start Up

Prior to computer logging and control the appropriate toggle switch action is undertaken, as shown by the non underlined states in section J.2.1. The following procedure is undertaken to provide computer data logging and control:

1 Turn on the power supplies in the data acquisition room for the following:-

- a) Digital in multiplexer
- b) Digital de-multiplexer
- c) Fast analog to digital converter and multiplexer

- 2 Set both banks of thumbwheel switches to zero.

- 3 LOG: turn on the power to the 0.27 inch L.E.D. lights and the thumbwheel switches.

- 4 Start the FADC data collection and analyzing programme on the S/7 by typing in at the teletype station AGO.

- 5 Type in the data required to the Eclipse S/130 using teletype station:
 - a) The hot and cold time periods in seconds up to 10 runs.
 - b) The letter for the set up, eg. giving SJHRUNAØ to SJHRUNA9 for a set up of 10 runs.
 - c) The set point temperature required on the front end.
 - d) The proportional constant.
 - e) The integral time constant.
 - f) The derivative time constant.

- 6 Start the assembler programme in the S/7 by typing in SYC.

- 7 On the apparatus actuate the variac and 'close circuit' the three variac heaters with the demand potentiometer set at zero.

VPON

H1

H12

H123

8 Turn thumbwheel switch A (top) to 01, this will actuate the timing sequence.

9 Activate the solenoid valves:

a) SV24V on

b) T24V on

The solenoid valves will then operate according to the pre-programmed timing sequence in SJHREGEN, usually of two minutes duration to assure operation.

10 Start the compressor and allow a known flowrate to pass through the apparatus by throttling valve control and noting the flowrate manometer level.

11 Actuate the test bed heater unit (Heenon 180/6) TBV240V with the demand potentiometer set at zero. This action should be taken during the cold stroke.

12 Actuate the temperature logging circuitry. This allows simultaneous analog and computer temperature logging.

K: Kent recorder on

WBT5V: Wheatstone bridge voltage on

AMP: Amplifier I15VDC supply on.

Allow up to 5 minutes for the recorder and amplification circuitry to warm up.

13 D/P. Turn on the Differential Pressure Cell power supply allowing pressure differential logging.

14 THY. Turn on the control supply unit, CSR thyristor regulator. No voltage will be transmitted to the heater wire until the suitable Bit range is instigated by thumbwheel switch B (bottom). The control temperature amplification circuitry is instigated when temperature logging is started.

15 Turn thumbwheel switch A (top) to 02. This will instigate the front end control.

16 Turn the thumbwheel switch A to 03 then 04. This will start temperature and flowrate logging as well as the first hot and cold periods.

17 Any two of the temperatures indicated by resistance thermometers 2 to 7 can then be observed by the 0.27" L.E.D. lights by the following thumbwheel switch action.

Thumbwheel switch A	31	RT2
	32	3
	33	4
Thumbwheel switch B	41	5
	42	6
	43	7

Once a resistance thermometer temperature is being observed, no matter what the thumbwheel switch action (other than 00 A) that temperature indication will remain until

one of the number above are dialed.

18 Cyclic steady state attainment and subsequent switching to the next run can be obtained by checking the temperature profiles within SJHREGEN to a required accuracy or by instigating the next run by dialing thumbwheel switch B to 08.

19 When a run has ended the time periods remain until 04 on thumbwheel switch A is actuated then the next time periods and temperature and flowrate logging starts under a new file name, eg. SJHRUNA1. Between run switch overs the number of cycles recorded are indicated by the bottom set of 0.27" L.E.D. lights.

J.3.2 Shut Down

1 The Eclipse programme is prevented from firing the S/7 assembler programme by automatically ending the series of time periods typed in or turning thumbwheel switch A to 00. This will stop timing, data logging and control procedures. However, the cold solenoid valves will remain open.

The following items will be switched off, in this order:-

2 Turn the Variac and test bed heater demand potentiometers to zero volts.

3 THY. Thyristor off.

4 Variac unit off.

VPON

H1)

H12) open circuit

H123)

5 TBH240V. Test bed heater off during the cold stroke.

6 D/P. Turn the Differential Pressure supply off.

7 Turn off the temperature logging circuit.

K: Kent recorder

WBT5V: Wheatstone bridge power supply

AMP: Amplifier \pm 15 VDC power supply.

8 Close the throttling valve

9 Close the solenoid valves:

T24V: Turn off the relay switching power supply.

SV24V: Turn off the solenoid valve power supply

10 LOG: Turn off the light and thumbwheel switches power supply.

11 Switch off the mains power.

12 In the computer room:

a) stop the S/7 assembler programme; SYD

b) stop the S/7 FADC data processing programme

- c) stop the real time programme running in the Eclipse CTRLF.

13 Turn off the following in the data acquisition room:

- a) digital in multiplexer
- b) digital de-multiplexer
- c) FADC-MPXR

14 Each separate run comprising of a number of cycles can then be processed using SJH (CYCT, CYCP).

This computer operation can also be used for co-current flow.

J.4 Analog Through to Computer Procedure

This procedure incorporates full analog start up as discussed in J.2.1 and finishes with computer running and eventual shut down. This aspect of running was designed to incorporate lengthy period runs for which the Eclipse S/130 disc capacity is not adequate. Changeover in computer logging and control is made for smaller time period runs.

J.4.1 Changeover Procedure

This must be undertaken in the following order, as the analog state is fully operational:

1 Activate the appropriate units in the data acquisition room as discussed in J.2.1 1.

2 Start the relevant computer programmes on the two computers as discussed in J.2.1 5.

3 LOG: Turn on the thumbwheel switch and 0.27 inch L.E.D. power supply, with both sets of thumbwheel switches set at 00.

4 D/P. Turn on the Differential Pressure cell power supply.

5 Instigate the computer timing at the end of a hot stroke:-

- a) Turn thumbwheel switch A to 01.
- b) Set the timer toggle switch up to COMP TIM.
- c) Turn off WT5V, the electronic timers power supply

6 Start the front end computer control if required.

Usually during this mode of operation analog control is maintained.

- a) Turn thumbwheel switch B to 02. This will by-pass the control algorithm in SJHREGEN setting the subsequent output voltage in the C.S.R. thyristor regulator to zero.
- b) Return the indicator pointer to 10°C then turn off the indicator controller, IC.
- c) Manipulate the toggle switches as indicated in section J.2.1 for computer control.
- d) Turn thumbwheel switch B to 12, so instigating the control procedure.

The subsequent running and shut down is discussed in section J.4. The thumbwheel switch actions are given in appendix E.

Appendix KSet Up Data

Set Up	A	B	C	D	E	F
Packing	Mild Steel		Lead Glass		Alumina	
PD	6.35		6		12.7	
LSEC	203.2		203.2		203.2	
GROSS	4.6560		1.957		2.783	
TARE	0.3960		0.287		0.747	
CS	0.461		0.6531		0.8373	
DS	7849.1		2948.6		1842.1	
kPACK	45.7		3.116		2.093	
INSU	1	1	1	1	1	1
BD	76.2		76.2		76.2	
^	20	15	20	15	20	15

Run Data for Each Set-UpRun Data for Steel (A)

N	1	2	3	4	5	6	7	8	9	10
FO	7									7
TFEND	18									18
REGSTEP	5									5
AMB	13	13	13	13	13.1	13.2	13.5	13.6	13.5	13.5
TG2	15	15.1	15.4	15.2	14.9	14.6	15	13	13.2	13.8
MANO	5									5
PO2	0.3									0.5
BARO	749.6	749.7	749.8	750	750	752.3	756.4	765.1	764.8	765.1
P _H	29	26	23	20	17	14	11	8	5	2
P _C	29	26	23	20	17	14	11	8	5	2
NCYCM	12	4	4	4	4	8	6	6	6	6
NCYCA	40	7	6	6	20	12	18	48	7	15
η H	0.507	0.627	0.581	0.681	0.724	0.777	0.824	0.90	0.8966	0.902
η C	0.391	0.353	0.491	0.533	0.587	0.657	0.693	0.80	0.721	0.773
η M	0.449	0.49	0.536	0.607	0.655	0.717	0.758	0.70	0.809	0.837

Run Data for Steel (B)

N	1	2	3	4	5	6	7	8	9	10
FO	7	—————→								7
TFEND	17.5	—————→								17.5
REGSTEP	5	—————→								5
AMB	17	16	16	16.5	16.7	16.3	16.5	17	17	17
TG2	19.5	21	22	20	19.5	19.8	19.8	19.8	19.1	19.2
MANO	25	—————→								25
PO2	0.98	—————→								0.98
BARO	750	751	752	753.1	753	753	752.6	751	749.1	749.3
PH	12	11	10	9	8	7	6	5	4	3
PC	12	11	10	9	8	7	6	5	4	3
NCYCM	14	4	4	4	4	4	6	6	6	6
NCYCA	31	7	4	4	7	4	6	7	10	14
η_H	0.520	0.5336	0.567	0.6152	0.664	0.721	0.7436	0.785	0.82	0.841
η_C	0.457	0.527	0.54	0.6128	0.624	0.687	0.726	0.784	0.762	0.782
η_M	0.488	0.530	0.553	0.614	0.644	0.703	0.735	0.784	0.792	0.812

Run Data for Glass (C)

N	1	2	3	4	5	6	7	8	9
FO	7	—————→							7
TFEND	23	—————→							23
REGSTEP	5	—————→							5
AMB	19.9	20	20.3	21	21	18	18.5	19.5	20.2
TG2	21.0	21.1	21.4	21.3	21.2	21.4	21.3	21.2	21.5
MANO	5	—————→							5
PO2	0.3	—————→							0.3
BARO	768.3	769	769	770	773.3	772.2	773.3	772.2	771.1
P _H	18	16	14	12	10	8	6	4	2
P _C	18	16	14	12	10	8	6	4	2
NCYCM	16	4	4	4	6	8	6	8	8
NCYCA	28	4	5	5	8	58	8	12	34
η H	0.556	0.598	0.673	0.657	0.688	0.823	0.913	0.936	0.932
η C	0.349	0.335	0.414	0.502	0.582	0.631	0.58	0.701	0.755
η M	0.458	0.465	0.543	0.579	0.636	0.727	0.747	0.820	0.843

Run Data for Glass (D)

N	1	2	3	4	5	6	7
FO	7	—————→					7
TFEND	23	—————→					23
REGSTEP	5	—————					5
AMB	19.5	19.7	19.9	20	20.4	20.5	20.5
TG2	26.1	26.2	26.4	26.6	26.5	26.8	26.9
MANO	25	—————→					25
PO2	1.0	—————→					1.0
BARO	759.8	761.0	762.2	762.2	762.2	763.0	763.1
P _H	7	6	5	4	3	2	1
P _C	7	6	5	4	3	2	1
NCYCM	16	4	4	8	8	6	6
NCYCA	50	79	16	49	8	11	12
η_H	0.464	0.558	0.591	0.643	0.746	0.816	0.794
η_C	0.428	0.517	0.558	0.663	0.743	0.802	0.860
η_M	0.446	0.537	0.575	0.653	0.744	0.809	0.827

Run Data for Alumina (E)

N	1	2	3	4	5	6	7	8	9
FO	7	—————→							7
TFEND	25	—————→							25
REGSTEP	5	—————→							5
AMB	20.6	20.6	20.6	20.4	20	20	19.8	19.5	19.1
TG2	23.0	23.1	23.3	23.2	23.0	23.5	23.4	23.5	23.5
MANO	5	—————→							5
PO2	0.3	—————→							0.3
BARO	765.1	765.1	765.2	765.3	765.4	765.4	765.6	766.0	765.9
P _H	18	16	14	12	10	8	6	4	2
P _C	18	16	14	12	10	8	6	4	2
NCYCM	16	4	4	4	6	8	6	8	8
NCYCA	16	4	4	6	8	53	10	18	18
η H	0.578	0.649	0.649	0.705	0.728	0.753	0.781	0.842	0.814
η C	0.279	0.30	0.324	0.774	0.7790	0.428	0.459	0.493	0.497
η M	0.43	0.475	0.487	0.539	0.553	0.591	0.620	0.667	0.655

Run Data for Alumina (F)

N	1	2	3	4	5	6	7
FO	7	—————→					7
TFEND	23	—————→					23
REGSTEP	5	—————→					5
AMB	20.1	20.8	20.4	21	21.2	20.9	20.4
TG2	25.1	25.3	25.2	25.3	25.4	25.6	25.8
MANO	25	—————→					25
PO2	1.0	—————→					1.0
BARO	756.7	756.7	756.9	757	756.4	754.8	754.1
P_H	7	6	5	4	3	2	1
P_C	7	6	5	4	3	2	1
NCYCM	46	7	10	20	15	21	40
η_H	0.585	0.598	0.589	0.595	0.585	0.672	0.6522
η_C	0.429	0.41	0.417	0.475	0.517	0.527	0.574
η_M	0.507	0.504	0.503	0.535	0.551	0.60	0.613

NOMENCLATURE

	<u>Units</u>	
A'	Surface area	m^2
A	Heat transfer area per unit volume	m^2/m^3
a	Constant $\sqrt{\frac{\Delta x}{2}}$	
A _x	Cross sectional area	m^2
Bi	Biot number	
b	constant $\frac{(\Delta s)}{2}$	
C	Specific heat	J/kgk
D	diameter (m except where stated)	m
e	temperature difference	k
Fo	Fourier number	
G	Superficial gas mass velocity	kg/m^2s
h	heat transfer coefficient (convective unless otherwise stated)	w/m^2k
J	Number of length points	
Jh	J factor	
j	denotes the current length point	
k	Thermal conductivity	w/km
L	Bed length (m except where stated)	m
M	Mass	kg
m	hydraulic mean radius	m
N	Number of time points	
n	denotes the current time point	s
Nu	Nusselt number	
P	Period (in seconds unless stated)	s
Pv	voidage	
Pr	Prandtl number	
Pe	Peclet number	
Q	Volumetric Flowrate	m^3/s

q	Electric input	w
Re	Reynolds number	
S	Eulerian dimensionless time co-ordinate	
t	Solid temperature) is K except where) stated
T	gas temperature	
U	Overall heat transfer coefficient	w/m^2k
u	interstitial velocity	m/s
V	volume	m^3
w	radius (in m except where stated)	m
W	Mass flowrate	kg/S
x	reduced distance co-ordinate	
y	distance along the bed	m
x	size of a reduced length step	m
z	size of a dimensionless time step	

SUBSCRIPTS

a	alumina
av	average value of the runs
C	Cold period
c	convective heat transfer
CH	control heater
cyc	cyclic
g	gas value
gl	glass
H	Hot period
HW	Heater wire
I	Inlet valve
i	Internal value
kl	Longitudinal conduction
L	Value in Lagrangian co-ordinate system
M	Mean value
MT	Mercury Thermometer
MIN	Smaller of the hot or cold values
MAX	Larger of the hot or cold values
n	Single shot exponent values
O	Outlet value
o	Overall value
PAC	Packing
PIP	Copper Pipe
PT	Pressure Tapping
RS	Radiation Shield
RT	Resistance thermometer
s	solid
st	steel
SS	Single Shot
T	Tipler Method

GREEK SYMBOLS

		<u>Units</u>
α	Thermal Diffusivity	m^2/s
Δ	An increment	
σ	Dimensionless outlet temperature swing	
η	Regenerator effectiveness	
θ	Time	s
Λ	Dimensionless length	
μ	Viscosity	
Π	Dimensionless time	
ρ	Bulk Density	kg/m^3
τ	Time constant	s
Φ	Hausen's factor	
ψ	Inefficiency ($1-\eta$)	

References

- R.A. ACKERMANN and W.E. GIFFORD - 'Small Cryogenic Regenerator Performance'. J. Eng. Ind. (Trans A.S.M.E. series B) 91 (February 1969) 273.
- ALCOA - 'Activate and Catalytic Aluminas'. Aluminium Company of America, 1969.
- O.A. ABSJORNSEN and B. WANG - 'Heat Transfer and Diffusion in Fixed Beds'. Chem. Eng. Sci. 26, 585, (1971)
- G. ADAMOPULIS - 'Development of Practical Stochastic Control Strategies of a Multi Effect Evaporator. PhD Thesis. University of Leeds, (1977).
- H.H. BOHM - 'Versuche zur Ermittlung der Konvektiven Wärmeübergangszahlen an gebaurnten engen Kanälen'. Archiv für das Eisenhüttenwesen, Vol. 6, 423, (1932/33).
- P. BUTTERFIELD, J.SCHOFFIELD and P.A. YOUNG - 'Hot Blast Stoves Part 2'. J. Iron Steel Inst. 201 (June 1963), 497.
- G.D. BAHNKE and C.P. HOWARD - 'The Effect of Longitudinal Heat Conduction on Periodic Flow Heat Exchanger Performance'. J. Eng.for Power (Trans. A.S.M.E. series A), 86 (1964), 105.
- J.J. BARKER - 'Heat Transfer in Packed Beds'. Ind. Eng. Chem, 57 (4) 43 (1965).

A.V. BRADSHAW, A. JOHNSON, N.H. McLAUHLAN and Y.T. CHIU - 'Heat Transfer Between Air and Nitrogen and Packed Beds of Non-Reacting Solids'. Trans. Inst. Chem. Engrs., 48 177 (1970).

A. BRETHERTON - 'The Performance of Small Scale Regenerators Operating at Low Temperatures'. PhD Thesis, University of Bradford (1970).

R. BROOKS - 'Computer and Interface Documentation'. Department of Chemical Engineering. Leeds University (1978).

B.CARNHAM, H.A. LUTHER and J.O. WILKES - 'Applied Numerical Methods'. J. Wiley and Sons Inc., New York (1969).

B.P. COOMBS - 'Transient Test Technique for Evaluating the Thermal Performance of Cross-Inclined Tube Bundles'. PhD Thesis. University of Newcastle (1970).

COMPUTER MANUFACTURERS MANUAL (IBM/S7) - Department of Chemical Engineering, Leeds University (1971).

K.J. CARPENTER - 'An Investigation of Thermal Regenerator Design'. PhD. Thesis, University of Leeds, (1976)

COMPUTER USERS LOG BOOK - 'Department of Chemical Engineering, Leeds University (1978).

F. DARABI - 'Thesis in Preparation'. Department of Chemical Engineering. Leeds University (1981).

N.K. ELUKHIN and S.I. STAROVITSKII - 'Heat Exchange and Hydraulic Resistance in Dumped Packings of Regenerators'. Int. Chem. Eng. 4. 114 (1964).

ENGLASS - 'Ballotini Technical Bulletin'. No. 33. Issue 4/276. (1976).

FOXBORO - 'Differential Pressure Cell Manual' (1975).

A.S. GUPTA and G. THODOS - 'Direct Analogy Heat and Mass Transfer to Beds of Spheres'. A.I. Chem. E.J. 9, 751, (1963).

W.E. GIFFORD - 'The Gifford - McMahon Cycle'. Adv. Cryo. Eng. 11 (1965), C-5. 152.

W.H. GRANVILLE, W.I. McDONALD and P. CUTLER - 'Comparison of Predicted and Experimental Thermal Efficiencies of Packed Regenerators'. Third Int. Heat Trans. Conf. (Chicago 1966). paper 149, 329.

W.E. GIFFORD, A. ACHARYA and R.A. ACKERMANN - 'Compact Cryogenic Thermal Regenerator Performance'. Adv. Cryo. Eng. 14 (1968), J-3 353.

D.J. GUNN and J.F.C. DE SOUZA - Heat Transfer and axial Dispersion in Packed Beds'. Chem.Eng. Sci.29,1363 (1974).

H. HAUSEN - 'Uber Die Theorie Von Warmeaustausches in Regeneratoren'. Z. Angew. Math. Und Mech. 9(1929), 173. R.A.E. Library Trans. 126.

H. HAUSEN - 'Naherungsverfahren zur Benechnung des Warmeaustausches in Regeneratoren'. Z. Angew. Math and Mech. 11 (1931), 105. R.A.E. Library Trans. 98.

H. HAUSEN - 'Vervollstandigte Berechnung des Warmeaustausches in Regeneratoren'. Z. VDI - Beiheft Verfahrenstechnik, No.2 (1942), 31.

W.HRYNSZAK - 'Heat Exchangers - Application to Gas Turbines'. Butterworths Scientific Publications. London (1958).

J.W. HLINKA, F.S. PUHR and V. PASCHKIS. 'AISE Manual for Thermal Regenerator Design'. Iron and Steel Eng. 59(Aug.1961)

B.S. HOLMES, C. ROUNTHWAITE, D.S.D. HUNTER and P.A. YOUNG - 'Hot Blast Stoves Parts 3 and 4'. J. Iron and Steel Inst. 202 (October 1964). 939.

P.J. HEGGS - 'Transfer Processes in Packings Used in Thermal Regenerators'. PhD Thesis, University of Leeds (1967).

P.J. HEGGS - 'Intraplate Conduction Effects in Fixed Bed Transient Heat Transfer'. Can. J. Chem. Eng. 47 1373 (1969).

P.J. HEGGS - 'Conduction Effects in Hasche Tiles'. 4th Int. Heat Trans. Conf. (Versailles) (Sept. 1970).

P.J. HEGGS and K.J. CARPENTER - 'The Effect of Fluid Hold Up on the Effectiveness of Contraflow Regenerators'. Trans. Inst. Chem. Eng. Vol 54, No. 4 P232, (1976).

P.J. HEGGS and S.J. HOLLINS - 'Development of an Apparatus to Investigate the Thermal Characteristics of Regenerator Heat Exchangers'. Annual Research Meeting, 6-7 April (1978). Birmingham University.

P.J. HEGGS and K.J. CARPENTER - 'The Effects of Packing Material, Size and Arrangement on the Performance of Thermal Regenerators'. Int. Heat and Mass Trans. Conf. Toronto, Canada. (Aug. 1978), Vol. 4, 303.

P.J. HEGGS and K.J. CARPENTER - 'A Modification of the Thermal Regenerator Infinite Conduction Model to Predict the Effects of Intraconduction'. Trans. I. Chem. E. Vol. 57, (1979), 228.

P.J. HEGGS, L.S. BANSAL, R.S. BOND and V. VAZAKAS - 'Thermal Regenerator Design Charts Including Intraconduction Effects'. Trans. I. Chem. E. Vol. 58, (1980), 265.

M. JAKOB - 'Heat Transfer' - Vol. 2, Wiley and Sons Ltd. New York. (1957).

H. KISTNER - 'Grossversuche an einer Zu Studien sweeken Gebauten Regeneratorenkammer.' Archu Fuer das Evsenhuettenwesen, Vol. 3, (1929/30), 751.

W.M. KAYS and A.L. LONDON - 'Compact Heat Exchangers' 2nd Ed. McGraw-Hill, New York (1964).

F. KRIETH - 'Principles of Heat Transfer'. 3rd Ed. (1973), Feffer and Simon's Int. Univ. Ed.

I. LUBBOCK and I.G. BOWEN - 'The Use of Rotary Heat Regenerators in Gas Turbines'. Shell Tech. Rep. ICT/5. (Sept. 1946).

G. LUND and B.F. DODGE - 'Frankl Regenerator Packings : Heat Transfer and Pressure Drop Characteristics'. Ind. and Eng. Chem. 40 1019 (1948).

T.J. LAMBERTSON - 'Performance Factors of a Periodic Flow Heat Exchanger'. Trans. A.S.M.E. 80 586, (1958).

G.N.LANCE - ' Numerical Methods for High Speed Computers' Iliffe (1960)

F.W.LARSEN - ' Rapid Calculation of Temperature in a Regenerative Heat Exchanger Having Arbitrary Initial Solid and Entering Fluid Temperatures'. Int. J. Heat and Mass Trans. 10 149, (1967).

W.J.MACDONALD - ' Comparison of Predicted and Experimental Thermal Efficiencies of Packed Regenerators'. M.Sc.Thesis, Bradford University, (1966).

MPXR Documentation - DEC-00-16AA-D, Department of Chemical Engineering, Leeds University, (1969).

M.I.S.P. Computer Program. P.J. HEGGS, Department of Chemical Engineering, Leeds, University, (1977).

A.J. St. J. MAIN - 'An Experimental Investigation into Heat Transfer and Momentum Effects in Packed Beds'. PhD Thesis, University of Leeds, (1978).

W. NUSSELT - 'Der Beharrungszustand in Winderhitzen'. Z. des Ver. Deut. Ing. 72 (1928), 1052.

N.B. ORR - 'The Rotary Regenerative Pre Heater - Low Cost Mechanism for Heat Recovery'. Low Cost Heat Recovery by Thermal Regenerators, Symposium, Department of Chemical Engineering, Leeds University (1976).

A.M. PEISER and J. LEHNER - 'Design Charts for Symmetric Regenerators'. Ind. Eng. Chem. 45, 4, 2166, (1953).

D.PETIT - 'Present State of Construction of Cowper Stoves'. J. Iron and Steel Inst. (1964), 202, 305.

C.B.A. PRICE - 'Heat and Momentum Transfer in Thermal Regenerators'. PhD Thesis, London University (1964).

V.PASCHKIS and P. RAZELOS - 'Blast Furnace Stove Design - A Progress Report'. Iron and Steel Eng. 115, (May 1966).

A. POLLARD - 'Process Control'. Heinemann Press. 1st Ed.
1971

P.G. POLETAVKIN and YU.S. MALYGIN - 'Heating of Air and Gases to
1500 - 2000°C in High Temperature Regenerators with a Pebble
Bed'. Int. Centre for Heat and Mass Trans. 1972, Int. Seminar
(Tragiv, Yugoslavia) Recent Developments in Heat Exchangers.

R.H. PERRY and C.H. CHILTON - 'Chemical Engineers Handbook,
5th Ed. 1973.

M. RUHEMANN - 'The Separation of Gases' Oxford Press,
2nd Ed. (1940).

J.M. RIDGION and B. KERRISON - 'Measurements of Heat Transfer
Coefficients for Stove Checkers'. J. Iron and Steel Inst.
202 (1964), 315.

P.A. RIOS and J.L. SMITH JNR. - 'The Effect of Variable
Specific Heat of the Matrix on the Performance of Thermal
Regenerators. Adv. Cyro. Eng. 13 (1967), 566.

P. RAZELOS and M.K. BENJAMIN - 'Computer Model of Thermal
Regenerators with Variable Mass Flow Rates'. Int. J. Heat
and Mass Trans. 21, 735 (1978).

T.E.W. SCHUMANN - 'Heat Transfer : A. Liquid Flowing Through
a Porous Prism'. J. Frank. Inst. 208, (1929), 405.

O.A. SAUNDERS and H. FORD - 'Heat Transfer in the Flow of a Gas Through a Bed of Solid Particles'. J. Iron and Steel Inst. 141,(1), 291, (1940).

J. SCHOFIELD, P. BUTTERFIELD and P.A. YOUNG - 'Hot Blast Stoves'. J. Iron and Steel Inst. 199 (Nov. 1961), 229.

L.K. SPINK - 'Principles and Practice of Flow Meter Engineering'. 8th Ed. Plimpton Press. (1961)

L.L. SIMPSON - 'Sizing Piping for Process Plants'. Chemical Engineering. June 17, (1968), 192.

J.M. STACEY - 'Development of a Novel Regenerative Furnace for High Temperature Reactions'. PhD Thesis, University of Leeds, (1970).

W. TIPLER - 'A Simple Theory of the Heat Regenerator'. Shell Tech. Rep. ICT/14, (July 1947).

R.J. THOMAS - 'Improved Computer Simulations of a Thermal Regenerator'. PhD Thesis, University of York, (1972).

A.J. WILLMOTT - 'B.I.S.R.A. Rep. IM/C/2/13. (1963)

A.J. WILLMOTT - 'Digital Computer Simulation of a Thermal Regenerator.' Int. J. Heat and Mass Trans. 7 (1964), 1291.

A.J. WILLMOTT - 'Simulation of a Thermal Regenerator Under Conditions of Variable Mass Flow'. Int. J. Heat and Mass Trans. 11, 1105, (1968). (2)

A.J. WILLMOTT - 'Operation of Cowper Stoves Under Conditions of Variable Flow : A computer Study'. J. Iron and Steel Inst. 206 (1), 33, (1968). (1)

A.J. WILLMOTT - 'The Regenerative Heat Exchanger Computer Representation'. Int. J. Heat and Mass Trans. 12, (1969), 997.

A.J. WILLMOTT and CLAIRE HINCHLIFFE - 'The Effect of Gas Heat Storage upon the Performance of the Thermal Regenerator'. Int. J. Heat and Mass Trans. 19, (1976), 821.

A.J. WILLMOTT and A. BURNS - 'Transient Response of Periodic - Flow Regenerators'. Int. J. Heat and Mass Trans. 20, 753, (1977).

A.J. WILLMOTT and A. BURNS - 'Periodic Flow Regenerators : Parametric Identification for Transient Performance'. Int. J. Heat and Mass Trans. Corp. Toronto, Canada, Vol. 4, 297 (1978).

A.J. WILLMOTT and A. BURNS - 'Heat Transfer Coefficient Correlating for Thermal Regenerator Calculations - Transient Response'. Int. J. Heat and Mass Trans. 22 (1980), 969

J.G. ZIEGLER and N.B. NICHOLS - Trans. A.S.M.E. 64, (1942),
759.

ZRDOS - Computer Manual, Department of Chemical Engineering,
Leeds University (1978).